COMPUTATIONAL STUDIES OF TRANSITION METAL CATALYSTS

by

RALUCA CRACIUN

A DISSERTATION

Submitted in partial fulfillment of the requirements
for the degree of Doctor of Philosophy
in the Department of Chemistry
in the Graduate School of
The University of Alabama

TUSCALOOSA, ALABAMA

2010

ABSTRACT

High level electronic structure calculations were used to evaluate reliable, self-consistent thermochemical data sets for the second and third row transition metal hexafluorides, as well as for metal phosphines (M=Ni, Pd, Pt). For the transition metal hexafluorides, the electron affinities, heats of formation, first ($MF_6 \rightarrow MF_5 + F$) and average M-F bond dissociation energies, and fluoride affinities of MF_6 ($MF_6 + F^- \rightarrow MF_7^-$) and MF_5 ($MF_5 + F^- \rightarrow MF_6^-$) were calculated. For the transition metal phosphines, the first metal-phosphine binding energy in MPH_3, $M(PH_3)_2$, MPH_3Cl_2 and $M(PH_3)_2Cl_2$ was calculated.

The electron affinities, which are a direct measure for the oxidizer strength, increase monotonically in the second and third row series, from WF_6 to AuF_6, and from MoF_6 to AgF_6. The hexafluorides of the last two elements of each series, Pt, Au in the third row and Pd and Ag in the second, form extremely powerful oxidizers. The inclusion of spin orbit corrections is necessary to obtain the correct qualitative order for the electron affinities. The calculated electron affinities increase with increasing atomic number, are in good agreement with the available experimental values and, for the third row are: WF_6 (3.15 eV), ReF_6 (4.58 eV), OsF_6 (5.92 eV), IrF_6 (5.99 eV), PtF_6 (7.09 eV), and AuF_6 (8.20 eV). The electron affinities of the second row hexafluorides are even larger than for the second row: MoF_6 (4.23 eV), TcF_6 (5.89 eV), RuF_6 (7.01 eV), RhF_6 (6.80 eV), PdF_6 (7.95 eV), AgF_6 (8.89 eV).

A wide range of density functional theory exchange-correlation functionals were also evaluated and only three gave satisfactory results as compared to the higher level electronic

structure calculations. The corresponding pentafluorides are extremely strong Lewis acids. The optimized geometries of the corresponding MF_7^- anions show classical structures with M-F bonds for W through Ir and for Mo, Tc and Rh; however, for PtF_7^-, AuF_7^-, RuF_7^-, PdF_7^-, and AgF_7^- nonclassical anions were found with a very weak external F-F bond between an MF_6^- fragment and a fluorine atom. These anions are text book examples for "superhalogens" and can serve as F atom sources under very mild conditions.

DEDICATION

To my parents.

LIST OF ABBREVIATIONS AND SYMBOLS

aug-cc-pVnZ	Augmented, correlation consistent, polarized valence n zeta basis sets, where n=double (D), triple (T), quadruple (Q)
aug-cc-pVTZ-PP	aug-cc-pVnZ basis sets with pseudo-potentials for heavy atoms
aug-cc-pwCVTZ	Augmented, correlation consistent, polarized weighted core valence triple zeta basis sets
aug-cc-pwCVnZ-PP	aug-cc-pwCVTZ basis set with pseudo-potentials for heavy atoms
B1B95	Becke 96 (exchange), Becke 95 (correlation) DFT functional
B1LYP	Becke 96 (exchange), Lee-Yang-Parr (correlation) DFT functional
B3LYP	Becke 93 (exchange), Lee-Yang-Parr (correlation) DFT functional
B3P86	Becke 93 (exchange), Perdew 86 (correlation) DFT functional
B3PW91	Becke 93 (exchange), Perdew-Wang 91(correlation) DFT functional
B971	Handy-Tozer's modification to B97
B972	Wilson-Bradley-Tozer's modification to B97
B98	Becke 98 hybrid DFT functional
BB95	Becke 88 (exchange), Becke 95 (correlation) DFT functional
BDE	Bond dissociation energy
BLYP	Becke 88 (exchange), Lee-Yang-Parr (correlation) DFT functional
BMK	Boese-Martin hybrid DFT functional

BP86	Becke 88 (exchange), Perdew 86 (correlation) DFT functional
BPW91	Becke 88 (exchange), Perdew-Wang 91(correlation) DFT functional
CBS	Complete basis set
CCSD(T)	Coupled cluster singles, doubles, and disconnected triples
CI	Configuration interaction
CISD	Configuration interaction singles and doubles
DFT	Density functional theory
DK	Douglas-Kroll
EA	Electron affinity
ΔE_{CBS}	Complete basis set energy change
ΔE_{CV}	Core valence energy change
ΔE_{MVD}	Mass-velocity and Darwin energy change
$\Delta E_{PP\text{-}error}$	Pseudopotential error energy change
ΔE_{Rel}	Scalar relativistic energy change
ΔE_{ZPE}	Zero point energy change
FA	Fluoride affinity
GGA	Generalized gradient approximation
HCTH	Handy (exchange), Handy (correlation) DFT functional
$\Delta H_{f,0K}$	Heat of formation at 0K
$\Delta H_{f,298K}$	Heat of formation at 298K
HGGA	Hybrid generalized gradient approximation
LSDA	Local spin density approximation
mPW	Adamo –Barone's modification to PW91 DFT functional

mPW1	Barone's modified PW91 (exchange), Perdew-Wang 91(correlation) DFT functional
MVD	Mass-velocity and Darwin term
NBS	National Bureau of Standards
NIST-JANAF	National Institute of Standards and Technology - Joint Army-Navy-Air Force
O3LYP	Handy's OPTX (exchange), Lee-Yang-Parr (correlation) DFT functional
PBE	Perdew-Burke-Ernzerhof (exchange), Perdew-Burke-Ernzerhof (correlation) DFT functional
PBE1	Perdew-Burke-Ernzerhof (exchange), Perdew-Burke-Ernzerhof (correlation) DFT functional
PW91	Perdew-Wang 91 (exchange), Perdew-Wang 91 (correlation) DFT functional
SO	Spin orbit
SVWN5	Slater (exchange), Vosko-Wilk-Nussair (correlation) DFT functional
TAE	Total atomization energy
TPSS	Tao-Perdew-Staroverov-Scuseria (exchange), Tao-Perdew-Staroverov-Scuseria (correlation) DFT functional
TPSSh	Tao-Perdew-Staroverov-Scuseria (exchange), Tao-Perdew-Staroverov-Scuseria (correlation) hybrid DFT functional
TZ2P	Triple zeta basis set with 2 polarization functions
VAE	Vertical attachment energy
VDE	Vertical detachment energy

VSXC	van Voorhis-Scuseria standalone DFT functional
ZORA	Zeroth order regular approximation to the Dirac equation
ZPE	Zero point energy
>	Greater than
<	Less than
=	Equal to
°	Degrees
±	Plus or minus

ACKNOWLEDGMENTS

I am forever grateful to my research adviser Dr. David A. Dixon for his tremendous support and constant guidance and encouragement. Always ready to help, and offering the perfect advice, he was a source of inspiration. I feel fortunate for having the opportunity to work with him. My life has forever changed.

Special thanks to the people that contributed to this work: Dr. Kirk A. Peterson from Washington State University, Dr. Karl O. Christe, Loker Hydrocarbon Research Institute and the University of Southern California, Dr. Shenggang Li and Dr. Kevin H. Shaughnessy, The University of Alabama, and the undergraduates I was fortunate to work with: Desiree Picone, Rebecca T. Long and Andrew Vincent. They are the co-authors of Chapter 2: Desiree Picone, Rebecca T. Long, Shenggang Li, David A. Dixon, Kirk A. Peterson and Karl O. Christe; Chapter 3: Rebecca T. Long, David A. Dixon and Karl O. Christe; and Chapter 4: Andrew Vincent, Kevin H. Shaughnessy and David A. Dixon.

I am indebted to my committee members, Dr. Martin Bakker, Dr. Kevin Shaughnessy, Dr. Gregory Szulczewski and Dr. Heath Turner for their inspiring questions, guidance and endless patience.

Many thanks to the Dixon group members, the best colleagues anyone could ask for, especially Dr. Shenggang Li and Dr. Myrna H. Matus for being great friends, always encouraging me.

I would like to thank the Graduate School for a one year Graduate Council Fellowship that allowed me to focus on my research. I am also grateful for the travel financial support from the Graduate School and the Department of Chemistry that allowed me to present my research at regional and national conferences.

And finally, I thank my dear husband Luigi for his love, support and understanding throughout my PhD years.

CONTENTS

ABSTRACT ii

DEDICATION iv

LIST OF ABBREVIATIONS AND SYMBOLS v

ACKNOWLEDGMENTS ix

LIST OF TABLES xiii

LIST OF FIGURES xvii

1. INTRODUCTION 1

1.1. Catalysis and Computational Chemistry 1

1.2. Molecular Orbital (MO) and Density Functional Theory (DFT) Methods 4

1.3. Energy Corrections 9

2. THIRD ROW TRANSITION METAL HEXAFLUORIDES, EXTRAORDINARY OXIDIZERS AND LEWIS ACIDS: ELECTRON AFFINITIES, FLUORIDE AFFINITIES, AND HEATS OF FORMATION OF WF_6, ReF_6, OsF_6, IrF_6, PtF_6, and AuF_6 12

References 61

Appendix 68

3. ELECTRON AFFINITIES, FLUORIDE AFFINITIES, AND HEATS OF FORMATION OF THE SECOND ROW

TRANSITION METAL HEXAFLUORIDES: (MoF_6, TcF_6, RuF_6, RhF_6, PdF_6, and AgF_6) 121
References 160
Appendix 164
4. PREDICTION OF RELIABLE METAL-PH3BOND ENERGIES FOR Ni, Pd AND Pt IN THE 0 AND +2 OXIDATION STATES 213
References 231
Appendix 237
5. CONCLUSIONS 253
REFERENCES 254

LIST OF TABLES

1.1. Benchmarked DFT Exchange-Correlation Functionals 8

2.1. MF_6 Electron Affinities in eV 46

2.2. Optimized Metal-Fluorine Bond Lengths (Å) and Bond Angles (degrees) at the CCSD(T) Level with the aT-PP Basis Set and at the ADF ZORA BLYP Level with the TZ2P Basis Set 47

2.3. Experimental and Calculated MF_6 Vibrational Frequencies (cm^{-1}) and IR Intensities at the B3LYP/aT-PP and BP86/aT-PP Levels.....49

2.4. Energy Components for Calculated Electron Affinities in kcal/mol 50

2.5. Adiabatic Electron Affinities of MF_6, Vertical Electron Detachment Energies (VDE) of MF_6^- and Vertical Electron Attachment Energies (VAE) of MF_6 in kcal/mol Calculated at the CCSD(T)/aT-DK//CCSD(T)/aT-PP Level.....51

2.6. Energy Components for Total Atomization Energies of MF_6 in kcal/mol at 0 K($\sum D_0$).....52

2.7. Heats of Formation of MF_6 in kcal/mol at 0 and 298 K ($\Delta H_{f,0K}$ and $\Delta H_{f,298K}$) Calculated at the CCSD(T) Level 53

2.8. Calculated Energy Components for the First Adiabatic and

Average M –F Bond Dissociation Energies for MF_6 in kcal/mol Calculated at CCSD(T) level 54

2.9. MF_6 Fluoride Affinities (kcal/mol) Calculated at CCSD(T) Level for the Classical and Non-Classical Structures 55

2.10. Calculated Fluoride Affinities for MF_5 in kcal/mol 56

2.11. Average Deviations of the MF_6 Electron Affinities, MF_5 and MF_6 Fluoride Affinities, and First Adiabatic M –F Bond Dissociation Energies from the CCSD(T) Calculated Values in kcal/mol 57

3.1. MF_6 Electron Affinities in eV 144

3.2. Optimized Metal-Fluorine Bond Lengths (Å) and Bond Angles (degrees) at the CCSD(T) Level with the aT-PP Basis Set and at the ADF ZORA BLYP Level with the TZ2P Basis Set for MF_6 and MF_6^- 145

3.3. Experimental and Calculated MF_6 Vibrational Frequencies (cm^{-1}) and IR Intensities (km/Mole) at the B3LYP/aT-PP Level 147

3.4. Energy Components for Calculated Electron Affinities in kcal/mol 148

3.5. Electronic Component of the Adiabatic Electron Affinities of MF_6, Vertical Electron Detachment Energies (VDE) of MF_6^- and Vertical Electron Attachment Energies (VAE) of MF_6 in kcal/mol Calculated at the CCSD(T)/aT-PP Level 149

3.6. Energy Components for Total Atomization Energies of MF_6 in kcal/mol at 0 K ($\sum D_0$).....150

3.7. Heats of Formation of MF_6 in kcal/mol at 0 and 298 K ($\Delta H_{f,0K}$ and $\Delta H_{f,298K}$) Calculated at the CCSD(T) Level 151

3.8. Calculated Energy Components for the First Adiabatic and Average M-F Bond Dissociation Energies for MF_6 in kcal/mol Calculated at CCSD(T) Level.....152

3.9. MF_6 Fluoride Affinities (kcal/mol) Calculated at the CCSD(T) Level for the Classical and Non-Classical Structures 153

3.10. Energies (kcal/mol) of Reactions (2) ($E(F)_{cluster}$) and (3) ($E(F_2^-)_{cluster}$) for the Second Row Transition Metals 154

3.11. Energies (kcal/mol) of Reactions (2) ($E(F)_{cluster}$), (3) ($E(F_2^-)_{cluster}$), and (4) ($FA(MF_5)$) for the Third Row Transition Metals.....155

3.12. MF_5 Fluoride Affinities in kcal/mol Calculated at the CCSD(T) Level.....156

3.13. Average Deviations of the MF_6 Electron Affinities, MF_5 and MF_6 Fluoride Affinities and First Adiabatic M –F Bond Dissociation Energies From the CCSD(T) Calculated Values.....157

4.1. Benchmarked DFT Exchange-Correlation Functionals.....224

4.2. MPH_3, $M(PH_3)_2$, MPH_3Cl_2 and $M(PH_3)_2Cl_2$ Optimized M-P and M-Cl Bond Lengths (Å) at the B3LYP and CCSD(T) Levels.....225

4.3. M-P and M-Cl **S**tretching Frequencies (cm^{-1}) and IR intensities (km/mol) at the B3LYP/aD-PP Level.....226

4.4. Components for Calculated M-PH3 Binding Energy for Reactions (1) to (4) (M = Ni, Pd, Pt).....227

4.5. Average Deviations of the Metal- Phosphine Bond Dissociation Energies from the CCSD(T) Calculated Values in kcal/mol.....228

LIST OF FIGURES

2.1. Schematic Energy Level Diagram for Use in Predicting the Molecular Electron Affinities for the MF_6 in kcal/mol 58

2.2. Symmetry Coordinates for the MF_6 Scissoring Mode Splitting into its Two components, i.e., Equatorial and Axial Scissoring upon Lowering of the Symmetry from O_h to D_{4h}.....59

2.3. Optimized Geometries for the Four Different Structures for MF_7^- as Exemplified by WF_7^- or PtF_7^-(nonclassical C_s).....60

3.1. Schematic Energy Level Diagram for Use in Predicting the Molecular Electron Affinities for the MF_6 Molecules in kcal/mol 158

4.1. General Catalytic Cycle for Palladium-Catalyzed Cross-Coupling Reactions.....229

4.2. MPH_3, $M(PH_3)_2$, MPH_3Cl_2 and $M(PH_3)_2Cl_2$ Structure.....230

1. INTRODUCTION

1.1 Catalysis and Computational Chemistry

Catalysis provides the means of changing the rates at which chemical bonds are formed and broken and of controlling the yields of desired products over undesired ones. Catalysts are chemical agents that bond selectively to reactant molecules to expedite the rapid, stepwise scission and formation of individual chemical bonds, and then disengage from product molecules in a manner that allows them to be used over and over again. Chemical catalysis lies at the heart of our quality of life. For example, the chemical industry relies on catalysis to produce commodity chemicals and the polymers that are so much a part of everyday living. The cleaner emissions of modern cars, the abundance of fresh food at our stores, and our healthier lives from new pharmaceuticals are created by the efficiency and stability of heterogeneous catalysts and the precision of homogeneous catalysts. Catalysis is critical to meet society's mounting energy demands while simultaneously protecting the environment, and thus is key to the new "Green chemistry" paradigm.[1,2] Energy consumption can be greatly reduced by employing efficient catalysts in the chemical industry, which lowers the operational cost. The environmental impact of a chemical process can be substantially reduced by using catalysts to eliminate undesirable by-products and/or solvents. Catalysis is also essential to enable the efficient utilization of renewable energy sources such as solar energy. The petroleum, chemical, and pharmaceutical industries that rely on catalysts contribute more than $1 trillion to the GNP of the United States.[2] Catalysis and catalytic processes account for nearly 20% of the U.S. GDP and nearly 20% of all

industrial products. About 2% of world energy usage per year is used in the production of the top 50 chemicals in the U.S. and catalytic routes account for the production of 30 of these chemicals, consuming ~1%. Improved catalysts can increase reaction efficiencies leading to reduced energy requirements, while increasing product selectivity and concomitantly decreasing wastes and emissions. A single process yield improvement of only 10% would save 0.02% of world energy usage per year! Production of the top 50 chemicals leads to >21 $x10^9$ lbs of CO_2 emitted to the atmosphere per year. Improved catalysts can reduce this carbon burden on the atmosphere.

There is a need to develop new catalysts for the control of chemical reactions to make new chemicals and materials with minimal energy input and minimal waste to minimize the environmental impact of the process. Catalysis, at its heart, involves important intermediates and transition states that "exist" in low concentrations with short lifetimes, properties which often thwart precise experimental evaluation, and for which state-of-the-art computations (appropriately integrated with cutting-edge experimental research) represent the best option for obtaining the detailed molecular-level understanding essential for next-generation catalyst development.[3] Computational methods hold the key to the fundamental understanding of catalytic processes thus enabling true first principles catalyst design. Catalysis is fundamentally about improving reaction kinetics and catalyst *design* will require quantitative information about *transition states* for critical reaction processes. Currently, information about transition states,[4] especially geometric and spectral information, is *only* readily accessible by computational methods. Yet such information is critical if we are to develop a language that can explain the events at the atomic level in order to design new homogeneous and heterogeneous catalysts.[5,6] Thus an important approach to catalyst design is the use of advanced computational chemistry techniques. The goal of the computational work is to provide unique insights at the atomic level

into the behavior of catalytic sites in terms of their structure, energetics, and reactivities in order to develop a fundamental understanding at the molecular level of how catalysts function. This will enable catalysts to be designed from first principles.

A critical goal of the research described in this dissertation is to develop new computational approaches that are highly accurate in order to design new catalysts. At the heart of quantum mechanics is the Schrödinger equation, for which the time-independent, non-relativistic form is

$$\hat{H}\Psi=E\Psi \tag{1.1}$$

where $\hat{H}$ is the molecular Hamiltonian (nuclear and electronic), Ψ is the total wavefunction and E is the total energy. Using the Born-Oppenheimer approximation, which assumes fixed nuclear positions due to the much slower movement of the nuclei as compared to that of the electrons due to the large mass differences, the electronic Hamiltonian may be written as

$$\hat{H} = -\frac{1}{2}\sum_{i} \nabla_i^2 - \sum_{iA} \frac{Z_A}{|R_A - r_i|} + \sum_{i<j} \frac{1}{|r_i - r_j|} \tag{1.2}$$

where the first term is the electronic kinetic energy and the last two are the nuclear-electron attraction and electron-electron repulsion potential energies respectively. R and r are the nuclear and electronic coordinates, Z is the atomic number and the subscripts i and j describe the different electrons and the subscript *A* defines the different nuclear positions. The solution of the electronic Schrödinger equation (1.1) with the appropriate Hamiltonian (1.2) yields the total electronic energy of the system. Mapping the electronic energy for all possible sets of nuclear coordinates defines the potential energy surface (PES). Searching for global energy minima on the PES leads to the identification of molecular structures and the calculation of second

derivatives of energy with respect to nuclear coordinates provides information about the vibrational modes in the molecule.

1.2 Molecular Orbital (MO) and Density Functional Theory (DFT) Methods

There are two commonly used computational approaches to predicting electronic structure at the *ab initio* (first principles) level: molecular orbital (MO) theory[7,8] and density functional theory (DFT).[9] An exact solution to eq 1.1 is not possible but for the most simple systems such as the hydrogen atom. To approximate the solution for larger systems the wave function is decomposed in a combination of molecular orbitals which are then expressed as linear combination of a predefined set of one electron functions known as basis functions.

$$\phi = \sum_{i=1}^{N} c_i \varphi_i \qquad (1.3)$$

Keeping the smallest number of basis functions, necessary to describe the electrons on an atom (for example for hydrogen: 1s and for carbon: 1s, 2s, $2p_x$, $2p_y$ and $2p_z$) results in a minimal basis set. To improve the flexibility of the basis set and better cover the spatial distribution of the electrons, the number of basis functions used per atomic orbital is doubled, tripled etc. Functions of higher angular momentum called polarization functions are added to allow the orbitals to change shape and better adapt to the molecular environment. Diffuse functions, primitives with small exponents, are added to describe the shape of the wave function far from nucleus, when dealing with anions, compounds with lone pairs of electrons or hydrogen bonded species. In our calculations we have used split valence basis sets such that only the valence orbitals are expanded to larger numbers of functions and the core orbitals are treated by a minimal basis set from the family of correlation-consistent basis sets developed by Dunning and

co-workers[10] of double, triple and quadruple zeta size. For the transition metal elements in our compounds we have used the basis sets[11] with the associated effective core potentials.[12] The high atomic numbers (Z) of the 3rd and potentially even the 1st and 2nd row transition metals imply that relativistic effects must be properly included to attain even semi-quantitative accuracy.[13,14] For many of the properties of interest in this work, the core electrons are chemically inert. It is possible to eliminate the core contributions from direct consideration by using pseudopotentials or effective core potentials (ECPs).[15,16] The simplest approach to solving the Schrödinger equation in molecular orbital theory is the Hartree-Fock method which neglects electron correlation since it treats each electron in the average field of all the other electrons. The neglected correlation energy, defined as the difference between the HF energy and the exact energy is small, but critical for the prediction of energetic properties of molecules.[17,18] A simple physical model of the correlation energy in an orbital is that classically the two electrons (spin up and spin down) avoid each other but quantum mechanically, they are allowed to overlap because they are fermions and have different sets of quantum numbers. The classical repulsion has to be obeyed so the electrons "avoid" each other and their motion in a given orbital is correlated, i.e., they "see" each other. This is missed in Hartree-Fock because of the average field approach.

One method designed to recover the correlation energy is the coupled cluster method.[19,20,21,22] It provides reliable energetics for smaller systems and benchmarks for DFT when used with very large correlation consistent basis sets extrapolated to the complete basis set (CBS) limit.[23] The coupled cluster wave function is given by the following expression

$$\Psi_{CC} = e^{T}\Psi_{HF} = (1 + T + \tfrac{1}{2} T^2 + 1/3!\, T^3 + \ldots)\, \Psi_{HF} \qquad (1.4)$$

where the cluster operator T takes the form

$$T = T_1 + T_2 + T_3 + \ldots + T_n \quad (1.5)$$

where n is the degree of excitations and we use the series expansion for the exponential. If all excitations are included, then this is equivalent to a full configuration interaction exact calculation within a given basis set. However, full CI scales as a factorial so it is computationally too expensive for all but the smallest molecules with modest basis sets. Thus the series in (1.5) is usually truncated at n =2. However, it is well known that the effect of triple excitations is important in the prediction of reliable energetics so they need to be included in some fashion. The inclusion of triple excitations is computationally expensive as CCSDT scales as iterative N^8, whereas CCSD scales as iterative N^6, where N is the number of basis functions. A reasonable approximation is to estimate the effect of triples from perturbation theory (e.g. MP4SDTQ) so CCSD(T) scales only as non-iterative N^7. Thus, this method has become to be considered the gold standard for calculations as it provides reliable results when large enough basis sets are used, even though it is still computationally quite expensive. However, the triples component can be done very efficiently computationally on modern parallel computers by taking advantage of fast linear algebra solvers. CC methods are completely size consistent and size extensive.

DFT provides a good description of the geometries and frequencies for a wide range of molecules including transition metal complexes and is more computationally efficient than the corresponding ab initio molecular orbital methods with the inclusion of electron correlation. The DFT method, is based on the theorems of Hohenberg and Kohn[24] and Kohn and Sham[25] who showed that the ground state electronic energy of a system is a functional of the electron density (ρ). The expression for the DFT energy is then given by

$$E[\rho] = T_s[\rho] + E_{ext}[\rho] + E_{coul}[\rho] + E_{XC}[\rho] \quad (1.3)$$

where T_s is the kinetic energy, E_{ext} is the electronic-nuclear external potential energy, E_{Coul} is the Coulombic interaction energy, and the E_{XC} is the exchange-correlation energy. If the exact density and form of each term is known, then the energy is exact in the non-relativistic approximation. The exact form of the exchange-correlation functional is not known and a variety of funcionals are available. In the work described in the dissertation, we have investigated the performance of different DFT exchange-correlation functionals for the prediction of the thermodynamic properties of transition metal complexes. Three different types of DFT functionals were benchmarked: LSDA, GGA, and HGGA where LSDA is the local density approximation,[26,27] GGA is the generalized gradient approximation which includes the gradient of the electron density but no Hartree-Fock exchange[28,29,30,31,32,33,34,35,36,37,38,39,40] and the hybrid-GGA (HGGA) which includes the density gradient and some Hartree-Fock exchange[41,42,43,44,45,46,47,48,49] (See Table 1.1).

Table 1.1 Benchmarked DFT Exchange-Correlation Functionals.

Functional	exchange	correlation	type
SVWN5	Slater	VWN5	LSDA
BLYP	Becke 88	Lee-Yang-Parr	GGA
BP86	Becke 88	Perdew 86	GGA
BPW91	Becke 88	Perdew-Wang 91	GGA
BB95	Becke 88	Becke 95	GGA
PW91	Perdew-Wang 91	Perdew-Wang 91	GGA
mPWPW91	Adamo & Barone's modified PW91	Perdew-Wang 91	GGA
PBE	Perdew-Burke-Ernzerhof	Perdew-Burke-Ernzerhof	GGA
OLYP	Handy's OPTX	Lee-Yang-Parr	GGA
TPSS	Tao-Perdew-Staroverov-Scuseria	Tao-Perdew-Staroverov-Scuseria	GGA
VSXC	van Voorhis -Scuseria	van Voorhis -Scuseria	GGA
HCTH	Handy	Handy	GGA
B3LYP	Becke 93	Lee-Yang-Parr	HGGA
B3P86	Becke 93	Perdew 86	HGGA
B3PW91	Becke 93	Perdew-Wang 91	HGGA
B1B95	Becke 96	Becke 95	HGGA
B1LYP	Becke 96	Lee-Yang-Parr	HGGA
mPW1	Barone's modified PW91	Perdew-Wang 91	HGGA
B971	Handy-Tozer's modified B97	Handy-Tozer's modified B97	HGGA
B972	Wilson-Bradley-Tozer's modified B97	Wilson-Bradley-Tozer's modified B97	HGGA
B98	Becke 98	Becke 98	HGGA
PBE1	Perdew-Burke-Ernzerhof	Perdew-Burke-Ernzerhof	HGGA
O3LYP	Handy's OPTX	Lee-Yang-Parr	HGGA
BMK	Boese -Martin	Boese -Martin	HGGA
TPSSh	Tao-Perdew-Staroverov-Scuseria	Tao-Perdew-Staroverov-Scuseria	HGGA

All properties are calculated for the species in their ground states so the molecular structures are first optimized through the use of analytic or numerical first derivatives. Second derivative calculations are performed to ensure that the geometry is indeed a minimum with all positive second derivatives; the second derivatives also yield the harmonic frequencies after projecting out the molecular translations and rotations. A variety of structures (symmetries) and orbital combinations have been studied for the open shell molecules in order to obtain the ground state structures. Geometries and frequencies were calculated at the DFT level with the range of functionals described above and also at the CCSD(T) level with the aD-PP and aT-PP basis sets.

1.3 Energy Corrections

Additional corrections are necessary to improve the calculations to reach "chemical accuracy" of ± 1 kcal/mol. The first correction is actually due to the nuclear motion, the nuclear zero point energy (ZPE), which accounts for the effects of molecular vibrations. It was obtained at the DFT level with various basis sets. Scalar relativistic corrections (ΔE_{SR}), which account for changes in the relativistic contributions to the total energies of the molecule and the constituent atoms, have been included at the CI-SD (configuration interaction singles and doubles) level of theory using the aug-cc-pVTZ/ECP basis set. ΔE_{SR} is taken as the sum of the mass-velocity and 1-electron Darwin (MVD) terms in the Breit-Pauli Hamiltonian.[50] This approach has been used for computational efficiency and because we are using ECPs for the metal atoms. A potential problem arises in computing the scalar relativistic correction for molecules as there is the possibility of "double counting" the relativistic effect on the atoms with an ECP when applying a MVD correction to an energy which already includes some relativistic effects via the ECP. Because the MVD operators mainly sample the core region where the pseudo-orbitals are small, it has been shown that any double counting is small in studies of heavy main group compounds.[51]

In order to estimate the errors for using the ECP basis sets in the above procedure, CCSD(T) calculations have been performed at the second order Douglass-Kroll-Hess (DKH) level[52] with all-electron DK basis sets. For the 2nd and 3rd row transition metals and their compounds, the CCSD(T)-DK calculations have been performed with the aug-cc-pVTZ-DK basis set,[53,54,55] which is the only valence correlation-consistent DK basis set available. DKH is a full two-component solution to the Dirac equation which includes the scalar relativistic terms. An electronic energy correction to the CCSD(T)/CBS valence energies, the core-valence correlation correction (ΔE_{CV}) was calculated at the CCSD(T) level with special basis sets, aug-cc-pwCVTZ basis set for F[56,57] and the aug-cc-pwCVTZ-PP basis set for the transition metal atoms. Spin orbit corrections account for the spin and angular momentum coupling. These have been calculated at the BLYP/TZ2P level using the spin orbit approach and scalar two-component zero-order regular approximation (ZORA)[58] as implemented in the ADF 2008.01 program.[59] The spin orbit (SO) correction is taken as the difference between the ZORA and ZORA + SO values for a specific thermodynamic property.

The different properties calculated: electron affinities, fluoride affinities and bond dissociation energies have been calculated as the sum of the different contributions:

$$E = E_{CBS} + \Delta E_{ZPE} + \Delta E_{CV} + \Delta E_{Rel} + \Delta E_{SO} \quad (1.6)$$

The above additive approach follows the general approach to the prediction of heats of formation developed at Washington State University, the Pacific Northwest National Laboratory, and The University of Alabama.[60]

In this dissertation, electron affinities of third and second row transition metal hexafluorides have been predicted for the design of strong oxidizers. These results provide the first accurate electron affinity/oxidizer scale for these important molecules. Also, the prediction

of fluoride affinities of MF_6 and MF_5 provide insights into the Lewis acidities of these molecules. The accurate PH_3-M bond energies for VIIIB (Ni, Pd, Pt) transition metals in the 0 and +2 oxidation states which are used to benchmark DFT for larger molecules provide the first accurate energies for these important types of models for catalysts for the design of "Green Chemical" processes.

2. Third Row Transition Metal Hexafluorides, Extraordinary Oxidizers and Lewis Acids: Electron Affinities, Fluoride Affinities, and Heats of Formation of WF_6, ReF_6, OsF_6, IrF_6, PtF_6, and AuF_6

Dedicated to the memory of Neil Bartlett

Abstract

High level electronic structure calculations were used to evaluate reliable, self-consistent thermochemical data sets for the third row transition metal hexafluorides. The electron affinities, heats of formation, first ($MF_6 \rightarrow MF_5 + F$) and average M-F bond dissociation energies, and fluoride affinities of MF_6 ($MF_6 + F^- \rightarrow MF_7^-$) and MF_5 ($MF_5 + F^- \rightarrow MF_6^-$) were calculated. The electron affinities which are a direct measure for the oxidizer strength increase monotonically from WF_6 to AuF_6, with PtF_6 and AuF_6 being extremely powerful oxidizers. The inclusion of spin orbit corrections is necessary to obtain the correct qualitative order for the electron affinities. The calculated electron affinities increase with increasing atomic number, are in good agreement with the available experimental values and are: WF_6 (3.15 eV), ReF_6 (4.58 eV), OsF_6 (5.92 eV), IrF_6 (5.99 eV), PtF_6 (7.09 eV), and AuF_6 (8.20 eV). A wide range of density functional theory exchange-correlation functionals were also evaluated and only three gave satisfactory results. The corresponding pentafluorides are extremely strong Lewis acids, with OsF_5, IrF_5, PtF_5 and AuF_5 significantly exceeding the acidity of SbF_5. The optimized geometries of the corresponding MF_7^- anions for W through Ir are classical MF_7^- anions with M-F bonds; however, for PtF_7^- and AuF_7^- nonclassical anions were found with a very weak external F-F bond between an MF_6^- fragment and a fluorine atom. These two anions are text book examples for

"superhalogens" and can serve as F atom sources under very mild conditions, explaining the ability of PtF_6 to convert NF_3 to NF_4^+, ClF_5 to ClF_6^+, and Xe to XeF^+ and Bartlett's failure to observe $XePtF_6$ as the reaction products of the PtF_6/Xe reaction.

Introduction

There is substantial interest in the development of strong electron acceptors in order to synthesize novel molecules with unique bonding properties as such syntheses often require very strong oxidizers. The first stable noble-gas compounds synthesized were the xenon fluorides[1,2] in the early 1960's. Bartlett first reported evidence for the xenon-containing compound, "$XePtF_6$",[3] which appears to be composed of $XeF^+PtF_6^-$, PtF_5 and $XeF^+Pt_2F_{11}^-$.[4] He used the metal hexafluoride PtF_6 in his reactions because of its ability to oxidize O_2, which has an ionization potential comparable to Xe, to form O_2^+ salts.[5] Bartlett[6,7] estimated that the electron affinities of the metal hexafluorides with the metal in the formal +6 oxidation state (starting from WF_6) would increase across the row by ~ 20 kcal/mol from molecule to molecule. He proposed that EA(ReF_6) > 90 kcal/mol, EA(IrF_6) > 125 kcal/mol, EA(PtF_6) > 156 kcal/mol and EA(AuF_6) > 176 kcal/mol (see Table 2.1) on the basis of their reactivity studies with reagents of different ionization potentials. On his scale, WF_6 would thus have an EA of ~ 70 kcal/mol (3.04eV).

About a decade later, George and Beauchamp[8] used ion cyclotron resonance spectroscopy (ICR) to measure the electron affinity of WF_6 using bracketing techniques. Their value of 3.5 eV supports Bartlett's prediction that WF_6 is the poorest oxidizer among the third row hexafluorides. A value of $3.36^{+0.04}_{-0.2}$ eV was later derived from studies of the ion chemistry of WF_6, WF_6^- and WF_7^-.[9] The latter ion molecule reaction bracketing studies showed that EA(WF_6) was between EA(Br) = 3.36 eV and EA(F) = 3.40 eV. The lower limit of 3.16 eV was due to the inclusion of the effects of internal and translational energy on the overall reaction energy. Sidorov and co-workers[10] used high temperature Knudsen cell mass spectrometry to obtain the electron affinities of OsF_6, IrF_6, and PtF_6 as shown in Table 2.1.

It is clear that the 3rd row metal hexafluorides have some of the highest known electron affinities of stable, neutral molecules. They also serve as a set of molecules to probe interesting electronic structure effects. Using formal oxidation state arguments, the MF_6 molecules can be considered to be an M^{6+} ion surrounded by six F^- in an approximate octahedral ligand field. This means that one is filling the t_{2g} orbitals (d_{xy}, d_{xz}, d_{yz}) as the atomic number increases from W to Au (See Supporting Information). This resembles the filling of the p orbitals in main group compounds. As noted early for the MF_6 compounds, the partially occupied d orbitals in such high symmetry species can lead to Jahn-Teller distortions. Moffitt and coworkers[11] first explained the UV-visible absorption spectra of ReF_6, OsF_6, IrF_6 and PtF_6 and showed that the Jahn-Teller effect may be present as a vibronic coupling as well as a symmetry distortion. The subsequent experimental vibrational spectra[12,13,14,15,16,17] of ReF_6, OsF_6 and PtF_6 supported the conclusions of Moffitt and co-workers. The results raised questions about the role of spin-orbit (relativistic) effects on the properties of these compounds.

Seppelt has reviewed the structures and properties of the metal hexafluorides.[18] Electron diffraction measurements[19] of MF_6 molecular structures (M = W, Re, Os, Ir and Pt) have been made by Hedberg and co-workers. These measurements show that the structures are all essentially octahedral under the experimental conditions. The M-F bond lengths for the first three members of the series are approximately the same, and the M-F bond lengths for the last two are longer. The same trend in the bond lengths was observed by Seppelt and co-workers[20] in their single-crystal structure determination study of second and third row transition metal hexafluorides. Seppelt and coworkers[21] have also discussed the stability of the octahedral structure of WF_6 relative to the regular or distorted trigonal prismatic structure and predicted the O_h structure to be more stable than the D_{3h} structure by 11 kcal/mol at the density functional

theory (DFT)[22] level with the B3LYP[23,24] exchange-correlation functional. Bartlett and co-workers[25] measured the M–F interatomic distances in $LiMF_6$ and Li_2MF_6 salts of the second and third row transition series by using synchrotron X-ray powder diffraction following the initial work of the Bartlett group[26] on the synthesis[27] and structural characterization of $LiMF_6$ salts for M = Pt and Au.

There are only a few experimental studies of the heats of formation of the third row transition metal hexafluorides[28] and no reliable theoretical predictions of this fundamental thermodynamic property. For WF_6, the first reported value of -422 ± 4 kcal/mol for $\Delta H_{f,298K}(WF_6)$ is from a solution calorimetry experiment.[29] Subsequent studies of tungsten combustion in fluorine in a bomb calorimeter yielded values of -411.5 ± 0.4 kcal/mol,[30] -411.7 ±0.5 kcal/mol,[31] and -411.4 ± 0.2 kcal/mol.[32] For ReF_6, an estimated value of -322.6 ± 2.3 kcal/mol is available from hydrolysis measurements.[33] The heat of formation of OsF_6 is not known and that of IrF_6, estimated in 1929 as -130 kcal/mol[34] from the temperature rise during its preparation, is probably not reliable. The heat of formation of PtF_6 was determined by Knudsen-cell mass spectrometry to be -161.6 ± 6.7 kcal/mol[35] and calculated from calorimetric literature data to be -160.6 ± 1.5 kcal/mol.[36]

A number of theoretical studies have predicted the electron affinities (EA) of the metal hexafluorides. Gutsev and Boldyrev[37,38] used the non-relativistic Xα method to calculate electron affinities for the MF_6 molecules relative to the experimental value[8] of 3.50 eV for WF_6. Miyoshi and co-workers[39,40] used modest level configuration interaction (CI) calculations to predict the electron affinities of WF_6 and AuF_6. The first and second electron affinities of the 5d metal hexafluorides and hexachlorides have been predicted by Macgregor and Moock using DFT.[41] More recently, Wesendrup and Schwerdtfeger[42] used different levels of theory up to the coupled

cluster theory (CCSD(T)) level to predict the structure and electron affinities of molecular platinum fluorides PtF_{2n} (n = 1 - 4). The structure of AuF_6 as well as its electron affinity (and that of PtF_6) have been investigated at different levels of theory by Riedel and Kaupp.[43] PtF_6 has been studied, in part, to predict the effect of including relativistic effects in the treatment of its geometry.[44,45,46]

Molecular fluoride affinities provide an estimate of the Lewis acid strength of a given species.[47] Bartlett[7] suggested, on the basis of the reactions of third row hexafluorides with ONF, that the fluoride affinity decreases along the MF_6 series in contrast to the increase in electron affinity. The fluoride affinity of WF_6 was measured in an ion cyclotron resonance bracketing study as 69 ± 5 kcal/mol (3.0 ± 0.2 eV); this value is based on the observation that SiF_5^- transfers F^- to WF_6 but BF_4^- does not.[8]

We describe the results of our high level electronic structure calculations at the CCSD(T) level of the structures, electron affinities, heats of formation, first ($MF_6 \rightarrow MF_5 + F$) and average M-F bond dissociation energies, and fluoride affinities ($MF_6 + F^- \rightarrow MF_7^-$) of MF_6 for M = W, Re, Os, Ir, Pt, and Au. We also report the fluoride affinities of MF_5 as these can be directly calculated from our data. The electron affinities can be used in the development of a quantitative scale of the strength of very strong oxidizers. The electron affinity and the fluoride affinity often compete with each other so good values for both are required in order to design the optimal oxidizing agent. In addition, we report on the ability of DFT to predict these energetic properties.

Computational Methods

Geometries and frequencies were calculated at the DFT level with a range of local,[48,49] gradient-corrected[24,50,51,52,53,54,55,56,57] and hybrid[23,24,58,59] exchange-correlation functionals including B3LYP (See Supporting Information). These calculations were performed with the

augmented correlation consistent double-ζ (aug-cc-pVDZ) basis set for F[60] and the aug-cc-pVDZ-PP basis sets with accompanying small-core relativistic pseudopotentials for the transition metal atoms;[61] we label the combined basis set as aN-PP with N = D, T, Q. For all of the calculations described below, the zero point energy corrections and the temperature corrections from 0 to 298 K were obtained at the B3LYP/aT-PP level unless it was necessary to use the frequencies obtained with the BP86 functional.

Geometries were also optimized at the CCSD(T) level[62,63,64,65] with the aD-PP and aT-PP basis sets, and single point CCSD(T) energies were calculated with the aQ-PP basis set. The CCSD(T) energies could then be extrapolated to the complete basis set (CBS) limit by using a mixed Gaussian/exponential formula.[66] An additional electronic energy correction to the CCSD(T)/CBS valence energies is the core-valence correlation correction (ΔE_{CV}) calculated at the CCSD(T) level with the aug-cc-pwCVTZ basis set for F[67,68] and the aug-cc-pwCVTZ-PP basis set for the transition metal atoms (denoted as awCVTZ). Scalar relativistic corrections on the F atoms and corrections for any errors in the metal pseudopotentials for the electron affinities (EAs) were obtained by taking the difference between the EA calculated at the Douglas-Kroll-Hess[69] level with the CCSD(T)-DK method and the aT-DK basis set[61,70,71] and the EA calculated at the CCSD(T)/aT-PP level (Equation (1)).

$$\Delta EA_{Rel} = EA(CCSD(T)\text{-}DK/aT\text{-}DK) - EA(CCSD(T)/aT\text{-}PP) \quad (1)$$

A separate estimate of just the pseudopotential error is described in the Supporting Information and is less than 2.5 kcal/mol (~0.1 eV) for the electron affinities. One final correction that needs to be considered is that of spin orbit. Molecular spin orbit corrections were calculated at the BLYP/TZ2P level using the spin orbit approach and scalar two-component zero-order regular approximation (ZORA)[72] as implemented in the ADF 2008.01 program.[73] The spin orbit (SO)

correction is taken as the difference between the ZORA and ZORA + SO values at a specific property. The electron affinity was thus calculated as the sum of different contributions (Equation (2)).

$$EA_{0K} = EA_{CBS} + \Delta EA_{ZPE} + \Delta EA_{CV} + \Delta EA_{Rel} + \Delta EA_{SO} \quad (2)$$

A similar equation was used to calculate the total atomization energies (TAEs), which are used to calculate the molecular heats of formation. In calculating the TAEs, we chose the low-lying atomic state with no SO splitting if possible, and used the experimental SO splittings otherwise.[74] The experimental atomic heats of formation at 0 K were taken from the JANAF Tables[28] for F and W and from the compilation of Wagman et al.[75] for the remaining metals (See Supporting Information). No error bars were reported for the latter values. The atomic heats of formation have also been given by Greenwood and Earnshaw[76] and these can be used to help provide ranges for the heats of formation. The heat of formation of Os is not given at 0 K so we estimated that its value is 0.2 kcal/mol lower than the 298 K value following the trends in the other metals. The above additive approach follows the general approach to the prediction of heats of formation developed at Washington State University, the Pacific Northwest National Laboratory, and The University of Alabama.[77]

Results and Discussion

Geometries of the Hexafluorides Table 2.2 lists the metal-fluorine bond distances of the neutral hexafluorides and their anions optimized at the CCSD(T) levels with aT-PP basis set and the ZORA and ZORA SO BLYP/TZ2P level. The Cartesian coordinates as well as the geometries optimized with the various DFT exchange correlation functionals as well as the CCSD(T)/aD-PP method are given as Supporting Information. We explored a variety of structures (symmetries)

and orbital combinations in our studies of the open shell molecules in order to obtain the ground state structures.

Qualitative description of MF_6 structures Before describing the results of the calculations, we describe the types of structures and states that are expected. The 5d orbitals in an octahedral field will split into a t_{2g} set and an e_g set with the t_{2g} orbitals below the e_g orbitals. We assume a formal +6 oxidation state on the metal atoms and no spin orbit coupling for the following argument. Thus, one is filling the t_{2g} orbitals starting from WF_6 with no d electrons so WF_6 should have O_h symmetry. WF_6^- has one d electron and will undergo a Jahn-Teller distortion to D_{4h} or D_{3d} symmetry. Distortion to D_{4h} symmetry gives an e_g and a b_{2g} orbital from the t_{2g} orbitals. Occupancy of the b_{2g} orbital leads to a structure with 2 short and 4 long M-F bonds. Distortion to D_{3d} symmetry gives an e_g and an a_{1g} orbital from the t_{2g} orbitals. Occupancy of the a_{1g} orbital leads to a structure with 6 equivalent M-F bonds with angles that deviate only slightly from 90°. ReF_6 will have a structure similar to WF_6^-. In D_{4h} symmetry, ReF_6^- has two potential electron occupancies, a $(b_{2g})^2$ occupancy giving rise to a $^1A_{1g}$ state or an $(e_g)^2$ occupancy leading to a $^3A_{1g}$ state. Thus the lowest energy state depends on which of the e_g and b_{2g} orbitals lies the lowest. If the b_{2g} orbital lies the lowest, then the $^1A_{1g}$ state should look like that of ReF_6 in terms of the geometry; if the $^3A_{1g}$ state is formed from the $(e_g)^2$ occupancy, then there should be 4 short and 2 long bonds. OsF_6 would be expected to exhibit the same type of behavior as ReF_6^-. In the distorted D_{3d} symmetry structure, the $(e_g)^2$ occupancy gives rise to a $^3A_{1g}$ state as well. For OsF_6^- and IrF_6, there are three d electrons so there is no need for a Jahn-Teller distortion as the $(t_{2g})^3$ electron configuration leads to the $^4A_{1g}$ high spin state in O_h symmetry. IrF_6^- and PtF_6 can be described by following the same considerations as for the triplet states in ReF_6^- or OsF_6. With four d electrons in D_{4h} symmetry, if the e_g orbital lies the lowest, then the state is $^1A_{1g}$ from the

$(e_g)^4$ occupancy with 4 short bonds and 2 long bonds. If the b_{2g} orbital lies the lowest, then the occupancy is $(b_{2g})^2(e_g)^2$ leading to a $^3A_{1g}$ state with 2 short bonds and 4 long bonds. In D_{3d} symmetry, there is the possibility of the $(a_{1g})^2(e_g)^2$ occupancy leading to a $^3A_{1g}$ state or of $(e_g)^4$ occupancy leading to a $^1A_{1g}$ state. With five d electrons, there is one hole so the electron configuration in D_{4h} symmetry is $(e_g)^4(b_{2g})^1$ for a $^2B_{2g}$ state for PtF_6^- and AuF_6 with 4 short bonds and 2 long bonds. In D_{3d} symmetry, the electron configuration is $(e_g)^4(a_{1g})^1$ for a $^2A_{1g}$ state. AuF_6^- has six d electrons so the electron occupancy is $(t_{2g})^6$ with O_h symmetry. A consequence of this analysis is that the D_{4h} structures should have two different M-F bond distances whereas the D_{3d} structures will have only one M-F bond distance just as in the O_h symmetry structure. If the three D_{4h}, D_{3d}, and O_h structures are all close in energy, it will be extremely difficult experimentally in a structural determination to observe any structure that does not have approximate O_h symmetry.. Contributions of the different corrections to the relative energy difference between the D_{4h} and D_{3d} structures are given in Supporting Information. The geometry discussion below focuses on the CCSD(T)/aT-PP structures and energies unless noted.

WF_6 The calculated W-F bond distance for WF_6 (O_h) of 1.835 Å is in good agreement with those reported by Marx et. al.[78] using neutron diffraction (1.825 Å) , by Richardson et. al.[19] using electron diffraction (r_g = 1.829(2) Å), and by Seppelt[20] in a single crystal structure determination (average of 1.826 Å). The previously reported values of 1.853 Å (Hartree-Fock) and 1.881 Å (single + double + Q correction CI (CI-SD+Q))[39] and of 1.886 Å (LDA/TZP/DFT[73])[41] are too long.

WF_6^- and ReF_6 In the D_{4h} structure with the b_{2g} orbital below the e_g orbital, WF_6^- and ReF_6 have two short axial bonds and four long equatorial bonds differing by 0.056 Å and 0.042 Å, respectively, with an average of 1.903 Å for r(W-F) and 1.830 Å for (Re-F). The O_h structures,

with the M-F bond distance calculated as the average of the bonds in the D_{4h} structures, were found to be no more than 1 kcal/mol higher in energy than the D_{4h} structures for both WF_6^- and ReF_6. The W-F bond length in the D_{3d} structure, which has essentially the same energy as the D_{4h} structure at the CCSD(T)/CBS level, is 1.902 Å.

We performed ZORA and ZORA-SO calculations to examine the effects of spin orbit coupling. For all MF_6 and MF_6^-, ZORA predicted an O_h or D_{3d} geometry to be the lowest energy structure. ZORA-SO predicted that WF_6^- distorts to a D_{4h} geometry with 2 long and 4 short bond distances, which is the opposite bonding pattern expected from simple orbital arguments without spin orbit. The D_{3d} structure for WF_6^- is only 0.59 kcal/mol higher in energy than the D_{4h} structure at ZORA-SO. When all of the energy contributions are combined, the D_{3d} structure for WF_6^- is only 0.5 kcal/mol above the D_{4h} structure (see Figure 2.1 for the state splittings). The ZORA-SO bond distance for WF_6 is 1.887 Å which is too long by about 0.06 Å as expected from other DFT calculations.[41] The spin orbit effect on the bond distance is a few thousandths of an angstrom.

For ReF_6, the D_{3d} structure is predicted to be slightly above the D_{4h} structure at the CCSD(T)/CBS level. The structure of ReF_6 has been measured by electron diffraction[19] and the bond distance for an O_h structure is r_g = 1.829(2) Å. This is in excellent agreement with our calculated values of 1.830 Å for the average distance in the D_{4h} structure and of 1.830 Å for the D_{3d} structure. ZORA-SO predicted the D_{3d} structure for ReF_6 to be 0.23 kcal/mol more stable than the D_{4h} structure. The ZORA-SO calculations with the BLYP functional give bond lengths that are too long by 0.06 Å as compared to experiment. The longer Re-F distance at the ZORA-SO level is consistent with a smaller difference between the long and short Re-F bond distances. ReF_6 may exhibit a Jahn-Teller distortion from the O_h structure as observed in its vibrational

spectra.[12,15] The CCSD(T)/CBS energy difference and the spin-orbit correction essentially cancel for the energy difference between the D_{4h} and D_{3d} structures of ReF_6 so that the difference of the zero point energies, which favors the D_{3d} structure, is the most important leading to the D_{3d} structure being more stable than the D_{4h} structure by 0.7 kcal/mol.

ReF_6^- and OsF_6 The $^3A_{1g}/D_{4h}$ state is predicted to be the ground state for both ReF_6^- and OsF_6 with the $^1A_{1g}/D_{4h}$ state 25.8 and 23.6 kcal/mol, respectively, higher in energy. Both ReF_6^- and OsF_6 have two long axial bonds and four short equatorial bonds with differences less than 0.05 Å and an average of 1.891 Å for Re-F and 1.830 Å for Os-F. Marx et al.[78] reported an average distance of 1.827 Å for the Os-F bond in OsF_6 with the axial bonds longer by 0.018 Å than the equatorial bonds using neutron diffraction. The gas phase electron diffraction value[19] for OsF_6 is r_g = 1.828(2) Å as compared to our average value of 1.829 Å. The X-ray crystal structure value of r(Os-F) = 1.827 Å is also in good agreement.[78] As in the case of WF_6^- and ReF_6, the O_h geometries are less than 1 kcal/mol above the D_{4h} structure. The D_{3d} structure for ReF_6^- is 1.04 kcal/mol higher than the D_{4h} structure at the CCSD(T)/CBS level but the difference in zero point energies essentially cancels this value and the D_{3d} structure is only 0.2 kcal/mol above the D_{4h} structure when all of the energy corrections are included. The Re-F distance in $CsReF_6$ was determined by X-ray crystallography[79] to be 1.863(4) Å, which is, surprisingly, almost 0.03 Å shorter than the calculated average value for the D_{4h} structure of 1.891 Å or the bond distance in the D_{3d} structure of 1.891 Å. The ZORA-SO D_{4h} structure for OsF_6 with 2 short and 4 long bond distances is only 0.15 kcal/mol higher in energy than the D_{3d} structure. The final result with all corrections is that the D_{4h} structure is 0.2 kcal/mol lower in energy than the D_{3d} structure for OsF_6.

OsF_6^- and IrF_6 Both OsF_6^- and IrF_6 have O_h symmetry. The calculated Os-F bond distance of 1.884 Å is close to the value of 1.8727 Å reported for the anion in the synchrotron X-ray powder diffraction study.[25] An X-ray powder diffraction study gives an Os-F bond length of 1.872(7) Å and the single crystal structure of $LiOsF_6$ gives r(Os-F) = 1.879(4) Å.[25] The calculated Ir-F bond distance at 1.832 Å is in excellent agreement with the electron diffraction value of 1.839 Å.[19] Again, the DFT value of 1.928 Å reported by Macgregor and Moock[41] for Os-F in OsF_6^- is too long. Thus, comparing the average calculated M-F bond distances shows that there is a slight decrease from WF_6 to OsF_6 and a slight increase to IrF_6 but they are all essentially the same within 0.006 Å. The experimental gas phase values for r_g are essentially the same for WF_6, ReF_6, and OsF_6 and increase by about 0.01 Å for IrF_6. At the ZORA-SO level, IrF_6 is predicted to have O_h symmetry and a bond distance of 1.894 Å, which is too long by 0.055 Å as compared to experiment.

IrF_6^- and PtF_6 IrF_6^- and PtF_6 are predicted to have a $^3A_{1g}/D_{4h}$ ground state with two short and four long bonds with differences of less than 0.05 Å. The average bond distance for PtF_6 is 1.845 Å, in good agreement with the electron diffraction value[19] of r_g =1.852(2) Å. The crystal structure[25] of $LiIrF_6$ determined by powder diffraction gives r(Ir-F) = 1.879(5) Å and a single crystal structure[80] gives r(Ir-F) = 1.875(3) Å. The calculated value of 1.881 Å for the average Ir-F bond distance from the D_{4h} structure or the Ir-F distance in the D_{3d} structure is in very good agreement with the experimental values. The $^1A_{1g}/D_{4h}$ structures are 23.4 and 16.3 kcal/mol, respectively for IrF_6^- and PtF_6, higher in energy than the $^3A_{1g}/D_{4h}$ geometry ground state. The O_h triplet structures are again only slightly higher than the D_{4h} geometries, and, for PtF_6, this difference is only 0.3 kcal/mol. The $^3A_{1g}/D_{3d}$ structure of IrF_6^- with a bond distance of 1.881 Å is 0.77 kcal/mol higher in energy than the $^3A_{1g}/D_{4h}$ ground state. At the ZORA-SO level, the D_{3d}

and D_{4h} structures for IrF_6^- have the same energy. The ZPE difference favors the D_{3d} structure so when all energy corrections are included, the D_{3d} and D_{4h} structures for IrF_6^- have the same energy. At the ZORA-SO level, the PtF_6 structure has approximate O_h symmetry with the D_{3d} and D_{4h} structures equal in energy. The energies of the D_{4h} and D_{3d} structures are equal and <0.4 kcal/mol more stable than an O_h structure, consistent with previous four-component or ZORA-SO calculations with the BLYP functional.[45] In this case, the ZPE difference favors the D_{4h} structure and the D_{4h} structure of PtF_6 is 1.5 kcal/mol more stable than the D_{3d} structure.

PtF_6^- and AuF_6 The D_{4h} structure has two long bonds and four short bonds with average values of 1.885 Å for PtF_6^- and 1.871 Å for AuF_6 with differences less than 0.05 Å. The calculated average value for r(Pt-F) in the D_{4h} structure for PtF_6^- as well as the bond distance in the D_{3d} structure are in good agreement with the experimental value of 1.887(6) Å from the powder diffraction study.[25] We would expect the bond distance for AuF_6 to be within 0.01 Å of the experimental r_g value when it becomes available. Wessendrup[42] predicted that PtF_6^- at the B3LYP level using the small core Stuttgart pseudopotential and basis set for Pt and aug-cc-pVDZ for F distorts to D_{4h} with axial Pt-F bonds of 1.960 Å and equatorial bonds of 1.908 Å consistent with our B3LYP optimized structures. At the CCSD(T)/CBS level, the D_{4h} structure is predicted to be more stable by 1.08 kcal/mol for AuF_6 and 1.04 kcal/mol for PtF_6^-. The O_h structure is again only less than 1 kcal/mol higher in energy. At the ZORA-SO level, both PtF_6^- and AuF_6 have O_h symmetry. Inclusion of all of the corrections leads to the D_{4h} structure being below the D_{3d} structure by 1.6 kcal/mol for PtF_6^- and by 0.9 kcal/mol for AuF_6.

AuF_6^- AuF_6^- has O_h symmetry with a calculated Au-F distance of 1.899 Å at the CCSD(T)/aT-PP level in excellent agreement with the crystal structure values of 1.890(4) Å[81], 1.899(3) Å[20], and 1.881 Å[82] for the Au-F distance in the $O_2^+AuF_6^-$ crystal and of 1.91±0.03 Å[82] for the Au-F

distance in the [KrF][AuF_6] crystal. The X-ray structure[83] of the AuF_6^- anion in $Xe_2F_{11}^+AuF_6^-$ shows an octahedral anion with an average Au-F distance of 1.861 Å. On the basis of all of our results, this bond distance is too short as is the value of 1.874(6) Å from the powder diffraction study.[25]

Vibrational Frequencies The six normal modes for MF_6 with O_h symmetry are ν_1 (a_{1g}), ν_2(e_g), ν_3(t_{1u}), ν_4(t_{1u}), ν_5(t_{2g}), and ν_6(t_{2u}). Under the Jahn-Teller distortion from O_h to D_{4h} the vibrational modes split as follows: $a_{1g} \rightarrow a_{1g}$, $e_g \rightarrow a_{1g} + b_{1g}$, each of the two $t_{1u} \rightarrow a_{2u} + e_u$, $t_{2g} \rightarrow b_{2g} + e_g$ and $t_{2u} \rightarrow b_{2u} + e_u$. The experimental[12,13,14,15,16,17] frequencies are compared to the B3LYP/aT-PP and/or BP86/aT-PP calculated MF_6 vibrational frequencies and their infrared intensities in Table 3 for M = W, Ir, Pt, and Au. For M = Re and Os, the B3LYP calculations gave two artificial imaginary frequencies possibly due to symmetry breaking, so we used the BP86/aT-PP frequencies. WF_6 and IrF_6, which have zero and three d electrons, respectively, have O_h symmetry and do not exhibit splitting of the vibrational modes. Our calculated values at the B3LYP/aT-PP level are smaller than the experimental values by 4 to 19 cm^{-1} for WF_6, and larger by 1 to 9 cm^{-1} for IrF_6, showing excellent agreement between theory and experiment. Weinstock et al.[13] interpreted the spectra of ReF_6, OsF_6 and PtF_6 assuming O_h symmetry, but noted that the vibrational mode ν_2 of symmetry e_g appears to be less intense for ReF_6 and OsF_6 and has a broader shape than for the other studied hexafluorides (SF_6, SeF_6, MoF_6, TeF_6, WF_6, UF_6, PtF_6, NpF_6 and PuF_6). This was considered to be evidence for a Jahn-Teller effect. Our calculated ReF_6 frequencies can qualitatively be compared to the experimental values. The a_{1g} stretch is smaller than the experimental one by 38 cm^{-1} and the e_g and t_{1u} stretches split by 31 cm^{-1} with their averages being in reasonable agreement with experiment. The lower t_{1u} mode splits by about 44 cm^{-1} and the t_{2u} mode by 50 cm^{-1} and both averages are qualitatively in agreement with

experiment. The t_{2g} scissoring mode shows a large splitting of 253 cm^{-1}, and the average is in poor agreement with experiment, Similar values have been obtained for OsF_6 with the stretches showing small splittings with averages in agreement with experiment. The calculated frequencies for PtF_6 are in good agreement with experiment with only small splittings, even for the t_{2g} mode. For AuF_6, our calculated values follow the same trends as for the other compounds with only a small splitting for the t_{2g} mode.

In many of these MF_6 compounds, the t_{2g} scissoring mode shows a very unusual behavior. It exhibits large splittings and, above all, the frequency order of the split components in ReF_6 and PtF_6 is reversed from that in OsF_6 and AuF_6. An inspection of the appropriate symmetry coordinates involved (Figure 2.2) provides a ready explanation. On lowering the symmetry from O_h to D_{4h}, the 4 equatorial and the two axial M-F bonds no longer possess the same bond lengths and the O_h t_{2g} mode splits into a b_{2g} equatorial scissoring mode and an e_g axial scissoring mode. If the equatorial M-F bonds are the shorter and stronger ones, the equatorial b_{2g} scissoring mode should have the higher frequency, and when the axial M-F bonds are shorter, the e_g axial scissoring mode should have the higher frequency. This is exactly the case. In ReF_6 and PtF_6 with shorter axial bonds, the e_g axial deformation modes have the higher frequencies, while in OsF_6 and AuF_6 with longer axial bonds the b_{2g} equatorial scissoring modes have the higher frequencies.

The frequencies for the D_{3d} structures are similar to those of the D_{4h} structures. The biggest differences are found for ReF_6 and OsF_6 for the modes derived from the e_g stretching mode in the O_h structures. This mode is not split in D_{3d} symmetry as it is in D_{4h} symmetry and is ~200 and 150 cm^{-1} lower than the average of the a_{1g} and b_{1g} modes in D_{4h} symmetry for ReF_6 and OsF_6 respectively.

Of interest to the prediction of the thermodynamic properties are the differences between the calculated and experimental zero point energies (ZPEs). These are compared in Table 2.6. All ZPEs calculated at the B3LYP level are within 0.3 kcal/mol of the experimental values as is the ZPE calculated at the BP86 level for ReF_6. The ZPE calculated at the BP86 level for OsF_6 is about 0.4 kcal/mol too small and is about 0.5 kcal/mol too small for WF_6.

Electron Affinities and Oxidizer Strengths Table 2.4 lists the valence CBS energies, the various additive energy corrections, and the calculated composite electron affinities, which are compared with the experimental values. The ZPE correction, calculated at the BP86/aD-PP or B3LYP/aT-PP levels, slightly increases the electron affinities (except for the EAs of WF_6 and PtF_6), whereas the core-valence correction, calculated at the CCSD(T)/awCVTZ level slightly decreases the electron affinities except for WF_6. An energy diagram showing the different states for the anions and neutrals used in predicting the electron affinities is shown in Figure 2.1.

If spin orbit interactions are not included, the electron affinity does not increase across the row, which is inconsistent with the prediction by Bartlett[6] that EA(IrF_6) is less than EA(OsF_6). Without spin orbit, the electron affinities of the MF_6 compounds follow the behavior expected for filling the t_{2g} orbitals (d_{xy}, d_{xz}, d_{yz}) as we increase the atomic number from W to Au. The electron affinity increases from WF_6 to OsF_6 as electrons are added to the the t_{2g} orbitals. The most stable species in this sequence is OsF_6^- which has 3 unpaired d electrons satisfying Hund's rule and would be expected to have the highest ionization potential like N in the first row (resulting in the highest electron affinity for OsF_6). Additional d electrons force spin pairing to occur and, as in the first row, the ionization potential of the anion (electron affinity of the corresponding neutral) would be expected to drop just as in main group elements. The ionization potential increases for AuF_6^- because it has a completely filled shell just like a noble gas. The

filling of the d orbitals in the transition metal hexafluorides differs from that of the s/p orbitals in main group fluorides. In the transition metal hexafluorides, the formal oxidation state of the central atom remains constant at +6 and does not change, contrary to the main group fluorides.

The SO correction (Table 2.4) to the EA was calculated as the difference between EA(ZORA+SO) and EA(ZORA). The electron affinities calculated with ZORA and ZORA+SO are given in Supporting Information. The effect of the SO correction is to increase the electron affinities for WF_6, ReF_6, IrF_6, and PtF_6 and to decrease those for OsF_6 and AuF_6. The SO effect on the electron affinity of OsF_6 is to decrease the EA by 2.67 kcal/mol and, for IrF_6, to increase it by 5.98 kcal/mol. When added to the CCSD(T) values, these SO corrections have the effect of reversing the order of the electron affinities for OsF_6 and IrF_6 so that EA(IrF_6) is greater than EA(OsF_6) by 0.07 eV. Thus, inclusion of molecular spin-orbit corrections results in a monotonic increase of the EAs for the third row transition metal hexafluorides. *The inclusion of molecular spin-orbit effects are essential for predicting the correct ordering of the electron affinities for these metal hexafluorides*.

Our calculated value of 3.15 eV for WF_6, which includes all corrections, differs from the ICR bracketing experimental[8] value of 3.5 eV. This difference of 0.35 eV is larger than expected on the basis of the agreement with experiment to within about 0.1 eV for the electron affinities of the metal oxide compounds[84] (WO_3 and W_2O_6), where W is also in the +6 oxidation state. Our calculated value is, however, in good agreement with the lower error bar of the $3.36^{+0.04}_{-0.2}$ eV value reported by Viggiano et al.[9] In the first bracketing study,[8] EA(WF_6) was estimated to be 3.5 eV between EA(F)[85] = 3.401 eV and EA(Cl) = 3.612 eV on the basis of the observation that WF_6 reacts with F^- in both charge transfer and association reactions but not with Cl^-. Viggiano et al.[9] did not observe charge transfer in the reaction of WF_6 with F^-, and only observed the

association reaction. They did observe charge transfer from Br^- to WF_6 so $EA(WF_6) > EA(Br) = 3.364$ eV. The lower error bar limit of 0.2 eV was estimated from the internal energy of WF_6 and translational energy effects. Thus, our calculated $EA(WF_6)$ value is consistent with the lower end of the energy range of Viggiano et al.[9]

The calculated electron affinities for OsF_6 and PtF_6 are in very good agreement with those from the charge transfer experiments by Sidorov and coworkers et al.[10] The calculated value of the electron affinity for IrF_6 is lower and lies just outside the experimental charge transfer error bar.[10] Friedman et al.[86] used a flowing afterglow to show that $EA(ReF_6) > EA(MoF_6) = 3.8 \pm 0.2$ eV and our calculated value is consistent with this experimental result.[87] On the basis of experiments such as the oxidation of NO and ONF by MF_6, Bartlett developed a scale of electron affinities. Our results are in good agreement with his approximate values and with the result that $EA(IrF_6) > EA(OsF_6)$.

Lower level calculations of the EAs as summarized in Table 2.1 are generally in agreement with our CCSD(T) values. We note that the CI-SD+Q values for WF_6[39] and AuF_6[40] are too large as compared to our values and those of others. The CCSD(T)/DZP calculation[42] for PtF_6 is in good agreement with our larger basis set value. The early DV-Xα values[37] are in reasonable agreement with our values except for IrF_6 which is 1 eV too large; these values are not purely theoretical as they are set relative to an experimental value of 3.5 eV for WF_6. The DFT/TZP/BP values[41] are in good agreement with our values for WF_6 and ReF_6 but start to show larger deviations beginning with OsF_6.

Vertical electron detachment (VDE) and attachment (VAE) energies have been calculated for the third row transition metal hexafluorides at the different levels of theory with the aT-PP basis set (Table 2.5) as these values are relevant to experimental measurements. The VDE of

MF_6^- was calculated from the difference between the energy of the neutral species MF_6 calculated at the corresponding anion geometry and the energy of the MF_6^- species. For the VAEs of MF_6, we calculated the energies of the anions at the geometries of the neutrals and subtracted them from the MF_6 energies. The VDEs of MF_6^- are 3 to 10 kcal/mol larger than the adiabatic EAs and the VAEs are 2 to 20 kcal/mol smaller than the adiabatic EAs. The largest differences between the VDE's and VAEs and the adiabatic EAs occur for the earlier transition metal atoms and the differences from the adiabatic EAs become much smaller as one proceeds from W to Au. For Au, the adiabatic EA, VDE, and VAE are all quite similar.

At the CCSD(T) level, we found a difference of less than 4 kcal/mol between the calculated values of the EAs with the aD-PP and aT-PP basis sets and of ≤1.5 kcal/mol between the aT-PP and aQ-PP basis sets (see Supporting Information). At the Hartree-Fock (HF) level a larger dependence was found, as the aD-PP and aT-PP values differ by an average of 6 kcal/mol with larger differences for the early metals of the series. The HF EAs are larger than the correlated EAs, and as one improves the correlation treatment, the EA decreases. This is opposite to what happens in typical electron affinities where the inclusion of the correlation energy in most cases leads to an increase in the electron affinity if the neutral molecule and its anion can be treated reasonably well with a single configuration wavefunction. In most of the simple molecules in which this is observed, the electron is added to a diffuse orbital that is on the exterior of the molecule. In these transition metal hexafluorides, however, the electron is added to a metal d orbital of the M(+6) center and is surrounded by negatively charged ligands (F^-). This difference between the HF and correlated values has been observed previously for WF_6 and attributed to the reduction of intra-closed shell correlation in the anions.[39]

One of the most fascinating problems from the onset of third row transition metal hexafluoride chemistry was concerned with the relative oxidizer strengths of these highly unusual oxidizers, and experiments were undertaken to establish qualitative measures for their oxidizing power based on their reaction chemistry.[7] In the following simple Born-Haber cycle for the one-electron oxidation of a given substrate S,

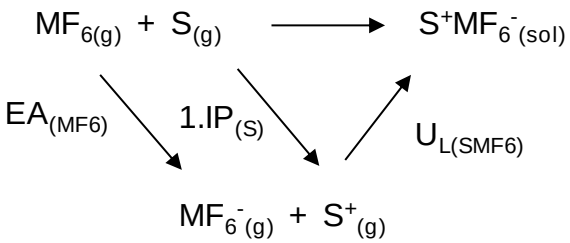

the free energy change of the reaction is a measure for the oxidizing power of MF_6. The free energy is given by the sum of the electron affinity of MF_6, the first ionization potential of S (1.IP), and the lattice energy of $S^+MF_6^-$. Since for a given substrate, 1.IP is always the same and the lattice energies of SMF_6 do not change much due to the radii of the MF_6^- being almost identical, the oxidizer strength of MF_6 is governed almost exclusively by the electron affinity of MF_6. Therefore, the oxidizer strength increases monotonously from WF_6 to AuF_6 with PtF_6 being the strongest presently known oxidizer within this series, and the electron affinity of MF_6 (Table 2.1) being an excellent quantitative measure of its oxidizing power.

Heats of Formation The total atomization energies (TAEs) (Table 2.6) which yield $\Delta H_{f,0K}$ and $\Delta H_{f,298K}$ (Table 2.7) were calculated at the CCSD(T) level and an atomic spin orbit correction is required.[74] The spin-orbit splitting is 0.39 kcal/mol for the ($^2P_{3/2}$) state of F. The ground states of Re ($^6S_{5/2}$) and Au ($^2S_{1/2}$) do not have any spin orbit splitting so they can be used directly to calculate the TAEs. For M = W, we calculated the TAE relative to the $^7S_3$ excited state of the atom which has no spin orbit correction and corrected the calculated TAE with the experimental

energy difference of 8.44 kcal/mol with respect to the $^5D_0$ ground state. For Pt, we used a similar approach and calculated the TAE for the $^1S_0$ excited state which was corrected by an energy difference of 17.54 kcal/mol with respect to the $^3D_3$ ground state. For Os and Ir, there are no convenient low lying excited states so we used the experimental ground states of Os ($^5D_4$) and Ir ($^4F_{9/2}$) with J-averaged spin orbit corrections of −7.57 and −10.38 kcal/mol, respectively. The TAEs decrease in the series from WF_6 to AuF_6.

We compare our calculated heats of formation with the available experimental values (Table 2.7). Excellent agreement is found between our calculated results and the experimental values for $\Delta H_f(WF_6)$, -423.2 vs. -422.0 kcal/mol[30], and for $\Delta H_f(ReF_6)$, -321.8 vs. -322.6 kcal/mol.[33] Other experimental values reported for $\Delta H_f(WF_6)$ are -411.5 ± 0.4,[30] -411.7 ± 0.5,[31] and -411.5 ± 0.2,[32] which are too positive. For PtF_6 the difference between our calculated value and the experimental estimate is 29 kcal/mol. Clearly, the prediction of $\Delta H_{f,298K}(IrF_6)$ = -130.0 kcal/mol, made by Ruff in 1929,[34] is incorrect.

What are the sources of errors in the calculated heats of formation of these metal fluorides? The first one is the experimental heat of formation of the metal atom, as the heats of formation of these transition metal atoms in the gas phase are not as well established and have larger error bars than do most main group elements (see Supporting Information). The error bars reported by Greenwood and Earnshaw[76] are not small and can be as large as ± 5.0 kcal/mol. The NBS tables[75] do not provide error bars, and although there is good agreement for $\Delta H_{f,298K}$ for W, Os and Ir between references 75 and 76, there is not as good an agreement for the other metals. Thus, it is likely that the largest source of error in the predicted heats of formation is due to the metal atomic values. The accurately calculated TAEs could be used together with experimental heats of formation of the fluorides, determined without the use of atomic energies, to obtain the

heats of the atoms as has been done for $\Delta H_f(B)$.[88] An additional source of error in the calculated heats of formation is due to the spin orbit correction for the metal atoms, as it is not clear whether the J-averaged approach for the atomic spin orbit correction that we have taken from our work on main group elements can be applied as reliably to the transition metals with more low lying excited states. As discussed above, the errors in the ZPEs are on the order of at most 0.5 kcal/mol. The last source of error is the molecular spin orbit effect, which was not included in the calculated heats of formation because of the difficulty in calculating the appropriate quantity for the atoms.

Bond Dissociation Energies Average adiabatic bond dissociation energies (BDEs) are calculated from the total atomization energies and are given in Table 2.8. The BDEs decrease in the series from WF_6 to AuF_6 consistent with the increase in bond length. Our findings are consistent with Bartlett's[7] prediction that the more powerful oxidizers in the MF_6 series (higher electron affinity) have lower average bond energies than the weaker oxidizers (lower electron affinity). Our calculated average M-F BDEs are quite high for the early metals of the series. The average BDEs range from 122.5 kcal/mol for the W-F bond energy to 42.1 kcal/mol for Au-F. The W-F BDE is only ~7 kcal/mol less than the C-F BDE in CF_4 and ~ 43 kcal/mol less than the Si-F BDE in SiF_4.[89]

The first adiabatic M-F BDEs have been calculated at different levels of theory from the reaction $MF_6 \rightarrow MF_5 + F$ with all species in their ground states (Table 2.8). DFT optimized geometries at the B3LYP/aT-PP level as well as scalar relativistic ZORA and ZORA-SO optimized geometries at the BLYP/TZ2P level are given in Supporting Information. Different molecular geometries and spin states were examined considering the way d orbitals split in the trigonal bipyramidal (D_{3h}) and square pyramidal (C_{4v}) ligand fields. WF_5 with only one 5d

electron distorts from the square pyramidal C_{4v} structure to a C_{2v} ($^2A_2$) structure with an average bond length of 1.854 Å. ReF_5 with two 5d electrons has a $^3A_1'/D_{3h}$ ground state with an average bond length of 1.851 Å; the $^3A_1'/D_{3h}$ state is ~6 kcal/mol more stable than the C_{4v} structure. OsF_5 with three 5d electrons has a $^4B_1/C_{4v}$ ground state with an average bond distance of 1.858 Å. Of all possible states for IrF_5, the $^5B_1/C_{4v}$ state is the most stable with an average bond distance of 1.875 Å. The $^1A_1$ and $^3A_1$ C_{4v} symmetry structures for IrF_5 are 9.9 and 4.7 kcal/mol higher in energy, respectively. The D_{3h} states for IrF_5 are up to 20 kcal/mol higher in energy than the $^5B_1/C_{4v}$ ground state. The PtF_5 $^2B_1/$ C_{4v} ground state has an average bond distance of 1.870 Å. The $^1A_1/C_{4v}$ ground state of AuF_5 has an average bond distance of 1.894 Å. The average M-F bond distances in the MF_5 series are approximately constant for M = W, Re, Os , increase in IrF_5 and PtF_5, and increase further in AuF_5. This trend is similar to that found for the metal hexafluorides (Table 2.2) where the average M-F bond distances are about the same from WF_6 through IrF_6 and then increase for PtF_6 and AuF_6.

The first adiabatic BDEs follow the same trend as the average BDEs and are up to 20 kcal/mol lower than the average BDEs, except for the 1st BDE for Ir-F, which is ~5 kcal/mol higher than its average BDE. The first BDEs as a function of the basis set are given in the Supporting Information and show that the effect of the basis set is not negligible even with the aT-PP basis set. The spin orbit corrections to the first BDEs were calculated to be less than 2 kcal/mol for all species except for M = Ir. The $^1A_{1g}$ state of WF_6 should be affected less by spin orbit coupling than the $^2A_2$ state of WF_5, so the total spin orbit effect reduces its first BDE. For AuF_6, the spin orbit effect for the $^1B_{2g}$ state nearly cancels that for the $^1A_1$ state of AuF_5 plus that for the F atom. For M = Re, Os, and Pt, the spin orbit corrections to the first BDEs depend on the relative magnitude of the spin orbit effects in MF_6 and MF_5, and our calculations show they all

increase the first BDEs by 1 to 2 kcal/mol. For IrF_6, the $^4A_{1g}$ state has a much smaller spin orbit correction as compared to the $^5B_1$ state of IrF_5, as the former has the degenerate t_{2g} orbitals half-filled. The total spin orbit correction substantially reduces the first BDE of IrF_6 by ~10 kcal/mol. The calculated spin orbit contributions for the first BDEs clearly show their importance, and significant error can be introduced if they are not included.

Fluoride Affinities and Lewis Acidities Table 2.9 lists the valence CBS energies and the various additive corrections included in the calculation of the MF_6 fluoride affinities. The results from DFT calculations with a selection of functionals and fluoride affinities calculated as a function of basis set at different levels of theory are given in Supporting Information.

The anionic heptafluorides have the same number of d electrons as the neutral hexafluorides. The addition of an F^- to an octahedral MF_6 structure would be expected to lead to three possible geometries on the basis of main group structures: pentagonal bipyramid (PBP, D_{5h}), mono-capped octahedron (MCO, C_{3v}) and mono-capped trigonal prism (MCTP, C_{2v}). Lin and Bytheway[90] predicted for WF_7^- that the MCO is more stable than the MCTP and the PBP by 0.1 and 1 kcal/mol, respectively, at the HF level; the MCTP and PBP structures had 1 and 2 imaginary frequencies. We found that at the B3LYP/aD-PP level, all three geometries have imaginary frequencies: two of 18*i* cm^{-1} for PBP, two of 34*i* cm^{-1} for MCO and one of 18*i* cm^{-1} for MCTP, consistent with the other DFT calculations on similar molecules.[91] All three are very close in energy with the MCO and MCTP structures being only 0.71 and 0.57 kcal/mol higher in energy, respectively, relative to the PBP at the B3LYP/aD-PP level. At the CCSD(T)/CBS level these differences are 0.66 for the MCO structure and 0.64 kcal/mol for the MCTP structure with respect to the lowest energy PBP structure. ReF_7^- with one 5d electron distorts to a doublet C_{2v} structure (not MCTP) which is a PBP structure distorted in the plane and more stable than the the

MCTP structure by 3.6 kcal/mol. The OsF_7^- PBP structure is lower in energy than the MCO and the MCTP structures by 5.6 and 4.9 kcal/mol, respectively; the two higher energy structures have imaginary frequencies of 74*i* cm^{-1} and 92*i* cm^{-1} respectively. IrF_7^-, like ReF_7^-, distorts to a doublet C_{2v} structure (an in-plane distorted PBP structure), which is more stable than the MCTP structure by 24.3 kcal/mol. For PtF_7^- with four 5d electrons, the PBP structure is more stable than the MCTP by ~4 kcal/mol, which has one imaginary frequency of 68*i* cm^{-1}.

For the three structures described above, the lowest energy structure for AuF_7^- with five 5d electrons is a doublet MCTP structure which is 37.4 kcal/mol lower in energy than a quartet PBP structure. However, the calculations at the B3LYP/aD-PP level showed two imaginary frequencies for the MCTP structure of 356*i* and 51*i* cm^{-1}, and one imaginary frequency of 277*i* cm^{-1} at the BP86/aT-PP level. The structures were distorted along the imaginary frequency direction and reoptimized. The reoptimization led to a C_s structure with one F atom bonded to an F atom ligand of the MF_6^- cluster for AuF_7^- and we found a similar result for PtF_7^-. The new structures, $^2A'/Cs$ for AuF_7^- and $^3A'/Cs$ for PtF_7^-, are more stable than the MCTP structures by 31.8 kcal/mol and 9kcal/mol respectively at the CCSD(T)/aT-PP level. The bond distance between the external F atom and the F atom on the cluster is 2.05 Å in PtF_7^- and 2.07 Å in AuF_7^- and the $M\text{-}F_{external}$ bond is 3.45 Å and 3.50 Å, respectively. The F-F bond distance is substantially longer than the F-F bond in F_2 of 1.412 Å[92] but is much shorter than the sum of the van der Waals radii[93] for two F atoms of 2.94 Å; the $M\text{-}F_{external}$ bond distance of ~ 3.5 Å in AuF_7^- is much longer than the average Au-F bond in AuF_6 of 1.895 Å at the B3LYP/aD-PP level. The M-F bond distance for the F atom bonded to the external F only lengthens by less than 0.05 Å. Thus this structure is quite unique. We optimized the same type of structures for the other metals in the series, and found that they are higher in energy than the classical structures by 87 kcal for the

WF_7^- $^3A''/C_s$ structure , 54 kcal/mol for the ReF_7^- $^4A''/C_s$ structure, 25 kcal/mol for the OsF_7^- $^5A''/C_s$ structure, and 32 kcal/mol for the IrF_7^- $^2A'/C_s$ structure at the CCSD(T)/aT-PP level.

The average M-F bond distances in the classical structures of the MF_7^- series follow the same trend as in the MF_6 and MF_5 series, with M-F bonds of approximately the same length for M=W, Re, and Os and increasing for M=Ir, Pt and Au. From WF_7^- to AuF_7^-, the average M-F bond distance is 1.901 Å, 1.900 Å, 1.902 Å, 1.921 Å, 1.922 Å and 2.025 Å (excluding the long bond structures in PtF_7^- and AuF_7^-).

The FAs for the addition of F^- to form one of three classical structures are consistently between 70 and 85 kcal/mol. For M = W, Re, and Os, the spin state of the MF_7^- is the same as for MF_6 as expected from the simplest model. Addition of F^- to IrF_6 ($^4A_{1g}/O_h$) leads to a $^2B_1/C_{2v}$ classical structure for IrF_7^- and addition of F^- to PtF_6 ($^3A_{1g}/D_{4h}$) leads to a $^1A_1'/D_{5h}$ classical structure for PtF_7^-. Our calculated value of 77.9 kcal/mol (3.38 eV) for FA(WF_6) is ~9 kcal/mol higher than the 69 kcal/mol (3.0 eV) estimated from ICR bracketing experiments.[8] Using more recent values[94] for the FAs (SiF_4 (77.4) < WF_6 < BF_3 (82.1)) we obtain excellent agreement between experiment and theory. The lowest value is for IrF_6 with a FA of ~ 70 kcal/mol.

The FAs for the formation of the nonclassical structures show a much greater variation with the metal, from near 0 for WF_6 to values of 84.4 and 111.5 kcal/mol, respectively, for PtF_6 and AuF_6; the non-classical structures are the more stable than the classical ones for the latter two MF_6 (Table 2.9). The FAs for the non-classical structures increase with an increase in the atomic number of the central metal atom. The spin orbit effects are not large for the fluoride affinities.

Examination of the calculated spin density and charges in the classical structures for MF_7^- shows that the negative charge is distributed relatively evenly over the F atoms in the cluster and

the spin is predominantly localized on the central metal atom. However, in the non-classical structure, one spin is localized on the external F atom with the remaining spin localized mostly on the metal atom with some spin on the F adjacent to the external F atom. The charge distribution also differs from the classical structures with the external F carrying much less negative charge. Thus, the nonclassical structure is best described as an F atom bonded to MF_6^-.

We can estimate the bond energy between the F atom and MF_6^- from the following thermodynamic cycle,

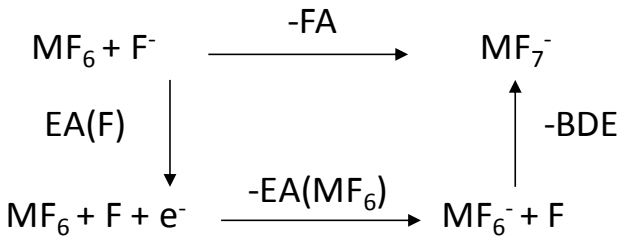

which uses available thermodynamic values to calculate the BDE of the process $MF_7^- \rightarrow MF_6^- + F$ given by BDE = EA(F) – EA(MF_6) + FA. The fluoride and electron affinities of MF_6 are available from our calculations and the experimental electron affinity[28] of F is 3.4012 eV (78.43 kcal/mol). The results in Table 2.9 show that the MF_6^--F BDE decreases from 84 kcal/mol for W to 10 kcal/mol for Ir for the classical MF_7^- structures, consistent with the increase in the MF_6 electron affinity. For PtF_7^-, the BDE is essentially zero, consistent with the formation of the F atom very weakly associated to PtF_6^-. A similar BDE of only 3.4 kcal/mol is predicted for AuF_7^-. Thus, when the electron affinity of MF_6 becomes large enough, the MF_6 will accept an F^- which then undergoes an electron transfer to MF_6 leaving a weak complex of an F atom with the MF_6^- anion. Thus, PtF_6 can oxidize F^- to $F^{\cdot}$, which explains its unusually high oxidizing power and reactivity. This is in excellent agreement with the previous experimental observations that PtF_6 can oxidize ClF_5 to ClF_6^+,[95,96] NF_3 to NF_4^+,[97] and Xe to XeF^+.[3,4] The mechanism of the NF_4^+

formation by different methods has been investigated in great detail[97] and been shown to involve the generation of F atoms as the crucial first step.

It is reasonable to assume that, in the reaction of Xe with PtF_6, the formation of an F atom is also the crucial first step. This would lead to the formation of a XeF radical which then gets oxidized by PtF_6 to give $XeF^+PtF_6^-$ and, by reacting with PtF_5, can yield $XeF^+Pt_2F_{11}^-$. This mechanism would account for the failure to observe experimentally any direct or indirect evidence for the formation of $Xe^+PtF_6^-$, with $XeF^+PtF_6^-$ and $XeF^+Pt_2F_{11}^-$ being the only observable products. Based on their extraordinarily high electron affinities, the third row transition metal hexafluorides ReF_6 (EA = 4.61 eV) through AuF_6 (EA = 8.20 eV) definitely fall in the category of "superhalogens", a term created in 1981 by Gutsev and Boldyrev for compounds having electron affinities exceeding those of the halogens (3.0-3.6 eV).[98] Its high EA of 8.20 eV makes AuF_6 one of the ultimate superhalogens.

The predicted F^- affinity of AuF_6, leading to the formation of an F radical, is 111.8 kcal/mol and is only about 10 kcal/mol below that of SbF_5.[47] This would make AuF_6 not only a very powerful oxidizer but also a very strong Lewis acid. Due to their lower electron affinities, WF_6, ReF_6, OsF_6 and IrF_6 favor the classical MF_7^- structures with M-F bonds and do not react in the nonclassical fashion.

Given the available results, it is also possible to calculate the MF_5 fluoride affinities ($MF_5 + F^- \rightarrow MF_6^-$). The resulting values calculated at the CCSD(T)/CBS level with ZPE, core-valence and scalar relativistic corrections are given in Table 2.10. The MF_5 fluoride affinities calculated as a function of the basis sets are given as Supporting Information. The MF_5 FAs increase from $FA(WF_5)$ = 113.0 to $FA(AuF_5)$ = 136.6 kcal/mol following the trends in the electron affinities. Our calculated value of 110.4 kcal/mol for $FA(WF_5)$ is in good agreement with the experimental

value of 107.6 kcal/mol.[99] The DFT calculated value for FA(AuF_5) = 141.2 kcal/mol[100] is in good agreement with our CCSD(T) value. Christe et al.[47] have used fluoride ion affinities to establish a quantitative Lewis acidity scale. The strongest Lewis acid on the list, SbF_5, has a fluoride affinity of 120.3 kcal/mol, lower than those of OsF_5, IrF_5, PtF_5 and AuF_5. WF_5 and ReF_5 with fluoride affinities of 112.1 and 115.0 kcal/mol, respectively, are comparable to strong Lewis acids such as AlF_3 and $AlCl_3$. The FAs of MF_5 are much larger by 35 to 58 kcal/mol than the FAs of the corresponding MF_6 molecules. This would be expected as going from a C_{4v} or D_{3h} structure for MF_5 to an approximate or actual octahedral structure for MF_6^- would have less steric crowding than going from an octahedral structure for MF_6 to the various structures for MF_7^-.

Performance of Density Functional Theory There is substantial interest in the performance of different DFT exchange-correlation functionals in predicting the thermodynamic properties of transition metal complexes. Calculated EAs for a selection of functionals , M-F bond dissociation energies, calculated MF_5 FAs and calculated MF_6 FAs are given in Supporting Information. The average deviations of these properties calculated with a selection of functional from the CCSD(T)/CBS values with all corrections except for spin orbit are given in Table 2.11. In general, the electron affinity differences between the CCSD(T) and DFT values are larger for the later transition metal fluorides than for the earlier ones. The largest differences are found for the LSDA functional SVWN5 with an average deviation of 26.0 kcal/mol. The GGA functionals perform somewhat better than SVWN5, but the differences from the CCSD(T) values are still quite large with average deviations of 15 to 20 kcal/mol. The hybrid functionals B3LYP, mPW1PW91, and PBE1 give the best performances with average deviations of 6-7 kcal/mol, but other hybrid functionals do not perform any better than the GGA functionals. Our B3LYP and

BP86 calculated values of 7.96 eV and 7.10 eV for the electron affinity of AuF_6 are in excellent agreement with those of 8.06 and 7.10 eV, respectively, calculated by Riedel and Kaupp,[43] but the B3LYP values are ~0.2 eV lower than our CCSD(T) value. For the M-F adiabatic BDEs of MF_6, the GGA functionals predict BDEs that are too large by up to 20 kcal/mol as compared to the CCSD(T) results. The hybrid functionals B3LYP, mPW91 and PBE1 predict M-F BDEs within 3 kcal/mol of the CCSD(T) results. For the MF_5 fluoride affinities, the GGA functionals predict values that are 8 to 19 kcal/mol smaller than the CCSD(T) values. Surprisingly, the best overall average agreement for the MF_5 FAs with the CCSD(T) values is with the local SVWN5 functional. The hybrid functionals also predict average values smaller than the CCSD(T) results by 3 to 16 kcal/mol. For the MF_6 fluoride affinities, the GGA functionals again show the largest differences on average with respect to the CCSD(T) values with average differences from 8 to 19 kcal/mol. The largest differences with these functionals are for FA(PtF_6) and AuF_6, where the lowest energy MF_7^- structure is the non-classical structure. All hybrid functionals, except for O3LYP, predict average FAs within 2 to 6 kcal/mol with respect to the CCSD(T) values. The local SVWN5 performs well for the classical MF_7^- structures but does not for the nonclassical structures for PtF_7^- and AuF_7^-.

Conclusions

High level coupled cluster CCSD(T) calculations, extrapolated to the complete basis set limit, were used to evaluate reliable, self-consistent thermochemical data sets for the third row transition metal hexafluorides. For MF_6 and MF_6^-, the Jahn-Teller distorted D_{4h} and D_{3d} structures where possible are very close in energy with an undistorted O_h structure about 1.0 kcal/mol higher in energy. Thus the MF_6 molecules are highly fluxional about the conical intersection and will exhibit an O_h geometry under most experimental conditions.

The electron affinities are direct measures for the oxidizer strengths of these hexafluorides and their oxidizing power increases monotonically from WF_6 to AuF_6, with PtF_6 and AuF_6 being extremely powerful oxidizers. The inclusion of spin orbit corrections was very important to obtain the correct qualitative order for the electron affinities. A wide range of DFT exchange-correlation functionals were also evaluated and only the B3LYP, mPW1PW91 and PBE1 functionals were found to approximate the coupled cluster values.

Based on their calculated fluoride ion affinities the corresponding pentafluorides are extremely strong Lewis acids, with OsF_5, IrF_5, PtF_5 and AuF_5 significantly exceeding the acidity of SbF_5.[94] A calculation of the minimum energy structures of the MF_6^- anions without or with (except for PtF_6^-) spin orbit corrections revealed that WF_6^-, ReF_6^-, IrF_6^- and PtF_6^- are all distorted from O_h to D_{4h} symmetry with concomitant splittings of the degenerate vibrational modes which, in the case of the scissoring deformation, can lead to interesting frequency reversals depending on whether the axial or the equatorial bonds are shorter.

The calculation of the minimum energy structures of the corresponding MF_7^- anions resulted in a very important discovery. Whereas the hexafluorides ranging from WF_6 through IrF_6 form the expected classical MF_7^- anions with M-F bonds, PtF_7^- and AuF_7^- form nonclassical anions with a very weak external F-F bond between an MF_6^- fragment and a fluorine atom. Therefore, these two anions are text book examples for "superhalogens" and can serve as F atom sources under very mild conditions. This ability of PtF_6 to generate, in the presence of fluoride anions, F atoms can explain its ability to convert NF_3 to NF_4^+, ClF_5 to ClF_6^+, and Xe to XeF^+. It also explains the failure of Bartlett's search for $XePtF_6$ and the observation of XeF^+ salts as the only reaction products of the PtF_6/Xe reaction.[3,4] The crucial first step appears to be the formation of a XeF radical which then is oxidized by PtF_6 to give $XeF^+PtF_6^-$.

Acknowledgment. This work was supported by the Chemical Sciences, Geosciences and Biosciences Division, Office of Basic Energy Sciences, U.S. Department of Energy (DOE) under grant no. DE-FG02-03ER15481 (catalysis center program). DAD also thanks the Robert Ramsay Chair Fund of The University of Alabama for support. Part of this work was performed at the W. R. Wiley Environmental Molecular Sciences Laboratory, a national scientific user facility sponsored by DOE's Office of Biological and Environmental Research and located at Pacific Northwest National Laboratory, operated for the DOE by Battelle. KOC is indebted to the Air Force Office of Scientific Research, the Office of Naval Reesearch, the National Science Foundation, and the Defense Threat Reduction Agency for financial support.

Supporting Information Experimental atomic heats of formation in kcal/mol, benchmarked DFT exchange-correlation functional, relative energy differences between the D_{4h} and D_{3d} MF_6 structures, EA(MF_6), FA(MF_5), FA(MF_6) and first M-F BDEs calculated with various exchange-correlation functional, adiabatic electron affinities of MF_6**,** vertical electron detachment energies (VDE) of MF_6^- and vertical electron attachment energies (VAE) of MF_6 in kcal/mol calculated at the CCSD(T)/aT-PP//CCSD(T)/aD-PP, B3LYP/aT-PP//B3LYP/aD-PP and CCSD(T)/aT-DK// CCSD(T)/aT-PP levels, MF_6 MF_6^-, MF_5, and MF_7^- total electronic energies and vibrational frequencies at the DFT level with various exchange-correlation functionals and the aD-PP basis set, zero point energies (ZPE), CCSD(T) total energies as a function of basis set, core and valence energies at the CCSD(T)/aug-cc-pWCVTZ-PP level, and scalar relativistic energies at the CISD/aT-PP and CCSD(T)-DK/aug-cc-pVTZ-DK levels, T1 diagnostics. Energy differences in kcal/mol of D_{4h} vs O_h structures for the same spin state and singlet –triplet splitting energies for the D_{4h} structures. Optimized geometry parameters with different DFT functionals. Pseudopotential errors and scalar relativistic corrections for EA(MF_6), 1st M –F BDEs, total

atomization energies, FA(MF_6), and FA(MF_5). Electron affinities calculated at the ZORA and ZORA+SO levels. Mulliken charges, NBO charges, and spin densities for MF_6 and MF_6^- and figures for the spin densities. First M –F BDEs, FA(MF_6), and FA(MF_5) calculated at the DFT and CCSD(T) levels as a function of basis set. MF_5 optimized geometry at the B3LYP/aT-PP, BLYP/TZ2P scalar relativistic ZORA and ZORA plus spin orbit levels .Cartesian xyz coordinates for all molecules. This material is available free of charge via the Internet at http://pubs.acs.org.

Table 2.1. MF_6 Electron Affinities in eV.

Molecule	Calculated[a]	Experiment	Reactivity Estimate[f]	Other calculated
WF_6	3.16	3.50 ± 0.1,[b] $3.36^{+0.04}_{-0.2}$ [c]	*>3.0*	3.34,[g] 3.85[h]
ReF_6	4.58	>3.8[d]	>3.90	4.50,[g] 4.8[i]
OsF_6	5.92	5.93 ± 0.28[e]	*>4.7*	5.55,[g] 6.0[i]
IrF_6	5.99	6.50 ± 0.38[e]	>5.46	5.34,[g] 7.2[i]
PtF_6	7.09	7.00 ± 0.35[e]	>6.76	6.36,[g] 7.4[i], 6.95,[j] 6.78[k]
AuF_6	8.20		*>7.6*	8.1,[i] 9.56[l]

[a] Final calculated value this work. [b] Reference 8. [c] Reference 9. [d] Reference 86. [e] Reference 10. [f] References 6 and 7. Values in italics obtained from data in Reference 7 using the estimate from this reference of a change in atomic number of 1 corresponds to a change of ~ 20 kcal/mol in the electron affinity. [g] DFT/BP86/TZP+DZP Reference 41. [h] CI-SD+Q Reference 39. [i] DV-Xα Reference 37. From calculated EAs relative to 3.5 eV for WF_6. [j] CCSD(T)/TZP+DZP. Reference 42, 43, 44. [k] B3LYP/ TZP+DZP. Reference 42. [l] CI-SD+Q Reference 40.

Table 2.2. Optimized Metal-Fluorine Bond Lengths (Å) and Bond Angles (degrees) at the CCSD(T) Level with the aT-PP Basis Set and at the ADF ZORA BLYP Level with the TZ2P Basis Set.

Molecule	**State/ sym**	**CCSD(T)/aT-PP**	**state/sym ZORA**	**ZORA TZ2P**	**Sym ZORA-SO**	**ZORA S-O TZ2P**	**EXPT**
WF_6	$^1A_{1g}/O_h$	1.835	$^1A_{1g}/O_h$	1.889	O_h	1.887	1.825[a],1.829[b],1.826[c]
WF_6^-	$^2B_{2g}/D_{4h}$	1.865 (x2),1.921 (x4)	$^2A_{1g}/D_{3d}$	1.951, 92.7°	D_{4h}	1.970 (x2), 1.943 (x4)	
WF_6^-	$^2A_{1g}/D_{3d}$	1.902, 92.7°			D_{3d}	1.950, 92.5°	
ReF_6	$^2B_{2g}/D_{4h}$	1.802 (x2), 1.844 (x4)	$^2A_{1g}/D_{3d}$	1.885, 91.8°	D_{4h}	1.899 (x2), 1.878 (x4)	1.829[b]
ReF_6	$^2A_{1g}/D_{3d}$	1.830, 91.8°			D_{3d}	1.883, 91.0°	
ReF_6^-	$^3A_{1g}/D_{4h}$	1.927 (x2), 1.873 (x4)	$^3A_{1g}/D_{3d}$	1.942, 91.6°	D_{4h}	1.928 (x2), 1.951 (x4)	1.863[d]
ReF_6^-	$^3A_{1g}/D_{3d}$	1.891, 90.8°			D_{3d}	1.941, 90.6°	
OsF_6	$^3A_{1g}/D_{4h}$	1.856 (x2), 1.816 (x4)	$^3A_{1g}/O_h$	1.887	D_{4h}	1.877 (x2), 1.892 (x4)	1.827[a], 1.828[b]
OsF_6	$^3A_{1g}/D_{3d}$	1.829, 90.7°	$^3A_{1g}/D_{3d}$	1.886, 91.2°	D_{3d}	1.885, 90.4°	
OsF_6^-	$^4A_{1g}/O_h$	1.884	$^4A_{1g}/O_h$	1.938	O_h	1.939	1.872[e], 1.879[e]
IrF_6	$^4A_{1g}/O_h$	1.832	$^4A_{1g}/O_h$	1.893	O_h	1.894	1.839[b]
IrF_6^-	$^3A_{1g}/D_{4h}$	1.849 (x2), 1.897 (x4)	$^3A_{1g}/D_{3d}$	1.941, 91.1°	D_{4h}	1.952 (x2), 1.938 (x4)	1.879[e], 1.875[f]
IrF_6^-	$^3A_{1g}/D_{3d}$	1.881, 91.3°			D_{3d}	1.940, 90.4°	
PtF_6	$^3A_{1g}/D_{4h}$	1.823 (x2), 1.856 (x4)	$^3A_{1g}/O_h$	1.911	D_{4h}	1.915 (x2), 1.909 (x4)	1.852[b]
PtF_6	$^3A_{1g}/D_{3d}$	1.845, 90.1°			D_{3d}	1.908, 90.2°	

PtF_6^-	$^2B_{2g}/D_{4h}$	1.917 (x2), 1.869 (x4)	$^2B_{2g}/O_h$	1.951	O_h	1.952	1.887[e]
PtF_6^-	$^2A_{1g}/D_{3d}$	1.884, 90.6°					
AuF_6	$^2B_{2g}/D_{4h}$	1.897 (x2), 1.858(x4)	$^2B_{2g}/O_h$	1.937	O_h	1.936	
AuF_6	$^2A_{1g}/D_{3d}$	1.870, 90.2°	$^2A_{1g}/D_{3d}$	1.938, 90.2°	D_{3d}	1.934, 90.1°	
AuF_6^-	$^1A_{1g}/O_h$	1.899	$^1A_{1g}/O_h$	1.966	Oh	1.967	1.899[c], 1.874[e], 1.861[g], 1.890[h]

[a] Reference 78. [b] Reference 19. [c] Reference 20. [d] Reference 79. [e] Reference 25. [f] Reference 80. [g] Reference 83. [h] Reference 81

Table 2.3. Experimental and Calculated MF_6 Vibrational Frequencies (cm^{-1}) and IR Intensities at the B3LYP/aT-PP and BP86/aT-PP Levels.

MF_6	State	a_{1g}		e_g		t_{1u}		t_{1u}		t_{2g}		t_{2u}	
	Sym	Calc	Expt	Calc	Expt	Calc	Expt	Calc	Expt	Calc	Expt	Calc	Expt
WF_6[a]	$^1A_{1g}/O_h$	757	771[b]	665	677[b]	699(810)	711[c]	239(102)	258[c]	304	320[b]	123(0)	[127][b]
ReF_6[d]	$^2B_{2g}/D_{4h}$	716	754[e]	a_{1g} 645	[671][c]	a_{2u} 705(205)	715[c]	e_u 261(28)	257[c]	e_g 467	[295][c]	e_u 168(4)	[147][e]
				b_{1g} 640		e_u 674(402)		a_{2u} 217(29)		b_{2g} 214		b_{2u} 118(0)	
ReF_6[a]	$^2A_{1g}/D_{3d}$	747		420		a_{2u} 698(238)		e_u 269(40)		a_{1g} 277		e_u 151(12)	
						e_u 712(488)		a_{2u} 254(24)		e_g 216		a_{1u} 133(0)	
OsF_6[d]	$^3A_{1g}/D_{4h}$	694	731[b]	b_{1g} 643	[668][c]	e_u 693(334)	720[f]	a_{2u} 282(7)	268[f]	e_g 285	[276][c]	b_{2u} 207(0)	[205][c]
				a_{1g} 629		a_{2u} 666(170)		e_u 245(34)		b_{2g} 308		e_u 161(4)	
OsF_6[a]	$^3A_{1g}/D_{3d}$	729		474		a_{2u} 717(210)		e_u 279(30)		a_{1g} 280		a_{1u} 213(0)	
						e_u 708(516)		a_{2u} 264(19)		e_g 191		e_u 154(8)	
IrF_6[a]	$^4A_{1g}/O_h$	704	702[b]	646	645[b]	710 (528)	719[c]	274(45)	276[c]	258	267[b]	200(0)	[206][c]
PtF_6[a]	$^3A_{1g}/D_{4h}$	664	656[b]	a_{1g} 622	[601][f]	a_{2u} 709(135)	705[f]	e_u 290(14)	273[f]	e_g 221	[242][f]	e_u 223(8)	[211][f]
				b_{1g} 635		e_u 688(202)		a_{2u} 249(19)		b_{2g} 195		b_{2u} 182(0)	
PtF_6[g]	$^3A_{1g}/D_{3d}$	691		641		e_u 729(184)		e_u 255(20)		e_g 226		a_{1u} 206(0)	
						a_{2u} 726(91)		a_{2u} 245(10)		a_{1g} 223		e_u 188(0)	
AuF_6[a]	$^2B_{2g}/D_{4h}$	619		b_{1g} 596		e_u 668(40)		a_{2u} 290(0)		b_{2g} 266		b_{2u} 234(0)	
				a_{1g} 589		a_{2u} 660(95)		e_u 259(24)		e_g 200		e_u197(14)	
AuF_6[a]	$^2A_{1g}/D_{3d}$	611		482		a_{2u} 664(56)		e_u 278(12)		a_{1g} 220		a_{1u} 242(0)	
						e_u 663(104)		a_{2u} 256(11)		e_g 218		e_u 190(6)	

[a] B3LYP/aT-PP. [b] Reference 16. [c] Reference 15. [d] BP86/aT-PP level [e] Reference 17. [f] Reference 13. [g] ADF Zora SO BLYP/TZ2P.

Table 2.4. Energy Components for the Calculated Electron Affinities in kcal/mol.

M	MF_6 State/Sym	MF_6^- State/Sym	ΔE_{CBS}[a]	ΔE_{ZPE}	ΔE_{CV}[b]	ΔE_{rel}[c]	EA	SO[d]	EA +SO
W	$^1A_{1g}/O_h$	$^2B_{2g}/D_{4h}$	67.36	0.73[e]	0.45	2.36	70.9	1.90	72.8
	$^1A_{1g}/O_h$	$^2A_{1g}/D_{3d}$	67.34	1.00[e]	0.34	2.35	71.0	1.31	72.3
Re	$^2A_{1g}/D_{3d}$	$^3A_{1g}/D_{4h}$	103.45	-0.01[f]	-0.17	1.38	104.7	0.88	105.6
	$^2B_{2g}/D_{4h}$	$^3A_{1g}/D_{4h}$	103.20	0.77[f]	-0.20	1.39	105.2	1.11	106.3
	$^2A_{1g}/D_{3d}$	$^3A_{1g}/D_{3d}$	102.41	0.90[f]	-0.14	1.18	104.4	1.00	105.4
Os	$^3A_{1g}/D_{4h}$	$^4A_{1g}/O_h$	138.30	0.91[f]	-0.71	0.29	138.8	-2.30	136.5
	$^3A_{1g}/D_{3d}$	$^4A_{1g}/O_h$	139.14	0.55[f]	-0.76	0.28	139.2	-2.45	136.7
Ir	$^4A_{1g}/O_h$	$^3A_{1g}/D_{4h}$	130.85	0.72[f]	-1.01	1.59	132.2	5.98	138.2
	$^4A_{1g}/O_h$	$^3A_{1g}/D_{3d}$	130.08	1.43[f]	-0.94	1.61	132.2	5.98	138.2
Pt	$^3A_{1g}/D_{4h}$	$^2B_{2g}/D_{4h}$	163.10	0.57[e]	-1.43	0.74	163.0	0.62	163.6
	$^3A_{1g}/D_{3d}$	$^2A_{1g}/D_{3d}$	162.49	0.76[e]	-1.32	0.98	162.9	0.61	163.5
Au	$^2B_{2g}/D_{4h}$	$^1A_{1g}/O_h$	194.25	0.30[g]	-1.42	-0.05	193.1	-3.90	189.2
	$^2A_{1g}/D_{3d}$	$^1A_{1g}/O_h$	195.34	-0.06[g]	-1.54	-0.06	193.7	-3.63	190.1

[a] Valence CCSD(T) electronic energy contribution extrapolated using the mixed Gaussian/exponential formula. [b] Core-valence correction obtained at the CCSD(T)/awCVTZ level. [c] See Equation (1). [d] Spin-orbit correction from BLYP/ZORA + SO/TZ2P calculation. [e]ADF Zora SO BLYP/TZ2P. [f] BP86/aD-PP. [g] B3LYP/aT-PP.

Table 2.5. Adiabatic Electron Affinities of MF_6**,** Vertical Electron Detachment Energies (VDE) of MF_6^- and Vertical Electron Attachment Energies (VAE) of MF_6 in kcal/mol Calculated at the CCSD(T)/aT-DK//CCSD(T)/aT-PP Level.

Molecule	**MF_6 State/Sym**	**MF_6^- State/Sym**	**ADE**	**VDE**	**VAE**
WF_6/WF_6^-	$^1A_{1g}/O_h$	$^2B_{2g}/D_{4h}$	68.7	79.4	54.1
ReF_6/ReF_6^-	$^2A_{1g}/D_{3d}$	$^3A_{1g}/D_{4h}$	103.8	115.0	94.7
ReF_6/ReF_6^-	$^2B_{2g}/D_{4h}$	$^3A_{1g}/D_{4h}$	103.6	115.0	88.4
OsF_6/OsF_6^-	$^3A_{1g}/D_{4h}$	$^4A_{1g}/O_h$	137.8	144.7	128.5
IrF_6/IrF_6^-	$^4A_{1g}/O_h$	$^3A_{1g}/D_{4h}$	130.5	136.1	123.3
PtF_6/PtF_6^-	$^3A_{1g}/D_{4h}$	$^2B_{2g}/D_{4h}$	161.7	166.7	154.6
AuF_6/AuF_6^-	$^2B_{2g}/D_{4h}$	$^1A_{1g}/O_h$	191.8	196.4	191.7

[a] $VDE = E_{\text{neutral at anion geom}} - E_{\text{anion}}$

[b] $VAE = E_{\text{neutral}} - E_{\text{anion at neutral geom.}}$

Table 2.6. Energy Components for Total Atomization Energies of MF_6 in kcal/mol at 0 K($\sum D_0$).

Molecule	**State/Sym**	ΔE_{CBS}[a]	ΔE_{ZPE}	ΔE_{CV}[b]	ΔE_{rel}[c]	**Atomic** ΔE_{SO}[d]	$\sum D_{0,0K}$[e]
WF_6	$^1A_{1g}/O_h$	759.29	-8.83[f](-9.10)[g]	-0.20	-4.22	-2.33	735.27
ReF_6	$^2A_{1g}/D_{3d}$	629.69	-8.07[f]	0.78	-2.56	-2.33	617.51
ReF_6	$^2B_{2g}/D_{4h}$	629.94	-9.14[h](-9.05)[g]	0.82	-2.58	-2.33	616.71
OsF_6		566.19	-8.86[h](-9.25)[g]	1.59	-1.83	-9.90	547.19
IrF_6	$^4A_{1g}/O_h$	495.99	-9.03[f](-9.14)[g]	2.66	-2.16	-12.71	474.75
PtF_6		381.37	-8.72[f](-8.79)[g]	11.70	1.12	-2.33	371.60
AuF_6	$^2B_{2g}/D_{4h}$	252.57	-8.44[f]	9.84	1.20	-2.33	252.84

[a] $\Delta E = \Delta E(M) + 6\Delta E(F) - \Delta E(MF_6)$. [b] CCSD(T)/awCVTZ. [c] See equation (1). [d] The spin-orbit splitting is -0.39 kcal/mol for the ($^2P_{3/2}$) state of F. See text for the metals. [e] $\sum D_{0,0K} = \Delta E_{CBS} + \Delta E_{ZPE} + \Delta E_{CV} + \Delta E_{rel} + \Delta E_{SO.}$ [f] B3LYP/aT-PP. [g] Experimental ZPE's. [h] BP86/aT-PP.

Table 2.7. Heats of Formation of MF_6 in kcal/mol at 0 and 298 K ($\Delta H_{f,0K}$ and $\Delta H_{f,298K}$) Calculated at the CCSD(T) Level.[a]

Molecule	**MF_6 State/Sym**	$\Delta H_{f,0K}$[b]	$\Delta H_{f,298K}$[b]	$\Delta H_{f,0K}$[c]	$\Delta H_{f,298K}$[c]	**Exp**
WF_6	$^1A_{1g}/O_h$	-421.4	-423.0			-422.0 ± 4,[29] -411.5 ± 0.4,[30] -411.7 ± 0.5,[31] -411.4 ± 0.2[32]
ReF_6	$^2B_{2g}/D_{4h}$	-322.1	-323.0	-319.7	-321.6	-322.6 ± 2.3[33]
ReF_6	$^2A_{1g}/D_{3d}$	-322.9	-323.3	-320.5	-321.9	
OsF_6	$^3A_{1g}/D_{4h}$	-247.6	-248.4	-247.3	-249.1	
IrF_6	$^4A_{1g}/O_h$	-205.1	-206.0	-204.0	-205.9	-130.0[34]
PtF_6	$^3A_{1g}/D_{4h}$	-125.9	-126.6	-130.6	-132.3	-161.6 ± 6.7,[34] -160.6 ± 1.5[35]
AuF_6	$^2B_{2g}/D_{4h}$	-54.5	-55.0	-51.4	-53.1	

[a] Heat of formation of F for all from the JANAF Tables. $\Delta H_{f,298K}(MF_6) = \Delta H_{f,0K}(MF_6) + \Delta H_{0K\rightarrow 298K}(MF_6) - \Delta H_{0K\rightarrow 298K}(M) - 6\Delta H_{0K\rightarrow 298K}(F)$. The experimental enthalpy change from 0 to 298 K ($\Delta H_{0K\rightarrow 298K}$) is 1.05 for F and 1.19 kcal/mol for W. For Re, Os, Ir, Pt and Au we have used a value of 1.20 kcal/mol. [b] Wagman et al. values (Ref. 75) for all metals except for W from JANAF Tables (Ref. 28). [c] Greenwood and Earnshaw (Ref. 76) values for all metals.

Table 2.8. Calculated Energy Components for the First Adiabatic and Average M –F Bond Dissociation Energies for MF_6 in kcal/mol Calculated at CCSD(T) level.

M-F Bond	MF_5 [a] State/Sym	MF_6 State/Sym	ΔE_{CBS} [b]	ΔE_{ZPE} [c]	ΔE_{CV} [d]	ΔE_{rel} [e]	ΔE_{SO} [f]	1st BDE [g]	Avg BDE [h]
W-F	$^2A_2/C_{2v}$	$^1A_{1g}/O_h$	124.0	-2.31[i]	0.13	-2.64	-1.51	117.7	122.5
Re-F	$^3A_1'/D_{3h}$	$^2B_{2g}/D_{4h}$	90.6	-2.54[j]	1.19	-1.63	1.10	88.7	102.8
Re-F	$^3A_1'/D_{3h}$	$^2A_{1g}/D_{3d}$	90.4	-1.30[k]	1.15	-1.86	1.33	89.7	102.9
Os-F	$^4B_1/C_{4v}$	$^3A_{1g}/D_{4h}$	74.0	-2.55[k]	1.72	-0.96	2.02	74.2	91.2
Ir-F	$^5B_1/C_{4v}$	$^4A_{1g}/O_h$	85.9	-2.31[i]	1.15	-0.69	-9.78	74.3	79.1
Pt-F	$^2B_1/C_{4v}$	$^3A_{1g}/D_{4h}$	45.1	-1.97[i]	2.52	-1.17	1.87	46.4	61.9
Au-F	$^1A_1/C_{4v}$	$^2B_{2g}/D_{4h}$	25.0	-2.24[i]	2.33	0.20	0.25	25.5	42.1

[a] All MF_5 structures optimized at the DFT level with the B3LYP functional with the aT-PP basis sets. DFT optimized geometries plus the scalar relativistic ZORA and ZORA-SO optimized geometries at the BLYP/TZ2P level are in Supporting Information. [b] Single point energies extrapolated to the CBS limit calculated at the CCSD(T) level with aD-PP, aT-PP and aQ-PP basis sets using the B3LYP/aT-PP geometries. [c] ZPE at the B3LYP or BP86 levels, [d] Core-valence corrections at the CCSD(T)/awCVTZ level. [e] See equation 1. [f] SO correction at the ADF ZORA BLYP/TZ2P level plus the experimental spin-orbit correction of -0.39 kcal/mol for F. [g] 1st BDE calculated as the sum of ΔE_{CBS} and of all corrections. [h] Average BDE = $\sum D_{0,0K}$ (MF_6)/6. [i] BP86/aD-PP. [j]BP86/aT-PP. [k] B3LYP/aT-PP.

Table 2.9. Calculated MF_6 Fluoride Affinities and MF_6^--F Bond Dissociation Energies in kcal/mol.

M	MF_6 State/Sym	MF_7^-[a] State/Sym[b]	CCSD(T)/ aD	CCSD(T)/ aT	ΔE_{CBS}[c]	ΔE_{ZPE}	ΔE_{CV}[d]	ΔE_{rel}[e]	ΔE_{SO}[f]	FA	BDE[g]
W	$^1A_{1g}/O_h$	$^1A_1'/D_{5h}$	76.63	77.91	78.08	-0.97[h]	0.04	0.96	0.01	78.1	83.7
W	$^1A_{1g}/O_h$	$^3A''/C_s$	-3.16	-9.02		1.19[i]				-7.8	3.5[j]
Re	$^2B_{2g}/D_{4h}$	$^2A_2/C_{2v}$	79.86	80.97	81.00	0.02[k]	0.33	0.18	-0.67	80.9	53.0
Re	$^2B_{2g}/D_{4h}$	$^4A''/C_s$	33.46	27.12		-0.40[i]				26.7	2.1[j]
Re	$^2A_{1g}/D_{3d}$	$^2A_2/C_{2v}$	80.08	81.21	81.25	-0.9[l]	0.36	0.41	-0.90	80.2	53.0
Re	$^2A_{1g}/D_{3d}$	$^4A''/C_s$	33.68	27.36		0.07[l]				27.4	3.4
Os	$^3A_{1g}/D_{4h}$	$^3A_1'/D_{5h}$	86.02	86.83	86.34	-0.90[k]	0.40	0.48	-3.85	82.5	24.4
Os	$^3A_{1g}/D_{4h}$	$^5A''/C_s$	68.30	61.46		1.23[i]				62.7	2.7[j]
Ir	$^4A_{1g}/O_h$	$^2B_1/C_{2v}$	61.80	62.72	64.18	-0.28[m]	2.21	1.42	2.49	70.0	10.2
Ir	$^4A_{1g}/O_h$	$^2A'/C_s$	34.01	30.42		1.06[i]				31.5	-19.8[j]
Pt	$^3A_{1g}/D_{4h}$	$^1A_1'/D_{5h}$	83.43	84.32	84.17	-1.08[m]	-0.61	0.13	-3.65	79.0	-6.2
Pt	$^3A_{1g}/D_{4h}$	$^3A'/C_s$	90.51	85.75		-0.16[i]		-1.30	0.08	84.4	-0.1[n]
Au	$^2B_{2g}/D_{4h}$	$^2B_2/C_{2v}$	87.82	83.91	83.30	-0.06[m]	-1.83	0.30	-3.24	78.5	-32.3
Au	$^2B_{2g}/D_{4h}$	$^2A'/C_s$	119.52	115.68		-0.23[i]		0.24	-3.93	111.8	2.0[n]

[a] See Supporting Information for details of calculations on MF_7^-. [b] The second row for each metal is for the MF_7^- non-classical structure. [c] Extrapolated using the mixed Gaussian/exponential formula. [d] CCSD(T)/awCVTZ. [e] See equation (1). [f] SO correction at the ADF ZORA BLYP/TZ2P level. [g] BDE = EA(F) – EA (MF_6) + FA (MF_6) (see text). [h] MP2/aD-PP. [i] B3LYP/aD-PP. [j] CCSD(T)/aT-PP values for the EA and FA(MF_6) are used together with the ZPE. [k] BP86/aT-PP. [l] BP86/aD-PP. [m] B3LYP/aT-PP. [n] CCSD(T)/aT-PP values for the EA and FA(MF_6) are used together with the ZPE, ΔE_{rel}, and ΔE_{SO} corrections.

Table 2.10. Calculated Fluoride Affinities for MF_5 in kcal/mol.

M	MF_5 State/Sym	MF_6^- State/Sym	ΔFA_{CBS}[a]	ΔE_{ZPE}	ΔE_{CV}[b]	ΔE_{rel}[c]	ΔE_{SO}[d]	FA
W	$^2A_2/C_{2v}$	$^2B_{2g}/D_{4h}$	112.5	-0.70[e]	0.33	-0.06	0.78	112.9
Re	$^3A_1'/D_{3h}$	$^3A_{1g}/D_{4h}$	114.9	-1.69[f]	0.89	-0.27	2.59	116.4
Os	$^4B_1/C_{4v}$	$^4A_{1g}/O_h$	133.4	-1.64[f]	0.91	-0.44	-0.27	132.0
Ir	$^5B_1/C_{4v}$	$^3A_{1g}/D_{4h}$	137.8	-1.12[g]	0.05	1.13	-3.25	134.6
Pt	$^2B_1/C_{4v}$	$^2B_{2g}/D_{4h}$	129.3	-2.19[g]	1.00	-0.22	2.87	130.7
Au	$^1A_1/C_{4v}$	$^1A_{1g}/O_h$	140.3	-1.94[g]	1.09	0.37	-3.27	136.6

[a] Extrapolated using the mixed Gaussian/exponential formula. [b] CCSD(T)/awCVTZ. [c] See equation (1). [d] SO correction at the ADF ZORA BLYP/TZ2P level. [e] ADF ZORA SO BLYP/TZ2P. [f] BP86/aD-PP. [g] B3LYP/aT-PP.

Table 2.11. Average deviations of the MF_6 electron affinities, MF_5 and MF_6 fluoride affinities, and first adiabatic M –F bond dissociation energies from the CCSD(T) calculated values in kcal/mol.

Functional	**References**	**EA(MF_6)**	**FA(MF_5)**	**FA(MF_6)**	**M-F BDE**
SVWN5	48,49	23.9	0.5	3.8	-41.1
BLYP	24, 50	20.6	16.3	15.7	-11.2
BP86	50, 51	20.7	14.3	13.9	-15.4
PW91	52, 53	20.5	8.2	8.1	-8.4
PBE	54, 55	22.6	13.1	12.7	-16.3
TPSS	56	21.9	10.2	9.7	-12.3
HCTH	57	15.8	19.0	19.2	-7.9
B3LYP	23, 24	4.5	8.6	6.4	1.2
mPW1	52, 53, 58	4.5	5.4	4.0	3.0
PBE1	54	6.0	5.2	3.3	1.8
O3LYP	24, 59	13.7	16.4	14.5	-38.8
TPSSh	56	21.8	2.8	2.0	-34.0

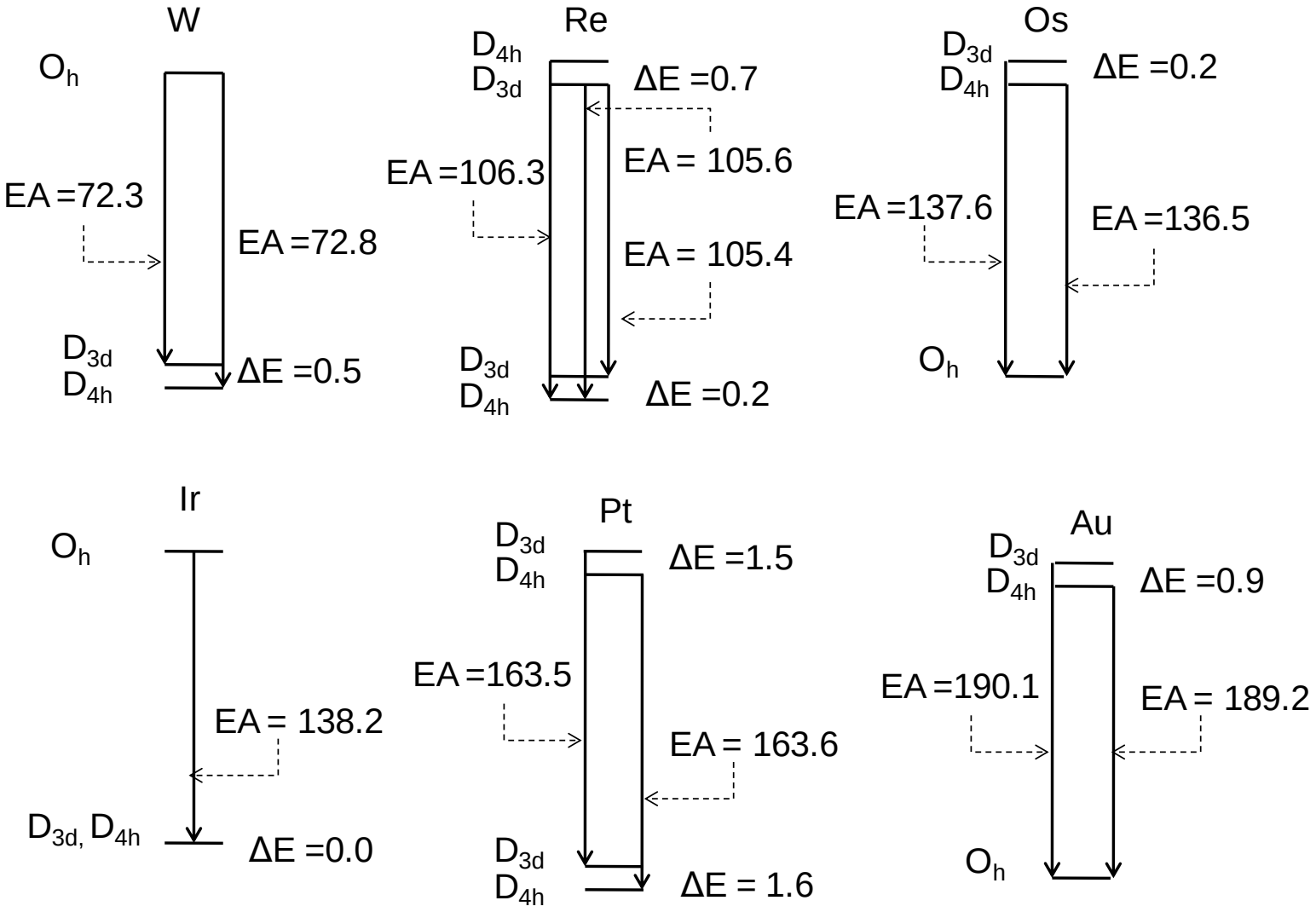

Figure 2.1. Schematic Energy Level Diagram for Use in Predicting the Molecular Electron Affinities for the MF_6 in kcal/mol.

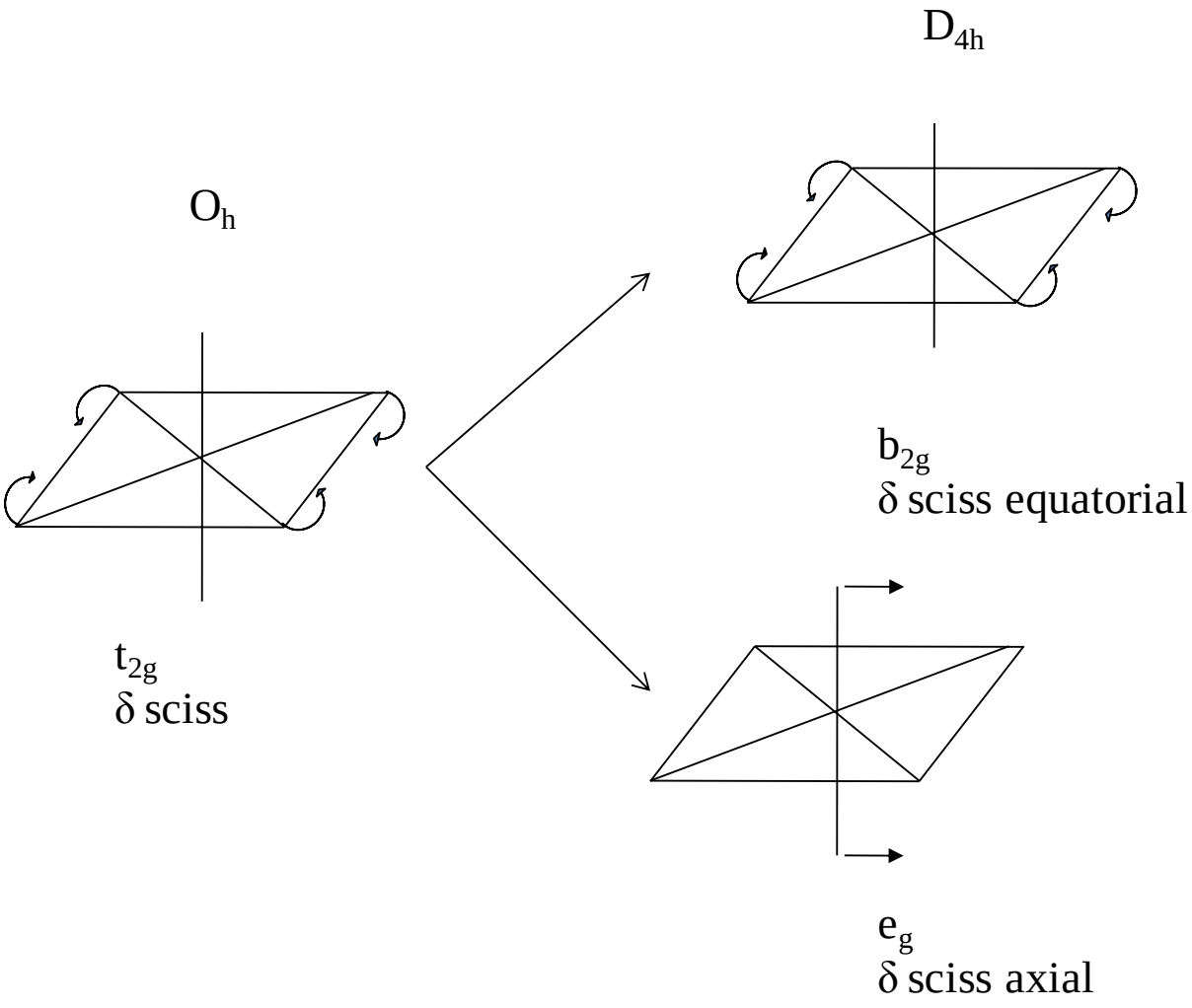

Figure 2.2. Symmetry coordinates for the MF_6 scissoring mode splitting into its two components, i.e., equatorial and axial scissoring upon lowering of the symmetry from O_h to D_{4h}. When the 4 equatorial bonds are shorter than the axial ones, the b_{2g} mode has the higher frequency and, when they are longer, the axial e_g deformation has the higher frequency.

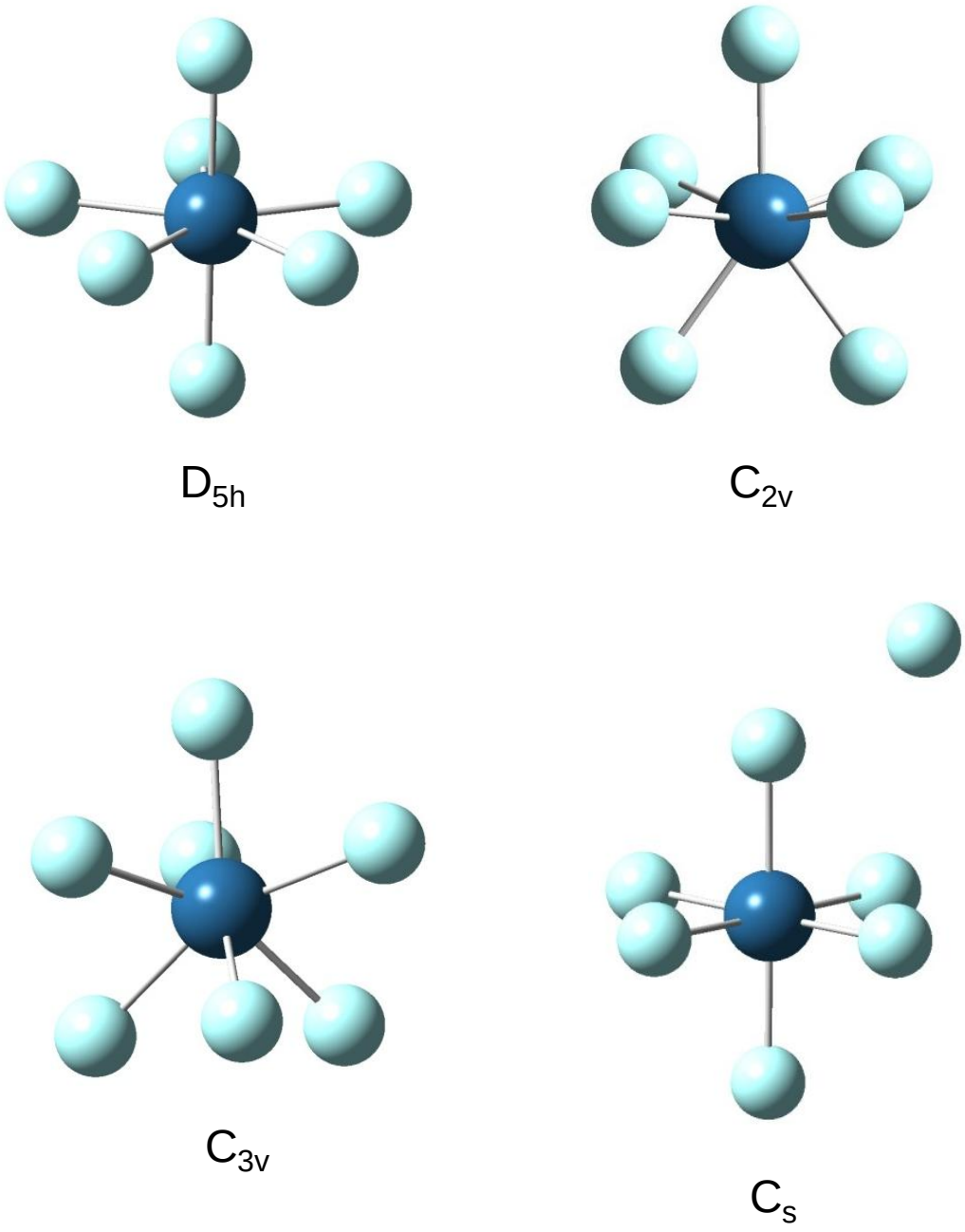

Figure 2.3. Optimized Geometries for the Four Different Structures for MF_7^- as Exemplified by WF_7^- or PtF_7^-. The structures are pentagonal bipyramid (D_{5h}), mono-capped octahedron (C_{3v}), mono-capped trigonal prism (C_{2v}), and the nonclassical (C_s).

References

[1] Bartlett, N.; Sladky, F. O. *The Chemistry of Krypton, Xenon and Radon*. In *Comprehensive Inorganic Chemistry*; Bailar, J. C., Jr.; Emeléus, H. J.; Nyholm, R.; Trotman-Dickenson, A. F.; Eds.; Pergamon Press: Oxford, U.K., **1973,** *Vol. 1,* 213-330.

[2] Malm, J. G.; Selig, H.; Jortner, J.; Rice, S .A. *Chem. Rev.*, **1965,** *65*, 199-236.

[3] Bartlett, N. *Proc. Chem. Soc.* **1962,** 218.

[4] Graham, L.; Gaudejus, O.; Jha, N. K.; Bartlett, N. *Coord. Chem. Rev.* **2000,** *197*, 321-334.

[5] Bartlett, N.; Lohmann, D. H. *Proc. Chem. Soc*. **1962**, 115.

[6] Bartlett, N; Beaton, S.P.; Jha, N.K.; *Chem. Commun.* **1966**, *6*, 169.

[7] Bartlett, N. *Angew. Chem. Int. Ed.* **1968,** *7*, 433.

[8] George, P M.; Beauchamp, J. L. *Chemical Physics* **1979**, *36*, 345.

[9] Viggiano, A. A.; Paulson, J. F.; Dale, F.; Henchman, M.; Adams, N. G.; Smith, D. *J. Phys. Chem*. **1985**, *89*, 2264.

[10] Korobov, M.V.; Kuznetsov, S.V.; Sidorov, L.N.; Shipachev, V.A.; Mit'kin, V.N. *Int. J. Mass. Spectrom. Ion Processes* **1989**, *87*, 13.

[11] Moffit, W.; Goodman, G.L.; fred, M.; Weinstock, B. *Mol. Phys.* **1959**, *2*, 109.

[12] Weinstock, B.; Claassen, H.H. *J. Chem. Phys*. **1959**, *31*, 262.

[13] Weinstock, B.; Claassen, H.H.; Malm, J.G. *J. Chem. Phys*. **1960**, *32*, 181.

[14] Weinstock, B.; Claassen, H.H.; Chernick, C.L. *J. Chem. Phys*. **1963**, *38*, 1470.

[15] Weinstock, B.; Goodman, G. *Advan. Chem. Phys*. **1965**, *9*, 169.

[16] Claassen, H.H.; Selig, H. *Israel J. Chem.* **1969**, *7*, 499.

[17] Claassen, H.H.; Goodman, G.L.; Holloway, J. H.; Selig, H. *J. Chem. Phys*. **1970**, *53*, 341.

[18] (a) Molski, M.J.; Seppelt, K. *Dalton Trans*, **2009**, 3379; (b) Seppelt, K. *Acc. Chem. Res.* **2003**, *36*, 147.

[19] Richardson, A. D.; Hedberg, K.; Lucier, G. M.; *Inorg. Chem*. **2000**, *39*, 2787.

[20] Drews, T.; Super, J.; Hagenbach, A.; Seppelt, K. *Inorg. Chem.* **2006**, *45*,3782.

[21] Quiñones, G.S.; Hägele, G.; Seppelt, K. *Chem. Eur. J*. **2004**, *10*, 4755.

[22] Parr, R. G.; Yang, M. *Density-Functional Theory of Atoms and Molecules*, Oxford University Press: New York, 1989

[23] Becke, A. D. *J. Chem. Phys.* **1993**, *98*, 5648.

[24] Lee, C.; Yang, W.; Parr, R. G. *Phys. Rev. B* **1988**, *37*, 785.

[25] Graudejus, O.; Wilkinson, A. P.; Chacon, L. C.; Bartlett, N. *Inorg. Chem* **2000**, *39*, 2794.

[26] Graudejus, O.; Elder, S. H.; Lucier, G. M.; Shen, C.; Bartlett, N. *Inor. Chem.* **1999**, *38*, 2503.

[27] Leary, K.; Bartlett, N. *J. Chem. Soc., Chem. Commun.* **1972**, 903.

[28] Chase, M.W. Jr. *NIST-JANAF Thermochemical Tables*, 4th ed., *J. Phys. Chem. Reference Data* **1998**, Mono. 9, Suppl. 1.

[29] Myers, O.E.; Brady, A.P. *J. Phys. Chem*. **1960**, *64*, 591.

[30] O'Hare, P.A.G.; Hubbard, W.N. *J. Phys. Chem.* **1966**, *70*, 3353.

[31] Schroeder, J.; Sieben, F.J. *Chemische Berichte*, **1970**, *103*,76.

[32] Pervov, V.S.; Klyuev, L.I.; Gaisinskaya, O.M.; Medvedev, V.A.; Nikolaev, N.S. *Doklady Akademii Nauk SSSR* **1972**, *205*, 349.

[33] Burgess, J.; Fraser, C.J.W.; Peacock, R.D *J. Chem. Soc., Dalton Trans.* **1973**, 501.

[34] Ruff, O.; Fischer, J. *Zeitschrift fuer Anorganische und Allgemeine Chemie*, **1929**, *179*, 161.

[35] Korobov, M.V.; Nikulin, V.V.; Chilingarov, N.S.; Sidorov, L.N. *J. Chem. Thermodynamics* **1986**, *18*, 235.

[36] Nikitin, M.I.; Karpukhina, E.V. *Zhurnal Neorganicheskoi Khimii*, **2007**, *52*, 531.

[37] Gutsev, G. L.; Boldyrev, A.I. *Chem. Phys. Lett*. **1983**, *101*, 441.

[38] Gutsev, G. L.; Levin, A.A. *Chem. Phys.* **1980**, *51*, 459.

[39] Miyoshi, E.; Sakai, Y.; Murakami, A.; Iwaki, H.; Terashima, H.; Shoda, T.; Kawaguchi, T. *J. Chem. Phys***. 1988**, *89*, 4193.

[40] Miyoshi, E.; Sakai, Y. *J. Chem. Phys.* **1988**, *89*, 7363.

[41] Macgregor, S. A; Moock, K. H. *Inorg. Chem.* **1998**, *37*, 3284.

[42] Wesendrup, R.; Schwerdtfeger, P. *Inorg. Chem.* **2001,** *40*, 3351.

[43] Riedel, S.; Kaupp, M. *Inorg. Chem.* **2006**, *45*, 1228.

[44] Riedel, S. *Journal of Fluorine Chemistry* **2007**, *128*, 938.

[45] Alvarez-Thon, L.; David, J.; Arratia-perez, R.; Seppelt, K. Phys. Rev. A 2008, 77, 034502 .

[46] David, J.; Fuentealba, P.; Restrepo, A. *Chem. Phys. Lett.* **2008**, *457*, 42.

[47] Christe, K. O.; Dixon, D. A.; McLemore, W.W., Wilson, Sheehy, J.; Boatz, J. A. *J. Fluorine Chem.* **2000**, *101*, 151; *Chem. Eng. News*, pp. 48-49, March 3, 2003.

[48] Slater, J. C. *Quantum Theory of Molecules and Solids*; McGraw-Hill: New York, 1974; Vol. 4.

[49] Vosko, S. H.; Wilk, L.; Nusair, M. *Can. J. Phys* **1980**, *58*, 1200.

[50] Becke, A. D. *Phys. Rev. A* **1988**, *38*, 3098.

[51] Perdew J. P. *Phys. Rev. B* **1986**, *33*, 8822.

[52] Perdew, J. P.; Wang, Y. *Phys. Rev. B* **1991**, *45*, 13244.

[53] Burke, K.; Perdew, J. P. Wang. Y. In *Electronic Density Functional Thoery: Recent Progress and New Directions*; Dobson, J. F., Vignale, G., Das, M. P., Eds.; Plenum: New York, 1998 p.81.

[54] Perdew, J. P.; Burke, K.; Ernzerhof, M. *Phys. Rev. Lett.* **1996**, *77*, 3865.

[55] Perdew, J. P.; Burke, K.; Ernzerhof, M. *Phys. Rev. Lett.* **1997**, *78*, 1396.

[56] Tao, J. M.; Perdew, J. P.; Staroverov, V. N.; Scuseria, G. E. *Phys. Rev. Lett.* **2003**, *91*, 146401.

[57] Hamprecht, F. A.; Cohen, A. J.; Tozer, D. J.; Handy, N. C. *J. Chem. Phys.* **1998**, *109*, 6264.

[58] Adamo, C.; Barone, V. *Chem. Phys. Lett.* **1997**, *274*, 242.

[59] Handy, N. C.; Cohen, A. J. *Mol. Phys.* **2001**, *99*, 403.

[60] Kendall, R. A.; Dunning, T. H. Jr. Harrison, R. J. *J. Chem. Phys.* **1994**, *96*, 6796.

[61] Figgen, D.; Peterson, K. A.; Dolg, M.; Stoll, H. *J. Chem. Phys*. **2009**, *130*, 164108.

[62] Purvis, G.D., III; Bartlett, R.J. J.Chem. Phys. 1982, 76, 1910.

[63] Raghavachari, K.; Truck, G.W.; pople, J.A.; Head-Gordon, M. *Chem. Phys. Lett*. **1989**, *157*, 479.

[64] Watts, J. D.; Gauss, J.; Bartlett, R. J. *J. Chem.. Phys.* **1993**, *98*, 8718.

[65] Bartlett, R. J.; Musial, M. *Rev. Mod. Phys.* **2007**, *79*, 291.

[66] Peterson, K. A.; Woon, D. E.; Dunning, T. H. Jr. *J. Chem. Phys.* **1994**, *100*, 7410.

[67] Woon, D. E.; Dunning, T. H. Jr. *J. Chem. Phys.* **1995**, *103*, 4572.

[68] Peterson, K. A.; Dunning, T. H. Jr. *J. Chem. Phys.* **2002**, *117*, 10548.

[69] (a) Douglas, M.; Kroll, N. M. *Ann. Phys.*, **1974**, *82*, 89; (b) Hess, B. A. *Phys. Rev. A.*, **1985**, *32*, 756. (c) Hess, B. A. *Phys. Rev. A.*, **1986**, *33*, 3742.

[70] de Jong, W. A.; Harrison, R. J. ; Dixon, D. A. *J. Chem. Phys.*, **2001**, *114*, 48.

[71] EMSL basis set library. http://www.emsl.pnl.gov/forms/basisform.html

[72] (a) van Lenthe, E.; Ehlers, A.E. Baerends, E.J. *J. Chem. Phys*. **1999**, *110*, 8943; (b) van Lenthe, E.; Baerends, E.J.; Snijders, J.G. *J. Chem. Phys* **1993,** *99*, 4597; (c) van Lenthe, E.; Baerends, E.J.; Snijders, J.G.. *J. Chem. Phys* **1994,** *101*, 9783 ; (d) van Lenthe, E.; Snijders,

J.G.; Baerends, E.J. *J. Chem. Phys* **1994,** *105*, 6505; (e) van Lenthe, E.; van Leeuwen, R.; Baerends, E.J.; Snijders, J.G. *Int. J. Quantum Chem*. **1996,** *57*, 281

[73] (a) G. te Velde, F.M. Bickelhaupt, S.J.A. van Gisbergen, C. Fonseca Guerra, E.J. Baerends, J.G. Snijders and T. Ziegler, *Chemistry with ADF.* ; (b) C. Fonseca Guerra, J.G. Snijders, G. te Velde and E.J. Baerends, *Towards an order-N DFT method.* Theoretical Chemistry Accounts **99**, 391 (1998); (c) ADF2008.01, SCM, Theoretical Chemistry, Vrije Universiteit, Amsterdam, The Netherlands, http://www.scm.com

[74] Moore, C. E. *Atomic energy levels as derived from the analysis of optical spectra, Volume 1, H to V*; U.S. National Bureau of Standards Circular 467, U.S. Department of Commerce, National Technical Information Service, COM-72-50282: Washington, D.C., 1949.

[75] Wagman, D.D.; Evans, W.H.; Parker, V.B.; Schumm, R.H.; Halow, I.; Bailey, S.M.; Churney, K.L.; Nuttall, R.L. *J. Phys. Chem. Ref. Data*, **1982**, *11*, Supplement 2.

[76] Greenwood, N.N.; Earnshaw, A. *Chemistry of the Elements*, Pergamon Press, Oxford, 1984 (W, Chapter 23, pg. 1170; Re, Chapter 24, pg. 1214, Os, Chapter 25, pg. 1248; Ir, Chapter 26, pg. 1294; Pt,Chapter 27, pg. 1333, Au, Chapter 28, pg 1368).

[77] (a) Feller, D.; Dixon, D. A. *J. Phys. Chem. A* **2000**, *104*, 3048; (b) Feller, D.; Dixon, D. A. *J. Chem. Phys.* **2001**, *115*, 3484; (c) Dixon, D.A.; Feller, D.; Peterson, K.A. *J. Chem. Phys*., **2001**, *115*, 2576; (d) Ruscic, B.; Wagner, A. F.; Harding, L. B.; Asher, R. L.; Feller, D.; Dixon, D. A.; Peterson, K. A.; Song, Y.; Qian, X.; Ng, C.; Liu, J.; Chen, W.; Schwenke, D. W. *J. Phys. Chem. A* **2002**, *106*, 2727. (e) Feller, D.; Dixon, D. A., *J. Phys. Chem. A*, **2003**, *107*, 9641 (f) Dixon, D.A.; Feller, D.; Christe, K. O.; Wilson, W. W.; Vij, A.; Vij, V.; Jenkins, H. D. B.; Olson, R. M.; Gordon, M. S. *J. Am. Chem. Soc.*, **2004**, *126*, 834; (g) Dixon, D. A.; Gutowski, M. *J. Phys. Chem. A*, **2005**, *109*, 5129; (h) Pollack, L.; Windus, T. L.; de Jong, W. A.; Dixon, D.A. *J. Phys.*

Chem. A, **2005**, *109*, 6934; (i) Gutowski K. E.; Dixon, D.A. *J. Phys. Chem. A*, **2006**, *110*, 12044 (j) Matus, M. H.; Anderson, K. D.; Camaioni, D. M.; Autrey, S. T.; Dixon, D. A. *J. Phys. Chem. A*, **2007**, *111*, 4411 ; (k) Feller, D.; Peterson, K.A.; Dixon, D.A. *J. Chem. Phys*., **2008**, *129* 204015.

[78] Marx, R.; Seppelt, K.; Ibberson, R.M. *J. Chem. Phys* **1996,** *104*, 7658.

[79] Hoskins, B.F.; Linden, A.; Mulvaney, Pc.C.; O'Donnell, T.A; *Inorg. Chim. Acta* **1984**, *88*, 217.

[80] Fitz, H.; Muller, B. G.; Graudejus, O.; Bartlett, N. *Z. Anorg. Allg. Chem*. **2002**, *628*, 133.

[81] Graudejus, O.; Muller, B.G. *Z. Anorg. Allg. Chem*. **1996**, *622*, 1076.

[82] Lehmnann, J. F.; Schrobilgen, G. J. *J. Fluorine Chem.* **2003**, *119*, 109.

[83] Leary, K.; Zalkin, A.; Bartlett, N. *Inorg. Chem*. **1974**, *13*, 775.

[84] Li, S.; Dixon, D.A. *J. Phys. Chem. A* **2007**, *111*, 11908.

[85] Blondel, C.**;** Delsart, C.; Goldfarb, F., *J. Phys. B*.**, 2001**, *34*, L281.

[86] Friedman, J.F.; Stevens, A.E.; Miller, T.M.; Viggiano, A.A. *J. Chem. Phys.* **2006**, *124*, 224306.

[87] Miller, T.M. in *Handbook of Chemistry and Physics, 86th ed*. Ed., Lide, D.R.; CRC, Boca Raton, FL; 2005, Sec. 10, pp 156-172.

[88] Karton, A.; Martin, J. M. L. *J. Phys. Chem. A* **2007**, *111*, 5936.

[89] Luo, T.-R. *Comprehensive Handbook of Chemical Bond Energies*; CRC Press, Taylor & Francis Group: Boca Raton, FL, 2007.

[90] Lin, Z.; Bytheway, I. *Inorg. Chem.* **1996**, *35*, 594.

[91] Christe, K. O.; Curtis E. C.; Dixon, D. A. *J. Am. Chem. Soc*., **1993**, *115*, 1520.

[92] Huber, K.P.; Herzberg, G., Molecular Spectra and Molecular Structure. IV. Constants of Diatomic Molecules,, Van Nostrand Reinhold Co., 1979.

[93] Bondi, A. *J. Phys. Chem*. **1964**, *68*, 441; Mantina, M.; Chamberlain, A.C.; Valero, R.; Cramer, C.J.; Truhlar, D.G. *J. Phys. Chem. A* **2009**, *113*, 5806.

[94] (a) Christe, K. O.; Dixon, D. A.; McLemore, D.; Wilson, W.W.; Sheehy, J.; Boatz, J. A. *J. Fluorine Chem.* **2000**, *101*, 151; (b) *Chem. Eng. News*, pp. 48-49, March 3, 2003.

[95] Christe, K. O. *Inorg. Nucl. Chem. Lett*. **1972,** *8,* 741.

[96] Roberto, F. Q. *Inorg. Nucl. Chem. Lett*. **1972,** *8,* 737.

[97] Christe, K. O.; Wilson, W. W.; Wilson, R. D. *Inorg. Chem* **1984,** *23,* 2058.

[98] Gutsev, G. L.; Boldyrev, A. I. *Chem. Phys,* **1981,** *56,* 277.

[99] Burgess, J.; Peacock, R.D *J. Fluorine Chem.* **1977**, *10*, 479.

[100] Hwang, I.C.; Seppelt, K. *Angew. Chem. Int. Ed.* **2001**, *40*, 19.

Appendix: Electron Affinities, Fluoride Affinities, and Heats of Formation of the Third Row Transition Metal Hexafluorides: MF_6 (M=W, Re, Os, Ir, Pt, Au)

Supporting Information Experimental atomic heats of formation in kcal/mol, benchmarked DFT exchange-correlation functional, relative energy differences between the D_{4h} and D_{3d} MF_6 structures, EA(MF_6), FA(MF_5), FA(MF_6) and first M-F BDEs calculated with various exchange-correlation functional, adiabatic electron affinities of MF_6**,** vertical electron detachment energies (VDE) of MF_6^- and vertical electron attachment energies (VAE) of MF_6 in kcal/mol calculated at the CCSD(T)/aT-PP//CCSD(T)/aD-PP, B3LYP/aT-PP//B3LYP/aD-PP and CCSD(T)/aT-DK// CCSD(T)/aT-PP levels, MF_6 MF_6^-, MF_5, and MF_7^- total electronic energies and vibrational frequencies at the DFT level with various exchange-correlation functionals and the aD-PP basis set, zero point energies (ZPE), CCSD(T) total energies as a function of basis set, core and valence energies at the CCSD(T)/aug-cc-pWCVTZ-PP level, and scalar relativistic energies at the CISD/aT-PP and CCSD(T)-DK/aug-cc-pVTZ-DK levels, T1 diagnostics. Energy differences in kcal/mol of D_{4h} vs O_h structures for the same spin state and singlet –triplet splitting energies for the D_{4h} structures. Optimized geometry parameters with different DFT functionals. Pseudopotential errors and scalar relativistic corrections for EA(MF_6), 1^{st} M –F BDEs, total atomization energies, FA(MF_6), and FA(MF_5). Electron affinities calculated at the ZORA and ZORA+SO levels. Mulliken charges, NBO charges, and spin densities for MF_6 and MF_6^- and figures for the spin densities. First M –F BDEs, FA(MF_6), and FA(MF_5) calculated at the DFT and CCSD(T) levels as a function of basis set. MF_5 optimized geometry at the B3LYP/aT-PP, BLYP/TZ2P scalar relativistic ZORA and ZORA plus spin orbit levels .Cartesian xyz coordinates for all molecules.

Figure A2.1. Electron spin densities of MF_6^- calculated at the B3LYP/aD-PP level.

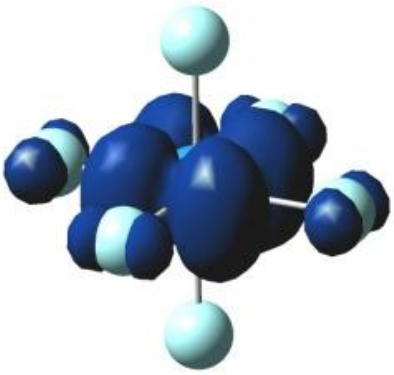

WF_6^- dt_{2g}^1

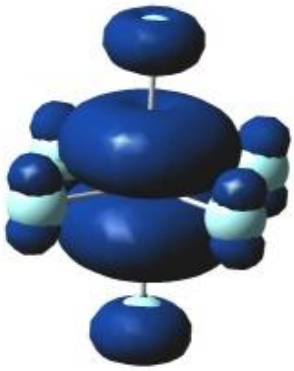

ReF_6^- dt_{2g}^2

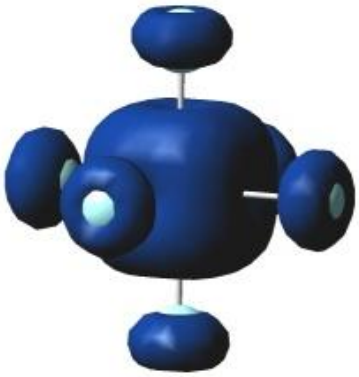

OsF_6^- dt_{2g}^3

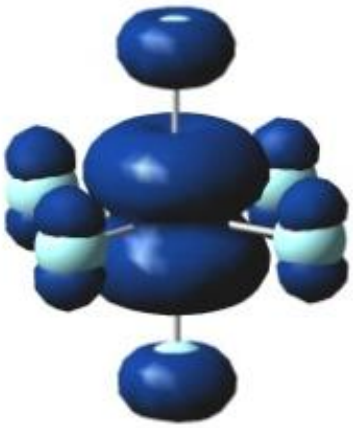

IrF_6^- dt_{2g}^4

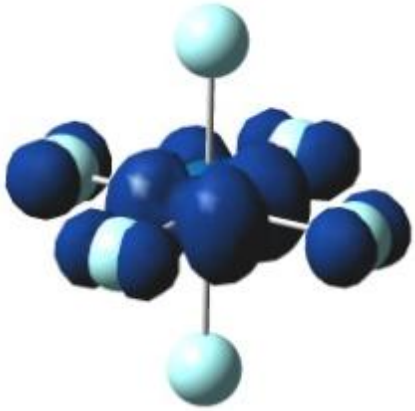

PtF_6^- dt_{2g}^5

Figure A2.2. Total electron spin densities of MF_6 at the B3LYP/aD-PP level.

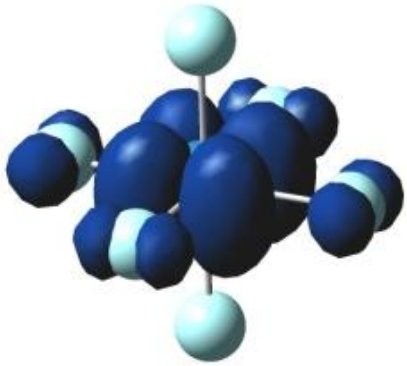

ReF_6 dt_{2g}^1

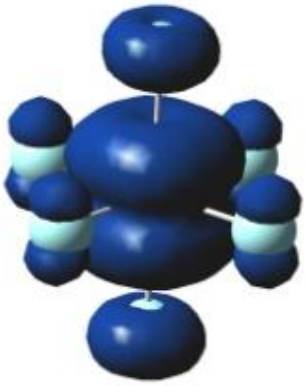

OsF_6 dt_{2g}^2

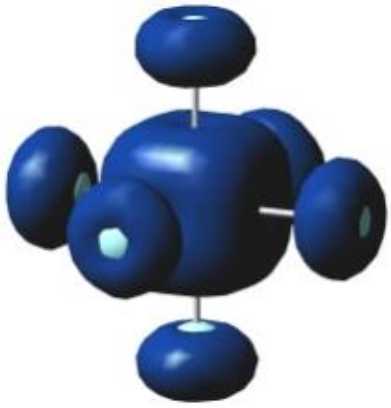

IrF_6 dt_{2g}^3

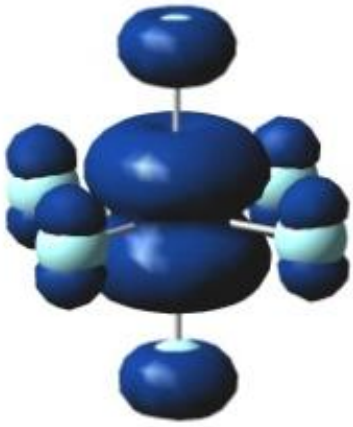

PtF_6 dt_{2g}^4

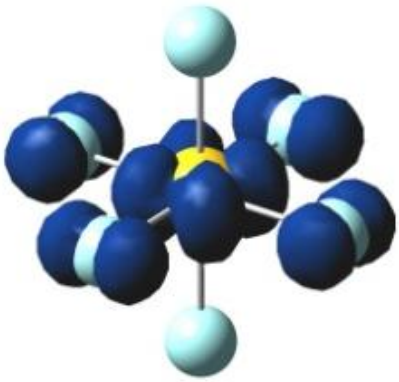

AuF_6 dt_{2g}^5

Table A2.1. MF_6 and MF_6^- number of d electrons and spin states.

molecule	neutral	Spin	Jahn-Teller distortion	anion	Spin	Jahn-Teller distortion
WF_6	t_{2g}^0	singlet	No	t_{2g}^1	doublet	Yes
ReF_6	t_{2g}^1	doublet	Yes	t_{2g}^2	triplet	Yes
OsF_6	t_{2g}^2	triplet	Yes	t_{2g}^3	quartet	No
IrF_6	t_{2g}^3	quartet	No	t_{2g}^4	triplet	Yes
PtF_6	t_{2g}^4	triplet	Yes	t_{2g}^5	doublet	Yes
AuF_6	t_{2g}^5	doublet	Yes	t_{2g}^6	singlet	No

Table A2.2. Experimental atomic heats of formation in kcal/mol.

Atom	**JANAF**[a] **0 K**	**Greenwood** [b] **298 K**	**Wagman et al.**[c] **0 K**	**Wagman et al.** [c] **298 K**
F	18.47 ± 0.07			
W	203.1 ± 1.5	202.9 ± 3.1	202.7	203.0
Re		186.2 ± 1.9	183.8	184.0
Os		189.0 ± 3.1	188.8[d]	189.0
Ir		159.9 ± 1.9	158.8	159.0
Pt		130.3 ± 5.0	134.9	135.1
Au		90.6 ± 1.9	87.5	87.5

[a] Reference 28. [b] Reference 76. [c] Reference 75. [d] estimated value. See text.

Table A2.3. Benchmarked DFT exchange-correlation functionals.

Functional	**exchange**	**correlation**	**type**	**refs.**
SVWN5	Slater	VWN5	LSDA	48,49
BLYP	Becke 88	Lee-Yang-Parr	GGA	24, 50
BP86	Becke 88	Perdew 86	GGA	50, 51
PW91	Perdew-Wang 91	Perdew-Wang 91	GGA	52, 53
PBE	Perdew-Burke-Ernzerhof	Perdew-Burke-Ernzerhof	GGA	54, 55
TPSS	Tao-Perdew-Staroverov-Scuseria	Tao-Perdew-Staroverov-Scuseria	GGA	56
HCTH	Handy	Handy	GGA	57
B3LYP	Becke 93	Lee-Yang-Parr	HGGA	23,24
mPW1	Barone's modified PW91	Perdew-Wang 91	HGGA	52, 53, 58
PBE1	Perdew-Burke-Ernzerhof	Perdew-Burke-Ernzerhof	HGGA	54
O3LYP	Handy's OPTX	Lee-Yang-Parr	HGGA	24, 59
TPSSh	Tao-Perdew-Staroverov-Scuseria	Tao-Perdew-Staroverov-Scuseria	HGGA	56

Table A2.4. Optimized metal-fluorine bond lengths (Å) and bond angles (degrees) with different DFT functionals and the aD-PP and aT-PP basis sets.

Molecule	**State/Sym**	**B3LYP**	**BLYP**	**CCSD(T)**	**B3LYP**	**BP86**	**TPSSh**	**TPSS**	**PW91**
		aD-PP	**aD-PP**	**aD-PP**	**aT-PP**	**aD-PP**	**aD-PP**	**aD-PP**	**aD-PP**
WF_6	$^1A_{1g}/O_h$	1.847	1.869	1.847	1.840	1.859	1.846	1.855	1.857
WF_6^-	$^2B_{2g}/D_{4h}$	1.878 (x2) 1.932 (x4)	1.898 (x2) 1.954 (x4)	1.878 (x2) 1.933 (x4)	1.869 (x2) 1.927 (x4)	1.888 (x2) 1.941 (x4)	1.875 (x2) 1.929 (x4)	1.884 (x2) 1.938 (x4)	1.886 (x2) 1.939 (x4)
WF_6^-	$^2A_{1g}/D_{3d}$	1.914 92.6°		1.914 92.5°	1.906 92.8°				
ReF_6	$^2B_{2g}/D_{4h}$	1.819 (x2) 1.859 (x4)	1.844 (x2) 1.884 (x4)	1.817 (x2) 1.857 (x4)	1.810 (x2) 1.852 (x4)	1.833 (x2) 1.872 (x4)	1.819 (x2) 1.857 (x4)	1.829 (x2) 1.868 (x4)	1.831 (x2) 1.870 (x4)
ReF_6	$^2A_{1g}/D_{3d}$	1.845 91.8°		1.844 91.7°	1.838 91.9°				
ReF_6^-	$^3A_{1g}/D_{4h}$	1.943 (x2) 1.891 (x4)	1.967 (x2) 1.914 (x4)	1.941 (x2) 1.888 (x4)	1.937 (x2) 1.883 (x4)	1.954 (x2) 1.902 (x4)	1.939 (x2) 1.888 (x4)	1.949 (x2) 1.897 (x4)	1.952 (x2) 1.899 (x4)
ReF_6^-	$^3A_{1g}/D_{3d}$	1.907 91.6°		1.905 90.7°	1.900 91.7°				
OsF_6	$^3A_{1g}/D_{4h}$	1.873 (x2) 1.836 (x4)	1.901 (x2) 1.865 (x4)	1.872 (x2) 1.834 (x4)	1.867 (x2) 1.828 (x4)	1.888 (x2) 1.852 (x4)	1.871 (x2) 1.836 (x4)	1.883 (x2) 1.847 (x4)	1.886 (x2) 1.850 (x4)
OsF_6	$^3A_{1g}/D_{3d}$	1.849 92.8°		1.847 90.7°					
OsF_6^-	$^4A_{1g}/O_h$	1.905	1.931	1.886	1.897	1.918	1.902	1.912	1.915
IrF_6	$^4A_{1g}/O_h$	1.872	1.887	1.851	1.846	1.873	1.854	1.866	1.870

IrF_6^-	$^3A_{1g}/D_{4h}$	1.877 (x2) 1.921 (x4)	1.907 (x2) 1.952 (x4)	1.870 (x2) 1.915 (x4)	1.866 (x2) 1.932 (x4)	1.893 (x2) 1.937 (x4)	1.875 (x2) 1.917 (x4)	1.887 (x2) 1.930 (x4)	1.891 (x2) 1.934 (x4)
IrF_6^-	$^3A_{1g}/D_{3d}$	1.906 91.1°		1.900 91.1°	1.897 91.2°				
PtF_6	$^3A_{1g}/D_{4h}$	1.854 (x2) 1.879 (x4)	1.889 (x2) 1.916 (x4)	1.846 (x2) 1.875 (x4)	1.841 (x2) 1.870 (x4)	1.873 (x2) 1.899 (x4)	1.853 (x2) 1.878 (x4)	1.868 (x2) 1.893 (x4)	1.870 (x2) 1.897 (x4)
PtF_6	$^3A_{1g}/D_{3d}$	1.870 90.7°		1.866 90.1°	1.860 90.7°				
PtF_6^-	$^2B_{2g}/D_{4h}$	1.948 (x2) 1.898 (x4)	1.9814(x2) 1.931 (x4)	1.936 (x2) 1.890 (x4)	1.939 (x2) 1.873 (x4)	1.963 (x2) 1.915 (x4)	1.943 (x2) 1.895 (x4)	1.956 (x2) 1.909 (x4)	1.961 (x2) 1.912 (x4)
PtF_6^-	$^2A_{1g}/D_{3d}$	1.913 90.6°		1.904 90.5°	1.904 90.7°				
AuF_6	$^2B_{2g}/D_{4h}$	1.918(x2) 1.883(x4)	1.956 (x2) 1.924 (x4)	1.9193 (2) 1.8824 (4)	1.9108 (2) 1.8728 (4)	1.9367 (2) 1.9054 (4)	1.915 (x2) 1.882 (x4)	1.930 (x2) 1.899 (x4)	1.934 (x2) 1.903 (x4)
AuF_6	$^2A_{1g}/D_{3d}$	1.893 90.4°		1.893 90.1°	1.885 90.4°				
AuF_6^-	$^1A_{1g}/O_h$	1.929	1.966	1.9205	1.920	1.9473	1.925	1.940	1.945

Table A2.5. Components of the relative energy difference (ΔE) between the D_{4h} and D_{3d} structures in kcal/mol.

MF_6/MF_6^-	State/Sym D_{4h}	State/Sym D_{3d}	ΔE_{CBS} [a]	ΔE_{ZPE}	ΔE_{CV} [b]	ΔE_{Rel} [c]	ΔE_{SO} [d]	ΔE
WF_6^-	$^2B_{2g}$	$^2A_{1g}$	0.02	-0.27[e]	0.11	0.01	0.59	0.5
ReF_6	$^2B_{2g}$	$^2A_{1g}$	0.25	-0.78[f]	0.04	-0.01	-0.23	-0.7
ReF_6^-	$^3A_{1g}$	$^3A_{1g}$	1.04	-0.91[f]	-0.02	0.19	-0.12	0.2
OsF_6	$^3A_{1g}$	$^3A_{1g}$	0.83	-0.36	-0.05	-0.02	-0.15	0.2
IrF_6^-	$^3A_{1g}$	$^3A_{1g}$	0.77	-0.71[f]	-0.07	-0.01	0.0	-0.01
PtF_6	$^3A_{1g}$	$^3A_{1g}$	0.46	0.71[e]	0.01	0.27	0.0	1.5
PtF_6^-	$^2B_{2g}$	$^2A_{1g}$	1.04	0.51[e]	-0.10	0.02	0.0	1.6
AuF_6	$^2B_{2g}$	$^2A_{1g}$	1.08	-0.36[g]	-0.11	-0.01	0.27[h]	0.9

[a] Valence CCSD(T) electronic energy contribution extrapolated using the mixed Gaussian/exponential formula.[b] CCSD(T)/awCVTZ. [c] See equation (1). [d] Spin-orbit correction from BLYP/ZORA + SO/TZ2P calculation.[e] ADF Zora SO BLYP/TZ2P.[f] BP86/aD-PP.[g] B3LYP/aT-PP. [h] Between the O_h and D_{3d} structures.

Table A2.6. Energy differences in kcal/mol of D_{4h} vs O_h structures for the same spin state and singlet –triplet splitting energies for the D_{4h} structures at the B3LYP/aD-PP, CCSD(T)/aD-PP and CCSD(T)/aT-PP levels.

Method	**ReF_6**			**OsF_6**				**PtF_6**				**AuF_6**		
State/symm	**$^2B_{2g}$ D_{4h}**	**$^2A_{1g}$ D_{3d}**	**O_h**	**$^3A_{1g}$ D_{4h}**	**$^3A_{1g}$ D_{3d}**	**O_h**	**$^1A_{1g}$ D_{4h}**	**$^3A_{1g}$ D_{4h}**	**$^3A_{1g}$ D_{3d}**	**O_h**	**$^1A_{1g}$ D_{4h}**	**$^2B_{2g}$ D_{4h}**	**$^2A_{1g}$ D_{3d}**	**O_h**
B3LYP/aD-PP	0.0	-0.6	0.7	0.0	-0.7	0.6	24.2	0.0	0.02	0.2	24.2	0.0	-1.3	0.5
CCSD(T)/aD-PP	0.0	0.2	0.8	0.0	0.7	0.7	24.1	0.0	0.3	0.3	16.8	0.0	1.1	0.5
CCSD(T)/aT-PP	0.0	0.2	1.4	0.0	0.8	1.5	23.6	0.0	0.5	1.3	16.3	0.0	1.2	1.6

Method	**WF_6^-**			**ReF_6^-**				**IrF_6^-**				**PtF_6^-**		
State/symm	**$^2B_{2g}$ D_{4h}**	**$^2A_{1g}$ D_{3d}**	**O_h**	**$^3A_{1g}$ D_{4h}**	**$^3A_{1g}$ D_{3d}**	**O_h**	**$^1A_{1g}$ D_{4h}**	**$^3A_{1g}$ D_{4h}**	**$^3A_{1g}$ D_{3d}**	**O_h**	**$^1A_{1g}$ D_{4h}**	**$^2B_{2g}$ D_{4h}**	**$^2A_{1g}$ D_{3d}**	**O_h**
B3LYP/aD-PP	0.0	-0.6	1.0	0.0	-0.5	1.0	26.8	0.0	-0.2	0.7	25.1	0.0	-0.5	0.9
CCSD(T)/aD-PP	0.0	0.04	1.1	0.0	1.0	1.1	26.8	0.0	0.7	0.8	23.5	0.0	0.9	0.9
CCSD(T)/aT-PP	0.0	0.02	1.2	0.0	1.1	1.2	25.8	0.0	0.8	0.9	23.4	0.0	1.0	1.0

Table A2.7. Pseudopotential errors[a] and scalar relativistic corrections in kcal/mol for the MF_6 electron affinities.

MF_6	State/Sym	$\Delta E_{PP\text{-}error}$[b]	ΔE_{MVD}[c]
WF_6	$^1A_{1g}/O_h$	2.52	-0.16
ReF_6	$^2B_{2g}/D_{4h}$	1.57	-0.18
ReF_6	$^2A_{1g}/D_{3d}$	1.56	-0.17
OsF_6	$^3A_{1g}/D_{4h}$	0.48	-0.19
IrF_6	$^4A_{1g}/O_h$	1.80	-0.21
PtF_6	$^3A_{1g}/D_{4h}$	0.97	-0.23
AuF_6	$^2B_{2g}/D_{4h}$	0.21	-0.26

[a] Estimate of the pseudopotential error was obtained by first calculating a scalar relativistic correction from the expectation values of the mass-velocity and Darwin terms in the Breit-Pauli Hamiltonian at the CISD/aT-PP level for MF_6 and MF_6^- (essentially the relativistic correction for the F atoms). This scalar relativistic correction was added to the CCSD(T)/aT-PP value and the pseudopotential error is given as the difference from the DKH value

[b] $\Delta EA_{PP\text{-}error}$ = EA(CCSD(T)-DK/aT-DK) – EA_{MVD}(CCSD(T)/aT-PP),where

EA_{MVD}(CCSD(T)/aT-PP) = EA(CCSD(T)/aT-PP) + ΔE_{MVD}.

[c] $\Delta E_{MVD} = \Delta E_{MVD}(MF_6) - \Delta E_{MVD}(MF_6^-)$

Table A2.8. Electron Affinities in kcal/mol calculated at the ZORA and ZORA+SO levels.

	BLYP/ZORA		BLYP/ZORA+SO	
Molecule	**Final State/Sym**	**EA**	**Final State/Sym**	**EA**
WF_6/WF_6^-	$^1O_h/^2D_{3d}$	61.39	$^1O_h/^2D_{4h}$	63.30
WF_6/WF_6^-	$^1O_h/^2D_{3d}$	61.40	$^1O_h/^2D_{3d}$	62.71
ReF_6/ReF_6^-	$^2D_{3d}/^3O_h$	87.48	$^2D_{4h}/^3D_{4h}$	88.59
ReF_6/ReF_6^-	$^2D_{3d}/^3D_{3d}$	87.48	$^2D_{3d}/^3D_{3d}$	88.48
OsF_6/OsF_6^-	$^2O_h/^4O_h$	114.08	$^3D_{4h}/^4O_h$	111.41
OsF_6/OsF_6^-	$^3D_{3d}/^4O_h$	113.71	$^3D_{3d}/^4O_h$	111.26
IrF_6/IrF_6^-	$^4O_h/^3D_{3d}$	111.04	$^4O_h/^3D_{4h}$	117.19
IrF_6/IrF_6^-	$^4O_h/^3D_{3d}$	111.24	$^4O_h/^3D_{3d}$	117.22
PtF_6/PtF_6^-	$^3O_h/^2O_h$	136.24	$^3D_{4h}/^2O_h$	136.86
PtF_6/PtF_6^-	$^3O_h/^2O_h$	137.05	$^3D_{3d}/^2O_h$	136.70
AuF_6/AuF_6^-	$^2O_h/^1O_h$	159.20	$^2O_h/^1O_h$	155.30
AuF_6/AuF_6^-	$^2D_{3d}/^1O_h$	162.40	$^2D_{3d}/^1O_h$	155.57

Table A2.9. Mulliken charges for MF_6 and MF_6^- (M = third row transition metals) at the B3LYP and BP86 levels with the aD-PP basis set.[a]

MF_6/MF_6^-	State	B3LYP			BP86		
		M	**F**	**F** (avg)	**M**	**F**	**F** (avg)
WF_6	$^1A_{1g}/O_h$	2.236	-0.370	-0.370	1.903	-0.3170	-0.317
WF_6^-	$^2B_{2g}/D_{4h}$	2.116	-0.466 (2s) -0.546 (4l)	-0.519	1.799	-0.414 (2s) -0.493 (4l)	-0.467
ReF_6	$^2B_{2g}/D_{4h}$	2.094	-0.386 (2s) -0.275(4l)	-0.312	1.763	-0.328 (2s) -0.226 (4l)	-0.260
ReF_6	$^2A_{1g}/D_{3d}$	2.096	-0.349	-0.349	1.765	-0.294(x6)	-0.294
ReF_6^-	$^3A_{1g}/D_{4h}$	2.051	-0.591 (2l) -0.467 (4s)	-0.508	1.735	-0.537 (2l) -0.415 (4s)	-0.456
OsF_6	$^3A_{1g}/D_{4h}$	2.082	-0.442 (2l) -0.299 (4s)	-0.347	1.785	-0.382 (2l) -0.255 (4s)	-0.297
OsF_6^-	$^4A_{1g}/O_h$	2.105	-0.517	-0.517	1.811	-0.468	-0.468
IrF_6	$^4A_{1g}/O_h$	2.175	-0.362	-0.362	1.899	-0.316	-0.316
IrF_6^-	$^3A_{1g}/D_{4h}$	2.137	-0.443 (2s) -0.562 (4l)	-0.522	1.855	-0.406 (2s) -0.511 (4l)	-0.476
PtF_6	$^3A_{1g}/D_{4h}$	2.125	-0.318 (2s) -0.372 (4l)	-0.354	1.871	-0.276 (2s) -0.330 (4l)	-0.312
PtF_6^-	$^2B_{2g}/D_{4h}$	2.099	-0.591 (2l) -0.479 (4s)	-0.516	1.824	-0.547 (2l) -0.435 (4s)	-0.472
AuF_6	$^2B_{2g}/D_{4h}$	2.181	-0.438 (2l) -0.326 (4s)	-0.363	1.935	-0.398 (2l) -0.285 (4s)	-0.323
AuF_6^-	$^1A_{1g}/O_h$	2.182	-0.530	-0.530	1.926	-0.488	-0.488

[a] s = short M-F bond distances. l = long M-F bond distances.

Table A2.10. Electron spin densities for MF_6 and MF_6^- (M = third row transition metals) calculated at the B3LYP/aD-PP and BP86/aD-PP and aT-PP levels ([a] s = short M-F bond distances. l = long M-F bond distances.)

MF_6/MF_6^-	state	B3LYP/aD-PP		BP86/aD-PP		BP86/aT-PP	
		M	**F**	**M**	**F**	**M**	**F**
WF_6^-	$^2B_{2g}/D_{4h}$	0.920	-0.009 (2s) 0.024 (4l)	0.928	-0.011 (2s) 0.023 (4l)	0.926	-0.012 (2s) 0.024 (4l)
ReF_6	$^2B_{2g}/D_{4h}$	0.832	-0.014 (2s) 0.049 (4l)	0.815	-0.014(2s) 0.053(4l)	0.813	-0.015(2s) 0.054 (4l)
ReF_6	$^2A_{1g}/D_{3d}$	0.833	0.028(x6)	0.824	0.029(x6)		
ReF_6^-	$^3A_{1g}/D_{4h}$	1.752	0.077 (2l) 0.024 (4s)	1.721	0.088 (2l) 0.026 (4s)	1.721	0.088 (2l) 0.026 (4s)
OsF_6	$^3A_{1g}/D_{4h}$	1.501	0.164 (2l) 0.042 (4s)	1.424	0.187 (2l) 0.051 (4s)	1.427	0.183 (2l) 0.052 (4s)
OsF_6^-	$^4A_{1g}/O_h$	2.425	0.096	2.314	0.114	2.322	0.113
IrF_6	$^4A_{1g}/O_h$	1.908	0.182	1.758	0.207	1.768	0.205
IrF_6^-	$^3A_{1g}/D_{4h}$	1.453	0.133 (2s) 0.070(4l)	1.336	0.153 (2s) 0.089 (4l)	1.347	0.150 (2s) 0.088 (4l)
PtF_6	$^3A_{1g}/D_{4h}$	0.964	0.196 (2s) 0.161 (4l)	0.860	0.220 (2s) 0.175 (4l)	0.867	0.221 (2s) 0.173 (4l)
PtF_6^-	$^2B_{2g}/D_{4h}$	0.601	-0.009 (2l) 0.104 (4s)	0.529	-0.007 (2l) 0.121 (4s)	0.533	-0.004 (2l) 0.119 (4s)
AuF_6	$^2B_{2g}/D_{4h}$	0.302	-0.007 (2l) 0.178 (4s)	0.261	-0.005 (2l) 0.187 (4s)	0.262	-0.003 (2l) 0.186 (4s)

Table A2.11. NBO Charges and electron spin densities for MF_6 and MF_6^- (M = third row transition metals) calculated at the B3LYP/aT-PP and BP86/aT-PP levels.[a]

molecule	state	Spin density B3LYP/aT-PP		NBO Charges B3LYP/aT-PP		
		M	**F**	**M**	**F**	**F** (avg)
WF_6	$^1A_{1g}/O_h$			2.170	-0.312	-0.312
WF_6^-	$^2B_{2g}/D_{4h}$	0.908	-0.009 (2s) 0.028 (4l)	1.430	-0.235 (2s) -0.240 (4l)	-0.238
ReF_6	$^2B_{2g}/D_{4h}$	0.819	-0.015 (2s) 0.053 (4l)	1.351	-0.149 (2s) -0.138 (4l)	-0.142
ReF_6^-	$^3A_{1g}/D_{4h}$	1.733	0.080 (2l) 0.027 (4s)	1.734	-0.208 (2l) -0.204 (4s)	-0.205
OsF_6	$^3A_{1g}/D_{4h}$	1.488	0.163 (2l) 0.046 (4s)	1.595	-0.079 (2l) -0. 109(4s)	-0.099
OsF_6^-	$^4A_{1g}/O_h$	2.410	0.098	2.021	-0.170	-0.170
IrF_6	$^4A_{1g}/O_h$	1.902	0.183	1.773	-0.045	-0.045
IrF_6^-	$^3A_{1g}/D_{4h}$	1.451	0.134 (2s) 0.070(4l)	1.540	-0. 125(2s) -0.197 (4l)	-0.173
PtF_6	$^3A_{1g}/D_{4h}$	0.793	0.199 (2s) 0.157 (4l)	1.335	-0.027 (2s) -0.070 (4l)	-0.056
PtF_6^-	$^2B_{2g}/D_{4h}$	0.605	-0.007 (2l) 0.102 (4s)	1.138	-0.259 (2l) -0.155 (4s)	-0.190
AuF_6	$^2B_{2g}/D_{4h}$	0.306	-0.005 (2l) 0.176 (4s)	1.061	-0.195 (2l) -0.043 (4s)	-0.094
AuF_6^-	$^1A_{1g}/O_h$			1.755	-0.459	-0.459

[a] s = short M-F bond distances. l = long M-F bond distances.

Table A2.12. First M –F bond dissociation energies in kcal/mol calculated at the DFT and CCSD(T) levels with the an-PP (n=2,3,4) basis sets.

Bond	**MF_5 State/Symm**	**MF_6 State/Symm**	**B3LYP/ aD-PP**	**B3LYP/ aT-PP**	**CCSD(T)/ aD-PP**	**CCSD(T)/ aT-PP**	**CCSD(T)/ aQ-PP**	**CBS**
W-F	$^2A_2/C_{2v}$	$^1A_{1g}/O_h$	116.0	117.8	117.0	121.0	122.8	124.0
Re-F	$^3A_1'/D_{3h}$	$^2B_{2g}/D_{4h}$	88.2	89.7	83.5	87.7	89.4	90.6
Re-F	$^3A_1'/D_{3h}$	$^2A_{1g}/D_{3d}$	88.7	89.8	83.3	87.4	89.2	90.4
Os-F	$^4B_1/C_{4v}$	$^3A_{1g}/D_{4h}$	70.4	74.2	64.9	71.0	72.8	74.0
Ir-F	$^5B_1/C_{4v}$	$^4A_{1g}/O_h$	79.8	82.2	75.5	82.7	84.6	85.9
Pt-F	$^2B_1/C_{4v}$	$^3A_{1g}/D_{4h}$	48.2	49.8	38.8	43.7	44.5	45.1
Au-F	$^1A_1/C_{4v}$	$^2B_{2g}/D_{4h}$	30.4	31.5	19.7	23.6	24.4	25.0

Table A2.13. MF_5 optimized geometry at the B3LYP/aT-PP, BLYP/TZ2P scalar relativistic ZORA and ZORA plus spin orbit levels.[a]

MF_5	**State/Symm**	B3LYP/aT-PP	ZORA	ZORA SO
WF_5	$^2A_2/C_{2v}$	1.893(x2)	1.936(x2)	1.933(x2)
		1.835(x2)	1.878(x2)	1.877(x2)
		1.815(x1)	1.860(x1)	1.860(x1)
ReF_5	$^3A_1'/D_{3h}$	1.903(x2)	1.943(x2)	1.940(x2)
		1.816(x3)	1.857(x3)	1.857(x3)
OsF_5	$^4B_1/C_{4v}$	1.822(x1)	1.863(x1)	1.864(x1)
		1.866(x4)	1.907(x4)	1.905(x4)
		97.6º	97.7º	97.1º
IrF_5	$^5B_1/C_{4v}$	1.979(x1)	2.025(x1)	1.897(x1)
		1.845(x4)	1.894(x4)	1.905(x4)
		95.9º	95.6º	94.3
PtF_5	$^2B_1/C_{4v}$	1.860(x1)	1.911(x1)	1.906(x1)
		1.872(x4)	1.918(x4)	1.919(x4)
		92.3º	92.4º	93.0º
AuF_5	$^1A_1/C_{4v}$	1.863(x1)	2.011(x1)	1.944(x1)
		1.902(x4)	1.939(x4)	1.943(x4)
		93.8º	93.2º	94.5

[a] The different bond lengths are listed separately and the times they occur are given in parentheses.

Table A2.14. Scalar relativistic corrections and pseudopotential errors in kcal/mol for the first M –F bond dissociation energies and the 1st BDE calculated at the ADF ZORA Scalar BLYP/TZ2P level.

Bond	**MF_5 State/Symm**	**MF_6 State/Symm**	**$\Delta E_{PP\text{-}error}$[a]**	**ΔE_{MVD}[b]**	**1st BDE ZORA[c]**
W-F	$^2A_2/C_{2v}$	$^1A_{1g}/O_h$	-2.37	-0.27	128.4
Re-F	$^3A_1'/D_{3h}$	$^2B_{2g}/D_{4h}$	-1.35	-0.28	106.1
Re-F	$^3A_1'/D_{3h}$	$^2A_{1g}/D_{3d}$	-1.58	-0.28	106.1
Os-F	$^4B_1/C_{4v}$	$^3A_{1g}/D_{4h}$	-0.69	-0.27	92.8
Ir-F	$^5B_1/C_{4v}$	$^4A_{1g}/O_h$	0.14	-0.83	97.4
Pt-F	$^2B_1/C_{4v}$	$^3A_{1g}/D_{4h}$	-0.92	-0.25	69.9
Au-F	$^1A_1/C_{4v}$	$^2B_{2g}/D_{4h}$	0.44	-0.24	57.6

[a] $\Delta E_{PP\text{-}error}$ = E(CCSD(T)-DK/aT-DK) – E_{MVD}(CCSD(T)/aT-PP); E_{MVD}(CCSD(T)/aT-PP) = E(CCSD(T)/aT-PP) + ΔE_{MVD}. [b] ΔE_{MVD} = $\Delta E_{MVD}(MF_5)$ + ΔE_{MVD}(F) - $\Delta E_{MVD}(MF_6)$. [c] 1st BDE ZORA calculated at the ADF ZORA Scalar BLYP/TZ2P level.

Table A2.15. Scalar relativistic corrections, pseudopotential errors and the atomic spin-orbit corrections in kcal/mol for the atomization energies at 0 K

Molecule	**State/Sym**	**$\Delta E_{PP\text{-}error}$[a]**	**ΔE_{MVD}[b]**	**Atomic ΔE_{SO}[c]**
WF_6	$^1A_{1g}/O_h$	-2.60	-1.62	-2.33
ReF_6	$^2B_{2g}/D_{4h}$	-0.95	-1.62	-2.33
ReF_6	$^2A_{1g}/D_{3d}$	-0.94	-1.62	-2.33
OsF_6	$^3A_{1g}/D_{4h}$	-0.23	-1.61	-9.90
IrF_6	$^4A_{1g}/O_h$	-0.59	-1.58	-12.71
PtF_6	$^3A_{1g}/D_{4h}$	2.57	-1.45	-2.33
AuF_6	$^2B_{2g}/D_{4h}$	2.57	-1.37	-2.33

[a] $\Delta E_{PP\text{-}error}$ = E(CCSD(T)-DK/aT-DK) – E_{MVD}(CCSD(T)/aT-PP); E_{MVD}(CCSD(T)/aT-PP) = E(CCSD(T)/aT-PP) + $\Delta E_{MVD.}$ [b] ΔE_{MVD} = 6*****ΔE_{MVD}(F) + ΔE_{MVD}(M) - ΔE_{MVD}(MF_6). [c] The spin-orbit splitting is -0.39 kcal/mol for the ($^2P_{3/2}$) state of F; 0.0 kcal/mol for the first excited state ($^7S_3$) of W (the calculated atomization energy was corrected by 8.43 kcal/mol, the experimental energy difference between the first excited state and the ground state $^5D_0$) and for the ground state ($^6S_{5/2}$) of Re and ($^2S_{1/2}$) of Au; 7.57 kcal/mol for Os ($^5D_4$); 10.38 kcal/mol for Ir ($^4F_{9/2}$); For Pt we have used the $^1S_0$ excited state with a spin-orbit splitting of 0.0 kcal/mol and we corrected the calculated atomization energy by 17.54 kcal/mol, the experimental energy difference between the first excited state and the ground state $^3D_3$. Reference 74.

Table A2.16. Optimized bond lengths (Å) for MF_7^- (M = third row transition metals) at the B3LYP and BP86 levels.

MF_7^-	State	B3LYP		BP86	
		aD-PP	aT-PP	aD-PP	aT-PP
WF_7^-	$^1A_1'/D_{5h}$	1.873 (x2)	1.866 (x2)	1.885 (x2)	1.878 (x2)
		1.921 (x5)	1.915 (x5)	1.933 (x5)	1.927 (x5)
ReF_7^-	$^2A_2/C_{2v}$	1.884 (x2)	1.878 (x2)	1.898 (x2)	1.891 (x2)
		1.938 (x2)	1.933 (x2)	1.951 (x2)	1.946 (x2)
		1.906 (x2)	1.899 (x2)	1.920 (x2)	1.912 (x2)
		1.888 (x1)	1.878 (x1)	1.951 (x1)	1.891 (x1)
OsF_7^-	$^3A_1'/D_{5h}$	1.898 (x2)	1.890 (x2)	1.912 (x2)	1.905 (x2)
		1.914 (x5)	1.906 (x5)	1.928 (x5)	1.921 (x5)
IrF_7^-	$^2B_1/C_{2v}$	1.914 (x2)	1.907 (x2)	1.931 (x2)	1.925 (x2)
		1.937 (x2)	1.931 (x2)	1.952 (x2)	1.946 (x2)
		1.912 (x2)	1.902 (x2)	1.928 (x2)	1.919 (x2)
		1.896 (x1)	1.885 (x1)	1.914 (x1)	1.903 (x1)
PtF_7^-	$^1A_1'/D_{5h}$	1.941 (x2)	1.933 (x2)	1.957 (x2)	1.951 (x2)
		1.928 (x5)	1.917 (x5)	1.945 (x5)	1.935 (x5)
PtF_7^-	$^3A'/C_s$	3.445(x1)	3.517(x1)	3.539(x1)	3.547(x1)
		1.963(x1)	1.935(x1)	1.958(x1)	1.948(x1)
		1.896(x2)	1.919(x2)	1.913(x2)	1.903(x2)
		1.890(x2)	1.915(x2)	1.905(x2)	1.895 (x2)
		1.931(x1)	1.908(x1)	1.942(x1)	1.935(x1)
AuF_7^-	$^2B_2/C_{2v}$	1.907 (x1)	1.896 (x1)	1.935 (x1)	1.924 (x1)
		1.929 (x4)	1.920 (x4)	1.948 (x4)	1.938 (x4)
		2.302 (x2)	2.299 (x2)	2.313 (x2)	2.310 (x2)
AuF_7^-	$^2A'/C_s$	3.501 (x1)	3.517(x1)	3.513(x1)	3.492(x1)
		1.946(x1)	1.935(x1)	1.966(x1)	1.956(x1)
		1.927(x2)	1.919(x2)	1.944(x2)	1.936(x2)
		1.923(x2)	1.915(x2)	1.939(x2)	1.931(x2)
		1.918(x1)	1.908(x1)	1.933(x1)	1.924(x1)

Table A2.17. MF_7^- Mulliken and NBO charges at the B3LYP/aT-PP level.

MF_7^-	State	Mulliken			NBO		
		M	**F**	**F** (avg)	**M**	**F**	**F** (avg)
WF_7^-	$^1A_1'/D_{5h}$	1.443	-0.297 (x2) -0.370 (x5)	-0.349	2.072	-0.411 (x2) -0.450 (x5)	-0.439
ReF_7^-	$^2A_2/C_{2v}$	1.279	-0.290 (x2) -0.323 (x2) -0.382 (x2) -0.287 (x1)	-0.325	1.607	-0.217 (x2) -0.237 (x2) -0.233 (x2) -0.232 (x1)	-0.229
OsF_7^-	$^3A_1'/D_{5h}$	1.312	-0.325 (x2) -0.333 (x5)	-0.331	1.156	-0.207 (x2) -0.071 (x5)	0.109
IrF_7^-	$^2A_2/C_{2v}$	1.357	-0.363 (x2) -0.311 (x2) -0.366 (x2) -0.277 (x1)	-0.337	1.454	-0.207 (x2) -0.240 (x2) -0.196 (x2) -0.167 (x1)	-0.207
PtF_7^-	$^1A_1'/D_{5h}$	1.346	-0.408 (x2) -0.305 (x5)	-0.334	1.669	-0.469 (x2) -0.346 (x5)	-0.381
PtF_7^-	$^3A'/C_s$	1.395	-0.152(x1) -0.302(x1) -0.396(x2) -0.390(x2) -0.369(x1)	-0.385	1.134	0.305(x1) -0.106(x1) -0.153(x2) -0.142(x2) -0.243(x1)	-0.091
AuF_7^-	$^2B_2/C_{2v}$	1.485	-0.299(x1) -0.368(x4) -0.356(x2)	-0.355	0.861	-0.194(x1) -0.223(x4) 0.112(x2)	-0.123
AuF_7^-	$^2A'/C_s$	1.395	-0.152(x1) -0.302(x1) -0.396(x2) -0.390(x2) -0.369(x1)	-0.342	0.879	0.354(x1) -0.116(x1) -0.228(x2) -0.223(x2) -0.214(x1)	-0.125

Table A2.18. MF_6 fluoride affinities in kcal/mol calculated at CCSD(T) level with the aVNZ-PP (N = D, T, Q) basis sets.

Calculation	**WF_6**	**ReF_6**	**ReF6**	**OsF_6**	**IrF_6**	**PtF_6**	**AuF_6**
State/Sym	$^1A_{1g}/O_h$	$^2B_{2g}/D_{4h}$	$^2A_{1g}/D_{3d}$	$^3A_{1g}/D_{4h}$	$^4A_{1g}/O_h$	$^3A_{1g}/D_{4h}$	$^2B_{2g}/D_{4h}$
CCSD(T)/aD-PP	76.6	79.9	80.1	86.1	61.8	90.51	119.52
CCSD(T)/aT-PP	78.3	81.2	81.2	86.8	62.7	85.75	115.68
CCSD(T)/aQ-PP	78.1	81.0	81.2	86.5	64.7		

Table A2.19. Scalar relativistic corrections and pseudopotential errors in kcal/mol for the MF_6 fluoride affinities and $FA(MF_6)$ calculated at the ADF ZORA Scalar BLYP/TZ2P level.

M	**MF_6 State/Symm**	**MF_7^- State/Symm**	**$\Delta E_{PP\text{-}error}$[a]**	**ΔE_{MVD}[b]**	**FA Zora[c]**
W	$^1A_{1g}/O_h$	$^1A_1'/D_{5h}$	1.19	-0.23	81.2
Re	$^2B_{2g}/D_{4h}$	$^2A_2/C_{2v}$	0.40	-0.22	82.4
Re	$^2A_{1g}/D_{3d}$	$^2A_2/C_{2v}$	0.63	-0.22	82.4
Os	$^3A_{1g}/D_{4h}$	$^3A_1'/D_{5h}$	0.67	-0.19	84.9
Ir	$^4A_{1g}/O_h$	$^2B_1/C_{2v}$	1.07	+0.35	65.4
Pt	$^3A_{1g}/D_{4h}$	$^3A'/C_s$	-1.42	-0.12	77.7
Au	$^2B_{2g}/D_{4h}$	$^2A'/C_s$	0.1	-0.14	98.0

[a] $\Delta E_{PP\text{-}error}$ = E(CCSD(T)-DK/aT-DK) – E_{MVD}(CCSD(T)/aT-PP); E_{MVD}(CCSD(T)/aT-PP) = E(CCSD(T)/aT-PP) + ΔE_{MVD}. [b] $\Delta E_{MVD} = \Delta E_{MVD}(MF_6) + \Delta E_{MVD}(F^-) - \Delta E_{MVD}(MF_7^-)$. [c] $FA(MF_6)$ calculated at the ADF ZORA Scalar BLYP/TZ2P level.

Table A2.20. MF_5 fluoride affinities (kcal/mol) calculated at the DFT and CCSD(T) level with aVnZ-PP (n= D, T, Q) basis sets

Calculation	WF_5	ReF_5	OsF_5	IrF_5	PtF_5	AuF_5
B3LYP/aD-PP	104.7	108.1	122.9	124.9	120.4	132.3
B3LYP/aT-PP	103.9	107.3	123.0	125.3	120.2	132.3
CCSD(T)/aD-PP	112.5	115.0	131.9	131.6	126.7	137.6
CCSD(T)/aT-PP	110.9	113.5	132.1	135.2	128.3	139.0
CCSD(T)/aQ-PP	111.8	114.3	132.8	136.8	128.8	139.8
CBS	112.5	114.9	133.4	137.8	129.3	140.3

Table A2.21. Scalar relativistic corrections and pseudopotential errors in kcal/mol for the MF_5 fluoride affinities.

M	MF_5 State/Symm	MF_6^- State/Symm	$\Delta E_{PP\text{-}error}$[a]	ΔE_{MVD}[b]	FA ZORA[c]
W	$^2A_2/C_{2v}$	$^2B_{2g}/D_{4h}$	0.21	-0.27	110.3
Re	$^3A_1'/D_{3h}$	$^3A_{1g}/D_{4h}$	0.02	-0.29	114.0
Os	$^4B_1/C_{4v}$	$^4A_{1g}/O_h$	-0.14	-0.30	127.4
Ir	$^5B_1/C_{4v}$	$^3A_{1g}/D_{4h}$	1.48	-0.35	128.9
Pt	$^2B_1/C_{4v}$	$^2B_{2g}/D_{4h}$	0.10	-0.32	126.6
Au	$^1A_1/C_{4v}$	$^1A_{1g}/O_h$	0.71	-0.34	137.3

[a] $\Delta E_{PP\text{-}error}$ = E(CCSD(T)-DK/aT-DK) – E_{MVD}(CCSD(T)/aT-PP); E_{MVD}(CCSD(T)/aT-PP) = E(CCSD(T)/aT-PP) + ΔE_{MVD}. [b] ΔE_{MVD} = $\Delta E_{MVD}(MF_5) + \Delta E_{MVD}(F^-) - \Delta E_{MVD}(MF_6^-)$. [c] FA(MF_5) calculated at the ADF ZORA Scalar BLYP/TZ2P level.

Table A2.22. Calculated MF_6^- vibrational frequencies (cm^{-1}). The IR intensities (km/mol) are given in the parentheses.

M	MF_6 State/Sym	a_{1g}	e_g	t_{1u}	t_{1u}	t_{2g}	t_{2u}
WF_6^{-a}	$^2B_{2g}/D_{4h}$	630(0)	a_{1g} 544(0) b_{1g} 392(0)	e_u 583(538) a_{2u} 562(268)	a_{2u} 228(20) e_u 214(58)	e_g 156(0) b_{2g} 146(0)	b_{2g} 129(2) b_{2u} 128(0)
WF_6^{-b}	$^2A_{1g}/D_{3d}$	642(0)	388(0)	e_u 594(562) a_{2u} 573(265)	e_u 247(38) a_{2u} 219(22)	e_g 238(0) a_{2g} 217(0)	a_{1u} 142(0) e_u 137(14)
ReF_6^{-b}	$^3A_{1g}/D_{4h}$	639(0)	b_{1g} 570(0) a_{1g} 550(0)	e_u 608(302) a_{2u} 568(256)	a_{2u} 257(7) e_u 226(21)	e_g 371(0) b_{2g} 274(0)	b_{2u} 193(4) e_u 149(0)
ReF_6^{-c}	$^3A_{1g}/D_{3d}$	668(0)	390(0)	a_{2u} 618(291) e_u 606(564)	e_u 257(34) a_{2u} 246(22)	a_{1g} 249(0) e_u 150(10)	a_{1u} 199(0) e_u 130(0)
OsF_6^{-c}	$^4A_{1g}/O_h$	659(0)	589(0)	620(795)	255(48)	225(0)	193(0)
IrF_6^{-c}	$^3A_{1g}/D_{4h}$	651(0)	b_{1g} 594(0) a_{1g} 581(0)	a_{2u} 650(243) e_u 615(448)	e_u 275(14) a_{2u} 243(21)	e_u 216(4) b_{2u} 184(0)	b_{2g} 178(0) e_g 100(0)
IrF_6^{-b}	$^3A_{1g}/D_{3d}$	605(0)	341(0)	e_u 605(388) a_{2u} 600(194)	a_{2u} 265(8) e_u 263(7)	a_{1g} 206(0) e_u 194(0)	e_u 205(6) a_{1u} 184(0)
PtF_6^{-c}	$^2B_{2g}/D_{4h}$	635(0)	b_{1g} 583(0) a_{1g} 580(0)	e_u 642(378) a_{2u} 603(179)	e_u 261(22) a_{2u} 289(1)	e_g 429(0) b_{2g} 251(0)	e_u 223(8) b_{2u} 182(0)
PtF_6^{-c}	$^2A_{1g}/D_{3d}$	620(0)	278(0)	a_{2u} 629(186) e_u 626(372)	e_u 280(10) a_{2u} 259(8)	a_{1g} 213(0) e_u 181(0)	a_{1u} 245(0) e_u 198(6)
AuF_6^{-c}	$^1A_{1g}/O_h$	582(0)	578(0)	623(438)	269(12)	226(0)	200(0)

[a] ADF Zora SO BLYP/TZ2P. [b] BP86/aD-PP. [c] B3LYP/aT-PP.

Table A2.23. Calculated MF_5 vibrational frequencies (cm^{-1}) at the B3LYP/aT-PP levels. The IR intensities (km/mol) are given in the parentheses.

Type	**WF_5**	**ReF_5**	**OsF_5**	**IrF_5**	**PtF_5**	**AuF_5**
State/Sym	$^2A_2/C_{2v}$	$^3A_1'/D_{3h}$	$^4B_1/C_{4v}$	$^5B_1/C_{4v}$	$^2B_1/C_{4v}$	$^1A_1/C_{4v}$
A_1	740(6); 729(7) 640(0); 208(15) 104(9)		728(29); 693(28) 218(17)	691(3); 526(51) 218(10)	687(5); 662(1) 267(10)	659(2); 609(0) 229(11)
B_1	688(277); 272(6) 220(12)		239(0)	267(0)	259(0)	191(0)
B_2	631(170); 188(22) 52(28)		650(0); 132(0)	628(0); 139(0)	619(0); 203(0)	605(0); 175(0)
A_2	129(0)					
E			678(215)x2 240(10)x2 56(4)x2	702(173)x2 239(9)x2 172(1)x2	679(151)x2 230(13)x2 102(1)x2	660(107)x2 253(2)x2 19(2)x2
A_1'		743(0); 639(0)				
E'		741(129)x2 218(14)x2 155(1)x2				
A_2"		644(260); 221(16)				
E"		171(0)x2				

Table A2.24. Calculated MF_7^- vibrational frequencies (cm^{-1}) at the B3LYP/aD-PP and aT-PP levels. The IR intensities (km/mol) are given in the parentheses.

Type	**WF_7^-**	**ReF_7^{-b}**	**OsF_7^{-c}**	**IrF_7^{-b}**	**PtF_7^{-c}**	**PtF_7^{-c}**	**AuF_7^{-c}**
Symm	**$^1A_1'/D_{5h}$**	**$^2A_1/C_{2v}$**	**$^3A_1'/D_{5h}$**	**$^2B_1/C_{2v}$**	**$^1A_1'/D_{5h}$**	**$^3A'/C_s$**	**$^2A'/C_s$**
A_1		668(0);621(258) 589(0); 524(0) 442(1); 339(29) 183(8)		624(0); 616(164) 586(0); 514(0) 432(0); 317(15) 210(4)			
B_1		639(275);281(23) 277(0); 58(0)		631(202); 300(6) 231(0); 91(0)			
B_2		592(257);460(1) 336(29);239(0) 42(0)		595(152);448(0) 317(12); 250(0) 58(0)			
A_2		236(0); 63(0)		206(0); 94(0)			
A_1'	663(0);572(0)				605(0);583(0)		
A_2''	628(338) 274(36)				617(162) 305(1)		
A'			659(0) 594(0)			648(144);638(23) 608(126);549(60) 328(7);292(1) 253(0);237(6) 202(2);155(1) 65(1)	627(132);618(144) 584(1);562(50) 309(8);266(3) 249(2);214(0) 199(0);150(3) 60(0)

A”			638(254) 296(13)			648(177);587(1) 257(10);244(0) 207(3);186(0) 23(0)	628(139);580(0) 266(3);226(0) 224(0);195(0) 23(0)
E_1’	586(328)x2 342(35)x2 207(7)x2		613(214)x2; 338(25)x2 226(2)x2		605(103)x2 308(7)x2 236(0)x2		
E_2’	511(0)x2; 433(0)x2		532(0)x2; 442(0)x2		512(0)x2 425(0)x2		
E_1”	293(0)x2		234(0)x2		195(0)x2;		
E_2”	60(0)x2		76(0)x2		91(0)x2		

[a] MP2/aD-PP. [b] B3LYP/aD-PP. [c] B3LYP/aT-PP.

Table A2.25. Adiabatic electron affinities of MF_6, vertical electron detachment energies (VDE) of MF_6^- and vertical electron attachment energies (VAE) of MF_6 in kcal/mol calculated at the CCSD(T)/aT-PP//CCSD(T)/aD-PP, B3LYP/aT-PP//B3LYP/aD-PP and CCSD(T)/aT-DK// CCSD(T)/aT-PP levels.

	MF_6	**MF_6^-**	**Adiabatic EA**			**VDE[a]**			**VAE[b]**		
Molecule	**State Sym**	**State Sym**	**CCSD(T)/ aT-PP**	**CCSD(T)/ aT-DK**	**B3LYP/ aT-PP**	**CCSD(T)/ aT-PP**	**CCSD(T)/ DK-aT**	**B3LYP/ aT-PP**	**CCSD(T)/ aT-PP**	**CCSD(T)/ aT-DK**	**B3LYP/ aT-PP**
WF_6/WF_6^-	$^1A_{1g}/O_h$	$^2B_{2g}/D_{4h}$	66.4	68.7	65.7	82.7	79.4	80.2	57.6	54.1	55.9
ReF_6/ReF_6^-	$^2A_{1g}/D_{3d}$	$^3A_{1g}/D_{4h}$	101.4	103.8	97.9	119.6	115	110.6	95.8	94.7	90.2
ReF_6/ReF_6^-	$^2B_{2g}/D_{4h}$	$^3A_{1g}/D_{4h}$	102.2	103.6	98.3	119.6	115	110.6	93.3	88.4	90.1
OsF_6/OsF_6^-	$^3A_{1g}/D_{4h}$	$^4A_{1g}/O_h$	137.5	137.8	130.0	146.0	144.7	140.1	134.1	128.5	123.9
IrF_6/IrF_6^-	$^4A_{1g}/O_h$	$^3A_{1g}/D_{4h}$	128.9	130.5	123.4	139.0	136.1	131.7	136.9	123.3	121.1
PtF_6/PtF_6^-	$^3A_{1g}/D_{4h}$	$^2B_{2g}/D_{4h}$	161.0	161.7	152.1	169.3	166.7	158.1	158.5	154.6	149.1
AuF_6/AuF_6^-	$^2B_{2g}/D_{4h}$	$^1A_{1g}/O_h$	191.9	191.8	181.9	195.8	196.4	185.6	191.3	191.7	180.3

[a] $VDE = E_{neutral\ at\ anion\ geom} - E_{anion.}$ [b] $VAE = E_{neutral} - E_{anion\ at\ neutral\ geom.}$

Table A2.26. Electron affinities[a] at 0 K (kcal/mol) for MF_6 (M = third row transition metals) calculated with various exchange-correlation functionals and the aD-PP basis sets and deviations (kcal/mol) from the CCSD(T) calculated electron affinities. Values in parentheses are the differences from the CCSD(T) values.

Method	**WF_6 O_h**	**ReF_6 D_{4h}**	**ReF_6 D_{3d}**	**OsF_6 D_{4h}**	**IrF_6 O_h**	**PtF_6 D_{4h}**	**AuF_6 D_{4h}**
SVWN5	52.1 (16.4)	81.3 (22.5)	84.1(19.2)	109.0 (29.5)	107.3 (23.2)	134.9 (27.4)	163.8 (29.3)
BLYP	58.7 (9.8)	87.5 (16.3)	85.5(17.8)	114.2 (24.3)	110.8 (19.7)	136.2 (26.1)	162.6 (30.5)
BP86	57.0 (11.5)	86.8 (17.0)	85.6(17.7)	115.5 (23.0)	110.2 (20.3)	136.3 (26.0)	163.9 (29.2)
PW91	56.9 (11.6)	86.9 (16.9)	85.6(17.7)	116.7 (21.8)	110.0 (20.5)	136.2 (26.1)	163.9 (29.2)
PBE	54.4 (14.1)	85.7 (18.1)	83.7(19.6)	112.8 (25.7)	108.4 (22.1)	134.6 (27.7)	161.9 (31.2)
TPSS	55.2 (13.3)	85.7 (18.1)	84.7(18.6)	115.1 (23.4)	108.6 (21.9)	134.9 (27.4)	162.3 (30.8)
HCTH	62.2 (6.3)	93.7 (10.1)	91.5(11.8)	120.4 (18.1)	112.8 (17.7)	140.1 (22.2)	168.7 (24.4)
B3LYP	69.0 (-0.5)	101.4 (2.4)	101.5(1.8)	132.9 (5.6)	125.7 (4.8)	154.1 (8.2)	183.7 (9.4)
mPW1	69.4 (-0.9)	101.4 (2.4)	100.8(2.5)	133.1 (5.4)	125.4 (5.1)	153.5 (8.8)	184.7 (8.4)
PBE1	68.0 (0.5)	100.0 (3.8)	99.5(3.8)	131.7 (6.8)	123.9 (6.6)	151.5 (10.8)	183.3 (9.8)
O3LYP	62.4(6.1)	95.0 (8.8)	92.4(10.9)	122.0 (16.5)	115.5 (15.0)	143.8 (18.5)	172.7 (20.4)
TPSSh	55.2 (13.3)	85.8 (18.0)	84.7(18.6)	115.2 (23.3)	108.7 (21.8)	135.0 (27.3)	162.8 (30.3)
CCSD(T)[b]	**65.5**	**103.8**	**103.3**	**138.5**	**130.5**	**162.3**	**193.1**

[a] $EA(DFT) = \Delta E_{elec}(DFT) + \Delta E_{ZPE}$. [b] $EA(CCSD(T)) = \Delta E_{CBS} + \Delta E_{ZPE} + \Delta E_{CV}$

Table A2.27. MF_5 fluoride affinities[a] at 0 K (kcal/mol) calculated with various exchange-correlation functionals and the aD-PP basis sets and deviations (kcal/mol) from the CCSD(T) calculated electron affinities. Values in parentheses are the differences from the CCSD(T) values.

Method	**WF_5**	**ReF_5**	**OsF_5**	**IrF_5**	**PtF_5**	**AuF_5**
SVWN5	112.2(1.3)	115.8(-1.7)	130.0(2.7)	132.6(4.1)	129.5(-1.4)	141.2(-1.7)
BLYP	98.6(14.9)	101.3(12.8)	114.3(18.4)	115.1(21.6)	113.5(14.6)	124.3(15.2)
BP86	95.9(17.6)	103.7(10.4)	118.0(14.7)	118.0(18.7)	116.2(11.9)	127.3(12.2)
PW91	104.1(9.4)	109.3(4.8)	123.8(8.9)	123.4(13.3)	121.9(6.2)	133.1(6.4)
PBE	99.2(14.3)	104.6(9.5)	118.2(14.5)	118.5(18.2)	117.3(10.8)	128.4(11.1)
TPSS	103.5(10.0)	107.1(7.0)	121.4(11.3)	122.0(14.7)	119.0(9.1)	130.2(9.3)
HCTH	95.8(17.7)	99.0(15.1)	112.4(20.3)	108.9(27.8)	111.6(16.5)	123.2(16.3)
B3LYP	105.0(8.5)	108.1(6.0)	123.1(9.6)	124.9(11.8)	119.7(8.4)	132.3(7.2)
mPW1	107.3(6.2)	110.9(3.2)	126.3(6.4)	127.9(8.8)	123.6(4.5)	135.9(3.6)
PBE1	107.6(5.9)	111.0(3.1)	126.8(5.9)	128.2(8.5)	123.3(4.8)	136.5(3.0)
O3LYP	96.8(16.7)	100.5(13.6)	114.4(18.3)	115.2(21.5)	113.7(14.4)	125.4(14.1)
TPSSh	111.0(2.5)	114.6(-0.5)	128.7(4.0)	129.5(7.2)	126.2(1.9)	137.7(1.8)
CCSD(T)[b]	113.5	114.1	132.7	136.7	128.1	139.5

[a] $EA(DFT) = \Delta E_{elec}(DFT) + \Delta E_{ZPE}$. [b] $EA(CCSD(T)) = \Delta E_{CBS} + \Delta E_{ZPE} + \Delta E_{CV}$

Table A2.28. MF_6 fluoride affinities[a] (kcal/mol) calculated with various local, gradient corrected and hybrid exchange-correlation functionals and the aD-PP basis set and and deviations (kcal/mol) from the CCSD(T) calculated fluoride affinities. Values in parentheses are the differences from the CCSD(T) values.

Method	WF_6 O_h	ReF_6 D_{4h}	ReF_6 D_{3d}	OsF_6 D_{4h}	IrF_6 O_h	PtF_6 D_{4h}	AuF_6 D_{4h}
SVWN5	82.8(-5.7)	86.4(-5.1)	84.1(-3.4)	86.9(-1.1)	67.2(-1.1)	67.84(17.8)	90.53(24.9)
BLYP	65.6(11.5)	69.4(12.0)	67.4(13.3)	70.7(15.1)	51.3(14.8)	68.16(17.4)	89.91(25.5)
BP86	69.4(7.7)	72.1(9.3)	70.0(10.7)	74.9(10.9)	52.9(13.2)	66.4(19.2)	88.85(26.6)
PW91	74.7(7.4)	78.4(2.9)	76.4(4.3)	80.4(5.4)	59.1(7.0)	71.95(13.2)	94.57(20.9)
PBE	70.2(6.9)	73.8(7.6)	71.8(8.9)	74.9(10.9)	54.3(11.8)	67.78(17.8)	90.24(25.2)
TPSS	73.3(3.8)	76.7(4.6)	74.5(6.2)	78.7(7.1)	56.9(9.2)	70.55(15.0)	93.55(21.9)
HCTH	61.5(15.6)	65.9(15.5)	63.7(17.0)	67.1(18.7)	43.7(22.4)	65.98(19.6)	89.64(25.8)
B3LYP	72.5(4.6)	75.7(5.6)	73.7(7.0)	79.9(5.9)	56.6(9.5)	81.13(4.5)	107.69(7.8)
mPW1	74.7(2.4)	77.7(3.6)	77.2(3.5)	81.5(4.3)	57.7(8.4)	83.3(2.3)	112.08(3.4)
PBE1	75.7(1.4)	78.6(2.8)	78.1(2.6)	82.3(3.5)	58.4(7.7)	83.67(1.9)	111.94(3.5)
O3LYP	64.8(12.3)	69.5(11.9)	66.9(13.8)	70.5(15.3)	48.3(17.8)	72.45(13.1)	97.98(17.5)
TPSSh	80.8(-3.7)	84.7(-3.4)	82.5(-1.8)	86.3(-0.5)	64.4(1.7)	78.31(7.3)	101.30(14.2)
CCSD(T)[b]	**77.1**	**81.4**	**80.7**	**85.8**	**66.1**	**85.6[c]**	**115.5[c]**

[a] $EA(DFT) = \Delta E_{elec}(DFT) + \Delta E_{ZPE}$. [b] $EA(CCSD(T)) = \Delta E_{CBS} + \Delta E_{ZPE} + \Delta E_{CV}$. [c] $EA(CCSD(T)) = \Delta E_{CCSD(T)/AT\text{-}PP} + \Delta E_{ZPE}$.

Table A2.29. First adiabatic M –F bond dissociation energies[a] in kcal/mol calculated with various exchange-correlation functionals and the aD-PP basis sets and deviations (kcal/mol) from the CCSD(T) calculated electron affinities. Values in parentheses are the differences from the CCSD(T) values.

Method	W-F	Re-F[b]	Re-F[c]	Os-F	Ir-F	Pt-F	Au-F
SVWN5	155.5(-33.7)	129.9(-40.6)	132.1(-41.8)	116.4(-43.2)	120.7(-36.0)	90.1(-44.4)	72.9(-47.8)
BLYP	125.0(-3.2)	99.0(-9.7)	100.9(-10.6)	85.2(-12.0)	89.4(-4.7)	62.5(-16.8)	46.8(-21.7)
BP86	129.1(-7.3)	103.3(-14.0)	105.3(-15.0)	88.8(-15.6)	94.4(-9.7)	66.6(-20.9)	50.3(-25.2)
PW91	130.9(-9.1)	105.0(-15.7)	107.0(-16.7)	90.6(-17.4)	96.1(-11.4)	68.4(-22.7)	52.3(-27.2)
PBE	129.8(-8.0)	103.9(-14.6)	105.9(-15.6)	90.3(-17.1)	95.1(-10.4)	67.7(-22.0)	51.4(-26.3)
TPSS	126.0(-4.2)	99.9(-10.6)	102.1(-11.8)	85.2(-12.0)	92.5(-7.8)	63.3(-17.6)	47.0(-21.9)
HCTH	122.8(-1.0)	94.6(-5.3)	96.7(-6.4)	81.1(-7.9)	85.3(-0.6)	60.7(-15.0)	44.3(-19.2)
B3LYP	116.0(5.8)	88.5(0.8)	88.71.6)	70.4(2.8)	79.8(4.9)	48.0(-2.3)	30.4(-5.3)
mPW1	114.3(7.5)	85.9(3.4)	86.4(3.9)	69.6(3.6)	78.8(5.9)	46.2(-0.5)	27.6(-2.5)
PBE1	115.5(6.3)	86.9(2.4)	87.4(2.9)	71.0(2.2)	80.2(4.5)	47.7(-2.0)	29.0(-3.9)
O3LYP	154.3(-32.5)	125.3(-36.0)	127.9(-37.6)	112.3(-39.1)	119.5(-34.8)	89.7(-44.0)	72.5(-47.4)
TPSSh	148.1(-26.3)	121.7(-32.4)	124.0(-33.7)	106.7(-33.5)	114.4(-29.7)	84.8(-39.1)	68.7(-43.6)
CCSD(T)[d]	121.8	89.3	90.3	73.2	84.7	45.7	25.1

[a] $EA(DFT) = \Delta E_{elec}(DFT) + \Delta E_{ZPE}$. [b] $BDE_{Re\text{-}F} = E(ReF_5) + E(F) - EA\ (ReF_{6,D4h})$. [c] $BDE_{Re\text{-}F} = E(ReF_5) + E(F) - EA\ (ReF_{6,D3d})$.

[d] $EA(CCSD(T)) = \Delta E_{CBS} + \Delta E_{ZPE} + \Delta E_{CV}$

Table A2.30. Total MF_6 electronic energies at the DFT level with various exchange-correlation functionals and the aD-PP basis set, zero point energies (ZPE) at the B3LYP/aT-PP or BP86/aD-PP levels, CCSD(T) energies with the aug-cc-pVnZ/aug-cc-pVnZ-PP basis sets (n = D, T, Q) and at the CBS level, core and valence energies at the CCSD(T)/aug-cc-pWCVTZ-PP level, scalar relativistic energies at the CISD/aT-PP and CCSD(T)-DK/aug-cc-pVTZ-DK energies in atomic units.

Method	**WF_6**	**ReF_6**	**ReF_6**	**OsF_6**	**IrF_6**	**PtF_6**	**AuF_6**
State/symm	$^1A_{1g}/O_h$	$^2B_{2g}/D_{4h}$	$^2A_{1g}/D_{3d}$	$^3A_{1g}/D_{4h}$	$^4A_{1g}/O_h$	$^3A_{1g}/D_{4h}$	$^2B_{2g}/D_{4h}$
CCSD(T) aD-PP	-665.226779	-676.184998	-665.226779	-688.365881	-701.857690	-716.627171	-732.744914
CCSD(T) aT-PP	-665.754003	-676.720582	-665.754003	-688.911098	-702.411588	-717.190951	-733.313352
CCSD(T) aQ-PP	-665.925202	-676.894249	-665.925202	-689.087729	-702.591116	-717.374213	-733.500784
CCSD(T) CBS	-666.024588	-676.995065	-666.024588	-689.190264	-702.695333	-717.480603	-733.609629
Core	-666.451891	-677.430983	-666.451891	-689.630304	-703.135238	-717.914948	-734.032563
Valence	-665.798989	-676.766636	-665.798989	-688.958466	-702.460011	-717.240900	-733.364774
SR	-0.522219	-0.522702	-0.522219	-0.523391	-0.524232	-0.525281	-0.526579
ZPE	0.014079[a]	0.014347[b]	0.013105[b]	0.013274[b]	0.014395[a]	0.013899[a]	0.013451[a]
CCSD(T) aT-DK	-16727.038773	-17276.098184	-16727.038773	-17837.063381	-18410.085933	-18995.275634	-19592.855731
SVWN5	-663.061468	-674.061926	-674.050535	-686.274253	-699.784494	-714.569346	
BLYP	-666.886966	-677.889890	-677.878912	-690.111954	-703.636029	-718.440630	-734.567053

BP86	-667.037159	-678.051178	-678.040026	-690.282575	-703.814480	-718.624904	-734.756023
PW91	-666.855521	-677.869361	-677.858296	-690.100155	-703.631432	-718.440642	-734.570663
PBE	-666.4172356	-677.427277	-677.416231	-689.653922	-703.180762	-717.984984	-734.109866
TPSS	-666.985543	-677.986952	-677.975697	-690.205534	-703.724489	-718.520467	-734.638084
HCTH	-667.017477	-678.054332	-678.043259	-690.312913	-703.876382	-718.717079	-734.883918
B3LYP	-666.928328	-677.926556	-677.91459	-690.144710	-703.668088	-718.468799	-734.599783
mPW1	-666.780286	-677.781200	-677.768955	-690.000916	-703.525378	-718.323218	-734.452942
PBE1	-666.324079	-677.321769	-677.309505	-689.537631	-703.057863	-717.850787	-733.975275
O3LYP	-666.788571	-677.803260	-677.791611	-690.038266	-703.578389	-718.395331	-734.540446
TPSSh	-666.985181	-677.986504	-677.975098	-690.205005	-703.723875	-718.519774	-734.637412

[a] B3LYP/aT-PP ZPE. [b] BP86/aD-PP ZPE.

Table A2.31. Total MF_6^- electronic energies at the DFT level with various exchange-correlation functionals and the aD-PP basis set, zero point energies at the B3LYP/aT-PP and BP86/aD-PP levels, CCSD(T) energies with the aug-cc-pVnZ/aug-cc-pVnZ-PP basis sets (n = D, T, Q) and at the CBS level, core and valence energies at the CCSD(T)/aug-cc-pWCVTZ-PP level, scalar relativistic energies at the CISD/aT-PP and CCSD(T)-DK/aug-cc-pVTZ-DK energies in atomic units.

Method	**WF_6^-**	**ReF_6^-**	**OsF_6^-**	**IrF_6^-**	**PtF_6^-**	**AuF_6^-**
State/symm	$^2B_{2g}/D_{4h}$	$^3A_{1g}/D_{4h}$	$^4A_{1g}/O_h$	$^3A_{1g}/D_{4h}$	$^2B_{2g}/D_{4h}$	$^1A_{1g}/O_h$
CCSD(T)/aD-PP	-665.338223	-676.353743	-688.591200	-702.065702	-716.885819	-733.051447
CCSD(T)/aT-PP	-665.859782	-676.883469	-689.130231	-702.617063	-717.447466	-733.619121
CCSD(T)/aQ-PP	-666.031950	-677.058112	-689.307617	-702.798504	-717.632831	-733.808936
CCSD(T)/CBS	-666.131933	-677.159529	-689.410692	-702.903865	-717.740478	-733.919197
Core	-666.558223	-677.593318	-689.847927	-703.339542	-718.169544	-734.336335
Valence	-665.904608	-676.929295	-689.177226	-702.665921	-717.497769	-733.670813
SR	-0.521969	-0.522422	-0.523080	-0.523901	-0.524908	-0.526159
CCSD(T)/aT-DK	-16727.148277	-17276.263286	-17837.282988	-18410.293956	-18995.533321	-19593.163179
ZPE	0.011183[b]	0.011818[b]	0.013021[b]	0.012506[a]	0.014248[a]	0.012971[a]
SVWN5	-663.142226	-674.190053	-686.449442	-699.954405	-714.783329	-730.930419
BLYP	-666.977707	-678.028010	-690.295379	-703.811580	-718.656871	-734.826200
BP86	-667.128061	-678.189581	-690.466564	-703.990113	-718.842167	-735.017263
PW91	-666.946201	-678.007819	-690.284494	-703.806653	-718.657744	-734.831857
PBE	-666.504858	-677.562648	-689.835105	-703.352384	-718.198523	-734.367519
TPSS	-667.073471	-678.123473	-690.388887	-703.897486	-718.735421	-734.897277

HCTH	-667.113881	-678.200455	-690.506416	-704.055094	-718.939489	-735.151472
B3LYP	-667.038353	-678.088085	-690.356498	-703.868461	-718.714412	-734.892599
mPW1	-666.887932	-677.941667	-690.213255	-703.722914	-718.567998	-734.746807
PBE1	-666.429559	-677.480073	-689.747818	-703.252916	-718.093239	-734.266946
O3LYP	-666.885062	-677.950415	-690.234487	-703.761526	-718.623351	-734.815254
TPSSh	-667.073207	-678.123158	-690.388513	-703.897026	-718.734894	-734.896775

[a] B3LYP/aT-PP ZPE. [b] BP86/aD-PP ZPE.

Table A2.32. MF_7^- classical structures total electronic energies at the DFT level with various exchange-correlation functionals and the aD-PP basis set, zero point energies at B3LYP/aD-PP and aT-PP levels and CCSD(T) energies with the aug-cc-pVnZ/aug-cc-pVnZ-PP basis sets (n = D, T, Q) and at the CBS level, core and valence energies at the CCSD(T)/aug-cc-pWCVTZ-PP level, scalar relativistic energies at the CISD/aT-PP and CCSD(T)-DK/aug-cc-pVTZ-DK energies in atomic units.

Method	**WF_7^-**	**ReF_7^-**	**OsF_7^-**	**IrF_7^-**	**PtF_7^-**	**AuF_7^-**
State/symm	$^1A_1'/D_{5h}$	$^2A_2/C_{2v}$	$^3A_1'/D_{5h}$	$^2B_1/C_{2v}$	$^1A_1'/D_{5h}$	$^2B_2/C_{2v}$
CCSD(T)/aD-PP	-765.017531	-775.980901	-788.171593	-801.624814	-816.428694	-832.553505
CCSD(T)/aT-PP	-765.627693	-776.599152	-788.799014	-802.261070	-817.073304	-833.196614
CCSD(T)/aQ-PP	-765.826714	-776.800409	-789.002574	-802.469483	-817.285402	-833.410832
CCSD(T)/CBS	-765.941907	-776.917035	-789.120744	-802.590496	-817.407632	-833.535258
Core	-766.387125	-777.371425	-789.579757	-803.047689	-817.859001	-833.974534
Valence	-765.678906	-776.651300	-788.852028	-802.317073	-817.130673	-833.254409
SR	-0.608523	-0.609020	-0.609736	-0.610618	-0.611696	-0.613103
CCSD(T)/aT-DK	-16827.00126	-17376.06446	-17937.03875	-18510.02436	-19095.24644	-19692.82790
ZPE	0.015892[a]	0.01502[a]	0.016197[b]	0.014856[a]	0.015619[b]	0.013353[a]
SVWN5	-762.406059	-773.411463	-785.626552	-799.103978	-813.900877	-829.960579
BLYP	-766.843465	-777.851825	-790.077841	-803.569816	-818.387454	-834.497844
BP86	-767.0025	-778.021742	-790.25661	-803.755313	-818.578448	-834.686618
PW91	-766.798087	-777.817307	-790.051595	-803.549114	-818.371021	-834.478133
PBE	-766.289985	-777.305268	-789.535352	-803.028134	-817.845396	-833.948551
TPSS	-766.9592	-777.965148	-790.187616	-803.672005	-818.481174	-834.57058

HCTH	-766.951489	-777.994368	-790.257028	-803.781944	-818.638371	-834.79315
B3LYP	-766.898382	-777.902489	-790.126378	-803.61384	-818.434685	-834.527667
mPW1	-766.723392	-777.730319	-789.955907	-803.441015	-818.260632	-834.343367
PBE1	-766.197654	-777.201351	-789.422927	-802.903609	-817.718464	-833.795853
O3LYP	-766.715205	-777.735468	-789.975128	-803.478485	-818.313423	-834.430099
TPSSh	-766.958551	-777.965179	-790.186823	-803.670915	-818.480282	-834.569748

[a]B3LYP/aD-PP (WF_7^- and AuF_7^- have 2 imaginary frequencies). [b]B3LYP/aT-PP.

Table A2.33. MF_7^- nonclassical structures total electronic energies at the CCSD(T) level with the aug-cc-pVnZ/aug-cc-pVnZ-PP basis sets (n = D, T) and zero point energies at B3LYP/aD-PP and aT-PP levels in atomic units.

Method	**WF_7^-**	**ReF_7^-**	**OsF_7^-**	**IrF_7^-**	**PtF_7^-**	**AuF_7^-**
State/symm	$^3A''/C_s$	$^4A''/C_s$	$^5A''/C_s$	$^2A'/C_s$	$^3A'/C_s$	$^2A'/C_s$
CCSD(T)/aD-PP	-764.890375	-775.906961	-788.143353	-801.580517	-816.440042	-832.604020
CCSD(T)/aT-PP	-765.489168	-776.513337	-788.758576	-802.209596	-817.077145	-833.247242
ZPE	0.0122633[a]	0.0134634[a]	0.013753[a]	0.012623[a]	0.013964[b]	0.013625[b]

[a]B3LYP/aD-PP (IrF_7^- has 2 imaginary frequencies).[b]B3LYP/aT-PP.

Table A2.34. MF_7^- (M=Pt and Au) nonclassical structures total electronic energies at the DFT level with various exchange-correlation functionals and the aD-PP basis set in atomic units.

Method	**PtF_7^-**	**AuF_7^-**
State/symm	**$^3A'/C_s$**	**$^2A'/C_s$**
SVWN5	-813.904303	-830.041548
BLYP	-818.414584	-834.576479
BP86	-818.600869	-834.768148
PW91	-818.392473	-834.559003
PBE	-817.867465	-834.028615
TPSS	-818.503677	-834.658216
HCTH	-818.67158	-834.876676
B3LYP	-818.468718	-834.642114
mPW1	-818.295351	-834.470176
PBE1	-817.751639	-833.921253
O3LYP	-818.347734	-834.533767
TPSSh	-818.503255	-834.657728

Table A2.35. MF_5 electronic energies at the DFT level with the B3LYP functional and the aD-PP basis set, zero point energies at the B3LYP/aT-PP level and CCSD(T) energies with the aug-cc-pVnZ/aug-cc-pVnZ-PP basis sets (n = D, T, Q) and at the CBS level, core and valence energies at the CCSD(T)/aug-cc-pWCVTZ-PP level, scalar relativistic energies at the CISD/aT-PP and CCSD(T)-DK/aug-cc-pVTZ-DK energies in atomic units.

Method	**WF_5**	**ReF_5**	**OsF_5**	**IrF_5**	**PtF_5**	**AuF_5**
State/symm	$^2A_2/C_{2v}$	$^3A_1'/D_{5h}$	$^4B_1/C_{4v}$	$^5B_1/C_{4v}$	$^2B_1/C_{4v}$	$^1A_1/C_{4v}$
CCSD(T)/aD-PP	-565.490323	-576.501881	-588.712391	-602.187413	-617.015332	-633.163511
CCSD(T)/aT-PP	-565.933451	-576.953079	-589.170249	-602.652057	-617.493525	-633.647997
CCSD(T)/aQ-PP	-566.076686	-577.098915	-589.318923	-602.803443	-617.650467	-633.809099
CCSD(T)/CBS	-566.159829	-577.183569	-589.405232	-602.891334	-617.741598	-633.90267
Core	-566.569207	-577.599541	-589.824485	-603.311818	-618.152123	-634.301549
Valence	-565.971621	-576.992193	-589.210501	-602.693532	-617.537193	-633.693023
SR	-0.43572746	-0.43621273	-0.43689681	-0.4377903	-0.43875633	-0.44002921
CCSD(T)/aT-DK	-16627.135394	-17176.246646	-17737.237034	-18310.240479	-18895.493045	-19493.104784
ZPE	0.010394	0.010973	0.010498	0.010715	0.010755	0.009874
SVWN5	-563.7350951	-574.7759462	-587.011226	-600.513795	-615.347316	-631.475427
BLYP	-566.9543642	-577.998552	-590.243949	-603.760336	-618.607925	-634.760598
BP86	-567.0965746	-578.151446	-590.405755	-603.929436	-618.784045	-634.941901
PW91	-566.938645	-577.993650	-590.247296	-603.770276	-618.623474	-634.780045
PBE	-566.5675436	-577.6186294	-589.868149	-603.386548	-618.234286	-634.386016
TPSS	-567.036821	-578.079707	-590.321959	-603.829824	-618.672327	-634.816476

HCTH	-567.110927	-578.1921357	-590.473729	-604.029523	-618.909548	-635.102558
B3LYP	-567.000228	-578.044542	-590.287895	-603.797713	-618.649737	-634.808379
mPW1	-567.034935	-577.9256251	-590.170799	-603.679285	-618.529536	-634.688857
PBE1	-566.489811	-577.5345197	-589.775641	-603.279871	-618.124973	-634.279146
O3LYP	-566.8926655	-577.9520995	-590.210575	-603.737902	-618.602355	-634.775094
TPSSh	-567.036621	-578.079459	-590.322129	-603.829418	-618.672631	-634.815913

Table A2.36. T_1 diagnostic at the CCSD(T)/aT-PP level (States and symmetry types as in tables S1 through S4).

M	MF_6	MF_6^-	MF_5	MF_7^-
W	0.022	0.021	0.022	0.021
Re	0.026	0.023	0.025	0.023
Os	0.030	0.024	0.029	0.026
Ir	0.032	0.028	0.026	0.027
Pt	0.038	0.028	0.032	0.029
Au	0.034	0.022	0.025	0.023

Table A2.37. MF_6 XYZ coordinates at BP86/aT-PP level or BP86/aD-PP level for the D_{3d} structures in Å.

WF_6

9	0.000000	0.000000	1.851724
9	0.000000	1.851724	0.000000
9	0.000000	-1.851724	0.000000
9	-1.851724	0.000000	0.000000
9	0.000000	0.000000	-1.851724
9	1.851724	0.000000	0.000000
74	0.000000	0.000000	0.000000

ReF_6

9	0.000000	1.866137	0.000000
9	0.000000	0.000000	1.824867
9	0.000000	0.000000	-1.824867
9	1.866137	0.000000	0.000000
9	0.000000	-1.866137	0.000000
9	-1.866137	0.000000	0.000000
75	0.000000	0.000000	0.000000

ReF_6, D_{3d}

9	0.000000	1.542402	1.037741
9	-1.335759	0.771201	-1.037741
9	1.335759	-0.771201	1.037741
9	-1.335759	-0.771201	1.037741
9	0.000000	-1.542402	-1.037741
9	1.335759	0.771201	-1.037741
75	0.000000	0.000000	0.000000

OsF_6

9	0.000000	1.843828	0.000000
9	0.000000	0.000000	1.882160
9	0.000000	0.000000	-1.882160
9	0.000000	-1.843828	0.000000
9	-1.843828	0.000000	0.000000
9	1.843828	0.000000	0.000000
76	0.000000	0.000000	0.000000

OsF_6, D_{3d}

9	0.000000	1.504588	1.100534
9	-1.303011	0.752294	-1.100534
9	0.000000	-1.504588	-1.100534
9	1.303011	-0.752294	1.100534
9	1.303011	0.752294	-1.100534
9	-1.303011	-0.752294	1.100534
76	0.000000	0.000000	0.000000

IrF_6

77	0.000000	0.000000	0.000000
9	0.000000	0.000000	1.863600
9	0.000000	1.863600	0.000000
9	0.000000	0.000000	-1.863600
9	0.000000	-1.863600	0.000000
9	1.863600	0.000000	0.000000
9	-1.863600	0.000000	0.000000

PtF_6

9	0.000000	0.000000	1.862639
9	0.000000	1.891244	0.000000
9	0.000000	0.000000	-1.862639
9	0.000000	-1.891244	0.000000
9	-1.891244	0.000000	0.000000
9	1.891244	0.000000	0.000000
78	0.000000	0.000000	0.000000

PtF_6, D_{3d} B3LYP/aT-PP

9	0.000000	1.528414	1.059997
9	-1.323645	0.764207	-1.059997
9	1.323645	-0.764207	1.059997
9	-1.323645	-0.764207	1.059997
9	0.000000	-1.528414	-1.059997
9	1.323645	0.764207	-1.059997
78	0.000000	0.000000	0.000000

AuF_6

79	0.000000	0.000000	0.000000
9	0.000000	0.000000	1.929096
9	0.000000	1.895098	0.000000
9	1.895098	0.000000	0.000000
9	-1.895098	0.000000	0.000000
9	0.000000	-1.895098	0.000000
9	0.000000	0.000000	-1.929096

AuF_6, D_{3d}

9	0.000000	1.559561	1.111830
9	-1.350620	0.779781	-1.111830
9	0.000000	-1.559561	-1.111830
9	1.350620	-0.779781	1.111830
9	1.350620	0.779781	-1.111830
9	-1.350620	-0.779781	1.111830
79	0.000000	0.000000	0.000000

Table A2.38. MF_6^- XYZ coordinates at BP86/aT-PP level and BP86/aD-PP level for the D3d structures in Å.

WF_6^-

9	0.000000	0.000000	1.879279
9	0.000000	1.936010	0.000000
9	0.000000	-1.936010	0.000000
9	-1.936010	0.000000	0.000000
9	0.000000	0.000000	-1.879279
9	1.936010	0.000000	0.000000
74	0.000000	0.000000	0.000000

WF_6^-, D_{3d}

9	0.000000	1.608575	1.053194
9	-1.393066	0.804287	-1.053194
9	1.393066	-0.804287	1.053194
9	-1.393066	-0.804287	1.053194
9	0.000000	-1.608575	-1.053194
9	1.393066	0.804287	-1.053194
74	0.000000	0.000000	0.000000

ReF_6^-

9	0.000000	1.893385	0.000000
9	0.000000	0.000000	1.947208
9	0.000000	0.000000	-1.947208
9	0.000000	-1.893385	0.000000
9	1.893385	0.000000	0.000000
9	-1.893385	0.000000	0.000000
75	0.000000	0.000000	0.000000

ReF_6^-, D_{3d}

9	0.000000	1.535794	1.131021
9	-1.330036	0.767897	-1.131021
9	0.000000	-1.535794	-1.131021
9	1.330036	-0.767897	1.131021
9	1.330036	0.767897	-1.131021
9	-1.330036	-0.767897	1.131021
75	0.000000	0.000000	0.000000

OsF_6^-

9	0.000000	0.000000	1.909175
9	0.000000	1.909175	0.000000
9	0.000000	-1.909175	0.000000
9	-1.909175	0.000000	0.000000
9	0.000000	0.000000	-1.909175
9	1.909175	0.000000	0.000000
76	0.000000	0.000000	0.000000

IrF_6^-

9	0.000000	0.000000	1.882363

9	0.000000	1.928126	0.000000
9	0.000000	0.000000	-1.882363
9	0.000000	-1.928126	0.000000
9	1.928126	0.000000	0.000000
9	-1.928126	0.000000	0.000000
77	0.000000	0.000000	0.000000

IrF_6^-, D_{3d}

9	0.000000	1.583848	1.087025
9	-1.371653	0.791924	-1.087025
9	1.371653	-0.791924	1.087025
9	-1.371653	-0.791924	1.087025
9	0.000000	-1.583848	-1.087025
9	1.371653	0.791924	-1.087025
77	0.000000	0.000000	0.000000

PtF_6^-

78	0.000000	0.000000	0.000000
9	0.000000	0.000000	1.956496
9	0.000000	1.905619	0.000000
9	1.905619	0.000000	0.000000
9	-1.905619	0.000000	0.000000
9	0.000000	-1.905619	0.000000
9	0.000000	0.000000	-1.956496

PtF_6^-, D_{3d}

9	0.000000	1.565928	1.128003
9	-1.356133	0.782964	-1.128003
9	0.000000	-1.565928	-1.128003
9	1.356133	-0.782964	1.128003
9	1.356133	0.782964	-1.128003
9	-1.356133	-0.782964	1.128003
78	0.000000	0.000000	0.000000

AuF_6^-

79	0.000000	0.000000	0.000000
9	0.000000	0.000000	1.938948
9	0.000000	1.938948	0.000000
9	0.000000	-1.938948	0.000000
9	0.000000	0.000000	-1.938948
9	-1.938948	0.000000	0.000000
9	1.938948	0.000000	0.000000

Table A2.39. MF_7^- XYZ coordinates at BP86/aT-PP level in Å.

WF_7^-

74	0.000000	0.000000	0.000000
9	0.000000	0.000000	1.878160
9	0.000000	1.927148	0.000000
9	1.832826	0.595521	0.000000
9	1.132749	-1.559095	0.000000
9	-1.132749	-1.559095	0.000000
9	0.000000	0.000000	-1.878160
9	-1.832826	0.595521	0.000000

ReF_7^-

9	1.892042	0.000000	0.000463
9	0.000000	1.850074	-0.604645
9	0.000000	0.000000	-1.893041
9	0.000000	-1.850074	-0.604645
9	0.000000	-1.121082	1.549694
9	-1.892042	0.000000	0.000463
9	0.000000	1.121082	1.549694
75	0.000000	0.000000	0.000242

OsF_7^-

9	0.000000	0.000000	1.905775
9	0.000000	1.921797	0.000000
9	1.827738	0.593868	0.000000
9	1.129604	-1.554766	0.000000
9	-1.129604	-1.554766	0.000000
9	0.000000	0.000000	-1.905775
9	-1.827738	0.593868	0.000000
76	0.000000	0.000000	0.000000

IrF_7^-

9	1.925016	0.000000	-0.000309
9	0.000000	1.850122	-0.603036
9	0.000000	1.125815	1.553918
9	0.000000	-1.125815	1.553918
9	0.000000	-1.850122	-0.603036
9	0.000000	0.000000	-1.903179
9	-1.925016	0.000000	-0.000309
77	0.000000	0.000000	0.000237

PtF_7^- C_s

9	-1.398687	1.340354	0.193905
9	0.000000	0.000000	2.050671

9	-1.398687	-1.340354	0.193905
9	1.398687	-1.340354	0.193905
9	1.398687	1.340354	0.193905
9	0.000000	0.971201	-1.969646
9	0.000000	-0.971201	-1.969646
79	0.000000	0.000000	0.126798

PtF_7^- D_{5h}

9	-1.398687	1.340354	0.193905
9	0.000000	0.000000	2.050671
9	-1.398687	-1.340354	0.193905
9	1.398687	-1.340354	0.193905
9	1.398687	1.340354	0.193905
9	0.000000	0.971201	-1.969646
9	0.000000	-0.971201	-1.969646
79	0.000000	0.000000	0.126798

AuF_7^- C_s

9	-0.202375	1.263661	1.369953
9	-2.120558	-0.091661	0.000000
9	-0.202375	-1.465493	1.369516
9	1.757534	-0.172564	0.000000
9	2.900854	1.515773	0.000000
9	-0.202375	-1.465493	-1.369516
9	-0.202375	1.263661	-1.369953
79	-0.196898	-0.096594	0.000000

AuF_7^- C2v

9	-1.398687	1.340354	0.193905
9	0.000000	0.000000	2.050671
9	-1.398687	-1.340354	0.193905
9	1.398687	-1.340354	0.193905
9	1.398687	1.340354	0.193905
9	0.000000	0.971201	-1.969646
9	0.000000	-0.971201	-1.969646
79	0.000000	0.000000	0.126798

Table A2.40. MF_5 XYZ coordinates at the B3LYP/aT level in Å.

WF_5			
9	0.000000	1.492595	-1.043421
9	1.892640	0.000000	0.023503
9	-1.892640	0.000000	0.023503
9	0.000000	0.000000	1.839251
9	0.000000	-1.492595	-1.043421
74	0.000000	0.000000	0.024395
ReF_5			
9	0.000000	1.815916	0.000000
9	0.000000	0.000000	1.903431
9	0.000000	0.000000	-1.903431
9	1.572630	-0.907958	0.000000
9	-1.572630	-0.907958	0.000000
75	0.000000	0.000000	0.000000
OsF_5			
9	0.000000	1.850061	0.309933
9	-1.850061	0.000000	0.309933
9	1.850061	0.000000	0.309933
9	0.000000	0.000000	-1.760717
9	0.000000	-1.850061	0.309933
76	0.000000	0.000000	0.061696
IrF_5			
9	0.000000	1.840008	0.281241
9	-1.840008	0.000000	0.281241
9	1.840008	0.000000	0.281241
9	0.000000	0.000000	-1.889495
9	0.000000	-1.840008	0.281241
77	0.000000	0.000000	0.089361
PtF_5			
9	0.000000	1.870960	0.189644
9	-1.870960	0.000000	0.189644
9	1.870960	0.000000	0.189644
9	0.000000	0.000000	-1.746377
9	0.000000	-1.870960	0.189644
78	0.000000	0.000000	0.113977
AuF_5			
9	0.000000	1.897984	0.224248
9	-1.897984	0.000000	0.224248
9	1.897984	0.000000	0.224248
9	0.000000	0.000000	-1.764245
9	0.000000	-1.897984	0.224248
79	0.000000	0.000000	0.098801

3. Electron Affinities, Fluoride Affinities, and Heats of Formation of the Second Row Transition Metal Hexafluorides: MF_6 (M = Mo, Tc, Ru, Rh, Pd, Ag)

Abstract

High level electronic structure calculations were used to evaluate reliable, self-consistent thermochemical data sets for the second row transition metal hexafluorides. The electron affinities, heats of formation, first ($MF_6 \rightarrow MF_5 + F$) and average M-F bond dissociation energies, and fluoride affinities of MF_6 ($MF_6 + F^- \rightarrow MF_7^-$) and MF_5 ($MF_5 + F^- \rightarrow MF_6^-$) were calculated. The electron affinities are higher than those of the corresponding third row hexafluorides making them stronger one-electron oxidizers. The calculated electron affinities, in good agreement with the available experimental values, are: MoF_6 (4.23 eV), TcF_6 (5.89 eV), RuF_6 (7.01 eV), RhF_6 (6.80 eV), PdF_6 (7.95 eV), AgF_6 (8.89 eV). The corresponding pentafluorides are also very strong Lewis acids, although their acidity on the pF^- scale is about one unit lower than those of the third row pentafluorides. The performance of a wide range of DFT exchange-correlation functionals was benchmarked by comparing them to our more accurate CCSD(T) results.

Introduction

There is substantial interest in the development of strong electron acceptors which can serve as strong oxidizers. We have just reported the reliable prediction of the electron affinities of the MF_6 compounds for the 3rd row transition metals.[1] We showed that the electron affinities increase monotonically from WF_6 to AuF_6 and that the inclusion of spin orbit corrections is essential to obtain the correct qualitative order for the electron affinities. In addition, we predicted the fluoride affinities of the MF_6 compounds and the corresponding pentafluorides. Our calculations show that these fluorides are strong Lewis acids. A new type of structure was predicted for PtF_7^- and AuF_7^- with a very weak external MF_6^--F bond between an MF_6^- fragment and a fluorine atom. We now extend our efforts to the 2nd row transition metal MF_6 compounds.

MF_6 molecules with the metal ion M in the +VI oxidation state surrounded by six F^- in an octahedral field can exhibit Jahn–Teller distortions.[2] For the second row transition metals, studies[3,4,5,6] of the experimental vibrational spectra of TcF_6 and RuF_6 showed Jahn-Teller effects. Seppelt has reviewed the structures and properties of a series of main group, actinide and transition metal hexafluorides, including MoF_6, TcF_6, RuF_6 and RhF_6.[7] Experimentally, the M-F bond lengths have been found to be essentially the same for M = Mo, Tc and Ru and slightly longer for M = Rh from single-crystal x-ray diffraction measurements.[8] This is consistent with the result that in the third row transition metal series, the M-F bond lengths for M = W, Re, and Os are approximately the same, with the Ir-F and Pt-F bond lengths being longer.[9] Holloway and co-workers[10] found in their EXAFS study that the M-F bond distance increased from Mo to Ru to Rh. Bartlett and co-workers[11] used synchrotron X-ray powder diffraction to study the $LiMF_6$ salts and obtained single-crystal data for $KRhF_6$. A number of theoretical studies have predicted the M-F bond distances in MoF_6,[12,13,14] MoF_6^-,[15] TcF_6,[12] RuF_6,[12] RhF_6,[12] PdF_6,[16] and AgF_6^-.[17]

For the second row transition metal hexafluorides, MoF_6 has been the most studied in terms of its electron affinity both experimentally and theoretically. Mathur et al.[18] set a lower limit for EA(MoF_6) = 4.5 eV from their study of ionization reactions between MoF_6 and alkali metal atoms. Compton and co-workers[19] also studied the collisions of alkali metal atoms with a series of hexafluorides including MoF_6 and found that EA(MoF_6) should be at least 5.1 eV. Sidorov and co-workers[20] investigated the electron affinities of higher molybdenum fluorides by measuring the equilibrium constants of ion-molecule reactions using high temperature Knudsen cell mass spectroscopy and determined EA(MoF_6) = 3.6 eV;. later, this group[21] revised the value to EA(MoF_6) = 3.8 eV. This group[22] also reported EA(RuF_6) = 6.47 eV and later[21] revised it to EA(RuF_6) = 7.5 eV. These results showed that EA(RuF_6) is higher than that of the corresponding third row OsF_6 (EA = 5.94 eV), in agreement with the observation that O_2 can be oxidized to O_2^+ by RuF_6, which in the third row hexafluorides does not occur until PtF_6.[23] Selig and co-workers[24] estimated EA(TcF_6) = 6.94 eV based on the correlation of layer spacing and charge transfer with the electron affinities of transition metal hexafluorides intercalated into graphite. Bartlett[25] found that the O_2RhF_6 salt is less stable towards dissociation to its constituent molecules than O_2RuF_6 and also has a larger unit cell volume, unlike the lithium salts where the unit cell volume of $LiRhF_6$ is smaller than that of $LiRuF_6$. This led to the conclusion that EA(RuF_6) is greater than that of RhF_6, in contrast to the third row transition metal hexafluorides where the electron affinities increase from WF_6 to AuF_6.[1]

There have been a number of theoretical studies of the electron affinities of the second row transition metal hexafluorides. Sakai, Miyoshi, and co-workers[15,26] calculated the MF_6 electron affinities for M = Cr, Mo, and W using the model potential method and predicted EA(MoF_6) > EA(WF_6) by ~ 2 eV. Adding an f function to the metal basis set and a d function to

the fluorine basis set led to a value of 5.37 eV for EA(MoF_6). Seppelt and co-workers[12] predicted the electron affinities of MoF_6, TcF_6, RuF_6 and RhF_6 to be 4.11, 5.64, 6.98, and 6.60 eV, respectively, at the B3LYP level with the Hay-Wadt (n+1) VDZ ECP basis set for the metals and the aug-cc-pVTZ basis set for F. The available experimental and calculated values of the electron affinities are summarized in Table 3.1.

There are only a few experimental studies of the heats of formation of the second row transition metal hexafluorides and no theoretical predictions. For MoF_6, the first reported value of -388 kcal/mol for $\Delta H_{f,298K}(MoF_6)$ is from solution calorimetry.[27] A second value of -372.3 ± 0.2 kcal/mol is from direct combination of the elements in a bomb calorimeter.[28]

Molecular fluoride affinities provide an estimate of the Lewis acid strength of a given species.[29] From the infrared spectra of UF_6, WF_6 and MoF_6 complexes codeposited with hydrogen fluoride, the fluoride affinity of MoF_6 was estimated to be greater than 70 kcal/mol .[30] The prediction was based on the assumption of a linear relationship between the fluoride affinities and the frequency shift of the HF stretching mode in the complex.

We describe here the results of high-level electronic structure calculations at the CCSD(T) level of the structures, electron affinities, heats of formation, first ($MF_6 \rightarrow MF_5 + F$) and average M-F bond dissociation energies, and fluoride affinities ($MF_6 + F^- \rightarrow MF_7^-$) of MF_6 for M = Mo, Tc, Ru, Rh, Pd and Ag. We also report the fluoride affinities of MF_5 as these can be directly calculated from our data. The electron affinities can be used in the development of a quantitative scale of the strength of very strong oxidizers. The electron affinity and the fluoride affinity often compete with each other, so good values for both are required for the design of the best oxidizing agent. In addition, we report on the ability of the DFT method to predict these energetic properties.

Computational Methods

We have followed the approach described in our previous paper on the third row transition metal hexafluorides.[1] Equilibrium geometries and vibrational frequencies were calculated first at the DFT level with a range of local, gradient-corrected, and hybrid exchange-correlation functionals (See Supporting Information for a list of functionals) and then at the CCSD(T) level.[31,32,33,34.] The initial DFT calculations were done with the Gaussian program system[35] and the CCSD(T) calculations with the Molpro program system.[36] The CCSD(T) energies were extrapolated to the complete basis set (CBS) limit by using a mixed Gaussian/exponential formula.[37] The calculations were performed with the augmented correlation consistent double-ζ (aug-cc-pVDZ) basis set for F[38] and the aug-cc-pVDZ-PP basis sets with accompanying small-core relativistic pseudopotentials for the transition metal atoms.[39] Several corrections have been used to adjust the CBS valence electronic energies: (1) a core-valence correlation correction (ΔE_{CV}); (2) scalar relativistic corrections on the F atoms and corrections for any errors in the metal pseudopotentials for the electron affinities (EAs). The latter is calculated by taking the difference between the EA calculated at the Douglas-Kroll-Hess[40] level with the CCSD(T)-DK method and the aT-DK basis set[41,42,43] and the EA calculated at the CCSD(T)/aT-PP level (a separate estimate of just the pseudopotential error is described in the Supporting Information); (3) molecular spin orbit corrections calculated using the spin orbit approach and scalar two-component zero-order regular approximation (ZORA)[44] as implemented in the ADF 2008.01 program;[45] and (4) the zero point energy calculated at the DFT level. The electron affinity was calculated as the sum of the different contributions (Equation (1)).

$$EA_{0K} = EA_{CBS} + \Delta EA_{ZPE} + \Delta EA_{CV} + \Delta EA_{Rel} + \Delta EA_{SO} \quad (1)$$

Total atomization energies (TAEs) for the prediction of the heats of formation were calculated using an equation similar to Equation (1). In calculating the TAEs, we chose the lowest lying atomic state with no SO splitting, and used the experimental SO splittings if needed.[46] The experimental atomic heats of formation at 0 K were taken from the JANAF Tables[47] for F and from the compilation of Wagman et al.[48] for the metals. The atomic heats of formation have also been given by Greenwood and Earnshaw[49] and these can be used to help provide an estimate of the range of errors for the molecular heats of formation due to the atomic heats of formation. The appropriate enthalpy change from 0 to 298 K ($\Delta H_{0K\rightarrow 298K}$) is 1.05 for F. For all the metal atoms we have used a value of 1.2 kcal/mol for $\Delta H_{0K\rightarrow 298K}$ as a best estimate from the available data.[1]

The calculations were performed on computers at The University of Alabama, the Alabama Supercomputing Center, and the Molecular Sciences Computing Facility in the William R. Wiley Environmental Molecular Sciences Laboratory at the Pacific Northwest National Laboratory.

Results and Discussion

Geometries of the Hexafluorides. Table 3.2 lists the metal-fluorine bond distances of the neutral hexafluorides and their anions optimized at the CCSD(T) levels with aT-PP basis set and the ZORA and ZORA SO BLYP/TZ2P level. The Cartesian coordinates as well as the geometries optimized with the various DFT exchange correlation functionals and the CCSD(T)/aD-PP method are given as Supporting Information. We explored a variety of structures (symmetries) and orbital combinations in our studies of the open shell molecules in order to obtain the ground state structures. We have previously discussed[1] the geometry behavior

on the orbital occupancies of the t_{2g} orbitals that are being filled for the third row transition metal atoms and the same models apply here.

MoF_6. The calculated Mo-F bond distance for MoF_6 (O_h) of 1.825 Å is in good agreement with the value of 1.817 Å reported by Seppelt[12] in a single crystal structure determination and that of 1.809 Å reported by Holloway[10] in the EXAFS study of MF_6 (M=Mo,Ru and Rh). The ZORA-SO/BLYP/TZ2P bond distance for MoF_6 is 1.870 Å, too long as compared to the CCSD(T) and the measured values.

MoF_6^- and TcF_6. The D_{4h} structures of MoF_6^- and TcF_6 have two short and four long bond distances with averages of 1.889 Å for r(Mo-F) and 1.816 Å for r(Tc-F). The O_h structures, with the M-F bond distance calculated as the average of the bonds in the D_{4h} structures, were found to be less than 1 kcal/mol higher in energy than the D_{4h} structures for both MoF_6^- and TcF_6. The Mo-F and Tc-F bond lengths in the D_{3d} structures, which have essentially the same energy as the D_{4h} structure at the CCSD(T)/CBS level, are 1.888 Å for r(Mo-F) and 1.816 Å for r(Tc-F). Our calculated value for r(Tc-F) is in excellent agreement with the experimentally determined value[12] of 1.812 Å. ZORA-SO predicted that the D_{4h} structures for both MoF_6^- and TcF_6 are less than 1 kcal/mol lower in energy than the D_{3d} structures. For both MoF_6^- and TcF_6 at the ZORA-SO level, the D_{4h} structures have two long and four short bond distances (an opposite bonding pattern from the predicted CCSD(T) structure) that differ by only 0.005 Å. Energetically, the D_{4h} structures are lower at the CCSD(T)/CBS and ZORA-SO levels, but after all corrections are included, the MoF_6^- D_{3d} structure is 1.1 kcal/mol lower in energy and the TcF_6 D_{3d} structure has basically the same energy, being lower by only 0.04 kcal/mol. (See Figure 3.1 for energy splittings). The D_{3d} structure becomes lower in energy due to the difference in zero point energies.

TcF_6^- and RuF_6. The $^3A_{1g}/D_{4h}$ structure is predicted to be the ground state for TcF_6^- with the $^1A_{1g}/D_{4h}$ structure 29.1 kcal/mol higher in energy at the CCSD(T)/aD-PP level. The $^3A_{1g}/D_{3d}$ structure, after all corrections have been included is above the $^3A_{1g}/D_{4h}$ structure by 0.6 kcal/mol. For RuF_6, the $^1A_{1g}/D_{4h}$ structure is 23.4 kcal/mol above the $^3A_{1g}/D_{4h}$ structure. The $^3A_{1g}/D_{3d}$ structure is predicted to be higher than the the $^1A_{1g}/D_{4h}$ structure by 0.54 kcal/mol at the CBS level, but lower by 0.24 kcal/mol at the ZORA-SO level, and after all corrections are included, the $^3A_{1g}/D_{3d}$ structure is more stable by almost 2 kcal/mol. This is mostly due to the difference in the zero point energies. As for MoF_6^- and TcF_6, the O_h geometries are less than 1 kcal/mol above the D_{4h} structures. The two long and four short bond distances in the D_{4h} structures of both TcF_6^- and RuF_6 average to 1.871 Å and 1.814 Å, respectively, and the D_{3d} structures have the same values. Our calculated average value for r(Ru-F) is in excellent agreement with the values of 1.818 Å reported by Seppelt[12] and of 1.824 Å reported by Holloway.[10] ZORA-SO/BLYP/TZ2P predicts an average bond distance of 1.921 Å for the TcF_6^- D_{4h} structure with two short and four long bond distances. The more stable D_{3d} structure at ZORA-SO in the case of RuF_6 shows a r(Ru-F) bond length of 1.876 Å, longer than the experimental and CCSD(T) values by ~0.05 Å.

RuF_6^- and RhF_6. Both RuF_6^- and RhF_6 have O_h symmetry. The calculated Ru-F bond distance of 1.860 Å is very close to the value of 1.851 Å reported by Bartlett and coworkers[11] in the x-ray powder diffraction study of the $LiRuF_6$ salt. The calculated Rh-F bond distance of 1.815 Å is also close to the measured values of 1.824 Å[12] and 1.838 Å.[10] ZORA-SO predicts O_h structures with bond distances of 1.921 Å for r(Ru-F) and 1.883Å for r(Rh-F), again too long as compared to experiment.

RhF_6^- and PdF_6. At the CCSD(T)/CBS level, the $^3A_{1g}/D_{4h}$ structure is predicted to be the ground state for both RhF_6^- and PdF_6. The $^1A_{1g}/D_{4h}$ structure is higher by 24.1 and 11.5 kcal/mol

for RhF_6^- and PdF_6, respectively, at the CCSD(T)/aD-PP level, and the O_h structure is within 0.5 kcal/mol of the ground state structure for both. ZORA-SO predicts the D_{3d} structure to be more stable by 0.16 and 0.13 kcal/mol for both RhF_6^- and PdF_6, and after all corrections are included, the D_{3d} structure remains lower in energy than the D_{4h} structure for RhF_6^-. The calculated values of 1.856 Å for r(Rh-F) in the D_{4h} structure and of 1.855 Å in the D_{3d} structure are in excellent agreement with the experimentally determined values of 1.855(5) Å[11] and 1.853(1) Å.[50] Our calculated average value of 1.849 Å for r(Pd-F) is consistent with the value of 1.852 Å for r(Pt-F) determined from electron diffraction measurements.[9] A calculated value of 1.893[51] at the B3LYP level with a smaller basis set than ours is clearly too long.

PdF_6^- and AgF_6. The D_{4h} structure has two long bonds and four short bonds with average values of 1.862 Å for PdF_6^- and 1.884 Å for AuF_6. At the CCSD(T)/CBS level, the D_{4h} structure is predicted to be more stable than the D_{3d} structure by 0.87 kcal/mol for PdF_6^- and less stable by 0.56 kcal/mol for AgF_6. The O_h structure is 0.6 kcal/mol higher in energy than the D_{4h} structure for PdF_6^- and 0.8 kcal/mol higher than the D_{3d} structure for AgF_6, both at the B3LYP/aD-PP level. After all corrections are included, the ground state for PdF_6^- is predicted to be the D_{4h} structure and for AgF_6 the D_{3d} structure. At the ZORA-SO level, the D_{4h} and D_{3d} structures for PdF_6^- have essentially the same energy within 0.1 kcal/mol with an average bond distance of 1.942 Å, and AgF_6 is predicted to be octahedral with a bond length of 1.949 Å.

AgF_6^-. The AgF_6^- anion has O_h symmetry with a calculated Ag-F distance of 1.884 Å at the CCSD(T)/aT-PP level and 1.960 Å at the ZORA-SO level. A calculated value of 1.920 was reported from an MP2 optimization.[52]

The average calculated M-F bond distances show a slight decrease from MoF_6 to TcF_6 with r(Tc-F), r(Ru-F) and r(Rh-F) being essentially the same and an increase to PdF_6 and AgF_6.

The experimental gas phase values for r_g(M-F), M=Mo to Rh are essentially the same within 0.008 Å. The average calculated M-F bond distances in the MF_6^- anions decrease from 1.889 Å for Mo-F to 1.856 Å for Rh-F and increase to 1.862 Å for Pd-F and 1.884 Å for Ag-F. Our calculated value for r(Ru-F) in RuF_6^- is within 0.009 Å of the powder diffraction value.[11]

Vibrational Frequencies. The six normal modes for MF_6 with O_h symmetry are ν_1 (a_{1g}), ν_2(e_g), ν_3(t_{1u}), ν_4(t_{1u}), ν_5(t_{2g}), and ν_6(t_{2u}). Under the Jahn-Teller distortion from O_h to D_{4h}, the vibrational modes split as follows: $a_{1g} \rightarrow a_{1g}$, $e_g \rightarrow a_{1g} + b_{1g}$, each of the two $t_{1u} \rightarrow a_{2u} + e_u$, $t_{2g} \rightarrow b_{2g} + e_g$ and $t_{2u} \rightarrow b_{2u} + e_u$.). Under the Jahn-Teller distortion from O_h to D_{3d}, the modes split as follows: $a_{1g} \rightarrow a_{1g}$, $e_g \rightarrow e_g$, each of the two $t_{1u} \rightarrow a_{2u} + e_u$, $t_{2g} \rightarrow a_{1g} + e_g$ and $t_{2u} \rightarrow a_{2u} + e_u$. In Table 3.3, the experimental frequencies[3,4,5,6] are compared to those calculated at the B3LYP/aT-PP and/or BP86/aD-PP levels.

MoF_6 and RhF_6, which have O_h symmetry, do not exhibit splittings of the vibrational modes. Our calculated B3LYP/aT-PP values for MoF_6 are smaller than the experimental values by 7 to 18 cm^{-1} showing excellent agreement between theory and experiment.[3,5] For RhF_6, the values for all modes except for the a_{1g} one are larger by up to 10 cm^{-1}, in good agreement with the experimental values.[6] The calculated value for the a_{1g} mode is larger than the experimental value by ~30 cm^{-1}.

Weinstock[6] described the Jahn-Teller effect on the e_g vibrational mode of the 4d and 5d hexafluoride molecules. He noted that the low intensity and the broad shape of the ReF_6 and OsF_6 ν_2(e_g) vibrational mode are evidence for the Jahn-Teller effect. For the 4d MF_6 molecules, the broadening was even more pronounced for TcF_6, and for RuF_6, the unusually large splitting did not allow for the assignment of the bandwidth. Our calculated BP86/aD-PP frequencies for D_{4h} TcF_6 can be compared to the experimental values.[3,4,5] The a_{1g} stretch is smaller than the

experimental value[3] by 41 cm^{-1} and there is a small splitting of 6 cm^{-1} f the e_g mode. There are larger splittings of the t_{1u} modes, of 20 and 45 cm^{-1}, with their averages being in reasonable agreement with the experiment.[5] The t_{2g} scissoring mode shows a large splitting of 120 cm^{-1}, but the average is qualitatively in agreement with experiment.[4] The value of the t_{2g} splitting is smaller than that of 253 cm^{-1} predicted[1] for the corresponding third row hexafluoride ReF_6. The D_{3d} structure of TcF_6 shows frequencies similar to those of the D_{4h} structure. The t_{2g} splitting is 13 cm^{-1} in the D_{3d} structure, much lower than that in the D_{4h} structure. The e_g mode does not split under D_{3d} symmetry and is 110 cm^{-1} lower than the average of the a_{1g} and b_{1g} modes in D_{4h} symmetry, and 140 cm^{-1} lower than the experimental value. This suggests that TcF_6 has D_{4h} symmetry.

In the other MF_6 compounds, the t_{2g} scissoring mode shows splitting ranging from 52 to 57 cm^{-1}. For the D_{4h} structures of TcF_6 and PdF_6, the e_g mode has the higher frequency , whereas for the AgF_6 D_{4h} structure the b_{2g} mode has the higher frequency. This behavior can be explained[1] by the two different types of bonding that appear on lowering the symmetry from O_h to D_{4h} when the O_h t_{2g} mode splits into a b_{2g} equatorial and an e_g axial scissoring mode. For TcF_6 and PdF_6 there are 2 shorter M-F axial bonds which lead to the e_g axial mode having the higher frequency. For AgF_6 there are four shorter equatorial bonds which lead to the b_{2g} equatorial scissoring mode to have the higher frequency.

The B3LYP/aT-PP calculated values for the frequencies of the RuF_6 D_{4h} and D_{3d} structures are similar to those of TcF_6. For both geometries, the a_{1g} stretch is larger than experiment[6] by 20 cm^{-1}. The e_g mode splits by 14 cm^{-1} in the D_{4h} structure and is larger by 3 cm^{-1} than the experimental value,[4] whereas in the D_{3d} structure, it is lower than experiment by 161 cm^{-1} and does not split. The t_{1u} modes split by 14 and 44 cm^{-1} in the D_{4h} structure, and their averages

are within 10 cm^{-1} of the experimental values.[6] In the D_{3d} structure, the t_{1u} modes split by 6 and 22 cm^{-1}, with the averages being within 14 cm^{-1} of experiment.[6] Our calculated values show larger splittings for the t_{2g} and t_{2u} modes. In the D_{4h} structure, the t_{2g} mode splits by 52 cm^{-1} and the t_{2u} mode by 56 cm^{-1}. In the D_{3d} structure, the splitting are 45 and 65 cm^{-1} for the t_{2g} and t_{2u} modes, respectively.

The differences between the calculated and the experimental[3,4,5,6] zero point energies (ZPEs) are given in Table 3.6. All ZPEs calculated at the B3LYP/aT-PP level, except for RuF_6, are within 0.3 kcal/mol of the experimental values, as is the ZPE calculated at the BP86/aD-PP level for TcF_6. The calculated ZPE for RuF_6 is 0.6 kcal/mol smaller than experiment.

Electron Affinities and Oxidizer Strengths. Table 3.4 lists the valence CBS energies, the various additive energy corrections, and the calculated composite electron affinities. In Table 3.1, the electron affinities are compared with the experimental values. The ZPE corrections, calculated at the BP86/aD-PP or B3LYP/aT-PP levels, slightly increase the electron affinities (except for the EAs of the D_{3d} structure of AgF_6), whereas the core-valence corrections, calculated at the CCSD(T)/awCVTZ level slightly decrease the electron affinities except for MoF_6 and the D_{3d} structures of PdF_6 and AgF_6. An energy diagram showing the different states for the anions and neutrals used in predicting the electron affinities is shown in Figure 3.1.

The SO correction (Table 3.4) to the EA was calculated as the difference between EA(ZORA+SO) and EA(ZORA). The electron affinities calculated with ZORA and ZORA+SO are given in the Supporting Information. The SO corrections increase the electron affinities for MoF_6, TcF_6, RhF_6, and PdF_6 and decrease those for RuF_6 and AgF_6; all of the SO corrections are small and are within 1.3 kcal/mol. We were specifically interested in the SO effect on the electron affinities of RuF_6 and RhF_6. The SO effect slightly decreases EA(RuF_6) by 0.41

kcal/mol and slightly increases EA(RhF_6) by 1.24 kcal/mol. The addition of the SO corrections to the CCSD(T)/CBS values does not reverse the order of the electron affinities for RuF_6 and RhF_6. This is in contrast to the difference in the electron affinities of OsF_6 and IrF_6, where the inclusion of molecular spin-orbit corrections inverts the order of the EAs from that at the CCSD(T)/CBS level and proved to be essential for predicting the correct monotonic increase of the EAs in the third row MF_6 compounds. This is consistent with the fact that the relativistic effects should be much smaller in the second row than in the third row transition metal compounds. Each second row transition metal hexafluoride has an electron affinity that is larger than the corresponding third row species in the same column, making them more powerful oxidizers.

In Table 3.1, our calculated electron affinities are compared to those either determined experimentally or predicted from lower level calculations. There has not been a consensus for EA(MoF_6). The reported values range from 3.6 eV to at least 5.1 eV. Our calculated value of 4.23 eV is closest to the value of 4.5 eV reported by Mathur.[18] Our calculated value for EA(RuF_6) falls half way between the experimental values of 7.5 eV[21] and 6.47 eV.[22] Our results support the conclusion of Bartlett[25] that the EA(RuF_6) is greater than that of RhF_6. Lower level DFT calculations for the EAs of MoF_6, TcF_6, RuF_6 and RhF_6 are only in qualitative agreement with our CCSD(T)/CBS values.

Vertical electron detachment (VDE) and attachment (VAE) energies have been calculated for the second row transition metal hexafluorides at the different levels of theory with the aT-PP basis set (Table 3.5). The VDEs of MF_6^- are larger than the adiabatic EAs by up to ~14 kcal/mol, and the VAEs are smaller than the adiabatic EAs by up to 11 kcal/mol, with the largest differences between the VDE's and VAEs and the adiabatic EAs occurring for the earlier

transition metal atoms. For example for Ag , the adiabatic EA, VDE, and VAE are all within 1.5 kcal/mol of each other.

Based on their extraordinarily high electron affinities, all of the second row transition metal hexafluorides fall in the category of "superhalogens", a term created in 1981 for compounds having electron affinities exceeding those of the halogens (3.0-3.6 eV).[53] The high EA of 8.89 eV for AgF_6 would make it a better superhalogen than AuF_6 with EA = 8.20 eV.

Heats of Formation. Total atomization energies (Table 3.6) for the prediction of $\Delta H_{f,0K}$ and $\Delta H_{f,298K}$ (Table 3.7) were calculated at the CCSD(T)/CBS level. The ground states of Mo ($^7S_3$), Tc ($^6S_{1/2}$), Pd ($^1S_0$) and Ag ($^2S_{1/2}$) do not have any spin orbit splitting, so they are used directly to calculate the TAEs. For Ru and Rh, there are no convenient low lying excited states, so we used the experimental ground states of Ru ($^5F_5$) and Rh ($^4F_{9/2}$) with J-averaged spin orbit corrections of −3.94 and −4.26 kcal/mol, respectively. The TAEs decrease in the series from MoF_6 to AgF_6, just like in the third row series, and are ~100 kcal/mol lower than the TAEs of the corresponding third row transition metal hexafluorides in the same column.

In Table 3.7, our calculated heats of formation are compared with the available experimental values. Our calculated value of -374.9 kcal/mol for $\Delta H_f(MoF_6)$ is in excellent agreement with the value of -372.3 ± 0.2 kcal/mol from the direct combination of the elements in a bomb calorimeter,[28] and slightly less negative than the value of -388 kcal/mol from a solution calorimetry experiment.[27] Besides errors in the electronic structure calculations, the major errors in the calculated heats of formation arise from the experimental heats of formation of the metal atoms, as the heats of formation of these transition metal atoms in the gas phase are not as well established and have larger error bars than those of most main group elements (see Supporting Information). Another source of error is the molecular spin orbit effect, which was not included

in the calculated heats of formation because of the difficulty in calculating the appropriate quantities for the atoms. However, based on the electron affinity calculations, we do not expect this contribution to be large.

Bond Dissociation Energies. Total atomization energies have been used to calculate the average adiabatic bond dissociation energies (BDEs) (Table 3.8). The average BDEs decrease in the series from Mo to Ag. The average BDEs range from 106.8 kcal/mol for MoF_6 to 28.6 kcal/mol for AgF_6. This decrease in the average bond energies with filling of the t_{2g} orbitals was also predicted for the third row hexafluorides. The second row hexafluorides have smaller BDEs than the corresponding third row compounds. For example, the average bond dissociation energy in PdF_6 is ~18 kcal/mol lower than that in PtF_6.

The first adiabatic M-F BDEs have also been calculated at different levels of theory from the reaction $MF_6 \rightarrow MF_5 + F$ with all species in their ground states. DFT optimized geometries at the B3LYP/aD-PP level as well as scalar relativistic ZORA and ZORA-SO optimized geometries at the BLYP/TZ2P level are given in the Supporting Information. The geometries of the MF_5 molecules depend on the way the 4d orbitals split in the trigonal bipyramidal (D_{3h}) and square pyramidal (C_{4v}) ligand fields. MoF_5 with one 4d electron distorts to a C_{2v} ($^2A_2$) structure with an average bond length of 1.849 Å. TcF_5 with two 4d electrons has, at the B3LYP/aD-PP level, a $^3A_1'/D_{3h}$ ground state with an average bond length of 1.839 Å, 8.7 kcal/mol more stable than the C_{4v} structure. RuF_5 with three 4d electrons has a $^4B_1/C_{4v}$ ground state with an average bond distance of 1.842 Å. The most stable state for RhF_5 is the $^3B_2/C_{2v}$ state with an average bond distance of 1.842 Å. The singlet, triplet and quintet C_{4v} states are 16.2, 4.0 and 5.8 kcal/mol, respectively, higher in energy. The PdF_5 $^2B_1/C_{4v}$ ground state has an average bond distance of 1.856 Å. AgF_5 has a $^1A_1/ C_{4v}$ ground state with an average bond distance of 1.880 Å. The triplet

C_{4v} and D_{3h} states are higher in energy by 1.7 and 3.1 kcal/mol, respectively, at the B3LYP/aD-PP level. The average M-F bond distances in the MF_5 series are approximately constant for the first four metals and increase for Pd and Ag, following the same trend as for the hexafluorides.

The calculated first adiabatic BDEs follow the same trend as the average BDEs, decreasing from Mo to Ag and, in all cases, are significantly lower than the average BDEs by up to 39 kcal/mol. For the first BDEs, there is a large change of more than 30 kcal/mol from MoF_6 to TcF_6 and a much smaller decrease of less than 10 kcal/mol from TcF_6 to RuF_6. The first BDE in RhF_6 is only 3 kcal/mol less than that in RuF_6. There is a much larger change again in the first BDE between RhF_6 and PdF_6 than between PdF_6 and AgF_6. We predict that AgF_6 is thermodynamically unstable with respect to loss of an F atom to form AgF_5. For all species, the spin orbit corrections to the first BDEs were calculated to be less than 2 kcal/mol. In general, the spin orbit effect reduces the first BDE except for M=Ru and Pd where the first BDE is slightly increased by up to 0.5 kcal/mol.

Fluoride Affinities and Lewis Acidities. Table 3.9 lists the valence CBS energies and the various additive corrections included in the calculation of the MF_6 fluoride affinities. The fluoride affinities from DFT calculations using different functionals and basis sets are given in the Supporting Information.

The heptafluoride anions, formed by the addition of a closed shell F^- to MF_6, nominally have the same number of d electrons as the neutral hexafluorides if electrons are not transferred from the F^- to the metal. On the basis of the known main group structures, the addition of an F^- ion to an octahedral MF_6 molecule would be expected to lead to three possible geometries: pentagonal bipyramid (PBP, D_{5h}), mono-capped octahedron (MCO, C_{3v}) or mono-capped trigonal prism (MCTP, C_{2v}). The average M-F bond distances in these classical MF_7^- structures

follow the same trend as in the MF_6 and MF_5 series, with M-F bonds of approximately the same length for M = Mo, Tc, and Ru and increasing for M = Rh, Pd and Ag. From MoF_7^- to AgF_7^-, the average M-F bond distances for the classical structures are 1.901 Å, 1.897 Å, 1.898 Å, 1.906 Å, 1.922 Å and 2.015 Å, respectively. It is also possible to form a non-classical structure that can be best described as a C_s structure with one F atom bonded to an F ligand of the MF_6^- cluster.[1] The F_{ligand}-$F_{external}$ average bond length in the non-classical MF_7^- structures is 2.060Å, which is considerably longer than r(F-F) = 1.412 Å[54] in F_2 or even r(F-F) = 1.920 Å (CCSD(T)/aQ) in F_2^-. The M-$F_{external}$ bond distance is ~3.5Å and is much longer than any of the average M-F bonds in the MF_6 structures.

For MoF_7^-, the three classical structures are very close in energy with MCTP lowest at the B3LYP/aD-PP level. The $^3A'/C_s$ non-classical structure, a local minimum on the potential energy surface, is substantially higher in higher in energy, 54.5 kcal/mol, than the MCTP structure at the CCSD(T) level (3.9). The high spin, non-classical structure $^4A''/C_s$ is 21.2 kcal/mol above the lowest energy classical MCTP structure at the CCSD(T) level (Table 3.9) for TcF_7^-. All three triplet classical structures of RuF_7^- are higher in energy than the non-classical $^5A''/C_s$ structure with the closest being the PBP structure which is 4.4 kcal/mol higher at the CCSD(T) level (3.9). For RhF_7^-, the non-classical $^4A''/C_s$ structure is predicted to be higher in energy the most stable classical MCTP structure by 31.6 kcal/mol. The relative energies of the classical and non-classical geometries for RhF_7^- and RuF_7^- are consistent with the inversion in the electron affinities. The singlet classical structures of PdF_7^- are up to 33 kcal/mol higher in energy than the non-classical $^3A'/C_s$ structure at the B3LYP/aD-PP level. At the CCSD(T) level (Table 3.9), the nonclassical structure of PdF_7^- is 18.9 kcal/mol more stable than the classical PBP structure. The

non-classical ^{2}A'/C*s* structure of AgF_7^- is more stable than the lowest energy classical distorted MCO structure by 30.0 kcal/mol at the CCSD(T) level (Table 3.9).

The FAs were calculated by extrapolating the CCSD(T) energies to the CBS limit and adding the various corrections as listed in Table 3.9. The FAs for the addition of F^- to form the non-classical structures were calculated by adding only the zero-point energy, scalar relativistic and spin-orbit corrections to the energies at the CCSD(T)/AT-PP level. The scalar relativistic correction was calculated from the expectation values of the mass-velocity and Darwin terms in the Breit-Pauli Hamiltonian [55] at the CISD/aT-PP level for MF_6 and MF_7^-. On the basis of our previous work on the FAs of the third row transition metal hexafluorides, [1] we estimate that the error introduced by the pseudopotential approximation is small. The SO correction was not included in the calculation of FA(MoF_6) and FA(TcF_6) to form the non-classical structures due to problems in converging the SCF to obtain the wavefunction.

The FAs for the addition of F^- to form one of the three classical structures are between ~74 and ~107 kcal/mol, but the FAs for the formation of the non-classical structures show a much greater variation with the metal, from 19.5 kcal/mol for MoF_6 to values of 87.4, 105.8 and 127.7 kcal/mol for RuF_6, PdF_6 and AgF_6, respectively (Table 3.9).

The bond energy between the F atom and MF_6^-, ($E(F)_{cluster}$), can be calculated from the following thermodynamic cycle.

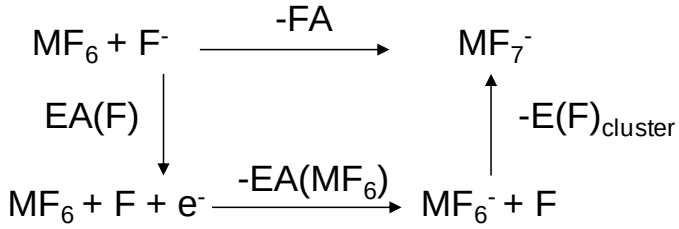

Using this cycle, $E(F)_{cluster}$ for MF_7^- (equation (2))

$$MF_7^- \rightarrow MF_6^- + F \qquad (2)$$

is given by $E(F)_{cluster} = EA(F) - EA(MF_6) + FA$. The calculated fluoride and electron affinities of MF_6 are available from our calculations, and the experimental value[47] for EA(F) is 3.4012 eV (78.43 kcal/mol).

The global decomposition of MF_7^- to F_2^- and MF_5 as shown in equation (3) is defined as $E(F_2^-)_{cluster}$ which is the energy difference between the MF_7^- and the products.

$$MF_7^- \rightarrow F_2^- + MF_5 \qquad (3)$$

We calculated the properties of F_2^- using the CCSD(T)/CBS plus additional corrections approach described above. The calculated $EA(F_2)$ = 3.04 eV is in excellent agreement with the experimental values of 3.005 ± 0.071 eV[56] and 3.120 ± 0.070 eV.[57] The heat of formation of MF_5 was obtained as described above and the heat of formation of MF_7^- was obtained from the fluoride affinity of MF_6. The energies of equations (2) and (3) at 0 K are given in Tables 3.10. The energies of equation (3), $E(F_2^-)_{cluster}$, are substantially more endothermic (Table 3.10) than $E(F)_{cluster}$, so equation (2) is more likely to occur thermodynamically as compared to equation (3).

For the most stable classical structures for MoF_7^- and TcF_7^-, $E(F)_{cluster}$ decreases from 54.9 to 19.1 kcal/mol, consistent with the increase in the $EA(MF_6)$. For RhF_7^-, $E(F)_{cluster}$ increases to 28.9 kcal/mol due to the high RhF_6 fluoride affinity. For RuF_7^-, $E(F)_{cluster}$ for the classical structures is essentially zero and becomes negative for PdF_7^- and AgF_7^-.

The $E(F)_{cluster}$ values for the non-classical structures exhibit a different type of behavior. For the MF_7^- ions where the classical structures are more stable than the non-classical ones (M = Mo, Tc, Rh), the $E(F)_{cluster}$ (non-classical) values are zero or negative. When the non-classical MF_7^- structure is more stable than the classical one, the $E(F)_{cluster}$ (non-classical) values are small (M = Ru, Pd, Ag) consistent with a weak complex of a fluorine radical atom with MF_6^-. In fact,

the $E(F)_{cluster}$ values of the non-classical structures are all near zero. Hence, if the non-classical MF_7^- ion were formed even in cases where it is not the most stable structure, it would also readily eliminate an F atom.

The $E(F_2^-)_{cluster}$ values increase from M = Mo to M = Ru, decrease for M = Rh and increase for M = Pd and Ag. We have also calculated the energy to release F_2^- from MF_7^- for the transition metals of the third row and compare them with our previously predicted $E(F)_{cluster}$ values (Table 3.11). The $E(F)_{cluster}$ and $E(F_2^-)_{cluster}$ values for the third row transition metals follow the same trends as for the second row. Again the $E(F)_{cluster}$ values are always less than the $E(F_2^-)_{cluster}$ values, so reaction (2) will preferentially occur as compared to reaction (3).

We have previously shown[1] that when the electron affinity of MF_6 becomes large enough, MF_6 will bind an F^- which then undergoes an electron transfer to MF_6 leaving the non-classical weak complex of an F atom with MF_6^-. With our additional data, we can conclude that when $EA(MF_6) > 6.9$ eV, MF_6 can abstract an electron from the F^- anion and form the non-classical complex MF_6^--F.

We also calculated the MF_5 fluoride affinities given by equation (4)

$$MF_5 + F^- \rightarrow MF_6^- \qquad (4)$$

The resulting values calculated at the CCSD(T)/CBS level with ZPE, core-valence and scalar relativistic corrections are given in Table 3.12. The MF_5 FAs increase from $FA(MoF_5) = 105.2$ to $FA(PdF_5) = 127.5$ kcal/mol following the trends in the electron affinities. The $FA(AgF_5)$ decreases slightly to 125.7 kcal/mol and its lower fluoride affinity as compared to $FA(PdF_5)$ may be connected with the weak Ag-F BDE in AgF_6. Christe et al.[29] have used fluoride ion affinities to establish a quantitative Lewis acidity scale. The strongest Lewis acid on the list, SbF_5, has a fluoride affinity of 120.3 kcal/mol, lower than those of RuF_5, RhF_5, PdF_5 and AgF_5. The FAs of

MF_5 are larger by 14 to 41 kcal/mol than the FAs of the corresponding MF_6 molecules, consistent with going from C_{4v} or D_{3h} structures for MF_5 to the energetically favored approximately octahedral structures for MF_6^-, while the transition from MF_6^- to the various classical structures of MF_7^- might involve some steric crowding.

It is useful to compare $FA(MF_5)$ (Equation (4), Table 3.4) with $E(F_2^-)_{cluster}$ (Equation (3), Table 3.10). If both F^- and F_2^- are present, then MoF_5 would prefer to bind F_2^- over F^- and for TcF_5, both anions are equally likely to bind to the pentafluoride. RuF_5 would preferentially bind F_2^- and again, RhF_5 would bind both anions equally well. PdF_5 and AgF_5 would both preferentially bind F^- over F_2^-. In the third row transition metal compounds (Table 3.11), WF_5 and ReF_5 will preferentially bind F_2^-. A crossover occurs at OsF_5 and the binding of F_2^- and F^- are comparable. IrF_5, PtF_5, and AuF_5 will all bind F^- over F_2^-.

Performance of Density Functional Theory. The calculated values for a selection of functionals for the EAs, M-F bond dissociation energies, MF_5 FAs and MF_6 FAs are given in the Supporting Information. The average deviations of these properties, calculated with a selection of functionals, from the CCSD(T)/CBS values with all corrections except for spin orbit are given in Table 3.13. In general, the differences in the electron affinities between the CCSD(T) and DFT values are larger for the later transition metal fluorides than for the earlier ones. For the GGA functionals, the differences from the CCSD(T) values are quite large with average deviations up to 29 kcal/mol and are even larger than for the 3rd row compounds. The hybrid functionals B3LYP, mPW1 and PBE1 give the best performances with average deviations of 5 to 6.5 kcal/mol. The O3LYP and TPSSh hybrid functionals do not perform any better than the GGA functionals. For the MF_5 fluoride affinities, the GGA functionals predict values that are 8 to 16 kcal/mol smaller than the CCSD(T) values. The hybrid functionals, except O3LYP, predict

smaller values than the CCSD(T) method within 10 kcal/mol. For the M-F adiabatic BDEs of MF_6, all GGA functionals predict BDEs that are too large by up to 21 kcal/mol as compared to the CCSD(T) results. The hybrid functionals, except TPSSh, predict BDEs within 5 kcal/mol of the CCSD(T) results.

Conclusions

High level coupled cluster CCSD(T) calculations, extrapolated to the complete basis set limit, were used to evaluate reliable, self-consistent thermochemical data sets for the second row transition metal hexafluorides. For MF_6 and MF_6^-, the Jahn-Teller distorted D_{4h} and D_{3d} structures are very close in energy while an undistorted O_h structure is about 1.0 kcal/mol higher in energy. Thus, the MF_6 molecules are highly fluxional about the conical intersection and will exhibit an average O_h geometry under most experimental conditions. The electron affinities are direct measures for the oxidizer strengths of these hexafluorides and their oxidizing power increases from MoF_6 to RuF_6, decreases to RhF_6 and then increases again to AgF_6. The RuF_6, RhF_6, PdF_6, and AgF_6 molecules are extremely powerful oxidizers with electron affinities ≥6.8 eV and are excellent representatives of the class of superhalogens. Contrary to the findings for the third row transition metal hexafluorides, the inclusion of spin-orbit effects for the correct prediction of the qualitative ordering of the electron affinities was found unimportant for the second row transition metal hexafluorides. Thus, EA(RhF_6) is less than EA(RuF_6), consistent with simple ideas from orbital filling and electron repulsion. On the basis of their calculated fluoride ion affinities, the corresponding pentafluorides are extremely strong Lewis acids, with RuF_5, RhF_5, PdF_5 and AgF_5 significantly exceeding the Lewis acidity of SbF_5. The MoF_7^-, TcF_7^- and RhF_7^- anions have classical heptacoordinated MF_7^- structures with the corresponding hexafluorides having fluoride affinities of 74, 77, and 107 kcal/mol, respectively. A lower energy

non-classical structure with a very weak external F-F bond between an MF_6^- fragment and a fluorine atom is predicted for MF_7^- for M = Ru, Pd and Ag, consistent with their high electron affinities; thus, RuF_7^-, PdF_7^- and AgF_7^-, should be excellent F atom sources under very mild conditions. Except for AgF_7^-, the loss of F^- from MF_7^- is much less endothermic than the loss of F_2^-, so the MF_7^- anions will always release F^- rather than F_2^-. A wide range of DFT exchange-correlation functionals were also evaluated and only the B3LYP, mPW1PW91 and PBE1 functionals were found to approximate the coupled cluster values.

Acknowledgment. This work was supported by the Chemical Sciences, Geosciences and Biosciences Division, Office of Basic Energy Sciences, U.S. Department of Energy (DOE) under grant no. DE-FG02-03ER15481 (catalysis center program). DAD also thanks the Robert Ramsay Chair Fund of The University of Alabama for support. Part of this work was performed at the W. R. Wiley Environmental Molecular Sciences Laboratory, a national scientific user facility sponsored by DOE's Office of Biological and Environmental Research and located at Pacific Northwest National Laboratory, operated for the DOE by Battelle. KOC is indebted to the Office of Naval Research, the National Science Foundation, and the Defense Threat Reduction Agency for financial support.

Supporting Information. MF_6, MF_6^-, MF_5, and MF_7^- total electronic energies and vibrational frequencies at the DFT level with various exchange-correlation functionals and the aD-PP basis set, zero point energies (ZPE), CCSD(T) total energies as a function of basis set, core and valence energies at the CCSD(T)/aug-cc-pWCVTZ-PP level, and scalar relativistic energies at the CISD/aT-PP and CCSD(T)-DK/aug-cc-pVTZ-DK levels, T1 diagnostics. Energy differences in kcal/mol of D_{4h} vs O_h structures for the same spin state and singlet –triplet splitting energies for the D_{4h} structures. Optimized geometry parameters with different DFT functionals.

Pseudopotential errors and scalar relativistic corrections for EA(MF_6), 1st M –F BDEs, total atomization energies, FA(MF_6), and FA(MF_5). Electron affinities calculated at the ZORA and ZORA+SO levels. Mulliken charges, NBO charges, and spin densities for MF_6 and MF_6^- and figures for the spin densities. First M –F BDEs, FA(MF_6), and FA(MF_5) calculated at the DFT and CCSD(T) levels as a function of basis set. Cartesian xyz coordinates for all molecules. This material is available free of charge via the Internet at http://pubs.acs.org.

Table 3.1. MF_6 Electron Affinities in eV.

Metal	Calculated[a]	Experiment	Reactivity Estimate	Other calculated
Mo	4.23	4.50[b], >5.1[c], 3.6[d], 3.8[e]		5.37[f], 4.11[g]
Tc	5.89		6.94[h]	5.64[g]
Ru	7.01	7.5[e], 6.47[i]		6.98[g]
Rh	6.80		< $EA(RuF_6)$[j]	6.60[g], 6.44[g]
Pd	7.95			
Ag	8.89			

[a] Final calculated value this work. [b] Reference 18. [c] Reference 19. [d] Reference 20. [e] Reference 21. [f] References 26 and 15. [g] Reference 12. [h] Reference 24. [i] Reference 22. [j] Reference 25.

Table 3.2. Optimized Metal-Fluorine Bond Lengths (Å) and Bond Angles (degrees) at the CCSD(T) Level with the aT-PP Basis Set and at the ADF/ZORA/BLYP Level with the TZ2P Basis Set for MF_6 and MF_6^-.

Molecule	State/sym	CCSD(T)/aT	State/sym ZORA	ZORA/ TZ2P	Sym ZORA-SO	ZORA-SO /TZ2P	EXPT
MoF_6	$^1A_{1g}/O_h$	1.825 (x6)	$^1A_{1g}/O_h$	1.870	O_h	1.870	1.817[a]
							1.809[b]
MoF_6^-	$^2B_{2g}/D_{4h}$	1.855 (x2)	$^2A_{1g}/D_{3d}$	1.932	D_{4h}	1.936 (x2)	
		1.906 (x4)		91.9°		1.931 (x4)	
	$^2A_{1g}/D_{3d}$	1.888			D_{3d}	1.933	
		91.9°				91.7°	
TcF_6	$^2B_{2g}/D_{4h}$	1.794 (x2)	$^2A_{1g}/D_{3d}$	1.868	D_{4h}	1.871(x2)	1.812[a]
		1.827 (x4)		91.2°		1.866(x4)	
	$^2A_{1g}/D_{3d}$	1.816			D_{3d}	1.867	
		91.2°				91.3°	
TcF_6^-	$^3A_{1g}/D_{4h}$	1.903 (x2)	$^3A_{1g}/D_{3d}$	1.921	D_{4h}	1.909(x2)	
		1.855 (x4)		88.9°		1.928(x4)	
	$^3A_{1g}/D_{3d}$	1.871			D_{3d}	1.923	
		90.4°				88.8°	
RuF_6	$^3A_{1g}/D_{4h}$	1.833 (x2)	$^3A_{1g}/D_{3d}$	1.874	D_{4h}	1.889(x2)	1.818[a]
		1.804 (x4)		90.7		1.868(x4)	1.824[b]
	$^3A_{1g}/D_{3d}$	1.813			D_{3d}	1.876	
		90.4°				90.3°	
RuF_6^-	$^4A_{1g}/O_h$	1.860 (x6)	$^4A_{1g}/O_h$	1.921	O_h	1.921	1.851[c]
RhF_6	$^4A_{1g}/O_h$	1.815 (x6)	$^4A_{1g}/O_h$	1.883	O_h	1.883	1.824[a]
							1.838[b]

RhF_6^-	$^3A_{1g}/D_{4h}$	1.828 (x2)	$^3A_{1g}/D_{3d}$	1.924	D_{4h}	1.937(x2)	1.855[c]
		1.870 (x4)		90.6°		1.919(x4)	1.853[c]
	$^3A_{1g}/D_{3d}$	1.855			D_{3d}	1.924	
		90.8°				89.6°	
PdF_6	$^3A_{1g}/D_{4h}$	1.850 (x2)	$^3A_{1g}/O_h$	1.911	D_{4h}	1.916(x2)	
		1.849 (x4)				1.908(x4)	
					D_{3d}	1.910	
						90.1	
PdF_6^-	$^2A_{1g}/D_{4h}$	1.891(x2)	$^2A_{1g}/O_h$	1.943	D_{4h}	1.939(x2)	
		1.847(x4)				1.944(x4)	
					O_h	1.942	
AgF_6	$^2B_{2g}/D_{4h}$	1.904(x2)	$^2A_{1g}/O_h$	1.948(x2)	O_h	1.947(x2)	
		1.874(x4)		1.950(x4)		1.949(x2)	
						1.951(x2)	
AgF_6^-	$^1A_{1g}/O_h$	1.884 (x6)	$^1A_{1g}/O_h$	1.959	O_h	1.960	

[a] Reference 12. [b] Reference 10. [c] Reference 11.

Table 3.3. Experimental and Calculated MF_6 Vibrational Frequencies (cm^{-1}) and IR Intensities (km/mole) at the B3LYP/aT Level.

M	State	a_{1g}		e_g		t_{1u}		t_{1u}		t_{2g}		t_{2u}	
	Sym	Calc	Exp	Calc	Exp	Calc	Exp	Calc	Exp	Calc	Exp	Calc	Exp
Mo[a]	$^1A_{1g}/O_h$	734	741[b]	641	652[b]	731(652)	741[b]	250(93)	264[c]	300	318[b]	112(0)	(116)[b]
Tc[d]	$^2A_{1g}/D_{3d}$	671		499		e_u 707 (426)		e_u 271(30)		a_{1g} 275		e_u 152(6)	
						a_{2u} 696 (211)		a_{2u} 267(16)		e_g 262		a_{2u} 128(0)	
	$^2B_{2g}/D_{4h}$	672	713[b]	a_{1g} 612	(639)[e]	a_{2u} 716(219)	748[c]	e_u 277(24)	265[c]	e_g 357	(297)[e]	e_u 161(2)	(145)[b]
				b_{1g} 606		e_u 696(208)		a_{2u} 232(27)		b_{2g} 237		b_{2u} 109(0)	
Ru[a]	$^3A_{1g}/D_{3d}$	696		463		a_{2u} 735(223)		e_u 297(28)		a_{1g} 284		a_{2u} 206(0)	
						e_u 729(444)		a_{2u} 275(18)		e_g 239		e_u 141(6)	
	$^3A_{1g}/D_{4h}$	695	(675)[f]	b_{1g} 630	(624)[e]	e_u 735(436)	735[f]	a_{2u} 313(9)	275[f]	e_g 372	(283)[e]	b_{2u} 204(0)	(186)[e]
				a_{1g} 624		a_{2u} 721(224)		e_u 269(42)		b_{2g} 320		e_u 148(5)	
Rh[a]	$^4A_{1g}/O_h$	665	(634)[f]	603	(595)[f]	724(525)	724[f]	288(52)	283[f]	275	(269)[f]	182(0)	(192)[f]
Pd[a]	$^3A_{1g}/D_{4h}$	608		a_{1g} 569		a_{2u} 692(124)		e_u 296(18)		e_g 271		e_u 206(16)	
				b_{1g} 580		e_u 671(80)		a_{2u} 240(24)		b_{2g} 218		b_{2u} 130(0)	
Ag[d]	$^2B_{2g}/D_{4h}$	515		a_{1g} 502		a_{2u} 624(59)		a_{2u} 271(0)		b_{2g} 250		b_{2u} 195(0)	
				b_{1g} 505		e_u 587(11)		e_u 258(20)		e_g 193		e_u 194(2)	

[a]B3LYP/aT-PP. [b] Reference 3. Experimental values in parentheses calculated from combination bands or overtones. [c] Reference 5. [d] BP86/aD-PP. [e] Reference 4. [f] Reference 6.

Table 3.4. Energy Components for Calculated Electron Affinities in kcal/mol.

M	MF_6 State/Sym	MF_6^- State/Sym	ΔE_{CBS}[a]	ΔE_{ZPE}	ΔE_{CV}[b]	ΔE_{rel}[c]	EA	SO[d]	EA + SO
Mo	$^1A_{1g}/O_h$	$^2B_{2g}/D_{4h}$	96.41	0.31[e]	0.30	-0.93	96.09	0.27	96.4
	$^1A_{1g}/O_h$	$^2A_{1g}/D_{3d}$	96.21	1.47[e]	0.19	-0.61	97.26	0.20	97.5
Tc	$^2A_{1g}/D_{3d}$	$^3A_{1g}/D_{4h}$	132.03	0.33[e]	-0.54	3.95	135.77	0.17	135.9
	$^2B_{2g}/D_{4h}$	$^3A_{1g}/D_{4h}$	131.73	0.83[e]	-0.56	3.95	135.95	0.03	136.0
	$^2A_{1g}/D_{3d}$	$^3A_{1g}/D_{3d}$	131.18	0.76[e]	-0.47	3.94	135.41	-0.06	135.3
Ru	$^3A_{1g}/D_{4h}$	$^4A_{1g}/O_h$	165.28	1.00[f]	-1.17	-1.43	163.68	-0.41	163.3
	$^3A_{1g}/D_{3d}$	$^4A_{1g}/O_h$	165.82	0.12[f]	-1.28	-2.41	162.25	-0.64	161.6
Rh	$^4A_{1g}/O_h$	$^3A_{1g}/D_{4h}$	155.79	0.51[e]	-1.17	-0.30	154.83	1.08	155.9
	$^4A_{1g}/O_h$	$^3A_{1g}/D_{3d}$	155.20	1.12[e]	-1.10	0.32	155.54	1.24	156.8
Pd	$^3A_{1g}/D_{4h}$	$^2B_{2g}/D_{4h}$	183.54	0.21[f]	-0.74	-0.14	182.87	0.45	183.3
	$^3A_{1g}/D_{3d}$	$^2A_{1g}/D_{3d}$	185.61	0.32[f]	0.87	-1.49	185.31	0.23	185.5
Ag	$^2B_{2g}/D_{4h}$	$^1A_{1g}/O_h$	205.25	0.10[e]	-0.19	-0.22	204.94	-0.03	204.9
	$^2A_{1g}/D_{3d}$	$^1A_{1g}/O_h$	204.68	-0.01[e]	0.62	-4.92	200.37	-0.87	199.5

[a] Valence CCSD(T) electronic energy contribution extrapolated using the mixed Gaussian/exponential formula.

[b] Core-valence correction obtained at the CCSD(T)/awCVTZ level. [c] ΔEA_{Rel} = EA(CCSD(T)-DK/aT-DK) - EA(CCSD(T)/aT-PP).

[d]Spin-orbit correction from BLYP/ZORA + SO/TZ2P calculation. [e] BP86/aD-PP. [f] B3LYP/aT-PP

Table 3.5. Electronic Component of the Adiabatic Electron Affinities of MF_6**,** Vertical Electron Detachment Energies (VDE) of MF_6^- and Vertical Electron Attachment Energies (VAE) of MF_6 in kcal/mol Calculated at the CCSD(T)/aT-PP Level.

Metal	MF_6 State/Sym	MF_6^- State/Sym	ADE	VDE[a]	VAE[b]
Mo	$^1A_{1g}/O_h$	$^2A_{1g}/D_{3d}$	95.4	105.7	88.6
Tc	$^2A_{1g}/D_{3d}$	$^3A_{1g}/D_{4h}$	131.1	144.4	122.8
Ru	$^3A_{1g}/D_{3d}$	$^4A_{1g}/O_h$	164.6	173.4	162.1
Rh	$^4A_{1g}/O_h$	$^3A_{1g}/D_{3d}$	152.8	160.8	149.7
Pd	$^3A_{1g}/D_{4h}$	$^2B_{2g}/D_{4h}$	180.7	188.1	179.7
Ag	$^2A_{1g}/D_{3d}$	$^1A_{1g}/O_h$	201.4	202.9	201.4

[a] $VDE = E_{\text{neutral at anion geom}} - E_{\text{anion}}$

[b] $VAE = E_{\text{neutral}} - E_{\text{anion at neutral geom.}}$

Table 3.6. Energy Components for Atomization Energies of MF_6 in kcal/mol at 0 K ($\sum D_0$).

M	State/Sym	ΔE_{CBS}[a]	ΔE_{ZPE}	ΔE_{CV}[b]	ΔE_{rel}[c]	Atomic ΔE_{SO}[d]	$\sum D_{0,0K}$[e]
Mo	$^1A_{1g}/O_h$	649.54	-8.86[f](-9.09)[g]	0.06	2.65	-2.33	641.06
Tc	$^2B_{2g}/D_{4h}$	562.25	-8.81[h](-9.09)[g]	2.40	1.69	-2.33	555.19
	$^2A_{1g}/D_{3d}$	561.94	-8.32[h]	2.37	1.68	-2.33	555.34
Ru	$^3B_{2g}/D_{4h}$	476.79	-9.37[f](-9.98)[g]	3.95	0.66	-6.27	465.76
	$^3A_{1g}/D_{3d}$	476.25	-8.49[f]	4.09	1.64	-6.27	467.22
Rh	$^4A_{1g}/O_h$	396.19	-8.98[f](-8.90)[g]	6.62	-0.77	-6.59	386.46
Pd	$^3A_{1g}/D_{4h}$	264.24	-8.47[f]	10.59	-0.37	-2.33	263.65
Ag	$^2B_{2g}/D_{4h}$	175.90	-7.71[h]	6.90	-1.03	-2.33	171.73

[a] $\Delta E = \Delta E(M) + 6\Delta E(F) - \Delta E(MF_6)$. [b] CCSD(T)/awCVTZ-DK. [c] ΔEA_{Rel} = EA(CCSD(T)-DK/aT-DK) - EA(CCSD(T)/aT-PP).[d] The spin-orbit splitting is -0.39 kcal/mol for the ($^2P_{3/2}$) state of F, 0.00 kcal/mol for the ground state ($^7S_3$) of Mo, ($^6S_{1/2}$) of Tc, ($^1S_0$) of Pd and ($^2S_{1/2}$) of Ag and: 3.94 for Ru ($^5F_5$), 4.26 for Rh ($^4F_{9/2}$). [e] $\sum D_{0,0K} = \Delta E_{CBS} + \Delta E_{ZPE} + \Delta E_{CV} + \Delta E_{rel} + \Delta E_{SO}$. [f] B3LYP/aT-PP. [g] Experimental ZPE's. [h] BP86/aD-PP.

Table 3.7. Heats of Formation of MF_6 in kcal/mol at 0 and 298 K ($\Delta H_{f,0K}$ and $\Delta H_{f,298K}$) Calculated at the CCSD(T) Level.[a]

M	State/Sym	$\Delta H_{f,0K}$[b]	$\Delta H_{f,298K}$[b]	$\Delta H_{f,0K}$[c]	$\Delta H_{f,298K}$[c]	Exp
Mo	$^1A_{1g}/O_h$	-373.3	-374.9	-371.5	-373.1	-388[27], -372.3 ± 0.2[28]
Tc	$^2B_{2g}/D_{4h}$	-282.5	-284.3			
	$^2A_{1g}/D_{3d}$	-282.7	-284.3			
Ru	$^3B_{2g}/D_{4h}$	-201.7	-203.8	-201.9	-204.0	
	$^3A_{1g}/D_{3d}$	-203.2	-204.9	-203.4	-205.1	
Rh	$^4A_{1g}/O_h$	-142.9	-144.6	-142.7	-144.5	
Pd	$^3A_{1g}/D_{4h}$	-62.6	-64.3	-62.7	-64.4	
Ag	$^2B_{2g}/D_{4h}$	7.0	5.5	7.0	5.5	

[a] Heat of formation of F from the JANAF Tables. $\Delta H_{f,298K}(MF_6) = \Delta H_{f,0K}(MF_6) + \Delta H_{0K\rightarrow 298K}(MF_6) - \Delta H_{0K\rightarrow 298K}(M) - 6\Delta H_{0K\rightarrow 298K}(F)$. The experimental enthalpy change from 0 to 298 K ($\Delta H_{0K\rightarrow 298K}$) is 1.05 for F. For the metal atoms we have used a value of 1.20 kcal/mol.

[b] Wagman et al.[48] values for all metals. [c] Greenwood and Earnshaw[49] values for all metals.

Table 3.8. Calculated Energy Components for the First Adiabatic and Average M –F Bond Dissociation Energies for MF_6 in kcal/mol Calculated at CCSD(T) Level.

M	MF_5 State/Sym	MF_6 State/Sym	ΔE_{CBS}[a]	ΔE_{ZPE}	ΔE_{CV}[b]	ΔE_{rel}[c]	ΔE_{SO}[d]	1st BDE[e]	Avg BDE[f]
Mo	$^2A_2/C_{2v}$	$^1A_{1g}/O_h$	87.6	-2.09[g]	0.62	0.43	-0.54	86.0	106.8
Tc	$^3A_1'/D_{3h}$	$^2B_{2g}/D_{4h}$	52.1	-2.01[h]	1.86	1.14	-0.10	53.0	92.5
	$^3A_1'/D_{3h}$	$^2A_{1g}/D_{3d}$	51.8	-1.51[h]	1.83	1.13	-0.24	53.0	92.6
Ru	$^4B_1/C_{4v}$	$^3A_{1g}/D_{4h}$	37.7	-2.14[g]	2.41	5.78	-0.03	43.7	77.6
	$^4B_1/C_{4v}$	$^3A_{1g}/D_{3d}$	37.1	-1.55[g]	2.52	6.76	0.21	45.0	77.9
Rh	$^3B_2/C_{2v}$	$^4A_{1g}/O_h$	43.9	-2.00[g]	2.59	-0.60	-1.65	42.2	64.4
Pd	$^2B_1/C_{4v}$	$^3A_{1g}/D_{4h}$	41.5	-1.69[g]	4.91	-0.12	0.51	25.9	43.9
Ag	$^1A_1/C_{4v}$	$^2B_{2g}/D_{4h}$	-0.40	-1.82[h]	2.02	0.12	-0.62	-0.2	28.6

[a] Extrapolated using the mixed Gaussian/exponential formula. [b] CCSD(T)/awCVTZ. [c] ΔEA_{Rel} = EA(CCSD(T)-DK/aT-DK) - EA(CCSD(T)/aT-PP). [d] SO correction at the ADF ZORA BLYP/TZ2P level plus the experimental spin-orbit correction of -0.39 kcal/mol for F. [e] 1st BDE calculated as the sum of ΔE_{CBS} and of all corrections. [f] BDE = $\sum D_{0,0K}$ (MF_6) / 6. [g] B3LYP/aD-PP. [h] BP86/aD-PP

Table 3.9. MF_6 Fluoride Affinities (kcal/mol) Calculated at CCSD(T) Level for the Lowest Energy Classical and Non-Classical Structures.

M	MF_6 State/Symm	MF_7^- State/Symm	CCSD(T) aD-PP	CCSD(T) aT-PP	ΔE_{CBS}[a]	ΔE_{ZPE}	ΔE_{CV}[b]	ΔE_{sr}[c]	ΔE_{SO}[d]	FA
Mo	$^1A_{1g}/O_h$	$^1A_1/C_{2v}$	74.11	76.23	75.49	-1.30[e]	0.06	-0.24	0.01	74.0
	$^1A_{1g}/O_h$	$^3A'/C_s$	25.050	19.47		0.08[e]		-0.07		19.5
Tc	$^2A_{1g}/D_{3d}$	$^2A_2/C_{2v}$	77.82	78.05	77.21	-0.88[e]	0.54	-0.21	-0.06	76.6
	$^2A_{1g}/D_{3d}$	$^4A''/C_s$	61.75	55.78		-0.32[e]		-0.08		55.4
Ru	$^3A_{1g}/D_{3d}$	$^3A_1'/D_{5h}$	85.22	85.08	84.89	-1.49[e]	0.51	-0.19	-0.75	83.0
	$^3A_{1g}/D_{3d}$	$^5A''/C_s$	94.18	88.34		-0.25[e]		-0.10	-0.63	87.4
Rh	$^4A_{1g}/O_h$	$^2A_1/C_{2v}$	134.11	108.84	102.72	0.22[f]		0.03	4.31	107.3
	$^4A_{1g}/O_h$	$^4A'/C_s$	78.79	75.27		0.21[e]		-0.12	0.35	75.7
Pd	$^3A_{1g}/D_{4h}$	$^1A_1'/D_{5h}$	88.66	88.86	89.87	-0.95[f]	-0.81	-0.17	-1.08	86.9
	$^3A_{1g}/D_{4h}$	$^3A'/C_s$	107.91	105.63		-0.32[e]		-0.20	0.66	105.8
Ag	$^2B_{2g}/D_{4h}$	$^2B_2/C_{2v}$	100.20	99.22	99.20	-0.36[e]	-1.05	-0.11	0.05	97.7
	$^2B_{2g}/D_{4h}$	$^2A'/C_s$	126.77	127.14		0.70[g]		-0.18	0.01	127.7

[a] Extrapolated using the mixed Gaussian/exponential formula. [b] CCSD(T)/awCVTZ. [c] $\Delta E_{SR} = 6 * \Delta E_{SR}(F) + \Delta E_{SR}(MF_6) - \Delta E_{SR}(MF_6^-)$. [d]SO correction at the ADF ZORA BLYP/TZ2P level; [e] B3LYP/aD-PP. [f] B3LYP/aT-PP. [g] BP86/aD-PP.

Table 3.10. Energies (kcal/mol) of Reactions (2) ($E(F)_{cluster}$) and (3) ($E(F_2^-)_{cluster}$) for the Second Row Transition Metals.

M	MF_7^- State/Sym	MF_6^- State/Sym	$E(F)_{cluster}$[a] Reaction (2)	MF_5 State/Sym	$E(F_2^-)_{cluster}$[b] Reaction (3)
Mo	$^1A_1/C_{2v}$	$^2A_{1g}/D_{3d}$	54.9	$^2A_2/C_{2v}$	131.4
	$^3A'/C_s$		0.4[c]		76.9
Tc	$^2A_2/C_{2v}$	$^3A_{1g}/D_{4h}$	19.1	$^3A_1'/D_{3h}$	101.0
	$^4A''/C_s$		-2.1[c]		79.8
Ru	$^3A_1'/D_{5h}$	$^4A_{1g}/O_h$	-0.2	$^4B_1/C_{4v}$	99.4
	$^5A''/C_s$		4.8[d]		104.5
Rh	$^2A_1/C_{2v}$	$^3A_{1g}/D_{3d}$	28.9	$^3B_2/C_{4v}$	121.0
	$^4A'/C_s$		-3.0[d]		89.0
Pd	$^1A_1'/D_{5h}$	$^2B_{2g}/D_{4h}$	-18.3	$^2B_1/C_{4v}$	103.3
	$^3A'/C_s$		-0.1[d]		121.6
Ag	$^2B_2/C_{2v}$	$^1A_{1g}/O_h$	-28.4	$^1A_1/C_{4v}$	68.9
	$^2A'/C_s$		1.6[d]		98.8

[a] $E(F)_{cluster} = EA(F) - EA(MF_6) + FA$. For the classical structures, the FAs were calculated using the CBS energies and all corrections (ZPE, CV, SR and SO) except M=Rh for which we did not calculate a core-valence corrections. For the non-classical structures the FAs were calculated using the CCSD(T)/aT-PP energies together with the ZPE and SR corrections. [b] $E(F_2^-)_{cluster} = \Delta H_{f,0K}(F_2^-) + \Delta H_{f,0K}(MF_5) - \Delta H_{f,0K}(MF_7^-)$; $\Delta H_{f,0K}(MF_5) = 1^{st}$ BDE $- \Delta H_{f,0K}(F) + \Delta H_{f,0K}(MF_6)$; $\Delta H_{f,0K}(MF_7^-) = -FA(MF_6) + \Delta H_{f,0K}(MF_6) + \Delta H_{f,0K}(F^-)$. $H_{f,0K}(F^-) = -EA(F) + \Delta H_{f,0K}(F) = -78.404 + 18.47 = -59.93$ kcal/mol; $H_{f,0K}(F_2^-) = -EA(F_2) = 70.06$ kcal/mol. [c] Use of $EA(MF_6)$ calculated at the CCSD(T)/aT-PP + ΔE_{ZPE} + ΔE_{SR} level gives 1.2 kcal/mol for M = Mo, 1.8 kcal/mol ro M = Tc. [d] Use of $EA(MF_6)$ calculated at the CCSD(T)/aT-PP + ΔE_{ZPE} + ΔE_{SR} + ΔE_{SO} level gives 1.9 kcal/mol for M = Ru, -0.8 kcal/mol for M = Rh, 2.9 kcal/mol for M = Pd, and 5.8 kcal/mol for M = Ag.

Table 3.11. Energies (kcal/mol) of Reactions (2) ($E(F)_{cluster}$), (3) ($E(F_2^-)_{cluster}$), and (4) ($FA(MF_5)$) for the Third Row Transition Metals.[a]

M	MF_7^- State/Sym	MF_6^- State/Sym	$E(F)_{cluster}$ Reaction (2)[b]	MF_5 State/Sym	$E(F_2^-)_{cluster}$ Reaction (3)	$FA(MF_5)$ Reaction (4)[b]
W	$^1A_1'/D_{5h}$	$^2B_{2g}/D_{4h}$	83.7	$^2A_2/C_{2v}$	167.2	112.9
	$^3A''/C_s$		-2.2		81.3	
Re	$^2A_2/C_{2v}$	$^3A_{1g}/D_{4h}$	53.0	$^3A_1'/D_{3h}$	141.3	116.4
	$^4A''/C_s$		0.2		88.5	
Os	$^3A_1'/D_{5h}$	$^4A_{1g}/O_h$	24.4	$^4B_1/C_{4v}$	128.1	132.0
	$^5A''/C_s$		4.6		108.3	
Ir	$^2B_1/C_{2v}$	$^3A_{1g}/D_{4h}$	10.2	$^5B_1/C_{4v}$	115.7	134.6
	$^2A'/C_s$		-28.3		77.2	
Pt	$^1A_1'/D_{5h}$	$^2B_{2g}/D_{4h}$	-6.2	$^2B_1/C_{4v}$	96.8	130.7
	$^3A'/C_s$		0.4		103.4	
Au	$^2B_2/C_{2v}$	$^1A_{1g}/O_h$	-32.3	$^1A_1/C_{4v}$	75.4	136.6
	$^2A'/C_s$		4.7		112.4	

[a] See footnotes to 3.10 for details of the calculations.

[b] Reference 1

Table 3.12. MF_5 Fluoride Affinities in kcal/mol Calculated at the CCSD(T) Level.

M	MF_5 State/Sym	MF_6^- State/Sym	ΔFA_{CBS}[a]	ΔE_{ZPE}[b]	ΔE_{CV}[c]	ΔE_{SR}[d]	Total FA kcal/mol
Mo	$^2A_2/C_{2v}$	$^2B_{2g}/D_{4h}$	105.1	-0.42	0.82	-0.28	105.2
Tc	$^3A_1'/D_{3h}$	$^3A_{1g}/D_{4h}$	104.9	-2.09	1.20	-0.30	103.7
Ru	$^4B_1/C_{4v}$	$^4A_{1g}/O_h$	124.0	-1.31	1.14	-0.32	123.6
Rh	$^3B_2/C_{2v}$	$^3A_{1g}/D_{4h}$	120.7	-0.69	1.32	-0.34	121.0
Pd	$^2B_1/C_{4v}$	$^2B_{2g}/D_{4h}$	145.3	-1.00	4.18	-0.40	127.5
Ag	$^1A_1/C_{4v}$	$^1A_{1g}/O_h$	125.9	-1.65	1.74	-0.36	125.7

[a] Extrapolated using the mixed Gaussian/exponential formula. [b] B3LYP/aD-PP. [c]CCSD(T)/awCVTZ. [d] Scalar relativistic correction at CISD/aT-PP level.

Table 3.13. Average Deviations of the MF_6 Electron Afinities, MF_5 and MF_6 Fluoride Affinities and First Adiabatic M –F Bond Dissociation Energies from the CCSD(T) Calculated Values.

Method	EA(MF_6)	FA(MF_5)	FA(MF_6)	M-F BDE
BLYP	27.3	16.01	28.98	-17.76
BP86	26.5	12.48	28.67	-20.71
PW91	24.47	8.11	22.44	-22.06
PBE	28.7	12.81	[a]	-21.37
TPSS	27.1	10.68	23.6	-17.45
B3LYP	6.4	-1.91	19.65	-2.48
mPW1	5.1	6.88	13.65	1.21
PBE1	6.5	6.48	13.28	-0.02
O3LYP	17.8	17.48	30.98	-4.61
TPSSh	28.3	3.15	20.54	-22.37

[a] Does not include Pd because the self consistent field did not converge for the energy of .

Figure 3.1. Schematic Energy Level Diagram for Use in Predicting the Molecular Electron Affinities for the MF_6 Molecules in kcal/mol.

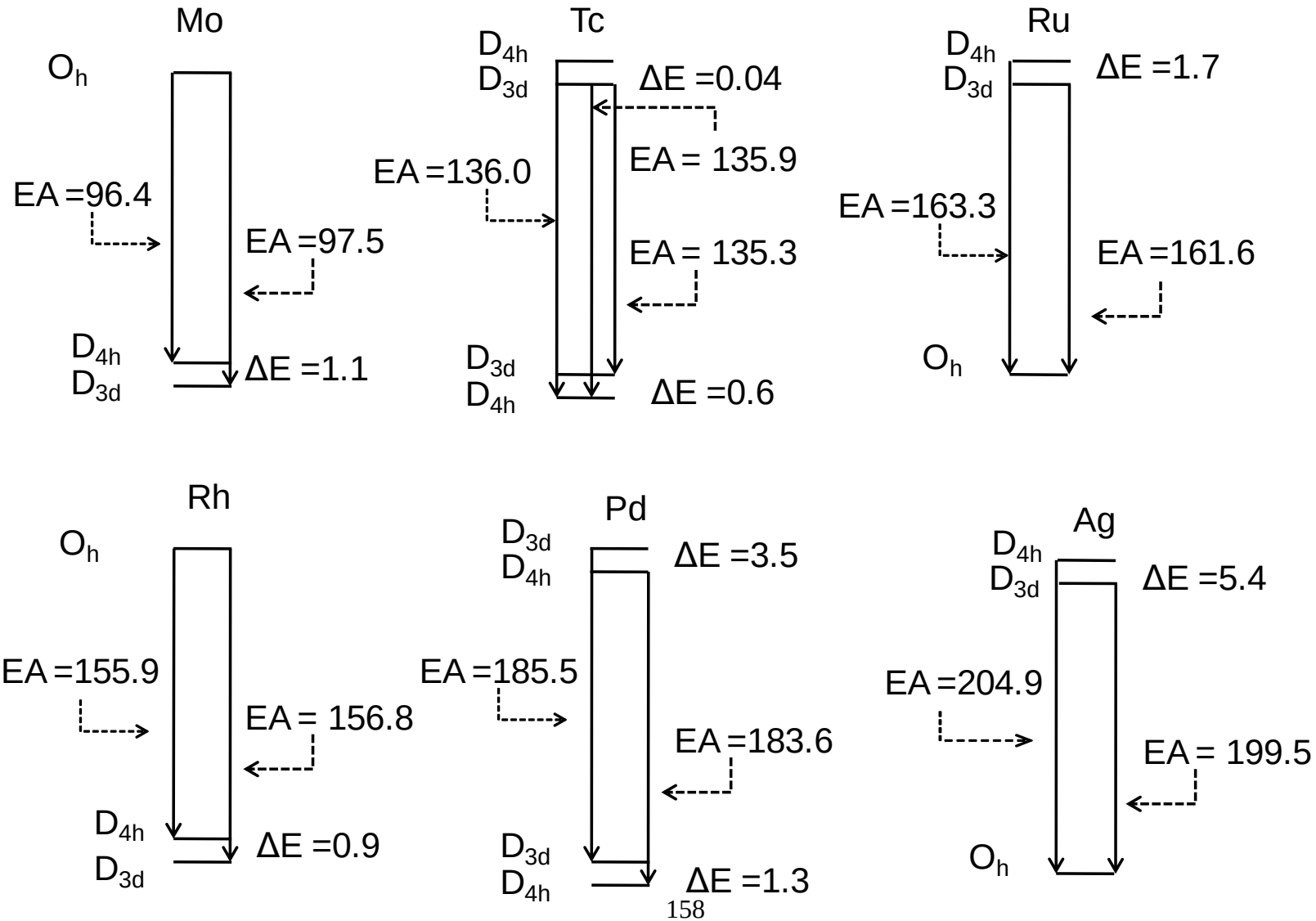

References

[1] Craciun, R.; Picone, D.; Long, R.T.; Li, S.; Dixon, D.A.; Peterson, K.A.; Christe, K.O. *Inorg. Chem* **2010**, *49*, 1056.

[2] Moffit, W.; Goodman, G.L.; Fred, M.; Weinstock, B. *Mol. Phys.* **1959**, *2*, 109.

[3] Claassen, H.H.; Goodman, G.L.; Holloway, J. H.; Selig, H. *J. Chem. Phys*. **1970**, *53*, 341.

[4] Weinstock, B.; Goodman, G. *Advan. Chem. Phys*. **1965**, *9*, 169.

[5] Claassen, H.H.; Selig, H.; Malm, J.G. *J. Chem. Phys. 1962*, **36**, 2888.

[6] Weinstock, B.; Claassen, H.H.; Chernick, C.L. *J. Chem. Phys*. **1963**, *38*, 1470.

[7] Molski, M.J.; Seppelt, K. *Dalton Trans*, **2009**, 3379; Seppelt, K. *Acc. Chem. Res.* **2003**, *36*, 147.

[8] Drews, T.; Super, J.; Hagenbach, A.; Seppelt, K. *Inorg. Chem.* **2006**, *45*,3782.

[9] Richardson, A. D.; Hedberg, K.; Lucier, G. M.; *Inorg. Chem*. **2000**, *39*, 2787.

[10] Brisdon, A. K.; Holloway, J. H.; Hope, E. G.; Levason, W.; Ogden, J. S.; Saad, A. K.; *J. Chem. Soc. Dalton, Trans*. **1992**, 447.

[11] Graudejus, O.; Wilkinson, A. P.; Chacon, L. C.; Bartlett, N. *Inorg. Chem* **2000**, *39*, 2794.

[12] Drews, T.; Supel, J.; Hagenbach, A.; Seppelt, K. *Inorg. Chem.* **2006**, *45*,3782.

[13] Miyoshi, E.; Sakai, Y.; Murakami, A.; Iwaki, H.; Terashima, H.; Shoda, T.; Kawaguchi, T. *J. Chem. Phys***. 1988**, *89*, 4193.

[14] Van Wüllen, C. *J. Comput. Chem.* **1999**, *20*,51.

[15] Miyoshi, E.; Sakai, Y.; Murakami, A.; Iwaki, H.; Terashima, H.; Shoda, T.; Kawaguchi, T. *J. Chem. Phys***. 1988**, *89*, 4193.

[16] Aullón, G.; Alvarez, S. *Inorg. Chem*. **2007**, *46*, 2700.

[17] Seth, M.; Cooke, F.; Schwerdtfeger, P.; Heully, J.L.; Pelissier, M.; *J. Chem. Phys.* **1998**, *109*, 3935.

[18] Mathur, B.P.; Rothe, E. W.; Reck, G. P. *J.Chem.Phys* **1977**, *67*, 377.

[19] Compton, R. N.; Reinhardt, P.W.; Cooper, C. D. *J. Chem. Phys.* **1978**, *68*, 2023.

[20] Sidorov, L. N.; Borshchevsky, A. Ya.; Rudny, E. B.; Butsky, V. D. *Chem. Phys.* **1982**, *71*, 145.

[21] Rudnyi, E. B.;Kaibicheva, E. A.; Sidorov, L. N. *Rapid. Commun. Mass. Spectrom.* **1992**, *6*, 356.

[22] Korobov, M.V.; Kuznetsov, S.V.; Sidorov, L.N.; Shipachev, V.A.; Mit'kin, V.N. *Int. J. Mass. Spectrom. Ion Processes* **1989**, *87*, 13.

[23] Edwards, A. J.; Falconer, W.E.; Griffiths, J.E.; Sunder, W.A.; Vasile, M.J. *J. Chem.Soc. Dalton Trans.* **1974**, 1129.

[24] Selig, H.; Vaknin, D.; Davidov, D.; Yeshurun, Y. *Synthetic Metals*, **1985**, *12*, 479.

[25] Bartlett, N. *J. Fluorine Chem*, **2006**, *127*, 1285.

[26] Sakai, Y.; Miyoshi, E. *J. Chem. Phys.* **1987**, *87*, 2885.

[27] Myers, O.E.; Brady, A.P. *J. Phys. Chem*. **1960**, *64*, 591.

[28] Settle, J. L.; Feder, H. M.; Hubbard, W. N. *J. Phys. Chem.* **1961**, *65*, 1337.

[29] Christe, K. O.; Dixon, D. A.; McLemore, W.W., Wilson, Sheehy, J.; Boatz, J. A. *J. Fluorine Chem.* **2000**, *101*, 151; *Chem. Eng. News*, pp. 48-49, March 3, 2003.

[30] Hunt, R.; Andrews, L.; Toth, L. M. *J. Phys. Chem.* **1991**, *95*, 1183.

[31] Purvis, G.D., III; Bartlett, R.J. J.Chem. Phys. 1982, 76, 1910.

[32] Raghavachari, K.; Truck, G.W.; pople, J.A.; Head-Gordon, M. *Chem. Phys. Lett*. **1989**, *157*, 479.

[33] Watts, J. D.; Gauss, J.; Bartlett, R. J. *J. Chem.. Phys.* **1993**, *98*, 8718.

[34] Bartlett, R. J.; Musial, M. *Rev. Mod. Phys.* **2007**, *79*, 291.

[35] Gaussian 03, Revision E.01, Frisch, M. J.; Trucks, G. W.; Schlegel, H. B.; Scuseria, G. E.; Robb, M. A.; Cheeseman, J. R.; Montgomery, Jr., J. A.; Vreven, T.; Kudin, K. N.; Burant, J. C.; Millam, J. M.; Iyengar, S. S.; Tomasi, J.; Barone, V.; Mennucci, B.; Cossi, M.; Scalmani, G.; Rega, N.; Petersson, G. A.; Nakatsuji, H.; Hada, M.; Ehara, M.; Toyota, K.; Fukuda, R.; Hasegawa, J.; Ishida, M.; Nakajima, T.; Honda, Y.; Kitao, O.; Nakai, H.; Klene, M.; Li, X.; Knox, J. E.; Hratchian, H. P.; Cross, J. B.; Bakken, V.; Adamo, C.; Jaramillo, J.; Gomperts, R.; Stratmann, R. E.; Yazyev, O.; Austin, A. J.; Cammi, R.; Pomelli, C.; Ochterski, J. W.; Ayala, P. Y.; Morokuma, K.; Voth, G. A.; Salvador, P.; Dannenberg, J. J.; Zakrzewski, V. G.; Dapprich, S.; Daniels, A. D.; Strain, M. C.; Farkas, O.; Malick, D. K.; Rabuck, A. D.; Raghavachari, K.; Foresman, J. B.; Ortiz, J. V.; Cui, Q.; Baboul, A. G.; Clifford, S.; Cioslowski, J.; Stefanov, B. B.; Liu, G.; Liashenko, A.; Piskorz, P.; Komaromi, I.; Martin, R. L.; Fox, D. J.; Keith, T.; Al-Laham, M. A.; Peng, C. Y.; Nanayakkara, A.; Challacombe, M.; Gill, P. M. W.; Johnson, B.; Chen, W.; Wong, M. W.; Gonzalez, C.; and Pople, J. A.; Gaussian, Inc., Wallingford CT, 2004.

[36] MOLPRO, version 2008.1, a package of ab initio programs, Werner, H.-J.; Knowles, P. J.; Lindh, R.; Manby, F. R.; Schütz, M.; Celani, P.; Korona, T.; Rauhut, G.; Amos, R. D.; Bernhardsson, A.; Berning, A.; Cooper, D. L.; Deegan, M. J. O.; Dobbyn, A. J.; Eckert, F.; Hampel C.; Hetzer, G.; Lloyd, A. W.; McNicholas, S. J.; Meyer W.; Mura, M. E.; Nicklass, A.; Palmieri, P.; Pitzer, R.; Schumann, U.; Stoll, H.; Stone, A. J.; Tarroni, R.; Thorsteinsson, T. See http://www.molpro.net.

[37] Peterson, K. A.; Woon, D. E.; Dunning, T. H. Jr. *J. Chem. Phys.* **1994**, *100*, 7410.

[38] Kendall, R. A.; Dunning, T. H. Jr. Harrison, R. J. *J. Chem. Phys.* **1994**, *96*, 6796.

[39] Figgen, D.; Peterson, K. A.; Dolg, M.; Stoll, H. *J. Chem. Phys*. **2009**, *130*, 164108.

[40] (a) Douglas, M.; Kroll, N. M. *Ann. Phys.*, **1974**, *82*, 89; (b) Hess, B. A. *Phys. Rev. A.*, **1985**, *32*, 756. (c) Hess, B. A. *Phys. Rev. A.*, **1986**, *33*, 3742.

[41] Figgen, D.; Peterson, K. A.; Dolg, M.; Stoll, H. *J. Chem. Phys*. **2009**, *130*, 164108.

[42] de Jong, W. A.; Harrison, R. J. ; Dixon, D. A. *J. Chem. Phys.*, **2001**, *114*, 48.

[43] EMSL basis set library. http://www.emsl.pnl.gov/forms/basisform.html

[44] (a) van Lenthe, E.; Ehlers, A.E. Baerends, E.J. *J. Chem. Phys*. **1999**, *110*, 8943; (b) van Lenthe, E.; Baerends, E.J.; Snijders, J.G. *J. Chem. Phys* **1993,** *99*, 4597; (c) van Lenthe, E.; Baerends, E.J.; Snijders, J.G.. *J. Chem. Phys* **1994,** *101*, 9783 ; (d) van Lenthe, E.; Snijders, J.G.; Baerends, E.J. *J. Chem. Phys* **1994,** *105*, 6505; (e) van Lenthe, E.; van Leeuwen, R.; Baerends, E.J.; Snijders, J.G. *Int. J. Quantum Chem*. **1996,** *57*, 281

[45] (a) G. te Velde, F.M. Bickelhaupt, S.J.A. van Gisbergen, C. Fonseca Guerra, E.J. Baerends, J.G. Snijders and T. Ziegler, *Chemistry with ADF*. ; (b) C. Fonseca Guerra, J.G. Snijders, G. te Velde and E.J. Baerends, *Towards an order-N DFT method.* Theoretical Chemistry Accounts **99**, 391 (1998); (c) ADF2008.01, SCM, Theoretical Chemistry, Vrije Universiteit, Amsterdam, The Netherlands, http://www.scm.com

[46] Moore, C. E. *Atomic energy levels as derived from the analysis of optical spectra, Volume 1, H to V*; U.S. National Bureau of Standards Circular 467, U.S. Department of Commerce, National Technical Information Service, COM-72-50282: Washington, D.C., 1949.

[47] Chase, M.W. Jr. *NIST-JANAF Thermochemical Tables*, 4th ed., *J. Phys. Chem. Reference Data* **1998**, Mono. 9, Suppl. 1.

[48] Wagman, D.D.; Evans, W.H.; Parker, V.B.; Schumm, R.H.; Halow, I.; Bailey, S.M.; Churney, K.L.; Nuttall, R.L. *J. Phys. Chem. Ref. Data*, **1982**, *11*, Supplement 2.

[49] Greenwood, N.N.; Earnshaw, A. *Chemistry of the Elements*, Pergamon Press, Oxford, 1984 (Mo, Chapter 23, pg. 1170; Ru, Chapter 25, pg. 1248; Rh, Chapter 26, pg. 1294;Pd,Chapter 27, pg. 1333, Ag, Chapter 28, pg 1368).

[50] Fitz, H.; Muller, B. G.; Graudejus, O.; Bartlett, N. *Z. Anorg. Allg. Chem*. **2002**, *628*, 133.

[51] Aullon, G.; Alvarez, S. *Inorg. Chem.* **2007**, *46*, 2700.

[52] Seth, M.; Cooke, F.; Schwerdtfeger, P.; Heully, J-L.; Pelissier, M. *J. Chem. Phys*. **1998**, *109*, 3935.

[53] Gutsev, G. L.; Boldyrev, A. I. *Chem. Phys*, **1981,** *56*, 277.

[54] Huber, K.P.; Herzberg, G., Molecular Spectra and Molecular Structure. IV. Constants of Diatomic Molecules,, Van Nostrand Reinhold Co., 1979.

[55] Davidson, E. R.; Ishikawa, Y.; Malli, G. L. *Chem. Phys. Lett*. **1981**, *84*, 226.

[56] Wenthold, P.G.; Squires, R.R., *J. Phys. Chem.*, **1995**, *99*, 2002

[57] Artau, A.; Nizzi, K.E.; Hill, B.T.; Sunderlin, L.S.; Wenthold, P.G. *J. Am. Chem. Soc.*, **2000**, *122*, 1066

Appendix: Electron Affinities, Fluoride Affinities, and Heats of Formation of the Second Row Transition Metal Hexafluorides: MF_6 (M=Mo, Tc, Ru, Rh, Pd, Ag)

Supporting Information Experimental atomic heats of formation in kcal/mol, benchmarked DFT exchange-correlation functional, relative energy differences between the D_{4h} and D_{3d} MF_6 structures, EA(MF_6), FA(MF_5), FA(MF_6) and first M-F BDEs calculated with various exchange-correlation functional, adiabatic electron affinities of MF_6**,** vertical electron detachment energies (VDE) of MF_6^- and vertical electron attachment energies (VAE) of MF_6 in kcal/mol calculated at the CCSD(T)/aT-PP//CCSD(T)/aD-PP, B3LYP/aT-PP//B3LYP/aD-PP and CCSD(T)/aT-DK// CCSD(T)/aT-PP levels, MF_6 MF_6^-, MF_5, and MF_7^- total electronic energies and vibrational frequencies at the DFT level with various exchange-correlation functionals and the aD-PP basis set, zero point energies (ZPE), CCSD(T) total energies as a function of basis set, core and valence energies at the CCSD(T)/aug-cc-pWCVTZ-PP level, and scalar relativistic energies at the CISD/aT-PP and CCSD(T)-DK/aug-cc-pVTZ-DK levels. Energy differences in kcal/mol of D_{4h} vs O_h structures for the same spin state and singlet –triplet splitting energies for the D_{4h} structures. Optimized geometry parameters with different DFT functionals. Pseudopotential errors and scalar relativistic corrections for EA(MF_6), 1^{st} M –F BDEs and total atomization energies.Electron affinities calculated at the ZORA and ZORA+SO levels. Mulliken charges, NBO charges, and spin densities for MF_6 and MF_6^- and figures for the spin densities. First M –F BDEs, FA(MF_6), and FA(MF_5) calculated at the DFT and CCSD(T) levels as a function of basis set. MF_5 optimized geometry at the B3LYP/aT-PP, BLYP/TZ2P scalar relativistic ZORA and ZORA plus spin orbit levels .Cartesian xyz coordinates for all molecules.

Table A3.1. MF_6 and MF_6^- number of d electrons and spin states.

molecule	neutral	Spin	Jahn-Teller distortion	anion	Spin	Jahn-Teller distortion
WF_6	t_{2g}^0	singlet	No	t_{2g}^1	doublet	Yes
ReF_6	t_{2g}^1	doublet	Yes	t_{2g}^2	triplet	Yes
OsF_6	t_{2g}^2	triplet	Yes	t_{2g}^3	quartet	No
IrF_6	t_{2g}^3	quartet	No	t_{2g}^4	triplet	Yes
PtF_6	t_{2g}^4	triplet	Yes	t_{2g}^5	doublet	Yes
AuF_6	t_{2g}^5	doublet	Yes	t_{2g}^6	singlet	No

Table A3.2. Experimental atomic heats of formation in kcal/mol.

Atom	**JANAF**[a] **0 K**	**Greenwood** [b] **0 K**	**Wagman et al.**[c] **0 K**	**Wagman et al.** [c] **298 K**
F	18.47 ± 0.07			
Mo		158.7±3.1	156.9	157.3
Tc			161.8	162.0
Ru		153	153.2	153.6
Rh		132.9±2.6	132.8	133.1
Pd		90.1±0.7	90.2	90.4
Ag		67.9±0.9	67.9	68.00

[a] Reference 45. [b] Reference 47. [c] Reference 46.

Table A3.3. Benchmarked DFT exchange-correlation functionals.

Functional	**exchange**	**correlation**	**type**
SVWN5	Slater	VWN5	LSDA
BLYP	Becke 88	Lee-Yang-Parr	GGA
BP86	Becke 88	Perdew 86	GGA
PW91	Perdew-Wang 91	Perdew-Wang 91	GGA
PBE	Perdew-Burke-Ernzerhof	Perdew-Burke-Ernzerhof	GGA
TPSS	Tao-Perdew-Staroverov-Scuseria	Tao-Perdew-Staroverov-Scuseria	GGA
HCTH	Handy	Handy	GGA
B3LYP	Becke 93	Lee-Yang-Parr	HGGA
mPW1	Barone's modified PW91	Perdew-Wang 91	HGGA
PBE1	Perdew-Burke-Ernzerhof	Perdew-Burke-Ernzerhof	HGGA
O3LYP	Handy's OPTX	Lee-Yang-Parr	HGGA
TPSSh	Tao-Perdew-Staroverov-Scuseria	Tao-Perdew-Staroverov-Scuseria	HGGA

Table A3.4. Optimized metal-fluorine bond lengths (Å) and bond angles (degrees) with the B3LYP and BLYP DFT functionals and the aD-PP and aT-PP basis sets.

Molecule	**state/symm**	**B3LYP**	**BLYP**	**CCSD(T)**	**B3LYP**
		aD-PP	**aD-PP**	**aD-PP**	**aT-PP**
MoF_6	$^1A_{1g}/O_h$	1.840 (x6)	1.865(x6)	1.838 (x6)	1.832(x6)
MoF_6^-	$^2B_{2g}/D_{4h}$	1.872(x2) 1.920(x4)	1.896(x2) 1.945(x4)	1.869 (x2) 1.918 (x4)	1.863(x2) 1.914(x4)
MoF_6^-	$^2A_{1g}/D_{3d}$	1.904 91.9°	1.928 91.9°	1.901 91.8°	1.897 92.0°
TcF_6	$^2B_{2g}/D_{4h}$	1.813 (x2) 1.845 (x4)	1.841(x2) 1.874(x4)	1.794 (x2) 1.828 (x4)	1.803(x2) 1.837(x4)
TcF_6	$^2A_{1g}/D_{3d}$	1.834 91.3°	1.863 91.3°	1.832 91.1°	1.826 91.3°
TcF_6^-	$^3A_{1g}/D_{4h}$	1.923 (x2) 1.877 (x4)	1.950(x2) 1.904(x4)	1.919 (x2) 1.872 (x4)	1.916(x2) 1.869(x4)
TcF_6^-	$^3A_{1g}/D_{3d}$	1.892 91.2°	1.919 91.1°	1.887 90.4°	1.884 91.2°
RuF_6	$^3A_{1g}/D_{4h}$	1.852 (x2) 1.825 (x4)	1.884(x2) 1.857(x4)	1.850 (x2) 1.824 (x4)	1.845(x2) 1.815(x4)
RuF_6	$^3A_{1g}/D_{3d}$	1.833 90.9°	1.866 90.8°	1.830 90.4°	1.825 90.9°
RuF_6^-	$^4A_{1g}/O_h$	1.884(x6)	1.915(x6)	1.879 (x6)	1.876(x6)
RhF_6	$^4A_{1g}/O_h$	1.838 (x6)	1.874(x6)	1.815 (x6)	1.829(x6)
RhF_6^-	$^3A_{1g}/D_{4h}$	1.859(x2) 1.895(x4)	1.894(x2) 1.929(x4)	1.849 (x2) 1.888 (x4)	1.849(x2) 1.888(x4)
RhF_6^-	$^3A_{1g}/D_{3d}$	1.882 90.7°	1.916 90.7°	1.875 90.8°	1.874 90.8°
PdF_6	$^3A_{1g}/D_{4h}$	1.849 (x2) 1.861 (x4)	1.886(x2) 1.902(x4)	1.848 (x2) 1.850 (x4)	1.841(x2) 1.853(x4)
PdF_6^-	$^2A_{1g}/D_{4h}$	1.919(x2) 1.876(x4)	1.957(x2) 1.915(x4)	1.909(x2) 1.868(x4)	1.914(x2) 1.869(x4)

AgF_6	$^2B_{2g}/D_{4h}$	1.899(x2) 1.876(x4)	1.935(x2) 1.918(x4)	1.909(x2) 1.913(x4)	1.887(x2) 1.890(x4)
AgF_6^-	$^1A_{1g}/O_h$	1.907(x6)	1.946(x6)	1.905 (x6)	1.899(x6)

Table A3.5. Components of the relative energy difference (ΔE) between the D_{4h} and D_{3d} structures in kcal/mol.

MF_6/ MF_6^-	State/Sym D_{4h}	State/Sym D_{3d}	ΔE_{CBS} [a]	ΔE_{ZPE}	ΔE_{CV} [b]	ΔE_{Rel} [c]	ΔE_{SO} [d]	ΔE
MoF_6^-	$^2B_{2g}$	$^2A_{1g}$	0.20	-1.16[e]	0.10	-0.32	0.07	-1.1
TcF_6	$^2B_{2g}$	$^2A_{1g}$	0.30	-0.50[e]	0.02	0.00	0.14	-0.04
TcF_6^-	$^3A_{1g}$	$^3A_{1g}$	0.85	-0.42[e]	-0.07	0.01	0.23	0.6
RuF_6	$^3A_{1g}$	$^3A_{1g}$	0.54	-0.88[f]	-0.11	-0.98	-0.24	-1.67
RhF_6^-	$^3A_{1g}$	$^3A_{1g}$	0.59	-0.61[e]	-0.07	-0.63	-0.16	-0.88
PdF_6	$^3A_{1g}$	$^3A_{1g}$	2.94	-0.57[f]	1.51	-0.21	-0.13	3.54
PdF_6^-	$^2B_{2g}$	$^2A_{1g}$	0.87	-0.68[f]	-0.11	1.14	0.09	1.31
AgF_6	$^2B_{2g}$	$^2A_{1g}$	-0.56	-0.09[e]	0.80	-4.70	-0.84	-5.39

[a] Valence CCSD(T) electronic energy contribution extrapolated using the mixed Gaussian/exponential formula.[b] CCSD(T)/awCVTZ. [c] See equation (2).[d] Spin-orbit correction from BLYP/ZORA + SO/TZ2P calculation. [e]BP86/aD-PP. [f]B3LYP/aT-PP.

Table A3.6. Energy differences of D_{4h} vs O_h structures for the same spin state and singlet –triplet splitting energies for the D_{4h} structures in kcal/mol at B3LYP/aD-PP and CCSD(T)/aD-PP levels.

Method	**TcF_6**		**RuF_6**			**PdF_6**			**AgF_6**		
State/symm	**$^2B_{2g}/D_{4h}$**	**O_h**	**$^3A_{1g}/D_{4h}$**	**O_h**	**$^1A_{1g}/D_{4h}$**	**$^3A_{1g}/D_{4h}$**	**O_h**	**$^1A_{1g}/D_{4h}$**	**$^2B_{2g}/D_{4h}$**	**O_h**	**D_{3d}**
B3LYP/aD	0.0	0.5	0.0	0.3	24.3	0.0	0.1	25.4	0.0	0.2	
CCSD(T)/aD	0.0	1.0	0.0	0.3	23.4	0.0	0.0	11.5	0.8	0.0	0.0

Method	**MoF_6^-**			**TcF_6^-**			**RhF_6^-**			**PdF_6^-**		
State/symm	**$^2B_{2g}/D_{4h}$**	**O_h**	**D_{3d}**	**$^3A_{1g}/D_{4h}$**	**O_h**	**$^1A_{1g}/D_{4h}$**	**$^3A_{1g}/D_{4h}$**	**O_h**	**$^1A_{1g}/D_{4h}$**	**$^2B_{2g}/D_{4h}$**	**O_h**	**D_{3d}**
B3LYP/aD	0.4	1.17	0.0	0.0	0.7	28.2	0.0	1.0	25.8	0.4	1.1	0.0
CCSD(T)/aD	0.0	0.8	0.2	0.0	0.8	29.1	0.0	0.5	24.1	0.0	29.3	0.7

Table A3.7. Pseudopotential errors[a] and scalar relativistic corrections in kcal/mol for the MF_6 electron affinities.

M	MF_6 State/Sym	MF_6^- State/Sym	$\Delta E_{PP\text{-}error}$[b]	ΔE_{MVD}[c]
Mo	$^1A_{1g}/O_h$	$^2A_{1g}/D_{3d}$	-0.61	-0.16
Tc	$^2A_{1g}/D_{3d}$	$^3A_{1g}/D_{4h}$	3.95	-0.18
Ru	$^3A_{1g}/D_{3d}$	$^4A_{1g}/O_h$	-2.41	-0.20
Rh	$^4A_{1g}/O_h$	$^3A_{1g}/D_{3d}$	0.55	-0.22
Pd	$^3A_{1g}/D_{4h}$	$^2B_{2g}/D_{4h}$	1.14	-0.31
Ag	$^2B_{2g}/D_{4h}$	$^1A_{1g}/O_h$	-0.22	-0.29

[a] Estimate of the pseudopotential error was obtained by first calculating a scalar relativistic correction from the expectation values of the mass-velocity and Darwin terms in the Breit-Pauli Hamiltonian at the CISD/aT-PP level for MF_6 and MF_6^- (essentially the relativistic correction for the F atoms). This scalar relativistic correction was added to the CCSD(T)/aT-PP value and the pseudopotential error is given as the difference from the DKH value

[b] $\Delta EA_{PP\text{-}error} = EA(CCSD(T)\text{-}DK/aT\text{-}DK) - EA_{MVD}(CCSD(T)/aT\text{-}PP)$, where

$EA_{MVD}(CCSD(T)/aT\text{-}PP) = EA(CCSD(T)/aT\text{-}PP) + \Delta E_{MVD}$.

[c] $\Delta E_{MVD} = 6 * \Delta E_{MVD}(F) + \Delta E_{MVD}(MF_6) - \Delta E_{MVD}(MF_6^-)$

Table A3.8. Electron Affinities in kcal/mol calculated at the ZORA and ZORA+SO levels.

	BLYP/ZORA		BLYP/ZORA+SO	
Molecule	**Final State/Sym**	**EA**	**Final Sym**	**EA**
MoF_6/MoF_6^-	$^1O_h/^2D_{3d}$	84.1	O_h / D_{4h}	84.3
MoF_6/MoF_6^-	$^1O_h/^2D_{3d}$	84.1	O_h / D_{3d}	84.4
TcF_6/TcF_6^-	$^2D_{3d}/^3D_{3d}$	110.8	D_{4h} / D_{4h}	110.8
TcF_6/TcF_6^-	$^2D_{3d}/^3D_{3d}$	110.8	D_{3d} / D_{3d}	110.7
RuF_6/RuF_6^-	$^3D_{3d}/^4O_h$	135.8	D_{4h} / O_h	135.4
RuF_6/RuF_6^-	$^3D_{3d} / ^4O_h$	135.8	D_{3d} / O_h	135.1
RhF_6/RhF_6^-	$^4O_h/^3D_{3d}$	132.2	O_h/D_{4h}	133.3
RhF_6/RhF_6^-	$^4O_h/^3D_{3d}$	132.2	O_h/D_{3d}	133.4
PdF_6/PdF_6^-	$^3O_h/^2O_h$	154.7	D_{4h}/D_{4h}	155.1
AgF_6/AgF_6^-	$^2O_h/^1O_h$	169.7	O_h/O_h	169.7

Table A3.9. Mulliken charges for MF_6 and MF_6^- (M = second row transition metals) at B3LYP and BP86 levels with aD basis set.

MF_6/MF_6^-	state	B3LYP			BP86		
		M	**F**	**F** (avg)	**M**	**F**	**F** (avg)
MoF_6	$^1A_{1g}/O_h$	2.317	-0.386	-0.386	1.990	-0.332	-0.332
MoF_6^-	$^2A_{1g}/D_{3d}$	2.271	-0.545	-0.545	1.953	-0.492	-0.492
MoF_6^-	$^2B_{2g}/D_{4h}$	2.270	-0.504(2s) -0.566(4l)	-0.545	1.953	-0.451(2s) -0.513(4l)	-0.492
TcF_6	$^2A_{1g}/D_{3d}$	2.177	-0.363	-0.363	1.862	-0.310	-0.310
TcF_6	$^2B_{2g}/D_{4h}$	2.176	-0.322(2s) -0.383(4l)	-0.362	1.861	-0.272(2s) -0.329(4l)	-0.310
TcF_6^-	$^3A_{1g}/D_{4h}$	2.148	-0.579(2l) -0.498(4s)	-0.525	1.841	-0.528(2l) -0.446(4s)	-0.473
RuF_6	$^3A_{1g}/D_{3d}$	2.025	-0.338	-0.338	1.856	-0.309	-0.309
RuF_6	$^3A_{1g}/D_{4h}$	2.022	-0.400(2l) -0.306(4s)	-0.337	1.740	-0.347(2l) -0.261(4s)	-0.90
RuF_6^-	$^4A_{1g}/O_h$	2.069	-0.511	-0.511	1.781	-0.463	-0.463
RhF_6	$^4A_{1g}/O_h$	2.144	-0.357	-0.357	1.866	-0.311	-0.311
RhF_6^-	$^3A_{1g}/D_{3d}$	2.115	-0.519	-0.519	1.827	-0.471	-0.471
RhF_6^-	$^3A_{1g}/D_{4h}$	2.106	-0.476(2s) -0.538(4l)	-0.517	1.824	-0.432(2s) -0.490(4l)	-0.470
PdF_6	$^3A_{1g}/D_{4h}$	1.999	-0.335(2s) -0.332(4l)	-0.333	1.756	-0.280(2s) -0.299(4l)	-0.293
PdF_6^-	$^2B_{2g}/D_{4h}$	1.989	-0.561(2l) -0.467(4s)	-0.498	1.735	-0.522(2l) -0.422(4s)	-0.455
AgF_6	$^2B_{2g}/D_{4h}$	1.876	-0.382(2l) -0.278(4s)	-0.439	1.671	-0.351(2l) -0.242(4s)	-0.278
AgF_6^-	$^1A_{1g}/O_h$	1.921	-0.487	-0.487	1.719	-0.453	-0.453

s = short M-F bond distances
l = long M-F bond distances

Table A3.10. Electron spin densities for MF_6 and MF_6^- (M = second row transition metals) calculated at the B3LYP/aD-PP and BP86/aD-PP and aT-PP levels ([a] s = short M-F bond distances. l = long M-F bond distances.)

MF_6/MF_6^-	state	B3LYP/aD-PP		BP86/aD-PP	
		M	F	M	F
$\mathbf{MoF_6^-}$	$^2A_{1g}/D_{3d}$	0.908	0.015	0.908	0.015
$\mathbf{MoF_6^-}$	$^2B_{2g}/D_{4h}$	0.907	-0.014 0.030	0.901	-0.014(2s) -0.032(4l)
$\mathbf{TcF_6}$	$^2A_{1g}/D_{3d}$	0.821	0.030	0.797	0.034
$\mathbf{TcF_6}$	$^2B_{2g}/D_{4h}$	0.820	-0.021(2s) 0.055(4l)	0.786	-0.019(2s) 0.063(4l)
$\mathbf{TcF_6^-}$	$^3A_{1g}/D_{4h}$	1.722	0.094(2l) 0.022(4s)	1.663	0.112(2l) 0.028(4s)
$\mathbf{RuF_6}$	$^3A_{1g}/D_{3d}$	1.468	0.089	1.376	0.104
$\mathbf{RuF_6}$	$^3A_{1g}/D_{4h}$	1.456	0.198(2l) 0.037(4s)	1.348	0.222(2l) 0.052(4s)
$\mathbf{RuF_6^-}$	$^4A_{1g}/O_h$	2.351	0.108	2.202	0.133
$\mathbf{RhF_6}$	$^4A_{1g}/O_h$	1.728	0.212	1.562	0.239
$\mathbf{RhF_6^-}$	$^3A_{1g}/D_{3d}$	1.355	0.107	1.213	0.131
$\mathbf{RhF_6^-}$	$^3A_{1g}/D_{4h}$	1.358	0.148(2s) 0.086(4l)	1.218	0.171(2s) 0.110(4l)
$\mathbf{PdF_6}$	$^3A_{1g}/D_{4h}$	0.761	0.193(2s) 0.213(4l)	0.691	0.234(2s) 0.210(4l)
$\mathbf{PdF_6^-}$	$^2B_{2g}/D_{4h}$	0.521	-0.014(2l) 0.127(4s0	0.446	-0.009(2l) 0.143(4s)
$\mathbf{AgF_6}$	$^2B_{2g}/D_{4h}$	0.201	-0.009(2l) 0.204(4s)	0.182	-0.007(2l) 0.208(4s)

Table A3.11. First M –F bond dissociation energies in kcal/mol calculated at DFT and CCSD(T) levels with the with the an-PP (n=2,3,4) basis sets.

Bond	MF_5 State/Sym	MF_6 State/Sym	B3LYP/aD-PP	CCSD(T)/aD-PP	CCSD(T)/aT-PP	CCSD(T)/aQ-PP	CBS
Mo-F	$^2A_2/C_{2v}$	$^1A_{1g}/O_h$	83.6	80.2	84.8	86.4	87.6
Tc-F	$^3A_1'/D_{3h}$	$^2B_{2g}/D_{4h}$	52.1	45.3	50.1	51.3	52.1
Ru-F	$^4B_1/C_{4v}$	$^3A_{1g}/D_{4h}$	39.1	29.3	35.5	36.8	37.7
Rh-F	$^3B_2/C_{4v}$	$^4A_{1g}/O_h$	47.4	39.0	42.5	43.2	43.9
Pd-F	$^2B_1/C_{4v}$	$^3A_{1g}/D_{4h}$	23.7	37.0	40.2	40.9	41.5
Ag-F	$^1A_1/C_{4v}$	$^2B_{2g}/D_{4h}$	9.2	-1.6	-1.4	-1.0	-0.4

Table A3.12. MF_5 optimized geometry at the B3LYP/aD-PP, BLYP/TZ2P scalar relativistic ZORA and ZORA plus spin orbit levels.[a]

MF_5	Initial State/Sym	B3LYP/aD-PP	ZORA Sym	ZORA	ZORA SO Sym	ZORA SO
MoF_5	$^2A_2/C_{2v}$	1.884(x2) 1.832(x2) 1.814(x1)	C_{2v}	1.912(x2) 1.859(x2) 1.841(x1)	C_{2v}	1.913(x2) 1.859(x2) 1.842(x1)
TcF_5	$^3A_1'/D_{3h}$	1.886(x2) 1.807(x3)	D_{3h}	1.916(x2) 1.836(x3)	D_{3h}	1.915(x2) 1.836(x3)
RuF_5	$^4B_1/C_{4v}$	1.811(x1) 1.850(x4) 98.1°	C_{4v}	1.843(x1) 1.887(x4) 97.7°	C_{4v}	1.843(x1) 1.887(x4) 97.8°
RhF_5	$^3B_1/C_{2v}$	1.870(x2) 1.828(x2) 1.814(x1)	C_{2v}	1.912(x2) 1.873(x2) 1.857(x1)	C_{4v}	1.865(x1) 1.891(x4) 94.5
PdF_5	$^2B_1/C_{4v}$	1.846(x1) 1.859(x4) 92.9°	C_{4v}	1.887(x1) 1.911(x4) 92.7°	C_{4v}	1.888(x1) 1.911(x4) 92.7°
AgF_5	$^1A_1/C_{4v}$	1.861(x1) 1.885(x4) 94.1°	C_{4v}	1.923(x1) 1.942(x4) 94.9°	C_{4v}	1.932(x1) 1.942(x4) 94.9

[a] The different bond lengths are listed separately and the times they occur are given in parentheses

Table A3.13. Scalar relativistic corrections and pseudopotential errors in kcal/mol for the first M –F bond dissociation energies and the 1st BDE calculated at the ADF ZORA Scalar BLYP/TZ2P level.

Bond	**MF_5 State/Sym**	**MF_6 State/Sym**	**$\Delta E_{PP\text{-}error}$[a]**	**ΔE_{MVD}[b]**	**1st BDE ZORA[c]**
Mo-F	$^2A_2/C_{2v}$	$^1A_{1g}/O_h$	0.72	-0.29	98.33
Tc-F	$^3A_1'/D_{3h}$	$^2A_{1g}/D_{3d}$	1.42	-0.29	74.59
Tc-F	$^3A_1'/D_{3h}$	$^2B_{2g}/D_{4h}$	1.43	-0.29	74.59
Ru-F	$^4B_1/C_{4v}$	$^3A_{1g}/D_{3d}$	7.05	-0.29	62.71
Ru-F	$^4B_1/C_{4v}$	$^3A_{1g}/D_{4h}$	6.07	-0.29	62.72
Rh-F	$^3B_2/C_{4v}$	$^4A_{1g}/O_h$	-0.32	-0.28	66.22
Pd-F	$^2B_1/C_{4v}$	$^3A_{1g}/D_{4h}$	0.13	-0.25	44.45
Ag-F	$^1A_1/C_{4v}$	$^2B_{2g}/D_{4h}$	0.35	-0.23	36.34

[a] $\Delta E_{PP\text{-}error}$ = E(CCSD(T)-DK/aT-DK) – E_{MVD}(CCSD(T)/aT-PP); E_{MVD}(CCSD(T)/aT-PP) = E(CCSD(T)/aT-PP) + $\Delta E_{MVD.}$ [b] $\Delta E_{MVD} = \Delta E_{MVD}(MF_5) + \Delta E_{MVD}(F) - \Delta E_{MVD}(MF_6)$. [c] 1st BDE ZORA calculated at the ADF ZORA Scalar BLYP/TZ2P level.

Table A3.14. Scalar relativistic corrections, pseudopotential errors and the atomic spin-orbit corrections in kcal/mol for the atomization energies at 0 K.

Molecule	**State/Sym**	**$\Delta E_{PP\text{-}error}$[a]**	**ΔE_{MVD}[b]**	**Atomic ΔE_{SO}[c]**
MoF_6	$^1A_{1g}/O_h$	4.30	-1.65	-2.33
TcF_6	$^2B_{2g}/D_{4h}$	3.33	-1.64	-2.33
RuF_6	$^3A_{1g}/D_{3d}$	3.27	-1.63	-6.27
RhF_6	$^4A_{1g}/O_h$	0.81	-1.58	-6.59
PdF_6	$^3A_{1g}/D_{4h}$	1.05	-1.42	-2.33
AgF_6	$^2B_{2g}/D_{4h}$	0.28	-1.31	-2.33

[a] $\Delta E_{PP\text{-}error}$ = E(CCSD(T)-DK/aT-DK) – E_{MVD}(CCSD(T)/aT-PP); E_{MVD}(CCSD(T)/aT-PP) = E(CCSD(T)/aT-PP) + $\Delta E_{MVD.}$ [b] ΔE_{MVD} = 6*****ΔE_{MVD}(F) + ΔE_{MVD}(M) - ΔE_{MVD}(MF_6). [c] The spin-orbit splitting is -0.39 kcal/mol for the ($^2P_{3/2}$) state of F; 0.0 kcal/mol for the ground state ($^7S_3$) of Mo, ($^6S_{5/2}$) of Tc, ($^1S_0$) of Pd and ($^2S_{1/2}$) of Ag; 3.94 kcal/mol for Ru ($^5F_5$) and 4.26 kcal/mol for Rh ($^4F_{9/2}$). Reference 42.

Table A3.15. Optimized bond lengths (Å) for MF_7^- (M = third row transition metals) at the B3LYP and BP86 levels.

MF_7^-	State	B3LYP		BP86	
		aD	aT	aD	aT
MoF_7^-	$^1A_1'/D_{5h}$	1.868(x2)	1.860(x2)	1.883(x2)	1.875(x2)
		1.916(x5)	1.911(x5)	1.931(x5)	1.925(x5)
	$^1A_1/C_{2v}$	1.916(x1)	1.909(x1)	1.929(x1)	1.922(x1)
		1.904(x2)	1.897(x2)	1.919(x2)	1.912(x2)
		1.896(x4)	1.888(x4)	1.910(x4)	1.903(x4)
	$^1A_1/C_{3v}$	1.908(x1)	1.901(x1)	1.923(x1)	1.916(x1)
		1.895(x3)	1.888(x3)	1.910(x3)	1.903(x3)
		1.904(x3)	1.897(x3)	1.917(x3)	1.909(x3)
TcF_7^-	$^2A_2/C_{2v}$	1.884(x1)	1.876(x1)	1.902(x1)	1.893(x1)
		1.871(x2)	1.864(x2)	1.888(x2)	1.881(x2)
		1.928(x2)	1.922(x2)	1.943(x2)	1.937(x2)
		1.900(x2)	1.893(x2)	1.917(x2)	1.909(x2)
RuF_7^-	$^3A_1'/D_{5h}$	1.876(x2)	1.869(x2)	1.895(x2)	1.888(x2)
		1.907(x5)	1.899(x5)	1.923(x5)	1.916(x5)
RuF_7^-	$^5A''/C_s$	3.555(x1)	3.546(x1)	3.524(x1)	3.509(x1)
		1.924(x1)	1.915(x1)	1.955(x1)	1.947(x1)
		1.879(x2)	1.871(x2)	1.893(x2)	1.885(x2)
		1.874(x2)	1.866(x2)	1.885(x2)	1.877(x2)
		1.875(x1)	1.867(x1)	1.888(x1)	1.879(x1)
RhF_7^-	$^2B_1/C_{2v}$	1.894(x1)	1.885(x1)	1.919(x1)	1.906(x1)
		1.888(x2)	1.881(x2)	1.910(x2)	1.904(x2)
		1.928(x2)	1.921(x2)	1.943(x2)	1.936(x2)
		1.907(x2)	1.899(x2)	1.914(x2)	1.907(x2)
PdF_7^-	$^1A_1'/D_{5h}$	1.916(x2)	1.911(x2)	1.936(x2)	1.930(x2)
		1.924(x5)	1.916(x5)	1.942(x5)	1.934(x5)

PdF_7^-	$^3A'/C_s$	3.423(x1)	3.441(x1)		
		1.944(x1)	1.938(x1)		
		1.874(x2)	1.866(x2)		
		1.869(x2)	1.861(x2)		
		1.904(x1)	1.898(x1)		
AgF_7^-	$^2B_2/C_{2v}$	1.896(x1)	1.885(x1)	1.926(x1)	1.915(x1)
		2.288(x2)	2.282(x2)	2.300(x2)	2.297(x2)
		1.909(x4)	1.9014(x4)	1.929(x4)	1.922(x4)
AgF_7^-	$^2A'/C_s$	3.499 (x1)	3.503(x1)	2.053(x1)	3.487(x1)
		1.928(x1)	1.920(x1)	1.927(x1)	1.956(x1)
		1.904(x2)	1.897(x2)	1.913(x2)	1.917(x2)
		1.900(x2)	1.893(x2)	1.905(x2)	1.912(x2)
		1.896(x1)	1.889(x1)	1.895(x1)	1.910(x1)

Table A3.16. MF_7^- Mulliken and NBO charges at B3LYP/aT level.

		Mulliken			NBO		
		M	**F**	**F** (avg)	**M**	**F**	**F** (avg)
MoF_7^-	$^1A_1'/D_{5h}$	1.672	-0.350(x2) -0.394(x5)	-0.381	2.360	-0.459(x2) -0.489(x5)	-0.480
TcF_7^-	$^2A_2/C_{2v}$	1.518	-0.317(x1) -0.363(x2) -0.391(x2) -0.346(x2)	-0.360	1.452	-0.215(x1) -0.193(x2) -0.213(x2) -0.212(x2)	-0.207
RuF_7^-	$^3A_1'/D_{5h}$	1.556	-0.417(x2) -0.344(x5)	-0.365	1.722	-0.147(x2) -0.186(x5)	-0.175
	$^5A''/C_s$	1.752	-0.444(x2) -0.447(x2) -0.439(x1) -0.371(x1) -0.159(away)	-0.393	1.876	-0.129(x2) -0.135(x2) -0.136(x1) -0.063(x1) 0.352(away)	-0.053
RhF_7^-	$^2A_1/C_{2v}$	1.429	-0.383(x2) -0.359(x2) -0.322(x2) -0.299(x1)	-0.376	0.999	-0.123(x2) -0.139(x2) -0.183(x2) -0.111(x1)	-0.143
PdF_6^-	$^1A_1'/D_{5h}$	1.386	-0.415(x2) -0.311(x5)	-0.341	1.956	-0.527(x2) -0.380(x5)	-0.422
	$^3A'/C_s$	1.342	-0.324(x2) -0.331(x2) -0.381(x1) -0.456(x1) -0.196(away)	-0.335	1.475	-0.361(x2) -0.377(x2) -0.362(x1) -0.442(x1) -0.196(away)	-0.354
	$^1A'/C_s$	1.285	-0.466(x2) -0.462(x2) -0.352(x1) -0.062(x1) -0.016(away)	-0.326	1.402	-0.521(x2) -0.526(x2) -0.373(x1) 0.041(x1) 0.026(away)	-0.362

AgF_7^-	$^2B_2/C_{2v}$	1.495	-0.380(x4) -0.304(x1) -0.336(x2)	-0.356	0.773	-0.205(x4) -0.191(x1) 0.112(x2)	-0.112
	$^2A'/C_s$	1.395	-0.396(x2) -0.391(x2) -0.396(x1) -0.299(x1) -0.154(away)	-0.346	0.788	-0.207(x2) -0.215(x2) -0.191(x1) -0.111(x1) 0.358(away)	-0.113

Table A3.17. MF_6 fluoride affinities to classical and non-classical structures (kcal/mol) calculated at CCSD(T) level with the aVNZ-PP (N = D, T, Q) basis sets.

Calculation	MoF_6[a]	TcF_6[a]	RuF_6[a]	RuF_6[b]	RhF_6[a]	PdF_6[a]	PdF_6[b]	AgF_6[a]	AgF_6[b]
State/Sym	$^1A_{1g}/O_h$	$^2A_{1g}/D_{3d}$	$^3A_{1g}/D_{3d}$	$^3A_{1g}/D_{3d}$	$^4A_{1g}/O_h$	$^3A_{1g}/D_{4h}$	$^3A_{1g}/D_{4h}$	$^2B_{2g}/D_{4h}$	$^2B_{2g}/D_{4h}$
B3LYP/aD	71.3	73.5	77.9	80.7	54.5	69.4	98.5	96.9	121.7
B3LYP/aT	72.0	73.7	77.8		61.3	70.1	97.5	96.4	121.7
CCSD(T)/aD	74.1	77.8	85.2	94.2	134.1	88.7	107.9	100.2	126.8
CCSD(T)/aT	76.2	78.1	85.1	88.3	108.8	88.9	105.6	99.2	127.1
CCSD(T)/aQ	75.7	77.5	84.9		104.9	89.7		99.1	
CBS	75.5	77.2	84.9		102.7	89.9		99.2	

[a] Addition of F^- to form one of the classical MF_7^- structures (C_{2v}, M=Mo, Tc, Rh, Ag and D_{5h}, M=Ru, Pd). [b] Addition of F^- to form the non-classical C_s MF_7^- structure.

Table A3.18. MF_5 fluoride affinities (kcal/mol) calculated at the DFT and CCSD(T) level with aVnZ-PP (n= D, T, Q) basis sets

Calculation	MoF_5	TcF_5	RuF_5	RhF_5	PdF_5	AgF_5
B3LYP/aD-PP	98.6	98.7	115.0	114.4	114.7	122.9
CCSD(T)/aD-PP	104.4	104.7	121.8	118.4	141.7	123.5
CCSD(T)/aT-PP	103.9	104.4	123.1	119.5	143.7	124.8
CCSD(T)/aQ-PP	104.6	104.7	123.6	120.2	144.6	125.4
CBS	105.1	104.9	124.0	120.7	145.3	125.9

Table A3.19. Calculated MF_6^- vibrational frequencies (cm^{-1}). The IR intensities (km/mol) are given in the parentheses.

M	MF_6 State/Sym	a_{1g}	e_g	t_{1u}	t_{1u}	t_{2g}	t_{2u}
MoF_6^- [a]	$^2B_{2g}/D_{4h}$	626(0)	a_{1g} 542(0) b_{1g} 536(0)	e_u 603(640) a_{2u} 635(329)	e_u 252(22) a_{2u} 215(30)	e_g 456(0) b_{2g} 199(0)	e_u 148(2) b_{2u} 103(0)
MoF_6^- [a]	$^2A_{1g}/D_{3d}$	622(0)	366(0)	e_u 619(656) a_{2u} 601(316)	e_u 250(28) a_{2u} 240(17)	a_{1g} 236(0) e_g 198(0)	e_u 136(8) a_{2u} 126(0)
TcF_6^- [b]	$^3A_{1g}/D_{4h}$	645(0)	b_{1g} 562(0) a_{1g} 550(0)	e_u 650(668) a_{2u} 618(330)	a_{2u} 286(6) e_u 252(20)	e_g 596(0) b_{2g} 282(0)	b_{2u} 194 (0) e_u 144 (3)
RuF_6^-	$^4A_{1g}/O_h$	638(0)	562(0)	649(906)	278(33)	248(0)	189(0)
RhF_6^- [c]	$^3A_{1g}/D_{4h}$	619(0)	b_{1g} 547(0) a_{1g} 536(0)	a_{2u} 667(265) e_u 243(474)	e_u 295(6) a_{2u} 260(17)	b_{2g} 212(0) e_g 128(0)	e_u 209(4) b_{2u} 176(0)
RhF_6^- [a]	$^3A_{1g}/D_{3d}$	576(0)	372(0)	e_u 622(384) a_{2u} 619(193)	a_{2u} 282(5) e_u 276(5)	a_{1g} 232(0) e_g 219(0)	e_u 200(4) a_{1u} 174(0)
PdF_6^- [c]	$^2B_{2g}/D_{4h}$	591(0)	a_{1g} 545(0) b_{1g} 537(0)	e_u 650(354) a_{2u} 624(177)	a_{2u} 302(0) e_u 274(16)	b_{2g} 267(0) e_g 221(0)	b_{2u} 230(0) e_u 194(8)
AgF_6^- [c]	$^1A_{1g}/O_h$	539(0)	531(0)	632(387)	279(3)	217(0)	215(0)

[a] BP86/aD-PP [b] B3LYP/aD-PP [c] B3LYP/aT-P

Table A3.20. Calculated MF_5 vibrational frequencies (cm^{-1}). The IR intensities (km/mol) are given in the parentheses.

Type	**MoF_5**[a]	**TcF_5**[a]	**RuF_5**[b]	**RhF_5**[b]	**PdF_5**[b]	**AgF_5**[b]
State/Sym	$^2A_2/C_{2v}$	$^3A_1'/D_{3h}$	$^4B_1/C_{4v}$	$^3B_2/C_{2v}$	$^2B_1/C_{4v}$	$^1A_1/C_{4v}$
A_1	760(215); 723(0) 625(0);215(16) 91(8)		718(60); 672(12) 241(20)	701(36); 653(5) 602(0); 268(13) 160(0)	666(8); 612(0) 278(11)	623(4); 559(0) 241(12)
B_1	647(229); 204(32) 63(30)		262(0)	714(169); 229(12) 159(0)	275(0)	
B_2	689(330); 278(7) 229(9)		620(0); 124(0)	686(180); 264(8) 159(0)	575(0); 184(0)	552(0); 162(0)
A_2	211(0)			247(0);		
E			709(227)x2 251(9)x2 161(1)x2		683(120)x2 226(17)x2 157(0)x2	664(77)x2 259(2)x2 125(0)x2
A_1'		714(0); 621(0)				
E'		760(154)x2 236(15)x2 151(1)x2				
A_2"		682(295); 220(15)				
E"		214(0)				

[a]B3LYP/aT-PP. [b]B3LYP/aD-PP

Table A3.21. Calculated MF_7^- vibrational frequencies (cm^{-1}) at the B3LYP/aD-PP and aT-PP levels. The IR intensities (km/mol) are given in the parentheses.

	MoF_7^{-a}	TcF_7^{-b}	RuF_7^{-a}	RuF_7^{-c}	RhF_7^{-d}	PdF_7^{-a}	PdF_7^-	AgF_7^{-b}
	$^1A_1/C_{2v}$	$^2A_2/C_{2v}$	$^3A_1'/D_{5h}$	$^5A''/C_s$	$^4A'/C_s$	$^1A_1'/D_{5h}$	$^3A'/C_s$	$^2A'/C_s$
A								
A_1	666(21) 632(316) 508(7) 416(0) 349(30) 273(0)	641(0) 634(280) 565(0) 509(0) 425(1) 356(15) 178(7)						
B_1	636(342) 410(1) 325(30) 248(0)	669(320) 296(15) 276(0) 55(1)						
B_2	647(365) 475(2) 355(8) 337(17) 20(2)	610(279) 459(0) 356(13) 235(0) 60(1)						
A_2	535(0)	253(0)						

	313(0) 25(0)	62(0)						
A_1'			628(0) 560(0)			552(0) 541(0)		
A_2"			669(281) 309(7)			632(155) 302(0)		
A'				642(201);621(121) 599(114);499(80) 312(5);260(5) 244(0);214(0) 156(0);60(1)	662(213);632(185) 610(35);530(27) 350(4);302(3) 265(0);264(3) 218(3);174(2) 64(0)		657(153)615(190) 598(1) 528(36) 334(9) 301(0) 268(0) 249(4) 203(3) 163(2) 68(0)	632(115);619(168) 538(0);529(0) 518(22);306(5) 271(0);248(2) 214(0);209(0) 155(3);58(0)
A"				642(225);556(2) 267(7);266(9) 225(0);184(0) 175(0);32(0)	667.5(234);426(0) 278(10);235(0) 215(0);173(0) 27(0)		657(164)541(0) 268(8) 234(0) 212(0) 192(4) 42(0)	632(122); 269(1) 214(0);212(0) 203(0);28(0)

E_1'			617(210)x2 353(12)x2 225(2)			583(70)x2 312(1)x2 225(1)x2		
E_2'			513(0)x2 420(0)x2			477(0)x2 393(0)x2		
E_1"			252(0)x2			207(0)x2		
E_2"			80(0)x2			83(0)x2		

[a]B3LYP/aT-PP.[b]B3LYP/aD-PP.[c]BP86/aT-PP. [d] At the B3LYP/aD-PP level, the non-classical structure is more stable by 19.8 kcal/mol than the MCTP structure which has imaginary frequencies.

Table A3.22. Adiabatic electron affinities of MF_6**,** vertical electron detachment energies (VDE) of MF_6^- and vertical electron attachment energies (VAE) of MF_6 in kcal/mol calculated at the CCSD(T)/aT-PP//CCSD(T)/aD-PP, B3LYP/aT-PP//B3LYP/aD-PP and CCSD(T)/aT-DK// CCSD(T)/aT-PP levels.

	MF_6	**MF_6^-**	**Adiabatic EA**		**VDE**		**VAE**	
Calculation	**State Sym**	**State Sym**	**CCSD(T)/ aT**	**B3LYP/ aT**	**CCSD(T)/ aT**	**B3LYP/ aT**	**CCSD(T)/ aT**	**B3LYP/ aT**
MoF_6/MoF_6^-	$^1A_{1g}/O_h$	$^2B_{2g}/D_{4h}$	99.6	92.4	109.7	104.9	88.6	84.0
TcF_6/TcF_6^-	$^2A_{1g}/D_{3d}$	$^3A_{1g}/D_{4h}$	130.7	124.4	144.4	134.6	124.8	118.1
RuF_6/RuF_6^-	$^3A_{1g}/D_{4h}$	$^4A_{1g}/O_h$	164.1	154.7	173.4	162.4	162.1	150.6
RhF_6/RhF_6^-	$^4A_{1g}/O_h$	$^3A_{1g}/D_{4h}$	153.4	146.2	160.8	156.0	149.7	143.0
PdF_6/PdF_6^-	$^3A_{1g}/D_{4h}$	$^2B_{2g}/D_{4h}$	180.7	171.0	188.1	173.6	179.7	169.3
AgF_6/AgF_6^-	$^2B_{2g}/D_{4h}$	$^1A_{1g}/O_h$	203.0	197.7	202.9	198.8	201.5	196.8

[a] VDE = $E_{\text{neutral at anion geom}} - E_{\text{anion.}}$ [b] VAE = $E_{\text{neutral}} - E_{\text{anion at neutral geom}}$.

Table A3.23. Electron affinities[a] at 0 K (kcal/mol) for MF_6 (M = third row transition metals) calculated with various exchange-correlation functionals and the aD-PP basis sets and deviations (kcal/mol) from the CCSD(T) calculated electron affinities. Values in parentheses are the differences from the CCSD(T) values.

Method	**MoF_6** $O_h \rightarrow D_{3d}$	**TcF_6** $D_{3d} \rightarrow D_{4h}$	**RuF_6** $D_{3d} \rightarrow O_h$	**RhF_6** $O_h \rightarrow D_{3d}$	**PdF_6** $D_{4h} \rightarrow D_{4h}$	**AgF_6** $D_{4h} \rightarrow O_h$
BLYP	81.5 (16.4)	107.1 (24.7)	133.5 (31.2)	129.3 (25.9)	150.0 (33.0)	172.7 (32.5)
BP86	81.1 (16.8)	106.9 (24.9)	133.7 (31.0)	129.9 (25.3)	151.3 (31.7)	175.7 (29.5)
PW91	81.2 (16.7)	107.1 (24.7)	134.1 (30.6)	129.7 (25.5)	151.2 (31.8)	175.7(29.5)
PBE	79.0 (18.9)	105.0 (26.8)	132.0 (32.7)	127.3 (27.9)	149.0 (34.0)	173.3 (31.9)
TPSS	80.6 (17.3)	106.8 (25.0)	133.9 (30.8)	129.0 (26.2)	150.2 (32.8)	174.7 (30.5)
B3LYP	98.0 (-0.1)	125.6 (6.2)	156.9 (7.8)	150.1 (5.1)	172.2 (10.8)	196.8 (8.4)
mPW1	97.1 (0.8)	127.3 (4.5)	158.2 (6.5)	149.8 (5.4)	173.3 (9.7)	201.5 (3.7)
PBE1	95.4 (2.5)	126.0 (5.8)	156.9 (7.8)	148.2 (7.0)	171.8 (11.2)	200.4 (4.8)
O3LYP	87.2 (10.7)	115.5 (16.3)	145.2 (19.5)	137.8 (17.4)	160.2 (22.8)	184.9 (20.3)
TPSSh	80.7 (17.2)	99.2 (32.6)	134.1 (30.6)	129.1 (26.1)	150.3 (32.7)	174.8 (30.4)
CCSD(T)[b]	**97.9**	**131.8**	**164.7**	**155.2**	**183.0**	**205.2**

[a] $EA(DFT) = \Delta E_{elec}(DFT) + \Delta E_{ZPE;}$ [b] $EA(CCSD(T)) = \Delta E_{CBS} + \Delta E_{ZPE} + \Delta E_{CV}$

Table A3.24. MF_5 fluoride affinities[a] at 0 K (kcal/mol) calculated with various exchange-correlation functionals and the aD-PP basis sets and deviations (kcal/mol) from the CCSD(T) calculated electron affinities. Values in parentheses are the differences from the CCSD(T) values.

Method	MoF_5 $C_{2v}\rightarrow D_{3d}$	TcF_5 $D_{3h}\rightarrow D4_h$	RuF_5 $C_{4v}\rightarrow O_h$	RhF_5 $C_{4v}\rightarrow D_{3d}$	PdF_5 $C_{4v}\rightarrow D_{4h}$	AgF_5 $C_{4v}\rightarrow O_h$
BLYP	94.27 (11.23)	95.05 (8.96)	108.44 (15.39)	112.18 (9.15)	107.83 (40.65)	115.33 (10.66)
BP86	95.65 (9.85)	97.00 (7.01)	110.79 (13.04)	122.9(-1.57)	110.02 (38.46)	117.88 (8.11)
PW91	101.45 (4.05)	102.56 (1.45)	116.54 (7.29)	120.70 (0.63)	115.64 (32.84)	123.58 (2.41)
PBE	96.78 (8.72)	97.90 (6.11)	111.93 (11.90)	115.67 (5.66)	111.08 (37.40)	118.95 (7.04)
TPSS	98.59 (6.91)	99.84 (4.17)	113.84 (9.99)	119.64 (1.69)	112.36 (36.12)	120.79 (5.20)
B3LYP	99.55 (5.95)	98.73 (5.28)	115.03 (8.80)	120.08 (1.25)	113.75 (34.73)	122.94 (3.05)
mPW1	101.47 (4.03)	102.57 (1.44)	118.10 (5.73)	123.80 (-2.47)	116.18 (32.30)	125.72 (0.27)
PBE1	101.66 (3.84)	102.94 (1.07)	118.61 (5.22)	124.06 (-2.73)	116.74 (31.74)	126.28 (-0.29)
O3LYP	91.15 (14.35)	91.66 (12.35)	107.56 (16.27)	111.60 (9.73)	106.59 (41.89)	115.71 (10.28)
TPSSh	106.08 (-0.58)	107.36 (-3.35)	121.35 (2.48)	127.17 (-5.84)	119.85 (28.63)	128.41 (-2.42)
CCSD(T)[b]	**105.50**	**104.01**	**123.83**	**121.33**	**148.48**	**125.99**

[a] $FA(DFT) = \Delta E_{elec}(DFT) + \Delta E_{ZPE}$. [b] $FA(CCSD(T)) = \Delta E_{CBS} + \Delta E_{ZPE} + \Delta E_{CV}$

Table A3.25. MF_6 fluoride affinities[a] (kcal/mol) calculated with various local, gradient corrected and hybrid exchange-correlation functionals and the aD-PP basis set and and deviations (kcal/mol) from the CCSD(T) calculated fluoride affinities. Values in parentheses are the differences from the CCSD(T) values.

Method	MoF_6 $O_h \rightarrow C_{2v}$	TcF_6 $D_{3d} \rightarrow C_{2v}$	RuF_6 $D_{3d} \rightarrow C_s$	RhF_6 $O_h \rightarrow C_{2v}$	PdF_6 $D_{4h} \rightarrow C_s$	PdF_6 $D_{4h} \rightarrow D_{5h}$	AgF_6 $D_{4h} \rightarrow C_s$
BLYP	64.64 (9.61)	65.97 (10.90)	60.40 (27.69)	42.34(66.72)		57.26(30.85)	99.75(28.09)
BP86	66.59(7.66)	68.04 (8.83)	57.80 (30.29)	41.07(67.99)		58.12(29.95)	100.54(27.3)
PW91	73.38 (0.87)	74.41 (2.46)	63.87 (24.22)	47.20(61.86)		64.47(23.64)	106.23(21.61)
PBE	68.58(5.67)	69.80 (7.07)	59.68 (28.41)	42.66(66.40)			101.49(26.35)
TPSS	71.77 (2.48)	72.64 (4.23)	64.09 (24.00)	46.42(62.64)		62.50(25.61)	105.19(22.65)
B3LYP	70.60 (3.65)	72.17 (4.70)	80.41 (7.68)	54.73(54.33)	98.25(13.58)	68.54(19.57)	113.42(14.42)
mPW1	73.38(0.87)	75.10 (1.77)	85.45 (2.64)	56.88(52.18)	102.57(9.26)	71.44(16.67)	129.32(-1.48)
PBE1	74.27(0.02)	75.90 (0.97)	85.31 (2.78)	57.15(51.91)	102.43(9.0)	72.12(15.99)	128.78(-0.94)
O3LYP	63.47 (10.78)	64.97 (11.90)	70.10 (17.99)	42.90(66.10)	87.88(23.95)	57.99(30.12)	102.80(25.04)
TPSSh	79.42 (-5.17)	72.50 (4.37)	71.85 (16.24)	54.08(54.98)	91.78(20.05)	70.19(17.92)	112.99(14.85)
CCSD(T)[b]	**74.25**	**76.87**	**88.09[c]**	**109.1[c]**	**111.83[c]**	**88.11**	**127.84[c]**

[a] $FA(DFT) = \Delta E_{elec}(DFT) + \Delta E_{ZPE}$. [b] $FA(CCSD(T)) = \Delta E_{CBS} + \Delta E_{ZPE} + \Delta E_{CV}$. [c] $FA(CCSD(T)) = \Delta E_{CCSD(T)/AT\text{-}PP} + \Delta E_{ZPE}$.

Table A3.26. First adiabatic M –F bond dissociation energies[a] in kcal/mol calculated with various exchange-correlation functionals and the aD-PP basis sets and deviations (kcal/mol) from the CCSD(T) calculated electron affinities. Values in parentheses are the differences from the CCSD(T) values.

Method	MoF_5	TcF_5	RuF_5	RhF_5	PdF_5	AgF_5
BLYP	99.89 (-13.76)	73.13 (-21.01)	60.08 (-22.01)	68.06 (-23.57)	42.97(1.75)	27.78(-27.98)
BP86	99.89 (-13.76)	77.29 (-25.17)	64.30 (-26.23)	72.74 (-28.25)	45.97(-1.25)	29.42(-29.62)
PW91	99.87 (-13.74)	78.82 (-26.70)	65.81 (-27.74)	74.34 (-29.85)	47.73(-3.01)	31.22(-31.42)
PBE	99.80 (-13.67)	77.85 (-25.73)	64.91 (-26.84)	73.30 (-28.81)	47.07(-2.35)	30.61(-30.81)
TPSS	99.90 (-13.77)	72.69 (-20.57)	59.56 (-21.49)	70.32 (-25.83)	41.83(2.89)	25.72(-25.92)
B3LYP	99.87 (-13.74)	55.23 (-3.11)	40.29 (-2.22)	52.92 (-8.43)	23.67(21.05)	8.26(-8.46)
mPW1	99.85 (-13.72)	51.64 (0.48)	36.28 (1.79)	50.39 (-5.90)	19.30(25.42)	0.61(-0.81)
PBE1	99.78 (-13.65)	52.83 (-0.71)	37.66 (0.41)	51.78 (-7.29)	20.82(23.90)	1.77(-1.97)
O3LYP	99.84 (-13.71)	56.88 (-4.76)	43.06 (-4.99)	54.52 (-10.03)	27.11(17.60)	11.54(-11.74)
TPSSh	99.90 (-13.77)	84.74 (-32.62)	63.89 (-25.82)	74.65 (-30.16)	46.19(-1.47)	30.18(-30.38)
CCSD(T)[b]	**86.13**	**52.12**	**38.07**	**44.49**	**44.72**	**-0.2**

[a] $E(DFT) = \Delta E_{elec}(DFT) + \Delta E_{ZPE}$. [b] $E(CCSD(T)) = \Delta E_{CBS} + \Delta E_{ZPE} + \Delta E_{CV}$.

Table A3.27. Total MF_6 electronic energies at the DFT level with various exchange-correlation functionals and the aD-PP basis set, zero point energies (ZPE), CCSD(T) energies with the aug-cc-pVnZ/aug-cc-pVnZ-PP basis sets (n = D, T, Q) and at the CBS level, core and valence energies at the CCSD(T)/aug-cc-pWCVTZ-PP level, scalar relativistic energies at the CISD/aT-PP and CCSD(T)-DK/aug-cc-pVTZ-DK energies in atomic units.

Method	**MoF_6**	**TcF_6**	**RuF_6**	**RhF_6**	**PdF_6**	**AgF_6**
State/symm	$^1A_{1g}/O_h$	$^2A_{1g}/D_{3d}$	$^3A_{1g}/D_{3d}$	$^4A_{1g}/O_h$	$^3A_{1g}/D_{4h}$	$^2B_{2g}/D_{4h}$
CCSD(T)/aD-PP	-665.683277	-678.067733	-691.972316	-707.477673	-724.591087	-743.920610
CCSD(T)/aT-PP	-666.208975	-678.605390	-692.5193788	-708.028799	-725.150437	-744.485014
CCSD(T)/aQ-PP	-666.380064	-678.778774	-692.6957072	-708.209681	-725.336511	-744.675461
CCSD(T)/CBS	-666.479391	-678.879413	-692.7980544	-708.314712	-725.444588	-744.786468
Core	-666.959608	-679.371445	-693.296289	-708.811040	-725.930722	-745.253241
Valence	-666.255519	-678.653602	-692.569682	-708.081810	-725.206625	-744.543510
SR	-0.521613	-0.522511	-0.523647676	-0.525120	-0.527089	-0.529675
ZPE	0.014083[a]	0.012668[b]	0.013524[b]	0.014311[b]	0.0135[b]	0.012288[c]
CCSD(T)/aT-DK	-4645.098972	-4881.776779	-5126.592892	-5379.628912	-5640.986439	-5910.837308
BLYP	-667.3128822	-679.752844	-693.697936	-709.227618	-726.368473	-745.69
BP86	-667.4563294	-679.903963	-693.855345	-709.390009	-726.533996	-745.852696
PW91	-667.2828376	-679.729876	-693.680550	-709.215069	-726.357806	-745.675519
PBE	-666.8441853	-679.286227	-693.231793	-708.760914	-725.897696	-745.209067
TPSS	-667.4092275	-679.843805	-693.782001	-709.302942	-726.432329	-745.735752

B3LYP	-667.3477157	-679.778508	-693.717191	-709.246571	-726.384769	-745.711012
mPW1	-667.1964319	-679.626634	-693.563878	-709.092094	-726.225683	-745.544938
PBE1	-666.7424857	-679.167622	-693.100028	-708.623202	-725.750610	-745.062627
O3LYP	-667.2182523	-679.666062	-693.623284	-709.171796	-726.327199	-745.667321
TPSSh	-667.4086642	-679.855304	-693.781115	-709.301906	-726.431302	-745.734798

[a]B3LYP/aD-PP**.** [b] B3LYP/aT-PP.[c]BP86/aD-PP.

Table A3.28. Total MF_6^- electronic energies at the DFT level with various exchange-correlation functionals and the aD-PP basis set, zero point energies at the B3LYP/aT-PP and BP86/aD-PP levels, CCSD(T) energies with the aug-cc-pVnZ/aug-cc-pVnZ-PP basis sets (n = D, T, Q) and at the CBS level, core and valence energies at the CCSD(T)/aug-cc-pWCVTZ-PP level, scalar relativistic energies at the CISD/aT-PP and CCSD(T)-DK/aug-cc-pVTZ-DK energies in atomic units.

Method	**MoF_6^-**	**TcF_6^-**	**RuF_6^-**	**RhF_6^-**	**PdF_6^-**	**AuF_6^-**
State/symm	$^2A_{1g}/D_{3d}$	$^3A_{1g}/D_{4h}$	$^4A_{1g}/O_h$	$^3A_{1g}/D_{3d}$	$^2B_{2g}/D_{4h}$	$^1A_{1g}/O_h$
CCSD(T)/aD-PP	-665.840123	-678.281424	-692.238805	-707.721971	-724.877846	-744.238591
CCSD(T)/aT-PP	-666.360933	-678.814238	-692.781643	-708.272345	-725.438427	-744.807879
CCSD(T)/aQ-PP	-666.532871	-678.988590	-692.959206	-708.4555961	-725.627337	-745.001214
CCSD(T)/CBS	-666.632721	-679.089823	-693.062303	-708.5620344	-725.737089	-745.113556
Core	-667.111368	-679.579062	-693.556235	-709.0533355	-726.218007	-745.575825
Valence	-666.406971	-678.862074	-692.831672	-708.3258578	-725.495097	-744.866394
SR	-0.521359	-0.522227	-0.523329	-0.524762265	-0.526592	-0.529207
CCSD(T)/aT-DK	-4645.249956	-4881.991929	-5126.851314	-5379.872976	-5641.2742	-5911.159826
ZPE	0.011309[a]	0.014629[b]	0.013334[c]	0.011986[a]	0.013162[c]	0.012832[c]
BLYP	-667.442726	-679.923449	-693.910681	-709.433606	-726.607527	-745.962554
BP86	-667.585624	-680.074357	-694.068423	-709.596952	-726.775060	-746.132662
PW91	-667.412175	-679.900521	-693.894204	-709.421749	-726.598834	-745.955495
PBE	-666.970106	-679.453548	-693.442099	-708.963810	-726.135082	-745.485219
TPSS	-667.537666	-680.014009	-693.995447	-709.508490	-726.671666	-746.014205

B3LYP	-667.503858	-679.978708	-693.967167	-709.485706	-726.659208	-746.024651
mPW1	-667.351198	-679.829507	-693.815987	-709.330786	-726.501780	-745.866021
PBE1	-666.894508	-679.368438	-693.350005	-708.859350	-726.024434	-745.382014
O3LYP	-667.357243	-679.850113	-693.854703	-709.391386	-726.582458	-745.961963
TPSSh	-667.537226	-680.013430	-693.994774	-709.507695	-726.670792	-746.013431

[a]BP86/aD-PP. [b]B3LYP/aD-PP. [c]B3LYP/aT-PP.

Table A3.29. MF_7^- classical structures total electronic energies at the DFT level with various exchange-correlation functionals and aD-PP basis set, zero point energies at B3LYP/aD-PP and aT-PP levels and CCSD(T) energies at aug-cc-pVnZ/aug-cc-pVnZ-PP basis sets (n=2,3,4) and at the CBS level, core and valence energies at the CCSD(T)/aug-cc-pWCVTZ-PP level, scalar relativistic energies at the CISD/aT-PP and CCSD(T)-DK/aug-cc-pVTZ-DK energies in atomic units.

Method	**MoF_7^-**	**TcF_7^-**	**RuF_7^-**	**RhF_7^-**	**PdF_7^-**	**AgF_7^-**
State/symm	$^1A_1/C_{2v}$	$^2A_2/C_{2v}$	$^3A_1'/D_{5h}$	$^2A_1/C_{2v}$	$^1A_1'/D_{5h}$	$^2B_2/C_{2v}$
CCSD(T)/aD-PP	-765.470009	-777.860385	-791.776766	-807.360035	-824.401231	-843.747738
CCSD(T)/aT-PP	-766.080003	-778.479311	-792.404502	-807.951785	-825.042762	-844.39307
CCSD(T)/aQ-PP	-766.277768	-778.679272	-792.608063	-808.153865	-825.256523	-844.610512
CCSD(T)/CBS	-766.392571	-778.795343	-792.726232	-808.271300	-825.380685	-844.73684
Core	-766.891300	-779.306653	-793.242941		-825.883511	-845.220993
Valence	-766.132056	-778.532692	-792.460252	-808.002846	-825.105449	-844.457682
SR	-0.60789155	-0.608845	-0.610012	-0.61183208	-0.613479	-0.61617008
CCSD(T)/aT-DK	-4745.056542	-4981.737714	-5226.555274	-6010.785495	-5740.965743	-6010.785495
ZPE	0.016333[a]	0.015132[b]	0.016146[a]	0.013963[a]	0.015008[a]	0.013080[a]
BLYP	-767.281353	-779.723430	-793.686729	-809.160548	-826.32514	
BP86	-767.432653	-779.882588	-793.852025	-809.325663	-826.496778	
PW91	-767.237077	-779.685754	-793.654612	-809.127581	-826.2978	
PBEPBE	-766.728092	-779.172078	-793.135716	-808.603500	-826.767515	
TPSS	-767.394319	-779.830280	-793.786918	-809.247630	-826.402598	

B3LYP	-767.330605	-779.763895	-793.725297	-809.204166	-826.364313	
mPW1	-767.151764	-779.584713	-793.545481	-809.021128	-826.177873	
PBE1	-766.628196	-779.055923	-793.011957	-808.481627	-825.632834	
O3LYP	-767.156689	-779.606892	-793.584874	-809.077456	-826.256871	
TPSSh	-767.393852	-779.829466	-793.786358	-809.246715	-826.401728	

[a] B3LYP/aT-PP(RhF_7^- and RhF_7^- have 1 imaginary frequency)

[b] B3LYP/aD-PP

Table A3.30. MF_7^- nonclassical structures total electronic energies at the CCSD(T) level with the aug-cc-pVnZ/aug-cc-pVnZ-PP basis sets (n = D, T) and zero point energies at B3LYP/aD-PP level in atomic units.

Method	**MoF_7^-**	**TcF_7^-**	**RuF_7^-**	**RhF_7^-**	**PdF_7^-**	**AgF_7^-**
State/symm	$^3A'/C_s$	$^4A''/C_s$	$^5A''/C_s$	$^4A'/C_s$	$^3A'/C_s$	$^2A'/C_s$
CCSD(T)/aD-PP	-765.391837	-777.834780	-791.791046	-807.271874	-824.431910	-843.791272
CCSD(T)/aT-PP	-765.989543	-778.443822	-792.409695	-807.898284	-825.068308	-844.437162
ZPE	0.013946	0.013764	0.013984	0.013887	0.013970	0.013320

Table A3.31. MF_7^- (M=Ru, Pd and Ag) nonclassical structures total electronic energies at the DFT level with various exchange-correlation functionals and aD-PP basis set in atomic units.

Method	**RuF_7^-**	**PdF_7^{-a}**	**AgF_7^-**
State/symm	$^5A'/C_s$	$^3A'/C_s$	$^2A'/C_s$
BLYP	-793.65965		-845.711780
BP86	-793.81765		-845.883124
PW91	-793.61963		-845.682107
PBEPBE	-793.10151		-845.145413
TPSS	-793.75485		-845.774109
B3LYP	-793.71571	-826.411639	-845.773108
mPW1	-793.53844	-826.227462	-845.589417
PBE1	-793.00333	-825.681128	-845.035206
O3LYP	-793.57229	-826.304474	-845.679349
TPSSh	-793.75424	-826.436114	-845.773492

[a] The wave function did not converge for the GGA functionals.

Table A3.32. MF_6 XYZ coordinates at B3LYP/aT level

MoF_6

42	0.000000	0.000000	0.000000
9	0.000000	0.000000	1.832300
9	0.000000	1.832300	0.000000
9	0.000000	-1.832300	0.000000
9	-1.832300	0.000000	0.000000
9	0.000000	0.000000	-1.832300
9	1.832300	0.000000	0.000000

TcF_6, D_{4h}

9	0.000000	1.837408	0.000000
9	0.000000	0.000000	1.803260
9	0.000000	0.000000	-1.803260
9	1.837408	0.000000	0.000000
9	0.000000	-1.837408	0.000000
9	-1.837408	0.000000	0.000000
43	0.000000	0.000000	0.000000

TcF_6, D_{3d}

9	0.000000	1.507752	1.029683
9	-1.305751	0.753876	-1.029683
9	1.305751	-0.753876	1.029683
9	-1.305751	-0.753876	1.029683
9	0.000000	-1.507752	-1.029683
9	1.305751	0.753876	-1.029683
43	0.000000	0.000000	0.000000

RuF_6

9	0.000000	1.815195	0.000000
9	-1.815195	0.000000	0.000000
9	1.815195	0.000000	0.000000
9	0.000000	-1.815195	0.000000
9	0.000000	0.000000	1.844865
9	0.000000	0.000000	-1.844865
44	0.000000	0.000000	0.000000

RuF_6, D_{3d}

9	0.000000	1.478114	1.069902
9	-1.280085	0.739057	-1.069902
9	0.000000	-1.478114	-1.069902
9	1.280085	-0.739057	1.069902
9	1.280085	0.739057	-1.069902
9	-1.280085	-0.739057	1.069902

44	0	0.000000	0.000000	0.000000

RhF_6

9	0.000000	0.000000	1.828742
9	0.000000	1.828742	0.000000
9	0.000000	0.000000	-1.828742
9	0.000000	-1.828742	0.000000
9	1.828742	0.000000	0.000000
9	-1.828742	0.000000	0.000000
45	0.000000	0.000000	0.000000

PdF_6

9	0.000000	0.000000	1.840471
9	0.000000	1.853448	0.000000
9	0.000000	0.000000	-1.840471
9	0.000000	-1.853448	0.000000
9	-1.853448	0.000000	0.000000
9	1.853448	0.000000	0.000000
46	0.000000	0.000000	0.000000

AgF_6, D_{4h}

9	0.000000	1.890038	0.000000
9	0.000000	0.000000	1.886903
9	0.000000	0.000000	-1.886903
9	0.000000	-1.890038	0.000000
9	-1.890038	0.000000	0.000000
9	1.890038	0.000000	0.000000
47	0.000000	0.000000	0.000000

AgF_6, D_{3d}

9	1.873169	0.001134	0.000000
9	0.000000	1.327166	1.323095
9	-1.873169	-0.001134	0.000000
9	0.000000	-1.327166	-1.323095
9	0.000000	1.327166	-1.323095
9	0.000000	-1.327166	1.323095
47	0.000000	0.000000	0.000000

Table A3.33. MF_6^- XYZ coordinates at B3LYP/aT level

MoF_6^-, D_{4h}

42	0.000000	0.000000	0.000000
9	0.000000	0.000000	1.863928
9	0.000000	1.914120	0.000000
9	1.914120	0.000000	0.000000
9	-1.914120	0.000000	0.000000
9	0.000000	-1.914120	0.000000
9	0.000000	0.000000	-1.863928

MoF_6^-, D_{3d}

42	0.000000	0.000000	0.000000
9	0.000000	1.575025	1.057072
9	1.364012	-0.787513	1.057072
9	-1.364012	-0.787513	1.057072
9	-1.364012	0.787513	-1.057072
9	0.000000	-1.575025	-1.057072
9	1.364012	0.787513	-1.057072

TcF_6^-

43	0.000000	0.000000	0.000000
9	0.000000	0.000000	1.916105
9	0.000000	1.868535	0.000000
9	1.868535	0.000000	0.000000
9	-1.868535	0.000000	0.000000
9	0.000000	-1.868535	0.000000
9	0.000000	0.000000	-1.916105

RuF_6^-

44	0.000000	0.000000	0.000000
9	0.000000	0.000000	1.876008
9	0.000000	1.876008	0.000000
9	0.000000	-1.876008	0.000000
9	-1.876008	0.000000	0.000000
9	0.000000	0.000000	-1.876008
9	1.876008	0.000000	0.000000

RhF_6^-

45	0.000000	0.000000	0.000000
9	0.000000	0.000000	1.848667
9	0.000000	1.888054	0.000000
9	1.888054	0.000000	0.000000
9	-1.888054	0.000000	0.000000
9	0.000000	-1.888054	0.000000

9	0.000000	0.000000	-1.848667

PdF_6^-

46	0.000000	0.000000	0.000000
9	0.000000	0.000000	1.913839
9	0.000000	1.868474	0.000000
9	1.868474	0.000000	0.000000
9	-1.868474	0.000000	0.000000
9	0.000000	-1.868474	0.000000
9	0.000000	0.000000	-1.913839

AgF_6^-

47	0.000000	0.000000	0.000000
9	0.000000	0.000000	1.899269
9	0.000000	1.899269	0.000000
9	0.000000	-1.899269	0.000000
9	-1.899269	0.000000	0.000000
9	0.000000	0.000000	-1.899269
9	1.899269	0.000000	0.000000

Ta**ble A3.34.** MF_7^- XYZ coordinates at B3LYP/aT level. (PBP=pentagonal bipyramid, MCTP=mono-capped trigonal prism, MCO=mono-capped octahedron)

MoF_7^-, PBP

9	0.000000	0.000000	1.860219
9	0.000000	1.910500	0.000000
9	1.816993	0.590377	0.000000
9	1.122963	-1.545627	0.000000
9	-1.122963	-1.545627	0.000000
9	0.000000	0.000000	-1.860219
9	-1.816993	0.590377	0.000000
42	0.000000	0.000000	0.000000

MoF_7^-, MCTP

9	1.388069	1.223734	-0.342906
9	0.000000	0.000000	-1.875639
9	1.388069	-1.223734	-0.342906
9	-1.388069	-1.223734	-0.342906
9	-1.388069	1.223734	-0.342906
9	0.000000	1.144217	1.546286
9	0.000000	-1.144217	1.546286
42	0.000000	0.000000	0.033148

MoF_7^-, MCO

9	0.000000	0.000000	1.935254
9	0.000000	1.826799	0.510788
9	1.582055	-0.913400	0.510788
9	-1.582055	-0.913400	0.510788
9	1.239394	0.715565	-1.209768
9	0.000000	-1.431129	-1.209768
9	-1.239394	0.715565	-1.209768
42	0.000000	0.000000	0.034647

TcF_7^- C_{2v}

43	0.000000	0.000000	0.000148
9	-1.863454	0.000000	-0.001652
9	0.000000	1.827519	0.595969
9	0.000000	1.111299	-1.532470
9	0.000000	-1.111299	-1.532470
9	0.000000	-1.827519	0.595969
9	0.000000	0.000000	1.875596
9	1.863454	0.000000	-0.001652

RuF_7^- PBP

9	0.000000	0.000000	1.868695
9	0.000000	1.898863	0.000000
9	1.805926	0.586781	0.000000
9	1.116124	-1.536213	0.000000
9	-1.116124	-1.536213	0.000000
9	0.000000	0.000000	-1.868695
9	-1.805926	0.586781	0.000000
44	0.000000	0.000000	0.000000

RuF_7^- ^{5}A"/C_s

9	-0.260252	1.187191	1.328968
9	-2.149020	-0.126520	0.000000
9	-0.260252	-1.466198	1.324798
9	1.650308	-0.171980	0.000000
9	2.877775	1.511135	0.000000
9	-0.260252	-1.466198	-1.324798
9	-0.260252	1.187191	-1.328968
44	-0.273693	-0.133899	0.000000

RhF_7^- MCTP

9	1.383598	1.240402	-0.318544
9	0.000000	0.000000	-1.869454
9	1.383598	-1.240402	-0.318544
9	-1.383598	-1.240402	-0.318544
9	-1.383598	1.240402	-0.318544
9	0.000000	1.118224	1.548232
9	0.000000	-1.118224	1.548232
44	0.000000	0.000000	0.009647

PdF_7^- $^1A_1$'/D_{5h}

9	0.000000	0.000000	1.910598
9	0.000000	1.915831	0.000000
9	1.822063	0.592024	0.000000
9	1.126097	-1.549939	0.000000
9	-1.126097	-1.549939	0.000000
9	0.000000	0.000000	-1.910598
9	-1.822063	0.592024	0.000000
46	0.000000	0.000000	0.000000

PdF_7^- ^{3}A'/Cs

9	-0.252119	1.175034	1.323517

9	-2.147874	-0.128114	0.000000
9	-0.252119	-1.458576	1.314555
9	1.687520	-0.185095	0.000000
9	2.744134	1.563073	0.000000
9	-0.252119	-1.458576	-1.314555
9	-0.252119	1.175034	-1.323517
46	-0.249516	-0.133587	0.000000

AgF_7^- MCTP

9	-1.371901	1.313885	0.239893
9	0.000000	0.000000	2.042311
9	-1.371901	-1.313885	0.239893
9	1.371901	-1.313885	0.239893
9	1.371901	1.313885	0.239893
9	0.000000	0.962541	-1.911923
9	0.000000	-0.962541	-1.911923
47	0.000000	0.000000	0.157397

AgF_7^- $^2A'/C_s$

9	-0.256818	1.204420	1.342096
9	-2.143084	-0.125912	0.000000
9	-0.256818	-1.473075	1.340522
9	1.665136	-0.175668	0.000000
9	2.833874	1.523275	0.000000
9	-0.256818	-1.473075	-1.340522
9	-0.256818	1.204420	-1.342096
47	-0.254423	-0.131053	0.000000

Ta**ble A3.35.** MF_5 XYZ coordinates at the B3LYP/aD level.

MoF_5

42	0.000000	0.000000	0.029281
9	0.000000	0.000000	1.843819
9	0.000000	1.883710	0.020234
9	-1.508766	0.000000	-1.010465
9	0.000000	-1.883710	0.020234
9	1.508766	0.000000	-1.010465

TcF_5

9	0.000000	0.000000	1.885914
9	0.000000	1.807303	0.000000
9	0.000000	0.000000	-1.885914
9	1.565170	-0.903651	0.000000
9	-1.565170	-0.903651	0.000000
43	0.000000	0.000000	0.000000

RuF_5

9	0.000000	1.831426	0.337890
9	-1.831426	0.000000	0.337890
9	1.831426	0.000000	0.337890
9	0.000000	0.000000	-1.733095
9	0.000000	-1.831426	0.337890
44	0.000000	0.000000	0.078041

RhF_5

9	0.000000	1.869060	0.164543
9	0.000000	0.000000	-1.711680
9	0.000000	-1.869060	0.164543
9	1.801243	0.000000	0.420061
9	-1.801243	0.000000	0.420061
45	0.000000	0.000000	0.108494

PdF_5

9	0.000000	1.856386	0.238659
9	-1.856386	0.000000	0.238659
9	1.856386	0.000000	0.238659
9	0.000000	0.000000	-1.700193
9	0.000000	-1.856386	0.238659
46	0.000000	0.000000	0.145870

AgF_5

9	0.000000	1.879928	0.263681
9	-1.879928	0.000000	0.263681
9	1.879928	0.000000	0.263681

9	0.000000	0.000000	-1.731639
9	0.000000	-1.879928	0.263681
47	0.000000	0.000000	0.129622

4. Prediction of Reliable Metal-PH_3 Bond Energies for Ni, Pd and Pt in the 0 and +2 Oxidation States

Abstract

Phosphine-based catalysts play an important role in many metal-catalyzed carbon-carbon bond formation reactions yet reliable values of their bond energies are not available. We have been studying homogeneous catalysts consisting of a phosphine bonded to a Pt, Pd or Ni. High level electronic structure calculations at the CCSD(T)/complete basis set level were used to predict the M-PH_3 bond energy (BE) for the 0 and + 2 oxidation states for M = Ni, Pd, and Pt. A wide range of exchange-correlation functionals were also evaluated to assess the performance of density theory for these important bond energies. These bond energies can then be used, for example, in the design of new catalyst systems.

Introduction

Cross-coupling reactions are powerful synthetic methods to form new C–C or C–heteroatom bonds. Although other metals such as nickel, copper, and iron have been successfully used in cross-coupling reactions, palladium[1] remains the most widely used metal in these reactions due to the generally high activity of palladium complexes for a wide range of substrates. It is generally accepted that the main steps[2] involved in the homogeneous palladium catalyzed cross-coupling reactions are: (1) dissociation of supporting ligands to provide the coordinatively unsaturated active species, (2) oxidative addition of the electrophilic substrate, (3) ligand substitution by the nucleophilic reagent and (4) reductive elimination to give the desired product and regenerate the active species (Figure 4.1). The active $PdL_n(0)$ species can be generated *in situ* by the reduction of Pd(II) sources in the presence of the supporting ligands. Supporting ligands play a critical role in catalyst activity as they solubilize the metal center, stabilize the Pd(0)/Pd(II) active species, and can promote the oxidative addition step.

Phosphine ligands are a popular choice for use in tailoring the catalytic reactivity of the transition metal complexes. Triarylphosphines were the first ligands used in palladium-catalyzed cross-coupling reactions and are still commonly used. Over the past decade, sterically demanding, electron rich phosphines have been shown to provide highly active catalysts for a wide range of metal-catalyzed cross-coupling reactions, however.[3,4] These sterically demanding ligands form stable 14-electron $L_2Pd(0)$ species that serve as the catalyst resting state in cross-coupling reactions. Critical species in the catalytic cycle are believed to be monophosphine complexes.[5] Mechanistic studies have shown that ligand dissociation occurs during the oxidative addition step by both dissociative and associative mechanisms depending on the aryl halide substrate.[6,7,8,9] A computational study at the density functional theory (DFT)[10] level with the PBE[11] functional and a polarized double zeta basis set showed that oxidative addition to the

LPd(0) species occurred with a lower barrier than for the $L_2Pd(0)$ complex.[12] These authors also showed that the bond dissociation energy (BDE) of the ligand was a good predictor of the rate of oxidative addition of aryl chlorides. We had previously used DFT to model the gas-phase Pd-L BDEs for a series of sterically demanding phosphine ligands and showed that there is a correlation between the catalyst activity and BDE.[13,14] We have also shown that the Pd-P BDEs are strongly dependent on the choice of exchange-correlation functional.[15] Since the cleavage of the metal-phosphorus bond is a key step in the catalytic mechanism, it is important to be able to predict such BDEs.

A variety of computational methods have been used to predict the M-L bond energies of different complexes L-MR_2 (M = transition metal, R = additional ligand): L = C_2H_2, M = Ni, and R = PR'_3 (R' = H, CH_3, F, CF_3, C_6H_5);[16] L = olefin, M = Pt, and R = PH_3;[17] L = O_2, C_2H_4 C_2H_2; M = Ni, Pd, Pt, and R = PH_3;[18,19] L = C_{60}, $C_{20}H_{10}$, and $C_{21}H_{12}$; M = Pd, Pt, and R = PH_3;[20] L = SiH_3X (X = H, CH_3, SiH_3), M = Pd, and R = PH_3;[21] L = organostannanes, M = Pd, and R = PH_3, PMe_3;[22] and L = alkyl, M = Ni, Pd, and R = olefins, CO, PH_3, H_2O, Cl.[23,24] The metal phosphine bond dissociation energies for M = Cr, Ni, Mo and Ru have been investigated at the density DFT level with various exchange-correlation functionals.[25]

Despite the importance of the M-PR_3 bond, there is not a consistent set of metal phosphine BDEs available which can be used for different Group 10 metals in the important catalytic oxidation states. Our goal is to provide reliable bond energies for the simplest ligand so that more approximate methods can be used, for example with isodesmic reaction schemes,[26] to predict bond energies for phosphines of practical interest. We describe the results of high level electronic structure calculations at the CCSD(T)[27,28,29,30] level with basis sets extrapolated to the complete basis set limit of the binding energy of the Group 10 transition metals Ni, Pd and Pt in

the 0 and +2 oxidation states to the simplest tertiary phosphorus ligand PH_3 in reactions (1) to (4).

$$MPH_3 \rightarrow M + PH_3 \quad (1)$$

$$M(PH_3)_2 \rightarrow MPH_3 + PH_3 \quad (2)$$

$$MPH_3Cl_2 \rightarrow MCl_2 + PH_3 \quad (3)$$

$$M(PH_3)_2Cl_2 \rightarrow MPH_3Cl + PH_3 \quad (4)$$

These bond energy calculations follow the procedures we have developed for the reliable prediction of a wide range of thermodynamic properties.[31] We also report on the ability of a wide range of DFT exchange-correlation functionals to predict these bond energies.

Computational Methods

Equilibrium geometries (Table 4.2) and vibrational frequencies (Table 4.3 for stretching frequencies) were calculated first at the DFT level with a range of local,[32,33] gradient-corrected[11,34,35,36,37,38,39,40,41,42,43,44] and hybrid exchange-correlation[11,45,46,47,48,49,50,51,52] functionals (See Table 4.1 for a list of functionals). The DFT calculations were performed with the augmented correlation consistent double-ζ (aug-cc-pVDZ) basis set for H[53], P[54] and Cl[54] and the aug-cc-pVDZ-PP basis sets with accompanying small-core relativistic pseudopotentials for the transition metal atoms;[55] we label the combined basis set as aN-PP with N = D, T, Q. The B3LYP geometries were used as a starting point for optimizations at the CCSD(T) level. For P and Cl we have used the aug-cc-pV(n+d)Z basis sets[56] in the CCSD(T) calculations with n = D and T for the geometry optimizations. The aug-cc-pV(T+d)Z geometries were used for single point aug-cc-pV(Q+d)Z calculations. The CCSD(T) energies were extrapolated to the complete basis set (CBS) limit by using a mixed Gaussian/exponential formula.[57] The bond energy is given as

$$BDE = E(MR_xL_n) – E(L) - E(MR_xL_{n-1}) \quad (5)$$

Several additional corrections have been used to adjust the CBS valence electronic energies: (1) a core-valence correlation correction (ΔE_{CV}) calculated at the CCSD(T) level with the aug-cc-pwCVTZ basis set[54] for P and Cl and the aug-cc-pwCVTZ-PP basis set[55,58,59] for the transition metal atoms (denoted as awCVTZ).; (2) scalar relativistic corrections on the F atoms and corrections for any errors in the metal pseudopotentials for the binding energies (BDEs). The latter is calculated by taking the difference between the BDE calculated at the Douglas-Kroll-Hess[60] level with the CCSD(T)-DK method and the aT-DK basis set[55,61,62] and the BDE calculated at the CCSD(T)/aT-PP level (Equation 6); and

$$\Delta BDE_{Rel} = BDE(CCSD(T)\text{-}DK/aT\text{-}DK) - BDE(CCSD(T)/aT\text{-}PP) \quad (6)$$

(3) the zero point energy calculated at the DFT level with aug-cc-pVDZ and aug-cc-pVDZ-PP basis sets. The bond dissociation energy is calculated as the sum of the different contributions (Equation 7).

$$BDE_{0K} = BDE_{CBS} + \Delta BDE_{ZPE} + \Delta BDE_{CV} + \Delta BDE_{Rel} \quad (7)$$

The DFT calculations were done with the Gaussian program system[63] and the CCSD(T) calculations with the Molpro program system[64] on computers at The University of Alabama, the Alabama Supercomputing Center, and the Molecular Sciences Computing Facility in the William R. Wiley Environmental Molecular Sciences Laboratory at the Pacific Northwest National Laboratory.

Results and Discussion

Geometries and Vibrational Frequencies

Schematics of the ground state geometries of the 4 possible complexes are given in Figure 4.2.

MPH_3 All structures were optimized as singlet states of C_{3v} symmetry. At the B3LYP/aD-PP level, the triplet states of $NiPH_3$ and $PtPH_3$ are 1.8 and 42.8 kcal/mol respectively higher in energy than the singlet. The energy of the triplet state of $NiPH_3$ was evaluated at higher levels and, at the CCSD(T)/CBS level, it was found to be 17.2 kcal/mol higher in energy than the singlet state. The M-P bond distance increases from Ni to Pd and then decreases slightly for Pt. Our calculated CCSD(T) values for the M-P bond distances are: 1.998 Å for M = Ni (aD-PP), 2.144 Å Å for M = Pd (aT-PP level), and 2.089 Å for M=Pt (aT-PP level). At the CI level with a modest basis set, the Ni-P bond distance is predicted to be 2.196 Å and the Pd-P bond distance is predicted to be 2.355 Å.[24]

$M(PH_3)_2$ The ground state structure for all three metals studied, Ni, Pd and Pt was found to be a singlet state with a linear geometry and D_{3h} symmetry. Our calculated Ni-P bond distance is 2.090 Å (CCSD(T)/aT-PP). A comparable calculated bond distance of 2.084 Å for the C_{2v} bent structure of $Ni(PH_3)_2$ at the BP86/TZV(2df,2pd) level has been reported[16] and a longer value of 2.249 Å at the CI level was reported.[23] Calculations[18,19] at the BP86/TZV and B3LYP/LANL2DZ levels have predicted $Ni(PH_3)_2$ to be linear. For Pd-P, our calculated CCSD(T)/aT-PP bond distance is 2.250 Å. A linear structure for $Pd(PH_3)_2$ with a Pd-P bond distance of 2.408 Å was also predicted[21] at the MP4 level.

MCl_2 Geometries have been optimized for both singlet and triplet states. The linear $NiCl_2$ triplet is lower in energy by 31.5 kcal/mol than the singlet bent C_{2v} structure at the CCSD(T)/CBS level. For $PdCl_2$ and $PtCl_2$, the linear triplet structures are also more stable than the singlet structures by 6.1 and 10.3 kcal/mol, respectively.

MPH_3Cl_2 All structures were optimized in the singlet state. The $NiPH_3Cl_2$ triplet state is 22.4 kcal/mol higher in energy than the singlet at the CCSD(T)/CBS level. The $PtPH_3Cl_2$ triplet state

is 22.5 kcal/mol higher than the singlet at the B3LYP/aD-PP level and was not optimized further with CCSD(T). The M-P bond distance follows the same trend as for M-PH_3, increasing from Ni to Pd and then decreasing for Pt. The two M-Cl bond distances are slightly different from each other due to the C_s symmetry of the molecule and the average value increases from Ni to Pt.

$M(PH_3)_2Cl_2$ The ground states of the dichloro diphosphine metal complexes are also singlets. For M = Ni, the singlet-triplet splitting at the B3LYP/aD-PP level is predicted to be only 2.3 kcal/mol, so CCSD(T) single point calculations have been performed up to the aT-PP level to differentiate between the two possible states. At the CCSD(T)/aT-PP level, the triplet state is higher in energy by 14.1 kcal/mol than the singlet. For M = Pt, triplet was found to be 44.9 kcal/mol higher than the singlet at the B3LYP/aD-PP level and was not optimized further with CCSD(T). The M-P and M-Cl bond distances follow the same trend as in MPH_3Cl_2 compounds.

Vibrational Frequencies The M-P and M-Cl stretching frequencies (cm^{-1}) calculated at the B3LYP/aD-PP level are given in Table 4.3. All M-P frequencies are predicted to be in the range of 300-450 cm^{-1} except for $M(PH_3)_2Cl_2$ compounds where they range from 267 to 345 cm^{-1}. The stretching frequencies values correlate with the bond lengths and are at higher values for shorter bonds.

Bond Dissociation Energies

M-PH_3 bond dissociation energies (BDEs) for reactions (1) to (4) have been calculated at different levels of theory with all species in their ground states. The results are in Table 4.4. For all of the reactions, the zero point energy correction is less than 3 kcal/mol and the effect is to decrease the BDEs. The core-valence corrections can either increase or decrease the BDEs but the effect is also small, less than 2 kcal/mol, except for M = Pd in reaction (1) where the ΔE_{CV} is

2.6 kcal/mol. The relativistic corrections are less than 2 kcal/mol except for M = Ni in reaction (1) where ΔE_{Rel} is 4.1 kcal/mol, and can either increase or decrease the BDEs.

Care has to be taken in the prediction of the atomic energies. For Ni, we calculated the Ni-PH_3 BDE of reaction (1) at the CCSD(T)/CBS level relative to the $^1S_0$ excited state of the atom which has no spin orbit correction and corrected the calculated BDE with the experimental energy difference[65] of 42.11 kcal/mol with respect to the $^3F_4$ ground state. At the CCSD(T)/CBS level, this energy splitting is predicted to be 42.7 kcal/mol in excellent agreement with the experimental value. The DFT functionals predict the correct wavefunction for the s^2d^8 triplet state of the Ni atom but not for the d^{10} singlet state. To assess the performance of the DFT functionals we calculated the Ni-PH_3 BDE of reaction (1) relative to the $^3F_4$ ground state at the CCSD(T)/CBS level together with the zero point energy and core-valence corrections and substracted the experimental J-averaged atomic spin orbit correction of 2.78 kcal/mol. The resulting value was used to compare the Ni-PH_3 BDEs calculated at the DFT level with each of the functionals listed in Table 4.1. Blomberg et al.[24] predicted that the triplet state of Ni is more stable than the singlet by only 8 kcal/mol at the CI level and noted that the corresponding calculated nickel-ligand binding energies are too small due to the small basis sets used in calculations. For Pd, the d^{10} singlet state is the ground state and this state is predicted to be lower than the triplet state by 25 kcal/mol at the CCSD(T)/CBS level. In calculating the Pt-PH_3 BDE of reaction (1), we used the same approach as for Ni-PH_3, and calculated the Pt-PH_3 BDE in reaction (1) for the $^1S_0$ excited state which was corrected by an energy difference of 17.54 kcal/mol with respect to the $^3D_3$ ground state.

In reactions (2) and, the metal is in the 0 oxidation state. The energy to break the first M-PH_3 is largest for Pt and lowest for Pd. A different trend is predicted for the metal in the +2

oxidation state as shown in reaction (4) with the M-PH_3 BDEs increasing from M = Ni to M = Pt. Comparing the BDEs for reactions 2 and 4, we see that the higher oxidation state has the lower BDE with the two BDEs being comparable for Pd within 2 kcal/mol. For reaction (1), the second BDE for $M(PH_3)_2$, the M-PH_3 BDEs increase from M = Ni to M = Pt with that for Pt being almost 40 kcal/mol greater than that for Ni. The second BDE is greater than the first for Pt and Pd and the opposite holds for Ni all in the 0 oxidation state. In reaction (3) where the metal is in the +2 oxidation state, the second BDEs increase from ~16 kcal/mol for M = Ni to ~ 56 kcal/mol for M = Pd and Pt. In the +2 oxidation state, the same trend for the first and second BDEs is found as for the 0 oxidation state.

Blomberg and co-workers[23] investigated the nature of the Ni binding to the H_2O, CO and PH_3 ligands at the SCF, MCSCF and CI levels. They predicted for $NiPH_3$ and $Ni(PH_3)_2$ (both singlets) that the binding energies are 13.7 (singlet atom) and 41.0 kcal/mol. The former value is much lower than our value of 72 kcal/mol and the latter is comparable to our value of 40 kcal/mol. Subsequently, Blomberg et al.[24] studied the interaction of palladium with various ligands including PH_3 and predicted a bond energy of 16 kcal/mol for reaction (1), less than half the BDE predicted by us at a higher level.

A useful comparison is the basis set dependence of the BDEs at the CCSD(T) level. If a smaller basis set can be used for the calculations, this is a clear computational advantage due to the N7 (N = number of basis functions) scaling of CCSD(T). For $M(PH_3)_2Cl_2$ with the M in the formal +2 oxidation state, the M-P BDE is not strongly basis set dependent with the aug-c-pVDZ-PP results within better than 1.5 kcal/mol of the aug-c-pVQZ-PP results. The basis set effect is larger for $M(PH_3)_2$ with M in the 0 oxidation state with the aug-cc-pVDZ-PP results within better than 3 kcal/mol of the aug-c-pVQZ-PP results. This basis set dependence is

consistent with the fact that the M-P bond in these compounds is an electron pair donor/acceptor type bond.[66] The basis set effects are substantially larger for $M(PH_3)Cl_2$ and $M(PH_3)$ with differences up to ~ 8 kcal/mol between the aug-cc-pVDZ-PP and aug-cc-pVQZ basis sets. The vacant binding site leads to a larger basis set effect on the M-PH_3 bond energies.

Performance of Density Functional Theory The calculated bond energies for each of the four reactions for the selection of functionals in Table 4.1 are given in Supporting Information. The average deviations from the CCSD(T)/CBS values with the zero point and core=valence corrections are given in Table 4.5. As expected from our previous studies[67,68,69] on the performance of DFT exchange-correlation functionals for the prediction of the thermodynamic properties of transition metal complexes, the local functional SVWN5 displays large average deviations, and predicts BDEs up to17 kcal/mol too large. This is the typical overbinding exhibited by the local approximation. The GGA functionals perform better. The predicted energies can be either larger or smaller than the CCSD(T) values with average deviations ranging from 2 kcal/mol for the reaction (1) to 13 kcal/mol for reaction (4). The widely used PW91 and PBE GGA functional are within 2 to 3 kcal/mol of the CCSD(T) values for all four reactions. The widely used B3LYP hybrid functional, together with B1LYP, B98, and BMK functionals show the poorest agreement with the coupled cluster values, especially for reactions (1) and (3), where the average deviations are as much as 23 kcal/mol. Only a few of the hybrid functionals predict BDEs which fall within 2 to 3 kcal/mol of the CCSD(T) values: TPSSh for reaction (1); B3PB86, PBE1, and TPSSh for reaction (2); and B3PB86, PBE1, BMK, and TPSSh for reaction (4). Most of the GGA functional show poor agreement with the CCSD(T) values for reaction (1) due to the difficulty in predicting the correct states of the metal atoms.

Conclusions

High level coupled cluster CCSD(T) calculations, extrapolated to the complete basis set limit, were used to evaluate the Group 10 transition metal M-PH_3 bond energies for the 0 and +2 oxidation states. The additional energy corrections can either increase or decrease the M-PH_3 BDE by up to 4 kcal/mol so they cannot be neglected. The M-P bond distance increases from Ni to Pd and then decreases slightly for Pt and this trend is reflected in the values of the stretching frequencies. The higher oxidation state has the lower first BDE (reactions (2) and (4) with the two BDEs being comparable for Pd within 2 kcal/mol. The second BDE (reactions (1) and (3)) is greater than the first for Pt and Pd and the opposite holds for Ni in both oxidation states. A wide range of density functional theory exchange-correlation functionals were also evaluated to assess the performance of density functional theory.

Acknowledgment. This work was supported by the Chemical Sciences, Geosciences and Biosciences Division, Office of Basic Energy Sciences, U.S. Department of Energy (DOE) under grant no. DE-FG02-03ER15481 (catalysis center program). DAD also thanks the Robert Ramsay Chair Fund of The University of Alabama for support. Part of this work was performed at the W. R. Wiley Environmental Molecular Sciences Laboratory, a national scientific user facility sponsored by DOE's Office of Biological and Environmental Research and located at Pacific Northwest National Laboratory, operated for the DOE by Battelle.

Table 4.1. Benchmarked DFT Exchange-Correlation Functionals.

Functional	exchange	correlation	type	refs.
SVWN5	Slater	VWN5	LSDA	32, 33
BLYP	Becke 88	Lee-Yang-Parr	GGA	34,35
BP86	Becke 88	Perdew 86	GGA	34,36
BPW91	Becke 88	Perdew-Wang 91	GGA	34,37
BB95	Becke 88	Becke 95	GGA	34,38
PW91	Perdew-Wang 91	Perdew-Wang 91	GGA	39,37
mPWPW91	Adamo & Barone's modified PW91	Perdew-Wang 91	GGA	40,37
PBE	Perdew-Burke-Ernzerhof	Perdew-Burke-Ernzerhof	GGA	11
OLYP	Handy's OPTX	Lee-Yang-Parr	GGA	41,35
TPSS	Tao-Perdew-Staroverov-Scuseria	Tao-Perdew-Staroverov-Scuseria	GGA	42
VSXC	van Voorhis -Scuseria	van Voorhis -Scuseria	GGA	43
HCTH	Handy	Handy	GGA	44
B3LYP	Becke 93	Lee-Yang-Parr	HGGA	45,35
B3P86	Becke 93	Perdew 86	HGGA	45,36
B3PW91	Becke 93	Perdew-Wang 91	HGGA	45,37
B1B95	Becke 96	Becke 95	HGGA	46,38
B1LYP	Becke 96	Lee-Yang-Parr	HGGA	46,35
mPW1	Barone's modified PW91	Perdew-Wang 91	HGGA	47,39,37
B971	Handy-Tozer's modified B97	Handy-Tozer's modified B97	HGGA	48
B972	Wilson-Bradley-Tozer's modified B97	Wilson-Bradley-Tozer's modified B97	HGGA	49
B98	Becke 98	Becke 98	HGGA	50
PBE1	Perdew-Burke-Ernzerhof	Perdew-Burke-Ernzerhof	HGGA	11
O3LYP	Handy's OPTX	Lee-Yang-Parr	HGGA	41,35
BMK	Boese -Martin	Boese -Martin	HGGA	51
TPSSh	Tao-Perdew-Staroverov-Scuseria	Tao-Perdew-Staroverov-Scuseria	HGGA	52

Table 4.2. MPH_3, $M(PH_3)_2$, MPH_3Cl_2 and $M(PH_3)_2Cl_2$ Optimized M-P and M-Cl Bond Lengths (Å) at the B3LYP and CCSD(T) Levels.

M	reactant	M-P (Å)			M-Cl (Å)		
	State/Sym	B3LYP/ aD-PP	CCSD(T)/ aD-PP	CCSD(T)/ aT-PP	B3LYP/ aD-PP	CCSD(T)/ aD-PP	CCSD(T)/ aT-PP
			Reactant = MPH_3				
Ni	$^1A_1/C_{3v}$	2.025	1.998				
Pd	$^1A_1/C_{3v}$	2.202	2.175	2.144			
Pt	$^1A_1/C_{3v}$	2.131	2.102	2.089			
			Reactant =$M(PH_3)_2$				
Ni	$^1A_1'/D_{3h}$	2.124	2.109	2.090			
Pd	$^1A_1'/D_{3h}$	2.291	2.272	2.250			
Pt	$^1A_1'/D_{3h}$		2.244	2.222			
			Reactant =MPH_3Cl_2				
Ni	$^1A'/C_s$	2.129	2.154	2.062	2.113 2 .124	2.250 2.245	2.080 2.095
Pd	$^1A'/C_s$	2.196	2.162	2.132	2.284 2.297	2.281 2.266	2.249 2.266
Pt	$^1A'/C_s$	2.168	2.134	2.114	2.296 2.310	2.276; 2.290	2.259 2.276
			Reactant = $M(PH_3)_2Cl_2$				
Ni	$^1A_g/C_{2h}$	2.234	2.202	2.152	2.189	2.174	2.178
Pd	$^1A_g/C_{2h}$	2.327	2.301	2.280	2.335	2.309	2.912
Pt	$^1A_g/C_{2h}$	2.312	2.277	2.270	2.353	2.336	2.309

Table 4.3. M-P and M-Cl Stretching Frequencies (cm^{-1}) and IR intensities (km/mol) at the B3LYP/aD-PP Level.

M	reactant State/Sym	M-P stretching freq		M-Cl stretching freq	
		Reactant = MPH_3			
Ni	$^1A_1/C_{3v}$	437(29)			
Pd	$^1A_1/C_{3v}$	352(11)			
Pt	$^1A_1/C_{3v}$	446(13)			
		Reactant =$M(PH_3)_2$			
		Sym A_1'	**Asym A_2"**		
Ni	$^1A_1'/D_{3h}$	325(0)	377(135)		
Pd	$^1A_1'/D_{3h}$	295(0)	295(73)		
Pt	$^1A_1'/D_{3h}$	364(0)	313(59)		
		Reactant =MPH_3Cl_2			
				Sym	**Asym**
Ni	$^1A'/C_s$	394(3)		331(3)	449(98)
Pd	$^1A'/C_s$	385(13)		321(1)	369(78)
Pt	$^1A'/C_s$	436(24)		357(73)	344(9)
		Reactant =$M(PH_3)_2Cl_2$			
		Sym A_g	**Asym B_u**	**Sym A_g**	**Asym B_u**
Ni	$^1A_g/C_{2h}$	267(0)	334(3)	302(0)	400(49)
Pd	$^1A_g/C_{2h}$	290(0); 305(0)	283(0)	290(0); 305(0)	348(52)
Pt	$^1A_g/C_{2h}$	345(0)	282(3)	319(0)	333(51)

Table 4.4. Components for Calculated M-PH_3 Binding Energy for Reactions (1) to (4) (M = Ni, Pd, Pt)

M	reactant State/Sym	product State/Sym	ΔE_{CBS}	ΔE_{ZPE}	ΔE_{CV}	ΔE_{rel}	BDE
			Reactant = MPH_3				
Ni-P[a]	$^1A_1/C_{3v}$	1	71.81	-1.74	-0.87	-4.10	23.0
Pd-P	$^1A_1/C_{3v}$	1	42.16	-1.69	2.60	-1.23	41.8
Pt-P[a]	$^1A_1/C_{3v}$	1	82.38	-2.27	3.47	-2.12	63.9
			Reactant = $M(PH_3)_2$				
Ni-P	$^1A_1'/D_{3h}$	$^1A_1/C_{3v}$	39.51	-1.69	0.27	1.62	39.7
Pd-P	$^1A_1'/D_{3h}$	$^1A_1/C_{3v}$	33.67	-1.72	1.82	-0.18	33.6
Pt-P	$^1A_1'/D_{3h}$	$^1A_1/C_{3v}$	45.91	-1.90	1.39	0.05	45.5
			Reactant = MPH_3Cl_2				
Ni-P	$^1A'/C_s$	$^3\Sigma_g/D_{\infty h}$	19.52	-2.74	1.67	-1.94	16.5
Pd-P	$^1A'/C_s$	$^3\Sigma_g/D_{\infty h}$	62.15	-2.83	-0.46	-0.46	58.4
Pt-P	$^1A'/C_s$	$^3\Sigma_g/D_{\infty h}$	60.30	-2.83	-1.95	-1.30	54.2
			Reactant = $M(PH_3)_2Cl_2$				
Ni-P	$^1A_g/C_{2h}$	$^1A'/C_s$	26.70	-2.21	0.50	-0.53	24.5
Pd-P	$^1A_g/C_{2h}$	$^1A'/C_s$	32.66	-2.05	1.37	0.14	32.1
Pt-P	$^1A_g/C_{2h}$	$^1A'/C_s$	41.26	-2.24	1.14	0.17	40.3

[a] BDE calculated with respect to the $^1S_0$ excited states of Ni and Pt and corrected with the experimental energy difference of 42.11 and 17.54 kcal/mol respectively with respect to the $^3F_4$ ground state of Ni and to the $^3D_3$ ground state of Pt.

Table 4.5. Average Deviations of the Metal- Phosphine Bond Dissociation Energies from the CCSD(T) Calculated Values in kcal/mol.

Functional	**Rxn (1)**	**Rxn (2)**	**Rxn (3)**	**Rxn (4)**
SVWN5	-16.90	-11.03	-13.22	-9.00
BLYP	10.79	6.34	12.28	8.65
BP86	3.20	1.89	5.43	4.16
BPW91	4.78	3.31	6.88	5.51
BB95	2.60	3.93	5.83	5.76
PW91	1.45	0.32	3.21	1.88
mPWPW91	3.28	1.92	5.18	3.78
PBE	1.77	0.85	3.81	2.60
OLYP	10.93	10.78	12.24	13.04
TPSS	3.88	2.27	5.75	3.09
VSXC	5.80	3.05	7.28	-0.51
HCTH	-2.85	8.72	9.22	10.41
B3LYP	18.24	6.14	13.66	6.21
B3P86	11.82	2.10	7.19	1.97
B3PW91	14.13	3.94	9.79	3.86
B1B95	16.03	5.00	9.66	3.61
B1LYP	21.89	7.13	15.96	6.74
mPW1PW91	15.71	3.22	9.60	2.37
B971	16.83	4.29	10.83	3.63
B972	13.88	6.08	9.62	5.48
B98	19.70	4.94	11.55	4.23
PBE1PBE	14.44	2.37	8.51	1.44
O3LYP	15.75	9.84	13.14	10.69
BMK	23.40	7.51	15.96	2.40
TPSSh	2.85	1.98	6.42	2.72

Figure 4.1. General Catalytic Cycle for Palladium-Catalyzed Cross-Coupling Reactions

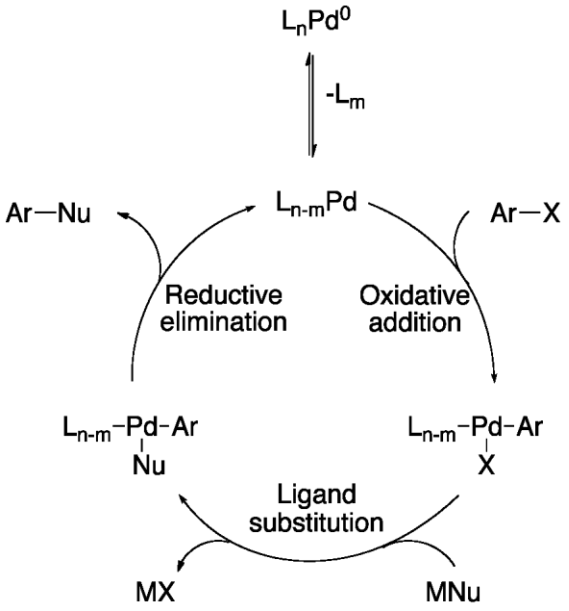

Figure 4.2. MPH_3, $M(PH_3)_2$, MPH_3Cl_2 and $M(PH_3)_2Cl_2$ Structures.

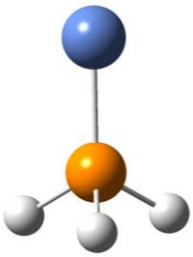

C_{3v}

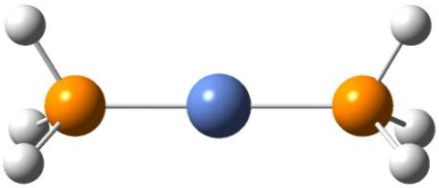

D_{3h}

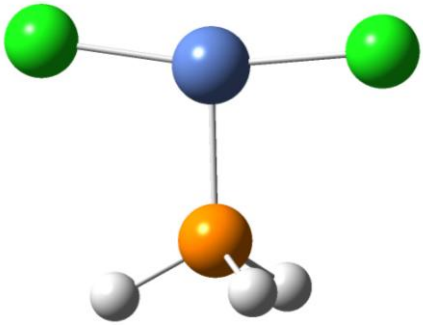

C_s

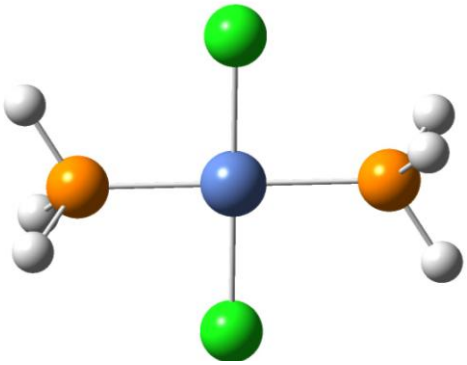

C_{2h}

References

[1] Tsuji, J. "Expanding Industrial Applications of Palladium Catalysts" *Synthesis* **1990**, *9*, 739-740.

[2] Crabtree, R.H. *The Organometallic Chemistry of the Transition Metals* John Wiley and sons, **2005**

[3] Fu, G. C. *Acc. Chem. Res.* **2008**, *41*, 1555.

[4] Fleckenstein, C. A.; Plenio, H. *Chem. Soc. Rev.* **2010**, *39*, 694.

[5] Christmann, U.; Vilar, R. *Angew. Chem., Int. Ed.* **2005**, *44*, 366.

[6] Stambuli, J. P.; Incarvito, C. D.; Bühl, M.; Hartwig, J. F. *J. Am. Chem. Soc.* **2004**, *126*, 1184.

[7] Galardon, E.; Ramdeehul, S.; Brown, J. M.; Cowley, A.; Hii, K. K.; Jutand, A. *Angew. Chem., Int. Ed.* **2002**, *41*, 1760.

[8] Barrios-Landeros, F.; Hartwig, J. F. *J. Am. Chem. Soc.* **2005**, *127*, 6944.

[9] Barrios-Landeros, F.; Carrow, B. P.; Hartwig, J. F. *J. Am. Chem. Soc.* **2009**, *131*, 8141.

[10] Parr, R. G.; Yang, M. *Density-Functional Theory of Atoms and Molecules*, Oxford University Press: New York, 1989

[11] (a) Perdew, J. P.; Burke, K.; Ernzerhof, M. *Phys. Rev. Lett.* **1996**, *77*, 3865. (b) Perdew, J. P.; Burke, K.; Ernzerhof, M. *Phys. Re*V. *Lett.* **1997**, *78*, 1396

[12] Li, Z.; Fu, Y.; Guo, Q.-X.; Liu, L. *Organometallics* **2008**, *27*, 4043.

[13] DeVasher, R.B.; Spruell, J.M.; Dixon, D.A.; Broker, G.A.; Griffin, S.T.; Rogers, R.D.; Shaughnessy, K.H. *Organometallics* **2005**, *24*, 962.

[14] Hill, L. L.; Smith, J. M. ; Brown, W. S. ; Moore, L. R.; Guevera, P.; Pair, E. S.; Porter, J.; Chou, J.; Wolterman, C. J.; Craciun, R.;Dixon, D. A.; Shaughnessy,K.H. *Tetrahedron*, **2008**, *64*, 6920.

[15] Hill, L. L.; Moore, L. R.; Huang, R.; Craciun, R.; Vincent, A.; Dixon, D. A.; Chou, J.; Woltermann, C. J.; Shaughnessy, K. H. *J. Org. Chem.*, **2006**, *71*, 5117.

[16] Piacenza, M.; Rakow, J.; Hyla-Kryspin, I.; Grimme, S. *Eur.J.Inorg.Chem.* **2006**, 213.

[17] Karhánek, D.; Kačer,P.; Kuzma,M.; Šplichalová, L. *J. Mol. Model* **2007**, *13*, 1009.

[18] Li,J.; Schreckenbach, G.; Ziegler,T. *Inorg. Chem.* **1995**, *34*, 3245.

[19] Massera,C.; Frenking,G. *Organometallics* **2003**, *22*, 2758.

[20] Kameno,Y.; Ikeda,A.; Nakao,Y.; Sato,H.; Sakaki,S. *J. Phys. Chem.A* **2005**, *109*, 8055.

[21] Sakaki,S.; Ogawa,M.; Musashi, Y.; Arai, T. *Inorg. Chem.* **1994**, *33*, 1660.

[22] Ariafard, A.; Lin,Z.; Fairlamb,J.S. *Organometallics* **2006**, *25*, 5788.

[23] Blomberg, M.R.A; Brandemark,U.B.; Siegbahn, P.E.M; Mathisen,K.B.; Karlstrom,G. *J.Phys.Chem.* **1985**, *89*, 2171.

[24] Blomberg, M.R.A; Schule, J.; Siegbahn, P.E.M. *J. Am. Chem. Soc.* **1989**, *111*, 6156.

[25] Minekov,Y.; Occhipinti,G.; Jensen,V.R. *J. Phys. Chem. A* **2009**, *113*, 11833.

[26] Hehre, W.J.; Radom, L.; Schleyer, P.V.R.; Pople, J.A.; *Ab Inition Molecular Orbital Theory;* Wiley-Interscience, 1986.

[27] Purvis, G.D., III; Bartlett, R.J. *J.Chem. Phys.* **1982**, *76*, 1910.

[28] Raghavachari, K.; Truck, G.W.; Pople, J.A.; Head-Gordon, M. *Chem. Phys. Lett.* **1989**, *157*, 479.

[29] Watts, J. D.; Gauss, J.; Bartlett, R. J. *J. Chem.. Phys.* **1993**, *98*, 8718.

[30] Bartlett, R. J.; Musial, M. *Rev. Mod. Phys.* **2007**, *79*, 291.

[31] (a) Feller, D.; Dixon, D. A. *J. Phys. Chem. A* **2000**, *104*, 3048. (b) Feller, D.; Dixon, D. A. *J. Chem. Phys.* **2001**, *115*, 3484. (c) Dixon, D.A.; Feller, D.; Peterson, K.A. *J. Chem. Phys.* **2001**, *115*, 2576. (d) Ruscic, B.; Wagner, A. F.; Harding, L. B.; Asher, R. L.; Feller, D.; Dixon, D. A.;

Peterson, K. A.; Song, Y.; Qian, X.; Ng, C.; Liu, J.; Chen, W.; Schwenke, D. W. *J. Phys. Chem. A* **2002**, *106*, 2727. (e) Feller, D.; Dixon, D. A. *J. Phys. Chem. A* **2003**, *107*, 9641. (f) Pollack, L.; Windus, T. L.; de Jong, W. A.; Dixon, D.A. *J. Phys. Chem. A* **2005**, *109*, 6934. (g) Feller, D.; Peterson, K.A.; Dixon, D.A. *J. Chem. Phys.* **2008**, *129*, 204015. (h) Dixon, D. A.; Grant, D. J.; Christe, K. O.; Peterson, K. A. *Inorg. Chem.* **2008**, *47*, 5485. (i) Dixon, D. A.; de Jong W. A. ; Peterson, K. A. ; Christe, K. O.; Schrobilgen, G. J. *J. Am. Chem. Soc.*, **2005**, *127*, 8627. (j) Dixon, D. A.; Grant , D. J.; Peterson , K. A.; Christe, K. O.; Schrobilgen, G. J. *Inorg. Chem.* **2008**, *47*, 5485.

[32] Slater, J. C. *Quantum Theory of Molecules and Solids*; McGraw-Hill: New York, 1974; Vol. 4.

[33] Vosko, S. H.; Wilk, L.; Nusair, M. *Can. J. Phys* **1980**, *58*, 1200.

[34] Becke, A. D. *Phys. Rev. A* **1988**, *38*, 3098.

[35] Lee, C.; Yang, W.; Parr, R. G. *Phys. Rev. B* **1988**, *37*, 785.

[36] Perdew J. P. *Phys. Rev. B* **1986**, *33*, 8822.

[37] Burke, K.; Perdew, J. P. Wang. Y. In *Electronic Density Functional Thoery: Recent Progress and New Directions*; Dobson, J. F., Vignale, G., Das, M. P., Eds.; Plenum: New York, 1998 p.81.

[38] Becke, A. D. *J. Chem. Phys.* **1996**, *104*, 1040.

[39] Perdew, J. P.; Wang, Y. *Phys. Rev. B* **1991**, *45*, 13244.

[40] Adamo, C.; Barone, V. *J. Chem. Phys.*, **1998**, *108*, 664.

[41] Handy, N. C.; Cohen, A. J. *Mol. Phys.* **2001**, *99*, 403.

[42] Tao, J. M.; Perdew, J. P.; Staroverov, V. N.; Scuseria, G. E. *Phys. Rev. Lett.* **2003**, *91*, 146401.

[43] Van Voorhis, T.; Scuseria, G. E. *J. Chem. Phys.*, **1998**, *109*, 400.

[44] Hamprecht, F. A.; Cohen, A. J.; Tozer, D. J.; Handy, N. C. *J. Chem. Phys.* **1998**, *109*, 6264.

[45] Becke, A. D. *J. Chem. Phys.* **1993**, *98*, 5648.

[46] Becke, A. D. *J. Chem. Phys.*, **1996**, *104***,** 1040.

[47] Adamo, C.; Barone, V. *Chem. Phys. Lett.* **1997**, *274*, 242.

[48] Hamprecht, F. A.; Cohen, A.; Tozer, D. J.; Handy, N. C. *J. Chem. Phys.* **1998**, *109*, 6264.

[49] Wilson, P. J.; Bradley, T. J.; Tozer, D. J. *J. Chem. Phys.* **2001**, *115*, 9233.

[50] Schmider, H. L.; Becke, A. D. *J. Chem. Phys.* **1998**, *108*, 9624.

[51] Boese, A. D.; Martin, J. M. L. *J. Chem. Phys.***2004**, *121*, 3405.

[52] Tao, J. M.; Perdew, J. P.; Staroverov, V. N.; Scuseria, G. E. *Phys. Rev. Lett.* **2003**, *91*, 146401.

[53] Dunning, Jr., T.H. *J.Chem. Phys*. **1989**, *90*, 1007.

[54] Woon, D.E.; Dunning, Jr., T.H. *J. Chem. Phys*. **1993**, *98*, 1358.

[55] Figgen, D.; Peterson, K. A.; Dolg, M.; Stoll, H. *J. Chem. Phys*. **2009**, *130*, 164108.

[56] Dunning, Jr., T.H.; Peterson, K. A.; Wilson, A.K. *J. Chem. Phys*. **2001**, *114*, 9244.

[57] Peterson, K. A.; Woon, D. E.; Dunning, T. H. Jr. *J. Chem. Phys.* **1994**, *100*, 7410.

[58] Peterson, K.A. ; Figgen, D.; Dolg, M.; Stoll, H. *J. Chem. Phys.* **2007**, *126*, 124101.

[59] (a) Balabanov, N.B.; Peterson, K.A. *J. Chem. Phys.* **2005**, *123*, 064107. (b) Balabanov, N.B.; Peterson, K.A. *J. Chem. Phys.* **2006**, *125*, 074110.

[60] (a) Douglas, M.; Kroll, N. M. *Ann. Phys.*, **1974**, *82*, 89; (b) Hess, B. A. *Phys. Rev. A.*, **1985**, *32*, 756. (c) Hess, B. A. *Phys. Rev. A.*, **1986**, *33*, 3742.

[61] de Jong, W. A.; Harrison, R. J. ; Dixon, D. A. *J. Chem. Phys.*, **2001**, *114*, 48.

[62] EMSL basis set library. http://www.emsl.pnl.gov/forms/basisform.html

[63] Gaussian 03, Revision E.01, Frisch, M. J.; Trucks, G. W.; Schlegel, H. B.; Scuseria, G. E.; Robb, M. A.; Cheeseman, J. R.; Montgomery, Jr., J. A.; Vreven, T.; Kudin, K. N.; Burant, J. C.; Millam, J. M.; Iyengar, S. S.; Tomasi, J.; Barone, V.; Mennucci, B.; Cossi, M.; Scalmani, G.;

Rega, N.; Petersson, G. A.; Nakatsuji, H.; Hada, M.; Ehara, M.; Toyota, K.; Fukuda, R.; Hasegawa, J.; Ishida, M.; Nakajima, T.; Honda, Y.; Kitao, O.; Nakai, H.; Klene, M.; Li, X.; Knox, J. E.; Hratchian, H. P.; Cross, J. B.; Bakken, V.; Adamo, C.; Jaramillo, J.; Gomperts, R.; Stratmann, R. E.; Yazyev, O.; Austin, A. J.; Cammi, R.; Pomelli, C.; Ochterski, J. W.; Ayala, P. Y.; Morokuma, K.; Voth, G. A.; Salvador, P.; Dannenberg, J. J.; Zakrzewski, V. G.; Dapprich, S.; Daniels, A. D.; Strain, M. C.; Farkas, O.; Malick, D. K.; Rabuck, A. D.; Raghavachari, K.; Foresman, J. B.; Ortiz, J. V.; Cui, Q.; Baboul, A. G.; Clifford, S.; Cioslowski, J.; Stefanov, B. B.; Liu, G.; Liashenko, A.; Piskorz, P.; Komaromi, I.; Martin, R. L.; Fox, D. J.; Keith, T.; Al-Laham, M. A.; Peng, C. Y.; Nanayakkara, A.; Challacombe, M.; Gill, P. M. W.; Johnson, B.; Chen, W.; Wong, M. W.; Gonzalez, C.; and Pople, J. A.; Gaussian, Inc., Wallingford CT, 2004.

[64] MOLPRO, version 2008.1, a package of ab initio programs, Werner, H.-J.; Knowles, P. J.; Lindh, R.; Manby, F. R.; Schütz, M.; Celani, P.; Korona, T.; Rauhut, G.; Amos, R. D.; Bernhardsson, A.; Berning, A.; Cooper, D. L.; Deegan, M. J. O.; Dobbyn, A. J.; Eckert, F.; Hampel C.; Hetzer, G.; Lloyd, A. W.; McNicholas, S. J.; Meyer W.; Mura, M. E.; Nicklass, A.; Palmieri, P.; Pitzer, R.; Schumann, U.; Stoll, H.; Stone, A. J.; Tarroni, R.; Thorsteinsson, T. See http://www.molpro.net.

[65] Moore, C. E. *Atomic Energy Levels as Derived from the Analysis of Optical Spectra, Volume 1, H to V*; U.S. National Bureau of Standards Circular 467; U.S. Department of Commerce, National Technical Information Service, COM-72-50282: Washington, D C, 1949.

[66] (a) Dixon, D.A.; Gutowski, M. *J. Phys. Chem. A*, **2005**, *109*, 5129. (b) Grant, D. J.; Dixon, D. A. *J. Phys. Chem. A* **2005**, *109*, 10138.

[67] Craciun, R.; Picone, D.; Long, R. T.; Li, S.; Dixon, D. A.; Peterson, K. A.; Christe, K. O., *Inorg Chem* **2010**, *49*, 1056

[68] Li, S.; Hennigan, J.M.; Dixon, D.A.; Peterson, K.A. *J. Phys. Chem. A* **2009**, *113*, 7861.

[69] Li, S.; Dixon, D. A. *J. Phys. Chem. A* **2010** *114*, 2665.

Appendix: Prediction of Reliable Metal-PH_3 Bond Energies for Ni, Pd and Pt in the 0 and +2 Oxidation States

Supporting Information

M-PH_3 binding energies , singlet-triplet energy splitting in kcal/mol, metal- phosphine bond dissociation energies[a] calculated with various exchange-correlation functionals and the aD-PP basis sets and deviations (kcal/mol) from the CCSD(T) calculated BDEs and MPH_3, $M(PH_3)_2$, MPH_3Cl_2, $M(PH_3)_2Cl_2$, and MCl_2 XYZ coordinates at B3LYP/aD-PP level .

Table A4.1. M-PH_3 binding energies in kcal/mol calculated at DFT and CCSD(T) levels with the aN-PP (N = D, T, Q) basis sets.

	reactant	**product**	**B3LYP aD-PP**	**CCSD(T) aD-PP**	**CCSD(T) aT-PP**	**CCSD(T) aQ-PP**
	State/Sym	**State/Sym**				
			Reactant = MPH_3			
Ni-P	$^1A_1/C_{3v}$	1	46.82	65.59	69.79	70.92
Pd-P	$^1A_1/C_{3v}$	1	34.83	35.89	39.88	41.18
Pt-P	$^1A_1/C_{3v}$	1	66.65	74.12	79.12	81.03
			Reactant = $M(PH_3)_2$			
Ni-P	$^1A_1'/D_{3h}$	$^1A_1/C_{3v}$	34.62	37.58	38.91	39.14
Pd-P	$^1A_1'/D_{3h}$	$^1A_1/C_{3v}$	28.75	30.80	32.42	33.06
Pt-P	$^1A_1'/D_{3h}$	$^1A_1/C_{3v}$	40.78	42.73	44.83	45.36
			Reactant = MPH_3Cl_2			
Ni-P	$^1A'/C_s$	$^3\Sigma_g/D_{\infty h}$	4.37	11.82	16.01	18.07
Pd-P	$^1A'/C_s$	$^3\Sigma_g/D_{\infty h}$	40.70	52.82	57.68	60.35
Pt-P	$^1A'/C_s$	$^3\Sigma_g/D_{\infty h}$	39.91	51.01	55.54	58.39
			Reactant = $M(PH_3)_2Cl_2$			
Ni-P	$^1A_g/C_{2h}$	$^1A'/C_s$	22.40	26.82	26.93	26.64
Pd-P	$^1A_g/C_{2h}$	$^1A'/C_s$	27.80	31.75	31.86	32.21
Pt-P	$^1A_g/C_{2h}$	$^1A'/C_s$	34.81	39.61	40.50	40.83

Table A4.2. Singlet-triplet energy splitting in kcal/mol for M, MCl_2, MPH_3, $M(PH_3)_2$, MPH_3Cl_2 and $M(PH_3)_2Cl_2$

M	**Ni**		**Pd**		**Pt**	
	S	**T**	**S**	**T**	**S**	**T**
M	42.7[a]	0	0	25.0[a]	0	5.8[a]
MCl_2	31.5[a]	0	6.1[a]	0	10.3[a]	0
MPH_3	0	17.2[a]			0	42.8[b]
$M(PH_3)_2$	0	34.1[c]			0	54.1[b]
MPH_3Cl_2	0	22.4[a]			0	22.5[c]
$M(PH_3)_2Cl_2$	0	14.1[d]			0	44.0*

[a] CCSD(T)/CBS. [b] CCSD(T)/aD-PP. [c] B3LYP/aD-PP. [d] CCSD(T)/aT-PP;

Table A4.3. First adiabatic metal- phosphine bond dissociation energies[a] calculated with various exchange-correlation functionals and the aD-PP basis sets and deviations (kcal/mol) from the CCSD(T) calculated BDEs. Values in parentheses are the differences from the CCSD(T) values.

$MPH_3 \rightarrow M + PH_3$

Functional	Ni (1→3)	Pd (1→1)	Pt (1→1)
SVWN5	68.9(-43.72)	59.86(-16.79)	79.78(-13.74)
BLYP	17.93(7.25)	37.43(5.64)	52.91(13.13)
BP86	25.9(-0.72)	43.79(-0.72)	61.37(4.67)
BPW91	24.65(0.53)	41.99(1.08)	59.66(6.38)
BB95	46.64(-21.46)	41.66(1.41)	59.21(6.83)
PW91	28.42(-3.24)	45.06(-1.99)	62.83(3.21)
mPWPW91	26.32(-1.14)	43.39(-0.32)	61.11(4.93)
PBE	28.42(-3.24)	44.57(-1.50)	62.37(3.67)
OLYP	23.13(2.05)	33.25(9.82)	51.49(14.55)
TPSS	24.22(0.96)	43.06(0.01)	61.72(4.32)
VSXC	29.38(-4.20)	40.21(2.86)	55.92(10.12)
HCTH	52.72(-27.54)	64.15(-21.08)	53.12(12.92)
B3LYP	1.64(23.54)	33.14(9.93)	46.84(19.20)
B3P86	12.34(12.84)	38.59(4.48)	54.21(11.83)
B3PW91	9.34(15.84)	36.53(6.54)	52.07(13.97)
B1B95	10.77(14.41)	34.90(8.17)	49.84(16.20)
B1LYP	-8.45(33.63)	31.10(11.97)	44.33(21.71)
mPW1PW91	2.87(22.31)	36.43(6.64)	52.04(14.00)
B971	-0.98(26.16)	35.23(7.84)	49.86(16.18)
B972	17.20(7.98)	33.79(9.28)	49.22(16.82)
B98	-2.21(27.39)	34.47(8.60)	49.29(16.75)
PBE1PBE	4.53(20.65)	37.45(5.62)	53.20(12.84)
O3LYP	23.81(1.37)	31.31(11.76)	47.38(18.66)
BMK	-45.71(70.89)	35.88(7.19)	44.96(21.08)

TPSSh	38.49(-13.31)	44.27(-1.20)	66.60(-0.56)
CCSD(T)[b]	**25.22**	**43.07**	**66.04**

[a] $E(DFT) = \Delta E_{elec}(DFT) + \Delta E_{ZPE} + \Delta E_{SO}$. For Ni we have used the atomic SO values of 2.38 kcal/mol. [b] $E(CCSD(T)) = \Delta E_{CBS} + \Delta E_{ZPE} + \Delta E_{CV} + \Delta E_{SO}$.

Table A4.4. First adiabatic metal- phosphine bond dissociation energies[a] calculated with various exchange-correlation functionals and the aD-PP basis sets and deviations (kcal/mol) from the CCSD(T) calculated BDEs. Values in parentheses are the differences from the CCSD(T) values.

$M(PH_3)_2 \rightarrow MPH_3 + PH_3$

Functional	**Ni**	**Pd**	**Pt**
SVWN5	50.02(-11.93)	44.35(-10.58)	55.98(-10.58)
BLYP	33.59(4.50)	27.38(6.39)	37.28(8.12)
BP86	37.63(0.46)	31.49(2.28)	42.48(2.92)
BPW91	36.40(1.69)	29.87(3.90)	41.07(4.33)
BB95	35.72(2.37)	29.31(4.46)	40.44(4.96)
PW91	39.34(-1.25)	32.86(0.91)	44.11(1.29)
mPWPW91	37.77(0.32)	31.26(2.51)	42.48(2.92)
PBE	38.80(-0.74)	32.32(1.45)	43.56(1.84)
OLYP	28.87(9.22)	22.28(11.49)	33.76(11.64)
TPSS	37.29(0.80)	30.79(2.98)	42.38(3.02)
VSXC	38.68(-0.59)	30.02(3.75)	39.42(5.98)
HCTH	30.60(7.49)	24.44(9.33)	36.06(9.34)
B3LYP	32.94(5.15)	27.03(6.74)	38.88(6.52)
B3P86	36.63(1.46)	30.74(3.03)	43.59(1.81)
B3PW91	34.90(3.19)	28.83(4.94)	41.72(3.68)
B1B95	33.63(4.46)	27.31(6.46)	41.32(4.08)
B1LYP	31.80(6.29)	26.00(7.77)	38.08(7.32)
mPW1PW91	35.41(2.68)	29.39(4.38)	42.81(2.59)
B971	34.56(3.53)	28.64(5.13)	41.20(4.20)
B972	32.56(5.53)	26.72(7.05)	39.75(5.65)
B98	33.75(4.34)	28.04(5.73)	40.65(4.75)
PBE1PBE	36.22(1.87)	30.24(3.53)	43.69(1.71)

O3LYP	29.29(8.80)	23.03(10.74)	35.43(9.97)
BMK	19.17(18.92)	32.17(1.60)	43.38(2.02)
TPSSh	37.63(0.55)	31.01(2.76)	42.78(2.62)
CCSD(T)[b]	**38.09**	**33.77**	**45.40**

[a] $E(DFT) = \Delta E_{elec}(DFT) + \Delta E_{ZPE}$; . [b] $E(CCSD(T)) = \Delta E_{CBS} + \Delta E_{ZPE} + \Delta E_{CV}$

Table A4.5. First adiabatic metal- phosphine bond dissociation energies[a] calculated with various exchange-correlation functionals and the aD-PP basis sets and deviations (kcal/mol) from the CCSD(T) calculated BDEs. Values in parentheses are the differences from the CCSD(T) values.

$MPH_3Cl_2 \rightarrow MCl_2 + PH_3$

Functional	**Ni**	**Pd**	**Pt**
SVWN5	33.26(-14.81)	81.46(-22.60)	57.78(-2.26)
BLYP	7.33(11.12)	53.63(5.23)	35.03(20.49)
BP86	13.25(5.20)	61.06(-2.20)	42.21(13.31)
BPW91	11.79(6.66)	58.92(-0.06)	41.49(14.03)
BB95	15.22(3.23)	58.70(0.16)	41.42(14.10)
PW91	15.42(3.03)	63.00(-4.14)	44.78(10.74)
mPWPW91	13.45(5.00)	60.79(-1.93)	43.05(12.47)
PBE	14.66(3.79)	62.33(-3.47)	44.41(11.11)
OLYP	7.49(10.96)	49.75(9.11)	38.86(16.66)
TPSS	12.22(6.23)	59.79(-0.93)	40.98(15.54)
VSXC	10.52(7.93)	62.01(-3.15)	38.45(17.07)
HCTH	11.12(7.33)	53.29(5.57)	40.76(14.76)
B3LYP	1.63(16.82)	53.15(5.71)	37.08(18.44)
B3P86	7.15(11.30)	59.96(-1.10)	44.15(11.37)
B3PW91	4.23(14.22)	57.12(1.74)	42.11(13.41)
B1B95	4.35(14.10)	56.04(2.82)	43.45(12.07)
B1LYP	-2.51(20.96)	51.28(7.58)	36.16(19.36)
mPW1PW91	2.17(16.28)	57.83(1.03)	44.02(11.50)
B971	4.19(14.26)	54.63(4.23)	41.51(14.01)
B972	5.80(12.65)	54.99(3.87)	43.19(12.33)
B98	3.19(15.26)	54.07(4.79)	40.93(14.59)
PBE1PBE	3.02(15.43)	59.13(-0.27)	45.15(10.37)
O3LYP	4.39(14.06)	50.42(8.44)	38.62(16.66)
BMK	1.47(16.98)	48.02(10.84)	35.46(20.06)
TPSSh	12.39(6.06)	60.21(-1.35)	40.98(15.54)
CCSD(T)[b]	**18.45**	**58.86**	**55.52**

[a] $E(DFT) = \Delta E_{elec}(DFT) + \Delta E_{ZPE}$; . [b] $E(CCSD(T)) = \Delta E_{CBS} + \Delta E_{ZPE} + \Delta E_{CV}$

Table A4.6. First adiabatic metal- phosphine bond dissociation energies[a] calculated with various exchange-correlation functionals and the aD-PP basis sets and deviations (kcal/mol) from the CCSD(T) calculated BDEs. Values in parentheses are the differences from the CCSD(T) values.

$M(PH_3)_2Cl_2 \rightarrow MPH_3Cl_2 + PH_3$

Functional	**Ni**	**Pd**	**Pt**
SVWN5	36.50(-11.51)	40.31(-8.33)	47.32(-7.16)
BLYP	18.71(6.28)	23.43(8.55)	29.04(11.12)
BP86	23.21(1.78)	27.56(4.42)	33.89(6.27)
BPW91	21.99(3.00)	26.09(5.89)	32.52(7.64)
BB95	22.39(2.60)	25.62(6.36)	31.83(8.33)
PW91	25.74(-0.75)	29.60(2.38)	36.14(4.02)
mPWPW91	23.78(1.21)	27.76()4.22	34.24(5.92)
PBE	25.08(-0.09)	29.60(2.38)	35.39(4.77)
OLYP	14.57(10.42)	18.41(13.57)	25.02(15.14)
TPSS	24.76(0.23)	28.15(3.83)	34.96(5.20)
VSXC	30.44(-5.45)	31.16(0.82)	37.05(3.11)
HCTH	16.90(8.09)	21.15(10.83)	27.84(12.32)
B3LYP	20.19(4.80)	25.75(6.23)	32.56(7.60)
B3P86	24.46(0.53)	29.58(2.40)	37.18(2.98)
B3PW91	22.64(2.35)	27.66(4.32)	35.25(4.91)
B1B95	23.22(1.77)	27.56(4.42)	35.51(4.65)
B1LYP	19.38(5.61)	25.29(6.69)	32.22(7.94)
mPW1PW91	23.95(1.04)	29.06(2.92)	37.02(3.14)
B971	22.71(2.28)	28.15(3.83)	35.37(4.79)
B972	20.96(4.03)	26.02(5.96)	33.70(6.46)
B98	21.97(3.02)	27.60(4.38)	34.85(5.31)
PBE1PBE	24.96(0.03)	29.91(2.07)	37.93(2.23)
O3LYP	16.30(8.69)	20.77(11.21)	27.98(12.18)
BMK	21.93(3.06)	30.55(1.43)	37.46(2.70)
TPSSh	25.08(-0.09)	28.52(3.46)	35.39(4.77)
CCSD(T)[b]	**24.99**	**31.98**	**40.16**

[a] $E(DFT) = \Delta E_{elec}(DFT) + \Delta E_{ZPE}$; . [b] $E(CCSD(T)) = \Delta E_{CBS} + \Delta E_{ZPE} + \Delta E_{CV}$

Table A4.7. MPH_3 $^1A_1/C_{3v}$ XYZ coordinates at B3LYP/aD-PP level .

$NiPH_3$

1	0.000000	1.238589	-1.906456
1	-1.072649	-0.619294	-1.906456
1	1.072649	-0.619294	-1.906456
28	0.000000	0.000000	0.839459
15	0.000000	0.000000	-1.185700

$PdPH_3$

46	0.000000	0.000000	0.653598
15	0.000000	0.000000	-1.548339
1	0.000000	1.228244	-2.280140
1	-1.063690	-0.614122	-2.280140
1	1.063690	-0.614122	-2.280140

$PtPH_3$

15	0.000000	0.000000	-1.710102
1	0.000000	1.252290	-2.394932
1	-1.084515	-0.626145	-2.394932
1	1.084515	-0.626145	-2.394932
78	0.000000	0.000000	0.420979

Table A4.8. $M(PH_3)_2$ $^1A_1'/D_{3h}$ XYZ coordinates at B3LYP/aD-PP level .

$Ni(PH_3)_2$

1	0.000000	1.222308	2.838772
15	0.000000	0.000000	2.115763
1	-1.058550	-0.611154	2.838772
1	1.058550	-0.611154	2.838772
28	0.000000	0.000000	0.000000
15	0.000000	0.000000	-2.115763
1	0.000000	1.222308	-2.838772
1	-1.058550	-0.611154	-2.838772
1	1.058550	-0.611154	-2.838772

$Pd(PH_3)_2$

15	0.000000	0.000000	2.291376
1	0.000000	1.226862	3.022721
1	1.062494	-0.613431	3.022721
1	-1.062494	-0.613431	3.022721
46	0.000000	0.000000	0.000000
15	0.000000	0.000000	-2.291376
1	-1.062494	-0.613431	-3.022721
1	1.062494	-0.613431	-3.022721
1	0.000000	1.226862	-3.022721

$Pt(PH_3)_2$

15	0.000000	0.000000	2.259610
1	0.000000	1.238932	2.967260
1	1.072947	-0.619466	2.967260
1	-1.072947	-0.619466	2.967260
15	0.000000	0.000000	-2.259610
1	-1.072947	-0.619466	-2.967260
1	1.072947	-0.619466	-2.967260
1	0.000000	1.238932	-2.967260
78	0.000000	0.000000	0.000000

Table A4.9. MPH_3Cl_2 $^1A'/C_s$ XYZ coordinates at B3LYP/aD-PP level .

$NiPH_3Cl_2$

15	-0.041969	-1.724880	0.000000
1	0.605244	-2.344338	1.098545
1	0.605244	-2.344338	-1.098545
1	-1.310204	-2.356801	0.000000
17	2.122351	0.492186	0.000000
17	-2.079453	0.779219	0.000000
28	0.000000	0.403743	0.000000

$PdPH_3Cl_2$

15	-0.022664	-1.798526	0.000000
1	0.625858	-2.404549	1.103685
1	0.625858	-2.404549	-1.103685
1	-1.301562	-2.407126	0.000000
46	0.000000	0.397124	0.000000
17	2.295118	0.311702	0.000000
17	-2.272188	0.625146	0.000000

$PtPH_3Cl_2$

15	-0.033886	-1.903566	0.000000
1	0.604785	-2.518174	1.106695
1	0.604785	-2.518174	-1.106695
1	-1.325529	-2.486751	0.000000
17	2.309343	0.319784	0.000000
17	-2.272623	0.590325	0.000000
78	0.000000	0.264163	0.000000

Table A4.10. $M(PH_3)Cl_2$ $^1A_g/C_{2h}$ XYZ coordinates at B3LYP/aD-PP level .

$Ni(PH_3)Cl_2$

1	3.004043	1.092975	0.000000
15	2.232192	-0.100576	0.000000
1	2.824730	-0.801230	1.083866
1	2.824730	-0.801230	-1.083866
28	0.000000	0.000000	0.000000
15	-2.232192	0.100576	0.000000
1	-2.824730	0.801230	-1.083866
1	-2.824730	0.801230	1.083866
1	-3.004043	-1.092975	0.000000
17	0.000000	2.188648	0.000000
17	0.000000	-2.188648	0.000000

$Pd(PH_3)Cl_2$

15	0.000000	2.327116	0.000000
1	1.242586	3.015026	0.000000
1	-0.661041	2.957385	1.086574
1	-0.661041	2.957385	-1.086574
46	0.000000	0.000000	0.000000
15	0.000000	-2.327116	0.000000
1	-1.242586	-3.015026	0.000000
1	0.661041	-2.957385	1.086574
1	0.661041	-2.957385	-1.086574
17	2.332902	-0.103461	0.000000
17	-2.332902	0.103461	0.000000

$Pt(PH_3)Cl_2$

1	-1.255347	2.975338	0.000000
15	0.000000	2.312522	0.000000
1	0.653824	2.946710	1.088709
1	0.653824	2.946710	-1.088709
15	0.000000	-2.312522	0.000000
1	-0.653824	-2.946710	-1.088709
1	-0.653824	-2.946710	1.088709
1	1.255347	-2.975338	0.000000
17	-2.351715	-0.077168	0.000000
17	2.351715	0.077168	0.000000
78	0.000000	0.000000	0.000000

Table A4.11. MCl_2 $^3\Sigma_g/D_{\infty h}$ XYZ coordinates at B3LYP/aD-PP level .

$NiCl_2$

17	0.000000	0.000000	2.072225
17	0.000000	0.000000	-2.072225
28	0.000000	0.000000	0.000000

$PdCl_2$

17	0.000000	0.000000	2.245810
17	0.000000	0.000000	-2.245810
46	0.000000	0.000000	0.000000

$PtCl_2$

17	0.000000	0.000000	2.190674
17	0.000000	0.000000	-2.190674
78	0.000000	0.000000	0.000000

5. CONCLUSIONS

High level coupled cluster CCSD(T) calculations, extrapolated to the complete basis set limit, were used to evaluate reliable, self-consistent thermochemical data sets for the third and second row transition metal hexafluorides and the Group 10 transition metals M-PH_3 bond energies critical to the innovation of metal phosphine catalysts. The electron affinities are direct measures for the oxidizer strengths of these hexafluorides and their oxidizing power increases monotonically from WF_6/MoF_6 to AuF_6/AgF_6. The inclusion of spin orbit corrections was very important to obtain the correct qualitative order for the electron affinitiesof the third row hexafluorides but not for the second row compounds. Based on their calculated fluoride ion affinities the corresponding pentafluorides are extremely strong Lewis acids. The MF_7^- anions exhibit the expected classical structure with M-F bonds, but a nonclassical structure with a very weak external F-F bond between an MF_6^- fragment and a fluorine atom is formed for M=Pt, Au, Ru, Pd and Ag, consistent with their high electron affinities. The $MF_7^- \rightarrow MF_6^- + F$ process is favored over the $MF_7^- \rightarrow MF_5 + F_2^-$ process for both second and third row transition metals. For PdF_7^-, AuF_7^-, RuF_7^-, PdF_7^- and AgF_7^-, nonclassical anions were found with a very weak external F-F bond between an MF_6^- fragment and a fluorine atom. These compounds should be excellent F atom sources under very mild conditions. A wide range of DFT exchange-correlation functionals were also evaluated and only the B3LYP, mPW1PW91 and PBE1 functionals were found to approximate the coupled cluster values.

References

[1] (a) Chorkendorff, I.; Niemantsverdriet, J. W. *Concepts of Modern Catalysis and Kinetics, 2nd Ed.* Wiley-VCH: Weinheim, Germany, 2007. (b) Sheldon, R.A.; Arends, I.; Hanefeld, U. *Green Chemistry and Catalysis*, Wiley-VCH: Weinheim, Germany, 2007. (c) Rothenberg, G. *Catalysis, Concepts and Green Applications*, Wiley-VCH: Weinheim, Germany, 2008.

[2] Bell, A.,Chair *Catalysis Looks to the Future*, Panel on New Directions in Catalytic Science and Technology, National Academy Press, 1992.

[3] Van Santen, R.A.; Neurock, M. *Concepts in Theoretical Heterogeneous Catalytic Reactivity*, *Catal.Rev.Sci.Eng* **1995**, *37*, 557.

[4] Truhlar, D.G.; Morokuma, K. *Transition State Modeling for Catalysis*, American Chemical Society, Washington DC, 1999

[5] Van Santen, R.A.; Neurock, M. *Molecular Heterogeneous Catalysis, a Conceptual and Computational Approach*, Wiley-VCH: Weinheim, Germany, 2006.

[6] Van Santen, R.A. *Theoretical Heterogeneous Catalysis*, World Scientific, Publishing: Singapore 1991

[7] Hirst, D. M. *A Computational Approach to Chemistry*, Blackwell Scientific: Oxford, **1990**.

[8] Grant, G. H.; Richards, W. G. *Computational Chemistry*, Oxford University Press: Oxford, 1995.

[9] Parr, R. G.; Yang, W. *Density Functional Theory of Atoms and Molecules*, Oxford University Press: New York, 1989.

[10] (a) Dunning, T. H., Jr. *J. Chem. Phys.* **1989**, *90*, 1007. (b) Kendall, R. A.; Dunning, T. H., Jr.; Harrison, R. J. *J. Chem. Phys.* **1992**, *96*, 6796.

[11] Peterson, K.A. In *Computational Inorganic and Bioinorganic Chemistry*, Solomon, E.I.; Scott, R.A.; King, R.B. Eds.; John Wiley and Sons 2009, p.187.

[12] (a) Frenking, G.; Antes, I.; Böhme, M.; Dapprich, S.; Ehlers, A.W.; Jonas, V.; Nauhaus, A.; Otto, M.; Stegmann, R.; Veldkamp, A.; Vyboishchikov, S.F. *Rev. Comp. Chem.*, **1996**, *8*, 63. (b) Cundari, T.R.; Benson, M. T.; Lutz, M. L.; Sommerer, S.O. *Rev. Comp. Chem.*, **1996**, *8*, 145.

[13] Wilson, S., Ed. *Methods in Computational Chemistry. Vol. 2. Relativistic Effects in Atoms and Molecules*, Plenum Press: New York, **1988.**

[14] Liu, W.; Kuchle, W.; Dolg, M. "Ab Initio Pseudopotential and Density Functional Studies of Lanthanide and Actinide Systems," In *Handbook on the Physics and Chemistry of Rare Earths*, Gschneider, K. A., Jr.; Eyring, L. eds.; Elsevier: Amsterdam, **1995**, Vol. 22, Chapter 170.

[15] Gropen, O. "The Relativistic Effective Core Potential Method," In *Methods in Computational Chemistry. Vol. 2. Relativistic Effects in Atoms and Molecules*, S. Wilson, ed., Plenum Press: New York, 1988, p. 109.

[16] (a) Küchle, W.; Dolg, M.; Stoll, H.; Preuss H. "Energy-Adjusted Pseudopotentials for the Actinides. Parameter Sets and Test Calculations for Thorium and Thorium Monoxide," *J. Chem. Phys.* **1994**, *100*, 7535 and references therein. (b) Küchle, W.; Dolg, M.; Stoll, H.; Preuss, H. "Pseudopotentials of the Stuttgart/Dresden Group **1998** (Revision: Tue Aug 11, 1998)." See World Wide Website: http://www.theochem.uni-stuttgart.de/pseudopotentiale.

[17] Cramer, C. *Essentials of Computational Chemistry: Theories and Models*, John Wiley&Sons, Chichester, 2004.

[18] Jensen, F. *Introduction to Computational Chemistry*, John Wiley&Sons, Chichester, 2007.

[19] Purvis, G.D., III; Bartlett, R.J. *J.Chem. Phys.* **1982**, *76*, 1910.

[20] Raghavachari, K.; Truck, G.W.; Pople, J.A.; Head-Gordon, M. *Chem. Phys. Lett*. **1989**, *157*, 479.

[21] Watts, J. D.; Gauss, J.; Bartlett, R. J. *J. Chem.. Phys.* **1993**, *98*, 8718.

[22] Bartlett, R. J.; Musial, M. *Rev. Mod. Phys.* **2007**, *79*, 291.

[23] Peterson, K. A.; Woon, D. E.; Dunning, T. H. Jr. *J. Chem. Phys.* **1994**, *100*, 7410.

[24] Hohenberg, P.; Kohn, W. *Phys. Rev. B* **1964**, *136*, 864.

[25] Kohn, W.; Sham, L. J. *Phys. Rev. A* **1965,** *140*, 1133.

[26] Slater, J. C. *Quantum Theory of Molecules and Solids*; McGraw-Hill: New York, 1974; Vol. 4.

[27] Vosko, S. H.; Wilk, L.; Nusair, M. *Can. J. Phys* **1980**, *58*, 1200.

[28] Becke, A. D. *Phys. Rev. A* **1988**, *38*, 3098.

[29] Lee, C.; Yang, W.; Parr, R. G. *Phys. Rev. B* **1988**, *37*, 785.

[30] Perdew J. P. *Phys. Rev. B* **1986**, *33*, 8822.

[31] Burke, K.; Perdew, J. P. Wang. Y. In *Electronic Density Functional Thoery: Recent Progress and New Directions*; Dobson, J. F., Vignale, G., Das, M. P., Eds.; Plenum: New York, 1998 p.81.

[32] Becke, A. D. *J. Chem. Phys.* **1996**, *104*, 1040.

[33] Perdew, J. P.; Wang, Y. *Phys. Rev. B* **1991**, *45*, 13244.

[34] Adamo, C.; Barone, V. *J. Chem. Phys.*, **1998**, *108*, 664.

[35] Perdew, J. P.; Burke, K.; Ernzerhof, M. *Phys. Rev. Lett.* **1996**, *77*, 3865.

[36] Perdew, J. P.; Burke, K.; Ernzerhof, M. *Phys. Rev. Lett.* **1997**, *78*, 1396.

[37] Handy, N. C.; Cohen, A. J. *Mol. Phys.* **2001**, *99*, 403.

[38] Tao, J. M.; Perdew, J. P.; Staroverov, V. N.; Scuseria, G. E. *Phys. Rev. Lett.* **2003**, *91*, 146401.

[39] Van Voorhis, T.; Scuseria, G. E. *J. Chem. Phys.*, **1998**, *109*, 400.

[40] Hamprecht, F. A.; Cohen, A. J.; Tozer, D. J.; Handy, N. C. *J. Chem. Phys.* **1998**, *109*, 6264.

[41] Becke, A. D. *J. Chem. Phys.* **1993**, *98*, 5648.

[42] Becke, A. D. *J. Chem. Phys.*, **1996**, *104***,** 1040.

[43] Adamo, C.; Barone, V. *Chem. Phys. Lett.* **1997**, *274*, 242.

[44] Hamprecht, F. A.; Cohen, A.; Tozer, D. J.; Handy, N. C. *J. Chem. Phys.* **1998**, *109*, 6264.

[45] Wilson, P. J.; Bradley, T. J.; Tozer, D. J. *J. Chem. Phys.* **2001**, *115*, 9233.

[46] Schmider, H. L.; Becke, A. D. *J. Chem. Phys.* **1998**, *108*, 9624.

[47] Perdew, J. P.; Burke, K.; Ernzerhof, M. *Phys. Rev. Lett.* **1996**, *77*, 3865.

[48] Boese, A. D.; Martin, J. M. L. *J. Chem. Phys.***2004**, *121*, 3405.

[49] Tao, J. M.; Perdew, J. P.; Staroverov, V. N.; Scuseria, G. E. *Phys. Rev. Lett.* **2003**, *91*, 146401.

[50] Davidson, E. R.; Ishikawa, Y.; Malli, G. L. "Validity of first-order perturbation theory for relativistic energy corrections," *Chem. Phys. Lett*. **1981,** *84*, 226.

[51] Feller, D.; Peterson, K.A.; de Jong, W. A.; Dixon, D. A. "Performance of coupled cluster theory in thermochemical calculations of small halogenated compounds," *J. Chem. Phys.* **2003**, *118*, 3510.

[52] (a) Douglas, M.; Kroll, N. M. *Ann. Phys.*, **1974**, *82*, 89; (b) Hess, B. A. *Phys. Rev. A.*, **1985**, *32*, 756. (c) Hess, B. A. *Phys. Rev. A.*, **1986**, *33*, 3742.

[53] Figgen, D.; Peterson, K. A.; Dolg, M.; Stoll, H. *J. Chem. Phys*. **2009**, *130*, 164108.

[54] de Jong, W. A.; Harrison, R. J. ; Dixon, D. A. *J. Chem. Phys.*, **2001**, *114*, 48.

[55] EMSL basis set library. http://www.emsl.pnl.gov/forms/basisform.html

[56] Woon, D. E.; Dunning, T. H. Jr. *J. Chem. Phys.* **1995**, *103*, 4572.

[57] Peterson, K. A.; Dunning, T. H. Jr. *J. Chem. Phys.* **2002**, *117*, 10548.

[58] (a) van Lenthe, E.; Ehlers, A.E. Baerends, E.J. *J. Chem. Phys*. **1999**, *110*, 8943; (b) van Lenthe, E.; Baerends, E.J.; Snijders, J.G. *J. Chem. Phys* **1993,** *99*, 4597; (c) van Lenthe, E.; Baerends, E.J.; Snijders, J.G.. *J. Chem. Phys* **1994,** *101*, 9783 ; (d) van Lenthe, E.; Snijders,

J.G.; Baerends, E.J. *J. Chem. Phys* **1994,** *105*, 6505; (e) van Lenthe, E.; van Leeuwen, R.; Baerends, E.J.; Snijders, J.G. *Int. J. Quantum Chem*. **1996,** *57*, 281

[59] (a) G. te Velde, F.M. Bickelhaupt, S.J.A. van Gisbergen, C. Fonseca Guerra, E.J. Baerends, J.G. Snijders and T. Ziegler, *J. Comput. Chem.* **2001**, *22*, 931; (b) C. Fonseca Guerra, J.G. Snijders, G. te Velde and E.J. Baerends, *Theor. Chem. Acc.* **1998**, *99*, 391; (c) ADF2008.01, SCM, Theoretical Chemistry, Vrije Universiteit, Amsterdam, The Netherlands, http://www.scm.com

[60] (a) Feller, D.; Dixon, D. A. *J. Phys. Chem. A* **2000**, *104*, 3048; (b) Feller, D.; Dixon, D. A. *J. Chem. Phys.* **2001**, *115*, 3484; (c) Dixon, D.A.; Feller, D.; Peterson, K.A. *J. Chem. Phys*., **2001**, *115*, 2576; (d) Ruscic, B.; Wagner, A. F.; Harding, L. B.; Asher, R. L.; Feller, D.; Dixon, D. A.; Peterson, K. A.; Song, Y.; Qian, X.; Ng, C.; Liu, J.; Chen, W.; Schwenke, D. W. *J. Phys. Chem. A* **2002**, *106*, 2727. (e) Feller, D.; Dixon, D. A., *J. Phys. Chem. A*, **2003**, *107*, 9641 (f) Dixon, D.A.; Feller, D.; Christe, K. O.; Wilson, W. W.; Vij, A.; Vij, V.; Jenkins, H. D. B.; Olson, R. M.; Gordon, M. S. *J. Am. Chem. Soc.*, **2004**, *126*, 834; (g) Dixon, D. A.; Gutowski, M. *J. Phys. Chem. A*, **2005**, *109*, 5129; (h) Pollack, L.; Windus, T. L.; de Jong, W. A.; Dixon, D.A. *J. Phys. Chem. A*, **2005**, *109*, 6934; (i) Gutowski K. E.; Dixon, D.A. *J. Phys. Chem. A*, **2006**, *110*, 12044 (j) Matus, M. H.; Anderson, K. D.; Camaioni, D. M.; Autrey, S. T.; Dixon, D. A. *J. Phys. Chem. A*, **2007**, *111*, 4411 ; (k) Feller, D.; Peterson, K.A.; Dixon, D.A. *J. Chem. Phys*., **2008**, *129* 204015.